THE UNIVERSITY *of* EDINBURGH

Uncertainty and complexity in pyrolysis modelling

Nicolas BAL

DOCTOR *of* PHILOSOPHY

THE UNIVERSITY *of* EDINBURGH
2012

Declaration

This thesis and the work described within have been conducted solely by Nicolas BAL under the supervision of Dr Guillermo REIN and Prof. José L. TORERO. Where others have contributed or other sources are quoted, references are given.

This research has been funded by BRE global.

The content of this work has been assessed by an examining committee composed by Dr Christopher W. LAUTENBERGER and Dr Stephen WELCH the 21st of August 2012.

Nicolas BAL

To my brother who made it all possible

Abstract

The use of numerical tools in fire safety engineering became usual nowadays and this tendency is expected to increase with the evolution of performance-based design. Despite the constant development of fire modelling tools, the current state of the art is still not capable of predicting accurately solid ignition, flame spread or fire growth rate from first principles. The condensed phase, which plays an important role in these phenomena, has been a large research area since few decades, resulting in an improvement of its global understanding and in the development of numerical pyrolysis models including a large number of physical and chemical mechanisms. This growth of complexity in the models has been justified by the implicit assumption that models with a higher number of mechanisms should be more accurate. However, as direct consequence, the number of parameters required to perform a simulation increased significantly. The problem is when the uncertainty in the input parameters accumulates in the model output beyond a certain level. The global error induced by the parameters uncertainty balances the improvements obtained with the incorporation of new mechanisms, leading to the existence of an optimum of model complexity.

While one of the first modelling tasks is to select the appropriate model to represent a physical phenomenon, this step is often subjective, and detailed justifications of the inclusion or exclusion of the different mechanisms are infrequent. The issue of how determining the most beneficial level of model complexity is becoming a major concern and this work presents a methodology to estimate the affordable level of complexity for polymer pyrolysis modelling prior ignition. The study is performed using PolyMethylMethAcrylate (PMMA) which is a reference material in fire dynamics due to the large number of studies available on its pyrolysis behaviour. The methodology employed is based on a combination of sensitivity and uncertainty analyses.

In the first chapter, the minimum level of complexity required to explain the delay times to ignition of black PMMA samples at high heat flux levels is obtained by exploring one by one the effect on the condensed phase of several mechanisms. It is found that the experimental results cannot be explained without considering the in-depth radiation absorption mechanism.

In the second chapter, a large literature review of the variability associated with the main parameters encountered in pyrolysis models is performed in order to establish the current level of confidence associated with the predictions using simple uncertainty analyses.

In the third chapter, a detailed analysis of the governing parameters (parametric sensitivity) is performed on the model obtained in chapter 1 to predict the delay time to ignition. Using the ranges obtained in chapter 2 for the input parameters, a detailed uncertainty analysis is performed revealing a large spread of the numerical predictions outside the experimental uncertainty. While several parameters, including the attenuation coefficient (from the in-depth radiation absorption mechanism), present large sensitivity, only a few are responsible for the large spread observed. The parameter uncertainty is shown as the limiting step in the prediction of solid ignition.

In the fourth chapter, a new methodology is developed in order to investigate the predominant mechanisms for the prediction of the transient pyrolysis behaviour of clear PMMA (no ignition). This approach, which corresponds to a mechanism sensitivity, consists of applying step-by-step assumptions to the most complex model used in the literature to model non-charring polymer pyrolysis behaviour. This study reveals the relatively high importance of the heat transfer mechanisms, including the process of in-depth radiation.

In the fifth chapter, an investigation of the uncertainty related to the calibration of pyrolysis models by inverse modelling is performed using several levels of model complexity. Inverse modelling couples the experimental data to the model equations and this dependency is often ignored. Varying the model complexity, this study reveals the presence of compensation effects between the different mechanisms. The phenomenon grows in importance with model complexity leading to unrealistic values for the calibrated parameters.

From the performed sensitivity and uncertainty analyses, the mechanism of in-depth absorption appeared critical for some applications. In the sixth chapter, an experimental investigation on specific conditions impacting the sensitivity of this mechanism shows its large dependency on the heat source emission wavelength when comparing the two heat sources of the most used pyrolysis test apparatuses in fire safety engineering. More fundamental investigations presented in the seventh chapter enabled to quantify this dependency that needs to be considered for modelling or experimental analyses. The impact of the heat source on the radiation absorption (depth and magnitude) is shown to be predictable thanks to the detailed measurements of the attenuation coefficient of PMMA and the emissive power of the heat sources.

The global uncertainty associated with the input parameters, extracted either from independent studies or by inverse modelling, appears as a limiting step in the improvement of pyrolysis modelling when a high level of complexity is implemented. A combination of numerical (sensitivity and uncertainty) analyses and experimental studies is required before increasing the level of complexity of a pyrolysis model.

Acknowledgements

First of all, I would like to thank Lucie for her presence and her patience. She has always been here for listening to me and her encouragements during the past 3 years have been essential. For that and for all the rest, I think that this work is also a bit hers.

Then my thanks go to Guillermo who has been a great supervisor. He had always faith in me and he allowed me losing time over different topics in the purpose to better understand mine. He is also the person who made me meeting many interesting people of the fire community and I would like to thank him a lot for that.

Of course, José has been one of the main actors of this global work by offering me the opportunity to join his group but also thanks to our technical conversations and its trust concerning knowledge transfer. For all of that, I would like to express him my gratitude. It has been a real pleasure to exchange and work closely with him.

Then I have to thank Hubert, Francesco and Thomas who have been my mentors and who are today close friends. I would like to tell them all my thankfulness for the time they spent explaining me the fundamentals and providing me their experimental knowledge. I should recognise that the best souvenirs I will keep from my time with them in Edinburgh are all the jokes that happened after 6pm in the office and the dinners which made this period of my life unforgettable. It is an honour for me to count them among my friends.

I have met incredible people at the BRE Centre for Fire Safety Engineering. I would like also to thank all of them, starting by the first generation that welcomed me in their group. Special thanks to Adam, Cécilia, Wolfram, David L. and Pedro: it was a pleasure to share your offices, to work and exchange with

you but also simply to be part of your life. I will not forget the second generation composed of very nice and enjoyable persons. Rory is great ambassador of this one and I need to express him my gratitude for all the suggestions he had about my research and more generally for the time we spent discussing. Among the third generation, I would like to thank Steffen for the long talks we had almost every day on our cultural similarities and John for sharing his vision on multitudes of topics including the French gastronomy. Cristian completes this beautiful trio. More than just a colleague, he has been a great flatmate (almost a perfect chef) who taught me more than he is thinking. I would never forget all the friends I made in the firegroup or more generally in John Muir, especially Josephine, Albert, Doug, Michal, François, Pierre, Nele and Joanne who have been really close to me

Special thanks to Frances, Iris, Jean, Aymeric and Pascal who helped me a lot and who explained me important notions such as the P+1 rule.

Last but not least, I would like to thank my parents and close relatives for their support and their continuous encouragements. More than everyone, they are the persons who made this adventure possible. I would never thank them enough for pushing me to follow my own path and for their valuable advice.

Contents

Introduction **1**

Numerical investigation of the ignition delay time of a translucent solid at high radiant heat fluxes **7**

1. Introduction 8
2. Behaviour at high heat fluxes 11
3. Pyrolysis model 13
4. Numerical investigation 15
   - 4.1. Kinetics, critical mass flux and heat losses 15
   - 4.2. Reaction scheme 17
   - 4.3. Temperature dependent material properties 18
   - 4.4. Incident radiation attenuation 19
   - 4.5. In-depth absorption 20
5. Effect of black-carbon coating 24
6. Conclusion 26

Pyrolysis modelling up to ignition – Part I: Literature review on sources of uncertainty and experimental variability **33**

1. Introduction 34
2. Piloted solid ignition 36
   - 2.1. Phenomenon complexity 36
   - 2.2. Modelling of the condensed phase 38
   - 2.3. Experimental state-of-the-art 40
   - 2.3.1 Time to ignition tign 41
   - 2.3.2 Variation of the condensed phase ignition criteria 43
3. Extraction of the input parameters 47
   - 3.1. Independent measurements 47
   - 3.2. Inverse modelling 48
   - 3.3. Expert judgment 48
   - 3.4. Literature 48
4. Literature review of main input parameters 49

4.1. Thermophysical properties 49
4.2. Pyrolysis kinetics 53
4.3. Radiative properties 58
4.4. Convective heat transfer coefficient 61
4.5. Heat of pyrolysis 62
4.6. Incident heat flux level 63
4.7. Range of variability 64
5. Conclusion 66

Pyrolysis modelling up to ignition – Part II: Parametric sensitivity and uncertainty analyses 75
1. Introduction 76
2. Piloted ignition model 81
3. Sensitivity and uncertainty analyses: concepts and methodologies 82
3.1. Sensitivity analyses 82
3.1.1 Scatter-plot (SP) 83
3.1.2 One-At-a-Time (OAT) 83
3.1.3 Design of Experiments (DoE) 84
3.2. Uncertainty analyses 84
3.2.1 Prediction intervals 85
3.2.2 Monte Carlo analysis 85
4. Input parameters 85
5. Results of parametric sensitivity analyses 87
5.1. Scatter plot (SP) 87
5.2. One-At-a-Time (OAT) 89
5.3. Design of Experiments (DoE) 90
5.4. Analysis and discussion 90
6. Uncertainty analyses 94
6.1. Prediction intervals 94
6.2. Monte Carlo 95
6.3. Analysis and discussion 98
7. Conclusion 100

Relevant model complexity for non-charring polymer pyrolysis **105**
1. Introduction 106
2. Several model complexities for one set of experiments 108
2.1. Comparison to experiments 108
2.2. Differences in the model equations 110
2.3. Parameter values 111
3. Mechanism sensitivity 113
3.1. Taxonomy of model complexity 113
3.2. Results and discussion 116
3.2.1 Taxonomy α 117
3.2.2 Taxonomy β 124
4. Conclusion 126

Uncertainty in the calibration process by inverse modelling for polymer pyrolysis **131**
1. Introduction 133
2. Experimental data 135
3. Model equations 136
3.1. Reference model 136
3.2. Model taxonomy 138
4. Optimisation process 139
5. Results and discussion 140
6. Conclusion 147

Comparison of pyrolysis behaviour results between the Cone Calorimeter and the Fire Propagation Apparatus heat sources **151**
1. Introduction 152
2. Experimental section 158
2.1. Sample preparation 158
2.2. Experimental procedure 158
2.3. Experimental results 160
2.3.1 Clear PMMA samples 160
2.3.2 Wood specimens 164

3. Discussion 165
4. Conclusion 170

Experimental study of radiative heat transfer in a translucent fuel sample exposed to different spectral sources 173
1. Introduction 174
2. Broadband measurements of the sample transmittance 177
3. Sample in-depth absorption 180
4. Spectral emission from heaters 184
5. Discussion 185
6. Conclusion 188

Achievements and prospects 193
1. Outcomes of the present research 193
2. Future work 197

Preface

This thesis is written in manuscript format. As such each chapter is a standalone document suitable for journal publication. The material is presented as follows:

Chapter 1 presents a numerical investigation on the failure of the classical ignition theory to explain experimental measurements at high heat flux levels. This manuscript has been published as:

> N. Bal and G. Rein, Numerical investigation of the ignition delay time of a translucent solid at high radiant heat fluxes, Combustion and flame 158 (2011) 1109–1116, http://dx.doi.org/10.1016/j.combustflame.2010.10.014.

Chapter 2 corresponds to a review of the state-of-the-art for piloted solid ignition of PolyMethylMethAcrylate and to the variability of the main parameters encountered in pyrolysis modelling. This chapter is intended to be a published manuscript.

Chapter 3 identifies, using sensitivity analyses, the governing parameters of a solid ignition model and assesses, using uncertainty analyses, the global level of confidence associated with the model predictions when the input parameters are calibrated with the literature database. This chapter is intended to be a published manuscript and a previous version has been presented to the fire community in a conference as part of a process of continuous improvement.

> N. Bal and G. Rein, Sensitivity and uncertainty of ignition modelling, Recent advances in flame retardancy of polymeric material 21(2010), BCC Research.

Chapter 4 presents a novel approach to study mechanism sensitivity in the context of pyrolysis modelling. This chapter is intended to be a published manuscript and a previous version has been presented to the fire community in a conference as part of a process of continuous improvement.

N. Bal and G. Rein, On the Uncertainty and Complexity in Model of Polymer Ignition, Recent advances in flame retardancy of polymeric material 22 (2011), BCC Research.

Chapter 5 investigates the influence of the model complexity in the context of pyrolysis modelling when the calibration process is performed by inverse modelling. This chapter has been submitted for publication to a relevant journal and is currently under review. It has been presented to the fire community in a conference as part of a process of continuous improvement.

N. Bal and G. Rein, Uncertainty and calibration in polymers pyrolysis modelling, Recent advances in flame retardancy of polymeric material 23 (2012), BCC Research.

Chapter 6 corresponds to an experimental sensitivity analysis where the differences in the pyrolysis behaviour induced by the use of two different heat sources are investigated. This manuscript has been published as:

P. Girods, N. Bal, H. Biteau, G. Rein and J.L. Torero, Comparison of pyrolysis behaviour results between the Cone Calorimeter and the Fire Propagation Apparatus heat sources, Fire safety science 10 (2011) 889-901, http://dx.doi.org/10.3801/IAFSS.FSS.10-889.

Chapter 7 reports fundamental investigations on the wavelength dependency of the radiative heat transfer in case of translucent solid. This manuscript has been submitted for publication to a relevant journal and is currently under review.

List of Figures

Figure 1.1: Times to piloted ignition of black PMMA samples for a wide range of experimental conditions in the literature. Continuous line is the classical theory which best fits for whole dataset between 20 and 70 kW/m^2. (a) inverse of the square root of the delay time to ignition (inset: zoom for heat fluxes up to 60 kW/m^2) and (b) delay time to ignition. 10

Figure 1.2: Effect of the different reaction schemes on the predictions of the inverse square root of the time to ignition. 18

Figure 1.3: Effect of the material property temperature dependency on the predictions of the inverse square root of the time to ignition. 19

Figure 1.4: Effect of the incident radiation attenuation by the pyrolysis gases on the predictions of the inverse square root of the time to ignition. 20

Figure 1.5: Effect of the attenuation coefficient on the predictions of the inverse square root of the time to ignition 21

Figure 1.6: Comparison of experimental temperature profiles (at ignition except for (a) 15 kW/m^2 - coated samples) with model predictions (attenuation coefficient of 1400 m^{-1}) with and without temperature dependency. Experimental errors: ±1.5 mm for depth and ±10 °C for temperature. Inset (d): comparison of the temperature profile with and without the in-depth radiation absorption phenomenon. 23

Figure 1.7: Surface temperature at the time to ignition over a wide range of heat fluxes for coated and uncoated samples 24

Figure 1.8: Predictions of the ignition delay times by combining surface absorption and in-depth absorption. 26

Figure 2.1: Schematic of the complexity encompassed in the pyrolysis process. 36

Figure 2.2: Times to piloted ignition of black PMMA samples for a wide range of experimental conditions (data extracted from the literature) 41

Figure 2.3: Variations of the measured delay time to ignition for different flow conditions and atmospheric compositions (black PMMA samples). 42

Figure 2.4: (a) Surface temperature and (b) mass flux measured at ignition with different experimental conditions for black and clear PMMA samples. ... 45

Figure 2.5: Surface temperature and mass loss rate for two samples sold under the trade name PMMA (18 kW/m^2 - air). 46

Figure 2.6: Thermal conductivity extracted from the literature for PMMA samples: (a) property function of temperature and (b) property considered as invariant. 50

Figure 2.7: Specific heat extracted from the literature for PMMA samples: (a) property function of temperature and (b) property considered as invariant. 50

Figure 2.8: Density extracted from the literature for PMMA samples: (a) property function of temperature and (b) property considered as invariant. 51

Figure 2.9: Thermogravimetric analyses extracted from the literature for PMMA at 5 K/min: (a) in air and (b) in inert gas. 54

Figure 2.10: Correlation between the Arrhenius kinetics parameters (activation energy and pre-exponential factor) for the chemical decomposition of PMMA (data extracted from the literature). 57

Figure 2.11: Reflectivity coefficients extracted from the literature for black PMMA. 59

Figure 2.12: Effective attenuation coefficients extracted from the literature for black PMMA. 61

Figure 2.13: Convective heat transfer coefficients extracted from the literature for bench-scale tests. 62

Figure 2.14: Heat of pyrolysis and gasification extracted from the literature for PMMA. 63

Figure 3.1: Delay times to piloted ignition of black PMMA samples for a wide range of experimental conditions (data from literature). 79

Figure 3.2: Correlation between the Arrhenius kinetics parameters for the chemical decomposition of PMMA samples simulated with 1-step reaction scheme (data extracted from the literature). 87

Figure 3.3: Evolution of the predicted delay time to ignition at four heat flux levels over the range of variation of the attenuation coefficient (SP technique). 88

Figure 3.4: Change in the effective sensitivity coefficient s_K at four heat flux levels as a function of the variation ΔX_i. 90

Figure 3.5: Relative sensitivity $s_i / s_{i\,max}$ of the different parameters (assessed from SP and OAT techniques) at four heat flux level. 91

Figure 3.6: Probability density functions of the predicted delay time to ignition resulting from the parameter uncertainty: (a) 50 kW/m², (b) 100 kW/m², (c) 150 kW/m² and (d) 200 kW/m². 96

Figure 3.7: Impact on the probability density function best fit at 100 kW/m² when a parameter is kept constant.....97

Figure 3.8: Relative differences in the average and standard deviation between the simulations where all parameters vary simultaneously and the simulations where one parameter is fixed: applied heat flux q_e''; specific heat c; density ρ; attenuation coefficient κ; kinetics parameters A; Ea or kinetics correlation $Ea = fA$. 98

Figure 4.1: Schematic of the relationship between prediction error, prediction uncertainty and model complexity.....108

Figure 4.2: Numerical predictions of surface temperature and mass loss rate from literature against experimental measurements for clear PMMA: (a-b) at 40 kW/m²; (c-d) at 17 kW/m²; (a-c) in 20 % of oxygen concentration and (b-d) in nitrogen atmosphere.....110

Figure 4.3: Kinetics parameters collected from the literature for PMMA decomposition. Inset: Comparison between experimental and numerical results of TGA at 5 K/min in inert atmosphere.....112

Figure 4.4: Model taxonomy α (diamond: models - square: assumptions).....116

Figure 4.5: Predictions against experimental measurements at 40 kW/m² in 20 % of O_2 for models in taxonomy α: (a) surface temperature and (b) mass loss rate.....117

Figure 4.6: Relationship between model complexity (taxonomy α) and prediction error for surface temperature and mass loss rate at 40 kW/m² in 20 % of oxygen. The x-axes represent (a) the number of parameters in the models and (b) the reference number of the models. 119

Figure 4.7: Predictions against experimental measurements at 40 kW/m² in nitrogen for models in taxonomy α: (a) surface temperature and (b) mass loss rate.....121

Figure 4.8: Relationship between model complexity (taxonomy α) and prediction error for surface temperature and mass loss rate at 40 kW/m² in nitrogen. The x-axes represent (a) the number of parameters in the models and (b) the reference number of the models.....122

Figure 4.9: Model taxonomy β (diamond: models - square: assumptions).....124

Figure 4.10: Predictions against experimental measurements at 40 kW/m² in 20 % of O_2 for models in taxonomy β: (a) surface temperature and (b) mass loss rate.....124

Figure 4.11: Relationship between model complexity (taxonomy β) and prediction error for surface temperature and mass loss rate at 40 kW/m² in 20 % of oxygen. The x-axes represent (a) the number of parameters in the models and (b) the reference number of the models. 126

Figure 5.1: Mass loss rate and surface temperature of clear PMMA at 40 kW/m² in 20 % oxygen (non flaming conditions): measurements and predictions. 136

Figure 5.2: Comparison of the 10 best simulations obtained with model M_1 against the experimental results: (a) mass loss rate and (b) surface temperature. 141

Figure 5.3: Comparison of the 10 best simulations obtained with model M_2 against the experimental results: (a) mass loss rate and (b) surface temperature. 141

Figure 5.4: Comparison of the 10 best simulations obtained with model M_3 against the experimental results: (a) mass loss rate and (b) surface temperature. 142

Figure 5.5: Comparison of the 10 best simulations obtained with model (a) M_4 and (b) M_5 against the experimental results for the surface temperature. 143

Figure 5.6: Mass loss rate evolution of the single best match from M_1, M_2 and M_3 to reference model prediction..... 143

Figure 5.7: Comparison of the optimised parameters from the 10 best fits for each model M_1 to M_5 with ranges found in the literature (solid lines) and values obtained with the reference model (dotted lines). 144

Figure 5.8: Comparison of the in-depth temperature prediction for the simulations presenting equivalent predictions of the mass loss rate..... 147

Figure 6.1: Inverse square root of the time to ignition for black PMMA samples extracted from the literature. The uncertainty is estimated at ± 2 s. 153

Figure 6.2: Ignition test measurements for (a) black PMMA and (b) clear PMMA with two heater sources: tungsten lamp and benzene flame. The uncertainty is estimated at ± 2s. 156

Figure 6.3: Schematic of the sample holder. 158

Figure 6.4: Schematic and picture of the experimental apparatus with both heaters: tungsten lamps and conical resistance..... 159

Figure 6.5: Temperature increase of the aluminium block located at the back of the clear PMMA samples for experiments with tungsten lamps and conical resistance.....161

Figure 6.6: Dimensionless mass loss coefficient γ versus time for tungsten lamps and conical resistance experiments with clear PMMA samples. 161

Figure 6.7: Vertical sections of clear PMMA samples showing the bubble layer depth. Samples were exposed to a heat flux level of 20 kW/m^2 for 35 min with: (a) conical resistance and (b) tungsten lamps. 162

Figure 6.8: Temperature measurement in-depth (below the exposed surface) for wood sample exposed to tungsten lamps and conical resistance: (a) temperature vs. time and (b) depth vs. temperature. 164

Figure 6.9: Dimensionless mass loss coefficient γ versus time for tungsten lamps and conical resistance experiments with wood samples. 165

Figure 6.10: Spectral distribution of the absorbance against the emissive power of a blackbody at the corresponding heater temperature providing a heat flux of 20 kW/m^2. (a) conical resistance, clear PMMA; (b) tungsten lamps, clear PMMA; (c) electrical cone resistance, wood; (d) tungsten lamps, wood. Shaded area is 60 % of the total intensity and centred on the peak emissive power value.....167

Figure 6.11: Spectral distribution of the transmittance of clear PMMA against the emissive power of a blackbody at the corresponding heater temperature providing a heat flux of 20 kW/m^2: (a) conical resistance; (b) tungsten lamps. Shaded area is 60 % of the total intensity and centred on the peak emissive power value. 168

Figure 7.1: Experimental set up of the heat source, the sample and the heat flux meters. Inset: Schematic of the multiple reflection mechanism. 176

Figure 7.2: Transmitted to incident heat flux ratio for clear PMMA samples (*Plexiglass* and *Lucite*) exposed to a radiative source (conical resistance and tungsten lamp) providing 10 and 20 kW/m^2 for thicknesses ranging between 0.375 and 51 mm.....179

Figure 7.3: Absorbance measurements for 0.375 mm and 30 mm thick *Plexiglass* samples. 181

Figure 7.4: Spectral distribution of the attenuation coefficient for *Plexiglass*. .183

Figure 7.5: Comparison of independent measurements of the absorbance with predictions based on the measured attenuation coefficient. 183

Figure 7.6: Spectral distribution of the emitted intensity (left axes) for (a) the tungsten lamp at 2610 K and (b) the conical resistance at 858 K. The

absorbance for the 1 mm *Plexiglass* sample is shown on the right axes for comparison. 185

List of Tables

Table 1.1: Parameter values used in the base case and range of values found in the literature, mostly, for black PMMA (References not exhaustive).....16

Table 1.2: Example of the material property temperature dependency equations. 18

Table 1.3: Comparison between model predictions and experimental measurements of the inverse square root of the delay time to ignition....21

Table 2.1: Sensitivity of tign to experimental conditions for PMMA samples. 42

Table 2.2: Equation coefficients for PMMA thermophysical properties. 52

Table 2.3: Ranges of variability extracted from the literature for the main input parameters of pyrolysis models applied to PMMA samples.....65

Table 3.1: Input parameters and uncertainty ranges extracted from literature for PMMA samples. 86

Table 3.2: Effective sensitivity coefficient si from SP and OAT techniques. 89

Table 3.3: Ratios between the prediction interval and the nominal prediction of tign. 94

Table 4.1: Assumptions and simplifications added to model M_1.....115

Table 5.1: Taxonomy of models complexity. 139

Table 5.2: Ranges of optimised values for best matched predictions of the mass loss rate between the reference model and M_1 to M_3.....146

Table 6.1: Operating temperatures for heat sources for Cone Calorimeter and FPA. 166

Introduction

While the ultimate goal of fire safety engineering has always been to protect the persons, properties and environment, its strategy has evolved since several decades. Historically, this one was based on the principles of flammability, failure and resistance capability of every element taken individually (combustible materials, safety device and structural elements). The regulation was based on a ranking system obtained from standardized tests. The strategy assumed therefore implicitly that the global level of safety corresponds to the weakest component. As a direct consequence of this methodology, large safety factors were implemented to cover the lack of understanding of the different interactions between the components (e.g. assumption of an infinite increase of temperature in the ISO 834 curve which attempts to envelop the worst temperature attainable in a compartment). Fire safety engineering was therefore fully prescriptive.

However, the research and the development of engineering tools enable more and more to understand the physics and chemistry controlling fires. The objective evolved from being able to rank the fire safety solutions to capturing the interaction between the different components in order to allow innovations and the inclusion of new technologies. In this context, fire safety engineering approaches progressed from standardizing experimental procedure to developing comprehensive models capable of predicting the evolution and the consequences of fire accident. The regulation is changing slowly, opening the path to performance-based design. While large safety factors were imposed before without proper knowledge of them, the new approach tends to quantify them, or at least to compare the safety between different strategies, in order to optimise the projects from a financial and innovative point of view. The freedom associated with this necessary evolution can be dangerous if the understanding does not follow the innovations.

The prediction of the fire growth is one of the main challenges of the fire safety engineering in this context of performance-based design. The pyrolysis of the solid material and their ignitability play a major role in this phenomenon. More than only being the initial event causing the fire start, solid ignition controls also the flame propagation: either from a continuous point of view (flame spread) or by the spread from an item to its neighbourhood.

The pyrolysis models have experienced a strong development as the global understanding of the phenomena occurring in the condensed and gas phases prior ignition increased. The first models, such as the classical ignition theory [1] were developed to analyse specific experimental procedures. The objective was not to predict the delay time to ignition but to extract internal parameters (material properties) to rank the material on a flammability scale. Then, correlations resulting from experimental understanding were developed [2,3], but their predictive capabilities are constrained to the range of tests performed (i.e. materials and experimental procedures). Since a decade ago, more comprehensive models, including mainly heat transfer and chemical degradation sub-models, have been developed [4-10]. However, even if the large part of solid ignition complexity is understood philosophically [1,11-14], its mathematical

formulation is still ill-defined. Some mechanisms are still not mature enough (e.g. bubble formation) and are neglected as a first approximation.

Such models have been developed with the constant willingness to get closer to the reality, including therefore more and more mechanisms. A direct consequence of this growth of complexity is the increasing number of input parameters required. The issue comes from the uncertainties associated with these parameters. They result mainly from the available resources (human, material and financial) to extract them and the experimental state-of-the-art. While often ignored, the parameter uncertainty directly impacts the level of confidence of model predictions. They accumulate in the model output up to a point that they overcome the error due to the simplicity of the model equations and potentially become the main source of error. It exists therefore an optimum level of complexity which depends on the knowledge of the phenomenon and of the model parameters. This optimum is not fixed and can move when more fundamental analysis are performed to reduce the parameters uncertainty. As the number of available mechanisms and sub-models grows rapidly, the issue of how determining the most beneficial level of model complexity to predict an event is becoming a major concern.

This concept is not specific to fire safety engineering and other disciplines have handled this issue [15,16]. They have demonstrated that the most complete models are not necessarily the most accurate.

The different chapters of this thesis represent a first attempt to characterise the balance between prediction accuracy and model complexity for the pyrolysis process leading to solid ignition. The methodology employed consists of a combination of sensitivity and uncertainty analyses. These studies diverge from previous analyses since they are focused on the required and affordable model complexity. The parameter uncertainty is investigated following two types of calibration process: literature review and inverse modelling.

These studies are performed with PolyMethylMethAcrylate (PMMA) which is a reference material in fire safety engineering. While its application is limited,

it is a very simple non-charring polymer which is by far the most studied since decades ago. The large amount of available analyses for this material provides a good representation of the experimental state-of-the-art for parameter variability. This later is therefore expected to be wider for any other materials.

Finally, fundamental studies are performed for the mechanism of in-depth absorption which appears in the sensitivity and uncertainty analyses as a critical mechanism for PMMA pyrolysis.

References

[1] J.L. Torero, Flaming ignition of solid fuels, in: The SFPE handbook of fire protection engineering 4th edition, P.J. DiNenno et al. (Eds.), National Fire Protection Association, 2008, chapter 2.11, pp. 2.260-2.278, ISBN-10: 0877658218.

[2] C. Vovelle, R. Akrich and J-L. Delfau, Mass loss rate measurements on solid materials under radiative heating, Combustion science and technology 36 (1984) 1-18, http://dx.doi.org/10.1080/00102208408923722.

[3] C. Vovelle, R. Akrich and J-L. Delfau, Thermal degradation of solid materials under a variable radiant heat flux, Proceedings of the symposium (international) on combustion 20 (1984) 1647-1654, http://dx.doi.org/10.1016/S0082-0784(85)80660-3.

[4] S.R. Wasan, P. Rauwoens, J. Vierendeels and B. Merci, An enthalpy-based pyrolysis model for charring and non-charring materials in case of fire, Combustion and flame 157 (2010) 715-734, http://dx.doi.org/10.1016/j.combustflame.2009.12.007

[5] K. McGrattan, S. Hostikka, J. Floyd, H. Baum, R. Rehm, W. Mell and R. McDermott, Fire dynamics simulator (version 5) technical reference guide volume 1: Mathematical model, NIST internal publication 1018-5, 2010.

[6] C. Lautenberger, A Generalized Pyrolysis Model for Combustible Solids, PhD dissertation, The University of California, Berkeley, 2007, <http://escholarship.org/uc/item/7wz5m7dg>.

[7] C. Lautenberger and C. Fernandez-Pello, Generalized pyrolysis model for combustible solids, Fire safety journal 44 (2009) 819-839, http://dx.doi.org/10.1016/j.firesaf.2009.03.011.

[8] S.I. Stoliarov and R.E. Lyon, Thermo-Kinetic model of burning, Federal Aviation Administration internal report DOT/FAA/AR-TN08/17, 2008.

[9] S.I. Stoliarov, S. Crowley, R. E. Lyon and G.T. Linteris, Prediction of the burning rates of non-charring polymers, Combustion and flame 156 (2009) 1068-1083, http://dx.doi.org/10.1016/j.combustflame.2008.11.010.

[10] M. Chaos, M.M. Khan, N. Krishnamoorthy, J.L. De Ris and S.B. Dorofeev, Evaluation of optimization schemes and determination of solid fuel properties for CFD

fire models using bench-scale pyrolysis tests, Proceedings of the Combustion Institute 33 (2011) 2599-2606, http://dx.doi.org/10.1016/j.proci.2010.07.018.

[11] A.C. Fernandez-Pello, On fire ignition, Fire safety science 10 (2011) 25-42, http://dx.doi.org/10.3801/IAFSS.FSS.10-25.

[12] J.G. Quintiere, Ignition of solids, in: Fundamentals of fire phenomena, John Wiley and sons Ltd, 2006, chapter 7, pp. 159-190, ISBN-10 0-470-09113-4.

[13] A. Atreya, Ignition of fires, Philosophical transactions: Mathematical, physical and engineering sciences 356 (1998) 2787-2813, http://www.jstor.org/stable/55049

[14] T. Kashiwagi, Polymer combustion and flammability – Role of the condensed phase, Proceedings of the symposium (international) on combustion 25 (1994) 1423-1437, http://dx.doi.org/10.1016/S0082-0784(06)80786-1

[15] S.D. Snowling and J.R. Kramer, Evaluation modelling uncertainty for model selection, Ecological modelling 138 (2001) 17-30, http://dx.doi.org/10.1016/S0304-3800(00)00390-2

[16] R. Astrup, K.D. Coates and E. Hall, Finding the appropriate level of complexity for simulation model: an example with forest growth model, Forest ecology and management 256 (2008) 1659-1665, http://dx.doi.org/10.1016/j.foreco.2008.07.016

Chapter 1

Numerical investigation of the ignition delay time of a translucent solid at high radiant heat fluxes

Summary

A one-dimensional numerical model describing the physical and chemical phenomena occurring in a translucent solid fuel up to ignition is used to investigate the failure of the classical ignition theory at radiant heat fluxes above 70 kW/m^2. Comparison with a very large dataset of experimental measurements of time to piloted ignition for black PMMA (PolyMethylMethAcrylate) samples shows that model predictions agree well for heat fluxes from 20 to 200 kW/m^2. The only two existing sets of experimental data for ignition at high heat fluxes for black-carbon coated and uncoated samples are used. Predictions of the transient temperature profiles inside the solid at different heat fluxes also agree well with measurements. Among all the

mechanisms investigated, agreement with measurements at heat fluxes above 70 kW/m^2 is only possible when in-depth radiation absorption is included in the model. Observed behaviour at high heat fluxes cannot be otherwise explained by the reaction scheme, ignition criterion, temperature dependency of material properties, surface heat losses or radiation attenuation by pyrolyzates. The model is also used to show that the traditional coating of black carbon added on the sample does not cancel in-depth radiation absorption but its effect is to absorb at the surface around 35 % ± 5% of the incoming radiation. This chapter explains the failure of the classical ignition theory at high heat fluxes and it is the first time that the effect of black-carbon coating is explained and quantified.

Collaboration

This chapter results from a joint work performed with Dr Guillermo Rein from the University of Edinburgh (UK).

Nomenclature

A	Pre-exponential factor [s^{-1}]
c	Specific heat [J/(kg.K)]
E_a	Activation energy [kJ/mol]
h	Convective heat transfer coef. [W/(m^2.K)]
k	Thermal conductivity [W/(m.K)]
L	Sample thickness [m]
$\dot{m}''$	Mass loss rate [g/(m^2.s)]
n	Order of reaction [-]
$\dot{q}''_e$	Heat flux [kW/m^2]
r	Surface reflectivity [-]
R	Ideal gas constant [J/(K.mol)]
t	Time [s]
T	Temperature [K]
w	Mass fraction [-]
y	Depth [m]

Subscripts

∞	Ambient conditions
i	Species
ign	At ignition
s	At the surface

Greek symbols

α	Thermal diffusivity [m^2/s]
γ	Fraction of non-reflected radiation absorbed at the surface [-]
ε	Surface emissivity [-]
ϕ	Gas phase absorptivity [-]
κ	Attenuation coefficient [m^{-1}]
ρ	Density [kg/m^3]
σ	Stefan-Boltzmann coef. [W/(m^2.K^4)]
υ	Yield of reaction [-]

1. Introduction

The key phenomena governing ignition and flame spread (continuous ignition over condensed fuels) are the radiant heat flux from the flame, the solid-phase response (heat and mass transfer and kinetics) and the gas-phase

processes (mixing and combustion). Of these three phenomena, the solid response is examined in this paper for a very wide range of heat fluxes up to 200 kW/m^2. Typical heat fluxes in small-scale experiments reach 10-60 kW/m^2. However, heat fluxes significantly above 60 kW/m^2 are observed close to the pyrolysis front during flame spread bench-scale test [1,2] and in large-scale fires [2-8]. Heat fluxes up to 100 or 200 kW/m^2 have been reported in real enclosure fires [3], forest fire [4], tunnel fires [5], jet fires [6], vapour explosion [6,7], and in industrial standard tests [2,8]. Therefore, the high end of the possible heat flux range (> 100 kW/m^2), which is often not experienced, is also very important for the understanding of fire behaviour.

The delay time to ignition of solid materials is a well studied subject. A theory (called classical ignition theory in this chapter), based on a fixed surface temperature as ignition criterion $T_{s\ ign}$, links linearly the inverse of the square root of the delay time to ignition $1/\sqrt{t_{ign}}$ with the heat flux imposed on the solid sample $\dot{q}''_e$ as shown in Eq. 1.1. The different steps to obtain Eq. 1.1 are shown in detail by Torero [9].

$$\frac{1}{\sqrt{t_{ign}}} = \frac{2}{\sqrt{\pi}\sqrt{k\rho c}} \frac{\dot{q}''_e}{(T_{s\ ign} - T_\infty)} \tag{1.1}$$

One of the best materials to investigate solid ignition is PolyMethylMethAcrylate (PMMA) because it is the material for which most experimental data, properties and numerical studies are available in the literature. Figure 1.1 shows the delay time to piloted ignition of black PMMA samples for a wide range of experimental conditions found in the literature [10-24]. For any set of data, the results below a heat flux of 70 kW/m^2 show that the inverse of the square root of the time to ignition varies linearly with the applied heat flux as predicted by the classical theory in Eq. 1.1. However, each set of data has a different slope. These differences in slope and time to ignition measurements stem from the different experimental conditions and from PMMA properties variability (i.e. ambient and flow conditions, pilot location, heat source type, sample orientation, black PMMA formulation, samples insulation, black-carbon coating, ignition detection method, etc.). Most of these parameters

are not taken into account by the classical theory. It could be concluded that the experimental data cloud in Fig. 1.1 represents the overall experimental uncertainty for the delay time to ignition of black PMMA.

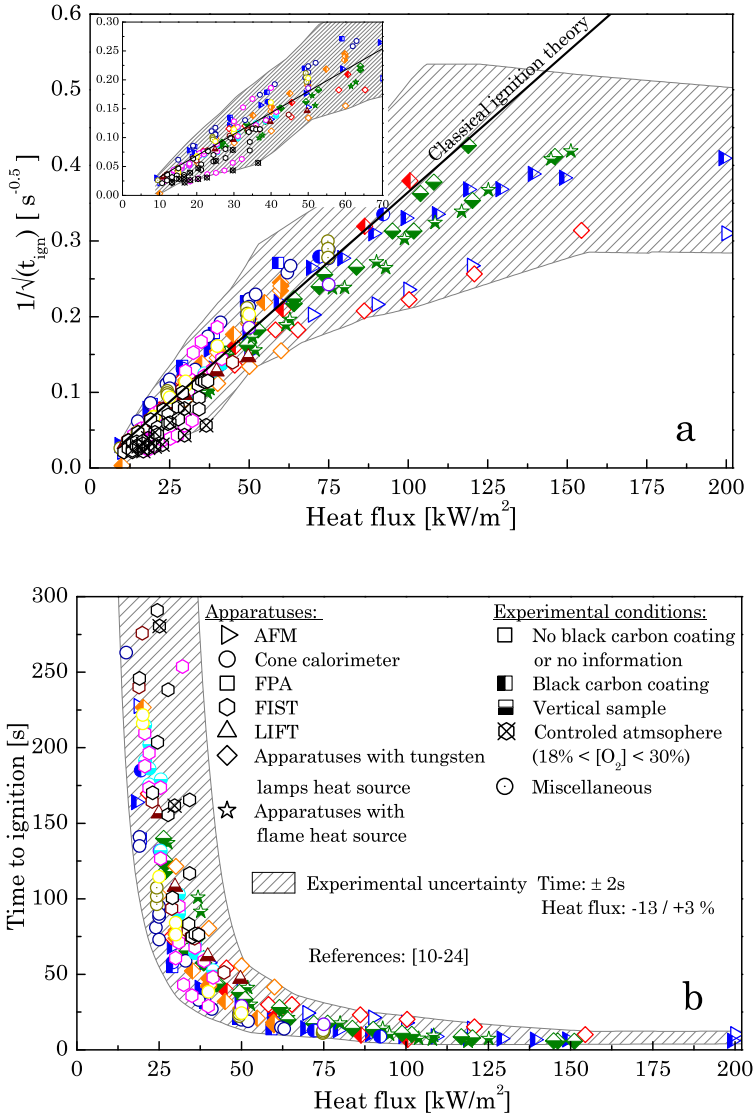

Figure 1.1: Times to piloted ignition of black PMMA samples for a wide range of experimental conditions in the literature. Continuous line is the classical theory which best fits for whole dataset between 20 and 70 kW/m². (a) inverse of the square root of the delay time to ignition (inset: zoom for heat fluxes up to 60 kW/m²) and (b) delay time to ignition.

The classical theory predicts well the experimental results for a wide range of materials, for heat fluxes up to 70 kW/m² [9,13,25]. However, as Beaulieu and

Dembsey [10,11] and Delichatsios and Saito [23,24] have measured experimentally, an unexpected curve divergence appears at high heat fluxes for $1/\sqrt{t_{ign}}$ in Fig. 1.1a. This curvature means that the measured delay times to ignition are significantly longer than those predicted by the classical theory for heat flux levels above 70 kW/m². This has also been observed for other materials [10,11] such as PolyOxyMethylene, PolyVinylChloride, pine wood, and asphalt shingle. The curvature implies that at least one of the classical theory's assumptions fails at high heat fluxes. This chapter investigates numerically the possible reasons causing it.

2. Behaviour at high heat fluxes

Torero [9] provides a detailed review of the classical ignition theory resulting in Eq. 1.1 which is presented in Fig. 1.1a by a straight line. A fundamental assumption of the theory is that the gas-phase chemical induction and mixing times are negligible in comparison to the solid heating time. This is known to be a good assumption at low heat fluxes [26]. In addition to this, the following six assumptions are made in the development of the theory:

1. The solid is inert.

2. The total incident heat flux is absorbed at the surface (the solid is opaque to radiation and the absorption coefficient is equal to 1).

3. The ignition criterion is specified as a fixed ignition temperature (considered traditionally as a material property).

4. All material properties are invariants (e.g. thermal diffusivity α is constant).

5. Heat losses at the exposed surface are negligible for high external heat fluxes.

6. The solid is semi-infinite (it behaves as thermally thick).

One or more of these assumptions break down at high heat fluxes as shown in Fig. 1.1. According to Beaulieu and Dembsey [10,11] the divergence is a true material response and they suggest that the assumption of an inert solid (#1) does not apply. During their experiments, they observed in-depth radiation absorption effects on their temperature measurements [11]. This observation would suggest that all the heat flux is not absorbed at the surface (assumption #2). However, Beaulieu and Dembsey do not consider the in-depth radiation absorption mechanism as the source of divergence at high heat fluxes.

Lautenberger and Fernandez-Pello [27] investigated the failure of the classical theory and developed an approximate analytical solution for the mass loss rate of a thermally thick degrading solid. They determined with this relation a link between the critical mass flux of pyrolyzate leaving the sample at ignition (chosen as the ignition criterion) and the non-constant surface temperature. Thus, from the six assumptions of the classical theory, assumptions #1 and #3 were not adopted whereas the others were used. However, the model failed to capture the behaviour at high heat fluxes as measured in the experiments of Beaulieu and Dembsey [10,11].

Jiang et al. [12] developed an analytical solution for the temperature profile inside a translucent sample by including the in-depth radiation absorption mechanism. They used the variable ignition temperature criterion calculated by Lautenberger and Fernandez-Pello [27], which is based on the temperature at the surface when the critical mass flux of pyrolyzate is reached. Jiang et al. [12] did not adopt assumptions #2, #3 and #5 of the classical theory, whereas the others were used. The model predicts well the ignition delay times at high heat fluxes on uncoated (i.e. without blackcarbon coating) samples measured by Delichatsios and Saito [23,24]. The authors concluded that the mechanism causing the failure of classical ignition theory is the in-depth radiation absorption (assumption #2).

The problem of ignition at high external heat fluxes is revisited in this work with a numerical model that includes all the important mechanisms for the response of a translucent solid at high external radiant fluxes. For the first time, several assumptions of the classical theory are investigated independently and combined. The numerical predictions are compared to the only two existing sets

of experimental measurements at high heat fluxes available in the literature [10,11,23,24]. Also, this study investigates for the first time both coated and uncoated samples.

3. Pyrolysis model

The main objective of the model is to simulate piloted solid ignition, especially at high heat fluxes. The system of equations used here includes all important mechanisms but is deliberately as simple as possible. Its development follows the rule that simplifications are required where the expected precision does not warrant the inclusion of higher levels of complexity.

A semi-infinite slab with coordinate y for the depth is considered with external radiant heat applied to the top surface. The one-dimensional pyrolysis model presented in [28] is used. It solves the heat transfer equation (Eq. 1.2) with an energy source term to account for in-depth radiation absorption in translucent media:

$$\rho c \frac{\partial T(y,t)}{\partial t} = k \frac{\partial^2 T(y,t)}{\partial y^2} + (1-\phi)(1-r)(1-\gamma)\dot{q}''_e \kappa e^{(-\kappa y)} \qquad (1.2)$$

As spectral radiation is emitted by a heat source, a fraction ϕ is absorbed in the gas phase by ambient gases and pyrolyzates. A fraction r of the radiation intensity that arrives to the surface of the solid is reflected away. Only a fraction $(1-\phi)(1-r)\gamma$ is absorbed at the surface and contributes to energy conservation in the sample through the boundary condition in Eq. 1.3. The remaining fraction $(1-\phi)(1-r)(1-\gamma)$ penetrates into the solid and is subjected to in-depth attenuation due to scattering and absorption in the translucent media (quantified by the attenuation coefficient κ also called in-depth radiation absorption coefficient in Eq. 1.2). For materials in general, radiation absorption is wavelength and temperature dependent [14,29,30] but an effective value (taken broadband over the range of temperature encountered) is considered here. The validity of this assumption is partly supported by the experimental study of Hallman [14] showing that the surface reflectivity r for black PMMA does not vary significantly with wavelength.

Material properties k (thermal conductivity), ρ (density) and c (specific heat) are function of the sample temperature. As a first step, it is considered that their variations with temperature are negligible and constant values are used. The effect of this assumption is investigated subsequently.

The slab is initially at ambient temperature T_∞ = 293 K (Eq. 1.5). The solid loses heat from the top surface by convection and re-radiation to the background environment (Eq. 1.3). The solid is approximated as semi-infinite by setting the back boundary as adiabatic (Eq. 1.4) at a large distance L from the exposed surface.

$$\forall t;\ -k\frac{\partial T}{\partial y}\Big|_{y=0} = \gamma(1-\phi)(1-r)\varepsilon\dot{q}''_e - h(T_s - T_\infty) - \varepsilon\sigma(T_s^4 - T_\infty^4) \quad (1.3)$$

$$\forall t;\ -k\frac{\partial T}{\partial y}\Big|_{y=L} = 0 \quad (1.4)$$

$$\forall y;\ T(y, t=0) = T_\infty \quad (1.5)$$

As the solid heats up, it undergoes pyrolysis. In general, the decomposition mechanism is made of several consecutive and parallel steps but only a few are important and control the process of ignition [18]. A global one-step reaction is considered here:

$$\text{PMMA} \rightarrow \upsilon_{MMA}\text{MMA} + (1-\upsilon_{MMA})\text{residue} \quad (1.6)$$

More complex kinetics schemes are explored later. This pyrolysis reaction produces the gas MethylMethAcrylate (MMA) [29]. The reaction rate $\dot{w}_{GAS}$, which is temperature dependent, is quantified using an Arrhenius law. Pyrolysis takes place not only at the surface but also in-depth, so the total mass loss is obtained by integrating the reaction rate over the entire depth (Eq. 1.7).

$$\dot{m}'' = \rho\int_{y=0}^{y=L}\dot{w}_{GAS}dy = \rho\int_{y=0}^{y=L} A\exp\left(\frac{-E}{RT(y,t)}\right)w_{PMMA}^{n}\,dy \quad (1.7)$$

When the pyrolysis gases leave the top surface, they mix with the surrounding air. As soon as a flammable concentration of pyrolyzate is reached

at the pilot location, flaming ignition takes place. The time for this concentration to be reached could be linked to a critical mass flux leaving the surface [21,31]. This is the ignition criterion assumed in this work.

The heat transfer equation (Eq. 1.2) neglects the endothermic and exothermic contributions respectively from the pyrolysis and oxidation reactions. The heat of pyrolysis for black PMMA is estimated to be within the range 0.84-1.2 kJ/g from the Refs. [10,11,37] (0.84 kJ/g is calculated in [37], and 1.2 kJ/g is estimated by deducting the sensible heat from the measured heat of gasification in Refs. [10,11].), and the pyrolysis mass flux at ignition is 2.42 g/(s m^2) (average value in the range from 1.82 to 4.5 g/(s m^2) found in the literature [31-36]). Thus, the endothermic contribution of pyrolysis is around 5-7 % of the power received from an external heat flux of 40 kW/m^2 or 1-2 % for a flux of 200 kW/m^2. Therefore, neglecting the pyrolysis endothermic contribution seems to appear as a valid assumption for medium and high external heat fluxes since the induced error is small. The advantage is that the solution to the heat transfer problem is decoupled from the pyrolysis process.

The model would not be valid for material forming a significant char layer before ignition since this modifies the heat arriving to the unreacted mass, but it is valid for PMMA which is a melting polymer.

4. Numerical investigation

The effects of each mechanism and assumption on the predictions are explored here. The base case considers all important mechanisms except in-depth absorption. Table 1.1 presents the set of parameters for the base case, all obtained from the literature for PMMA.

4.1. Kinetics, critical mass flux and heat losses

Assumptions #1, #3 and #5 of the classical theory for ignition were tested by considering a reacting solid without in-depth radiation absorption ($\gamma = 1$), implementing the critical mass flux as ignition criterion and adding the convection and radiation heat losses at the exposed surface. Simulations were

run covering a wide range of values (see Table 1.1) for the kinetics parameters, the critical mass flux and the convective heat transfer coefficient.

Table 1.1: Parameter values used in the base case and range of values found in the literature, mostly, for black PMMA (References not exhaustive).

Material parameters				
Parameter		Value	Range	References
Density	ρ [kg/m^3]	1187.8	[1180 ; 1191]	[10-12,15,17,37,38]
Thermal conductivity	k [W/(m.K)]	0.21	[0.19 ; 0.27]	[10-12,15,17,37,38]
Specific heat	c [J/(kg.K)]	1664.66	[1420 ; 2090]	[10-12,15,17,37,38]
Attenuation coefficient	κ [m^{-1}]	500	[333 ; 2000]	[11,12,39,40]
Reflectivity	r [-]	0	[0 ; 0.055]	[12,14]
Surface emissivity	ε [-]	0.945	[0.9945 ; 1]	[12,14]
Non-reflected radiation absorbed at the surface	γ [-]	1	[0 ; 1]	-

Kinetics parameters				
Parameter		Value	Range	References
Pre-exponential factor	A [1/s]	5 10^8	[2$\cdot 10^4$; 9.$\cdot 10^{13}$]	[35,36,41-44]
Activation energy	E_a [kJ/mol]	125	[74 ; 196]	[35,36,41-44]
Reaction order	n [-]	1	-	[45]
Yield of MMA	υ_{MMA} [-]	1	Non charring material	[11,17]

Other parameters				
Parameter		Value	Range	References
Critical mass flux at ignition	$\dot{m}''_{ign}$ [g/(m^2.s)]	2.42	[1.82 ; 3.75]	[31-36]
Convective heat transfer coefficient	h [W/(m^2.K)]	10	[5 ; 25]	[12,46,47]
Gas-phase absorbed fraction	Φ [-]	0	[0 ; 0.1]	[48]

The results show that the term $1/\sqrt{t_{ign}}$ varies linearly with the heat flux and no curvature is obtained at high heat fluxes. Thus, assumptions #3 and #5 are

not responsible for the divergence of the classical theory at high heat fluxes. Concerning assumption #1, it cannot be concluded entirely since only 1-step pyrolysis reaction with constant kinetics parameters was explored at this stage.

4.2. Reaction scheme

Assumption #1 is further investigated by expanding the 1-step reaction scheme in Eq. 1.6 to a two-step reaction scheme. A two-step scheme allows considering the possibility of an apparent 1-step scheme with non-constant kinetics parameters as well.

Both consecutive reactions (Eq. 1.8) and competitive reactions (Eq. 1.9) are considered. The additional kinetics parameters are taken from Lautenberger and Fernandez-Pello [39].

Consecutive reactions:

$$\begin{aligned} &\text{PMMA} \rightarrow \beta\,\text{PMMA} \\ &\beta\,\text{PMMA} \rightarrow \upsilon_{\text{MMA}}\text{MMA} + (1-\upsilon_{\text{MMA}})\text{residue} \end{aligned} \tag{1.8}$$

Competitive reactions:

$$\begin{aligned} &\text{PMMA} \rightarrow \beta\,\text{PMMA} \\ &\text{PMMA} \rightarrow \upsilon_{\text{MMA}}\text{MMA} + (1-\upsilon_{\text{MMA}})\text{residue} \end{aligned} \tag{1.9}$$

The specie β PMMA is a solid-phase species. The mass loss rate is therefore the same as for the 1-step scheme expressed in Eq. 1.7.

The results for each of the three schemes are presented in Fig. 1.2. The competitive scheme predicts shorter ignition delay times than the consecutive scheme. For all schemes, the prediction of $1/\sqrt{t_{ign}}$ varying linearly with the heat flux and no curvature is obtained at high heat fluxes. This further confirms that multistep kinetics reactions (and assumption #1) are not responsible for the failure of classical theory.

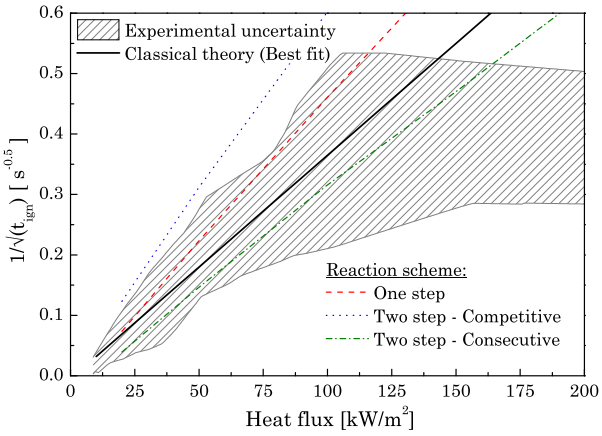

Figure 1.2: Effect of the different reaction schemes on the predictions of the inverse square root of the time to ignition.

4.3. Temperature dependent material properties

The material properties density ρ, thermal conductivity k and specific heat c are known to be temperature dependent. These dependencies are provided as polynomial functions for black PMMA in Refs. [17,38]. One set is shown in Table 1.2. Figure 1.3 shows the effect of the temperature dependency on the predictions. The dependency leads to longer delay times to ignition but $1/\sqrt{t_{ign}}$ still varies linearly with the heat flux. It is concluded that assumption #4 is not responsible for the failure of classical theory.

Table 1.2: Example of the material property temperature dependency equations.

Property	Equations	
Density ρ [kg/m^3]	$\rho(T\,[K]) = 1404.5 - 0.7316\,T$	(1.10)
Thermal conductivity k [W/(m.K)]	$k(T\,[K] < 378) = 0.1959 + 4.954 \cdot 10^{-5}\,(T - 273.15)$ $k(T\,[K] > 378) = 0.2249 - 2.318 \cdot 10^{-4}\,(T - 273.15)$	(1.11)
Specific heat c [J/(kg.K)]	$c(T\,[K] < 378) = 173 + 204.1 \cdot 10^{3}\,T^{-2} + 4.341\,T$ $c(T\,[K] > 378) = 1212 + 2.547\,T$	(1.12)

Reference [38]

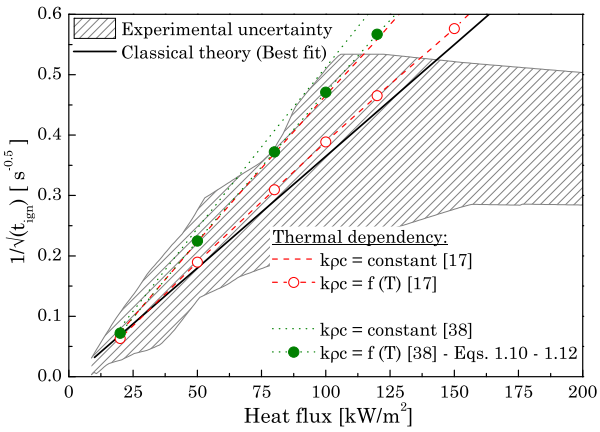

Figure 1.3: Effect of the material property temperature dependency on the predictions of the inverse square root of the time to ignition.

4.4. Incident radiation attenuation

Prior to ignition, the pyrolysis gases leaving the solid absorb a fraction of the external radiation (represented by the factor ϕ in Eq. 1.2) and therefore partially shield the exposed solid surface. It has been suggested that the assumption (#2) (the total radiation heat flux is absorbed at the surface) could explain the behaviour at high heat fluxes. Recent experimental measurements by Zhou et al. [48] on PMMA samples at heat fluxes up to 60 kW/m² show that this absorption at the time of ignition reaches a maximum of 10 %. Figure 1.4 shows the two limiting curves of $1/\sqrt{t_{ign}}$ against the applied heat flux when ϕ is equal to 0 and 0.1.

Even if the attenuations were to start at 0 and increase up to 0.1, the curvature associated is not significant and does not explain the experimental observations at high heat fluxes. Thus, the radiation attenuation by the pyrolysis gases is not responsible for the failure of classical theory at high heat fluxes.

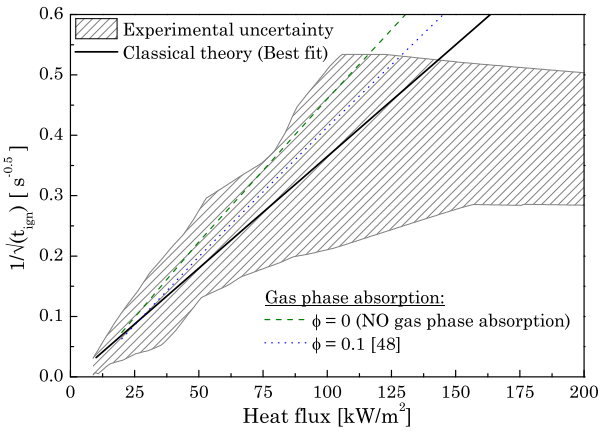

Figure 1.4: Effect of the incident radiation attenuation by the pyrolysis gases on the predictions of the inverse square root of the time to ignition.

4.5. In-depth absorption

The effect of in-depth radiation absorption, also related to assumption #2, is investigated by setting $\gamma = 0$ (no surface absorption) in Eqs. 1.2 and 1.3, and by varying the attenuation coefficient κ over a wide range of values found in the literature (see Table 1.1). Results are presented in Fig. 1.5. The in-depth absorption brings a significant curvature to $1/\sqrt{t_{ign}}$ as the heat flux is increased. For different values of κ, different radii of curvature are found. Therefore, it is concluded that assumption #2 and the translucency of black PMMA is responsible for the failure of the classical theory at high heat fluxes. This finding agrees with the conclusions in previous works [12,15,23,49] which showed that in-depth radiation is important at medium and high heat flux levels.

As shown in Table 1.3, the model predicts within 10 % (in average) both experimental measurements for ignition delay times by Beaulieu and Dembsey [10,11] and by Delichatsios and Saito [23,24] when κ equals 500 m^{-1} and 1400 m^{-1}, respectively for uncoated and coated samples (other parameter values shown in Table 1.1). However, it should be emphasized that these comparisons are only discrete and do not quantify the curvature. Moreover, the range of κ that would explain the experimental variability in $1/\sqrt{t_{ign}}$ measurements for uncoated samples between 40 and 200 kW/m^2 varies between 300 and 900 m^{-1} with best predictions between 500 to 600 m^{-1} (work using Monte-Carlo

methodology with parameter variability presented in Table 1.1 – results not presented here).

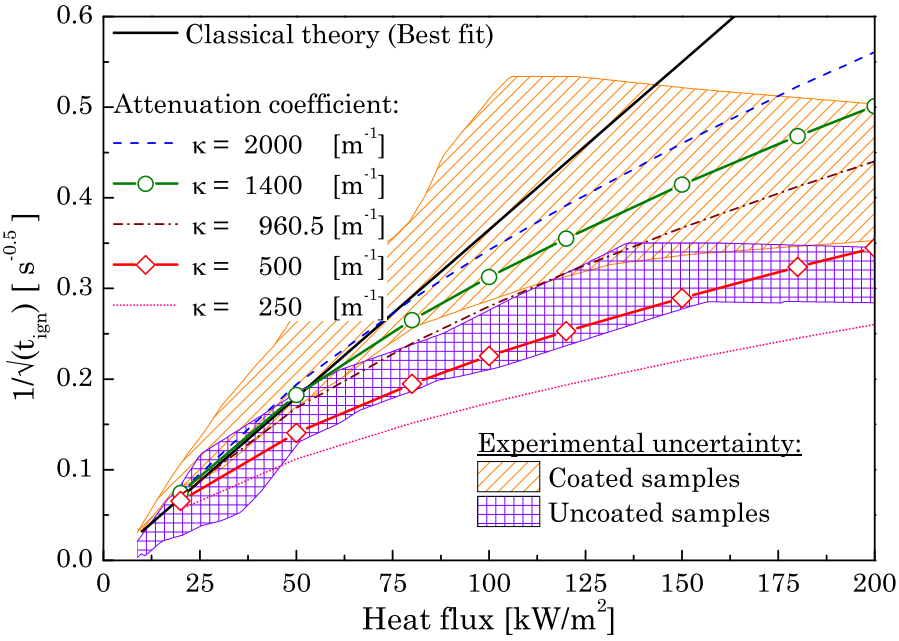

Figure 1.5: Effect of the attenuation coefficient on the predictions of the inverse square root of the time to ignition.

Table 1.3: Comparison between model predictions and experimental measurements of the inverse square root of the delay time to ignition.

Experimental results for $20 < \dot{q}''_e < 200$ kW/m² K = 500 m⁻¹ uncoated | κ = 1400 m⁻¹ coated	Maximum error (%)	Averaged error (%)
Uncoated samples Beaulieu and Dembsey [11]	11 %	7 %
Coated samples Beaulieu and Dembsey [10,11]	22 %	7 %
Uncoated samples Saito et al. [23,24]	21 %	8 %
Coated samples Saito et al. [23,24]	17 %	10 %

Error is defined as 100 × | Experimental - Simulated | / Experimental

Jiang et al. [12] measured the attenuation coefficient for uncoated black PMMA samples in the range of heat fluxes from 3 to 30 kW/m² and found a value of 960.5 m⁻¹ ± 14.3 %. They used this value in an analytical model and their predictions agree with the experimental measurements within 11 %

average error (maximum error 29 %). The value of 500 m^{-1} estimated here for a heat flux range from 20 to 200 kW/m^2 is 50 % smaller.

Moreover, the predictions from the numerical model presented in this chapter (Eqs. 1.2-1.7) with an attenuation coefficient of 960.5 m^{-1} are not the same as those from the analytical model of Jiang et al. [12] with the same coefficient. The numerical predictions for a coefficient κ of 960.5 m^{-1} fall inside the global experimental cloud area but not inside the uncoated sample experimental cloud area as it should be (see Fig. 1.5). This discrepancy is mainly due to the use of different material properties and a different ignition criterion. Although the analytical model of Jiang et al. [12] includes in-depth radiation absorption, they used a variable ignition temperature criterion calculated by the model of Lautenberger and Fernandez-Pello [27] which does not include in-depth radiation absorption. Comparing with the surface temperature obtained with the numerical model presented in this chapter and the material properties in Table 1.1 with an attenuation coefficient of 500 m^{-1}, the ignition criterion from Lautenberger and Fernandez-Pello [27] overpredicts the surface temperature at ignition by 11 % in the heat flux range from 20 to 200 kW/m^2. This over-prediction results in an over-prediction of the time to ignition by 38 %. Thus the different ignition criterion used by Jiang et al. [12] explains most of the discrepancy with our results.

Model predictions of the in-depth temperature profile for different heat fluxes are shown in Fig. 1.6. Profiles are shown at the time to ignition, except for the 15 kW/m^2 case that did not ignite (it is below the critical heat flux for ignition [9]). The comparison to the only experimental measurements of temperature profiles available (Beaulieu and Dembsey [10,11] for coated samples) shows a good agreement with the result obtained using the parameters in Table 1.1 and an effective attenuation coefficient of 1400 m^{-1}. These temperature profiles span over a wide range of heat fluxes and confirm that all the important mechanisms in the solid response are included and solved correctly in the model.

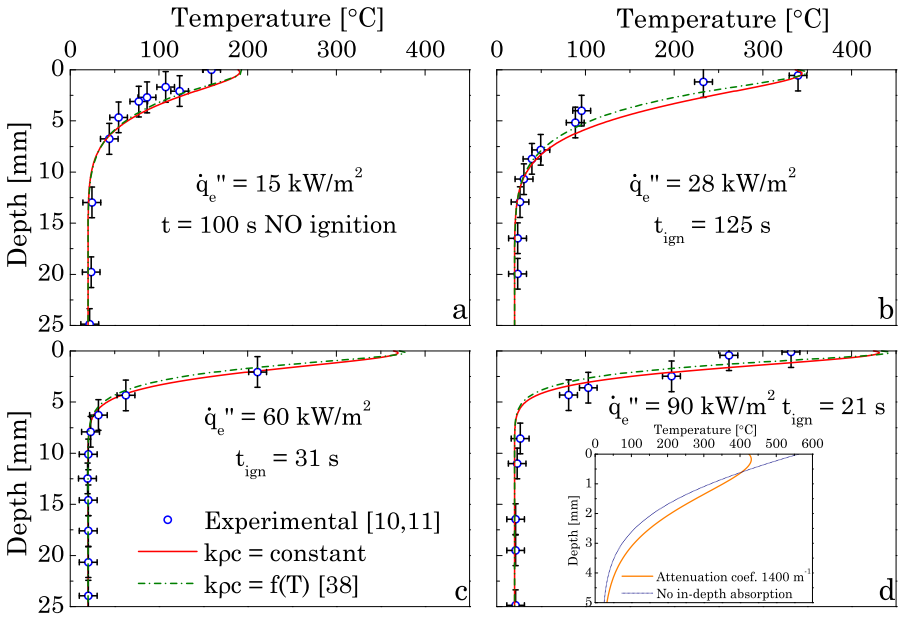

Figure 1.6: Comparison of experimental temperature profiles (at ignition except for (a) 15 kW/m² - coated samples) with model predictions (attenuation coefficient of 1400 m^{-1}) with and without temperature dependency. Experimental errors: ±1.5 mm for depth and ±10 °C for temperature. Inset (d): comparison of the temperature profile with and without the in-depth radiation absorption phenomenon.

Figure 1.6 serves to illustrate the effect of the in-depth radiation absorption, manifested physically by the presence of the peak temperature inside the solid (at about 0.2 mm in inset Fig. 1.6d and 0.3 mm with $\kappa = 500$ m^{-1} when ignition occurs) and not at the surface. The peak location is related to the depth penetration by radiation which is proportional to the inverse of the attenuation coefficient. The total thermal depth by combined conduction and radiation is seen in Fig. 1.6 to decrease from 12.5 (at 15 kW/m²) to 7.5 mm (at 90 kW/m²). The thermal depth by radiation is independent of the heat flux level and is established instantaneously, whereas the thermal depth by conduction grows with time (proportional to $\sqrt{\alpha t}$ [25]). Thus, at high heat fluxes, since the delay time to ignition is short, the depth penetration by conduction is much shorter than the depth penetration by radiation. The opposite is true at low heat fluxes. The peak produced by radiation absorption is more pronounced as the heat flux level increases.

Figure 1.6 also shows the resulting temperature profiles when temperature dependency of the material properties is considered (see Table 1.2). It is seen that the results are not significantly different from those using constant properties. This is against the suggestion in Ref. [12] that the increasing thermal conductivity and the specific heat at higher temperatures would bring further curvature to $1/\sqrt{t_{ign}}$ at high heat fluxes.

The model is used in Fig. 1.7 to investigate the surface temperature at the time to ignition. Coated samples ignite at surface temperatures 7 % higher (on average) than uncoated samples. Moreover, the surface temperature is not strictly constant as the heat flux level varies from 40 to 200 kW/m² but monotonically increases from 284 to 305 °C for uncoated samples (from 304 to 325 °C for coated samples) as it was already reported experimentally by Cordoba et al. [21]. This confirms that the surface temperature at ignition is not a material property but it varies slightly with imposed heat flux and thus is approximately invariant.

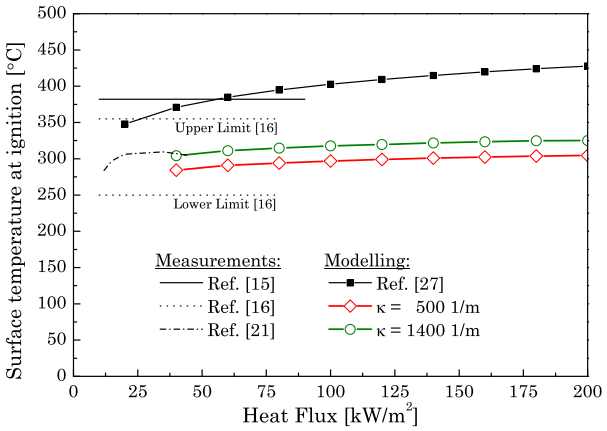

Figure 1.7: Surface temperature at the time to ignition over a wide range of heat fluxes for coated and uncoated samples.

5. Effect of black-carbon coating

In some standard flammability tests and experimental research [10,11,15,40,50], the exposed surface of the sample is coated with a thin layer of

black carbon in order to absorb radiation at the surface and attempt to eliminate the in-depth radiation absorption phenomenon. The effect of the black carbon on PMMA for ignition tests has not been often investigated and reported. Beaulieu [11] carried out ignition experiments on coated and uncoated samples of black PMMA in the same apparatus and controlled environmental conditions. The measured time to ignition was significantly different for coated and uncoated samples, and the difference increased with the heat flux (Fig. 1.1: AFM apparatus). Similar experimental observations were done independently by Delichatsios and Saito [23,24] (Fig. 1.1: Tungsten lamp heat source) and Tewarson and Ogden [15].

The previous section shows a three-fold increase of the attenuation coefficient when black-carbon coating is present (see Fig. 1.5). However, this coefficient is considered as a material property and should not change by a surface treatment. The effective change is caused by a surface phenomenon taken into account by the model in Eqs. 1.2 and 1.3 via the surface absorptivity γ. In principle this coefficient can vary between 1 (all irradiation is absorbed at the coating) to 0 (all radiation is absorbed in-depth). The effect of changing γ while keeping κ fixed at 500 m^{-1} is shown in Fig. 1.8 for a range of values of γ from 0 to 0.5.

Predictions with a surface absorptivity γ of $0.35 \pm 5\%$ are as close to the experimental results for coated samples as the predictions with an effective attenuation coefficient equals to 1400 m^{-1} and no surface absorption. Thus, the significant surface absorption explains the effect of the carbon coating. The remaining 0.65 fraction, not absorbed at the surface, is transmitted through the coating. Even when the attenuation coefficient of black carbon is high (>10^4 m^{-1} [49]), it is reasonable that the very thin layer (<0.1 mm) is optically thin and therefore transmits a significant amount of the incident radiation.

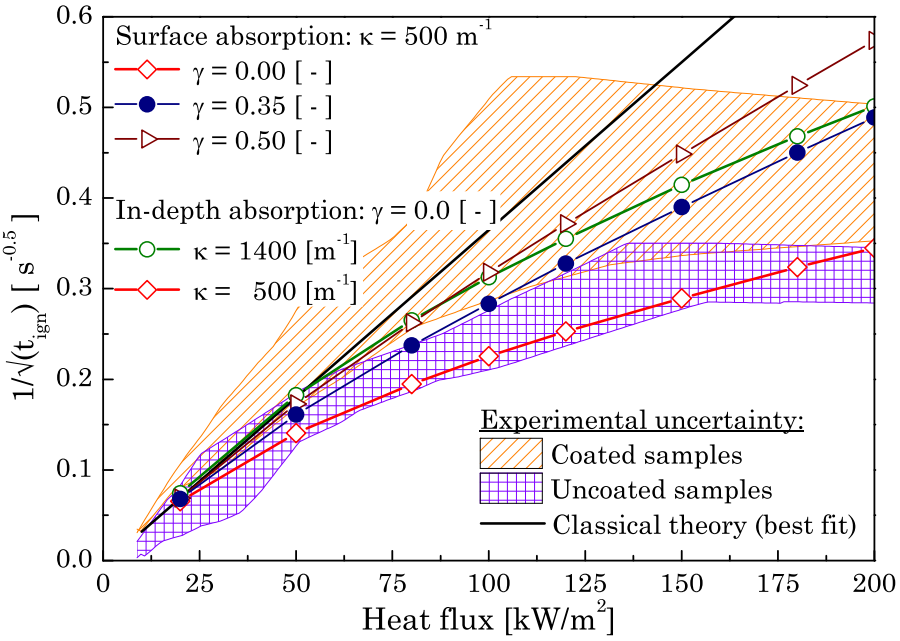

Figure 1.8: Predictions of the ignition delay times by combining surface absorption and in-depth absorption.

6. Conclusion

A one-dimensional pyrolysis model decoupling the heat transfer and the chemical kinetics is used for solving the transient radiant heating of a translucent solid. The model is especially apt for medium and high heat flux range which is the most important in large-scale fire behaviour.

The model predictions of transient temperature profiles and delay time to ignition over a wide range of heat fluxes agree well with measurements (less than 10 % in average error with a maximum at 22 %). The model is able to explain the failure of the classical ignition theory at high heat fluxes for black PMMA only when in-depth radiation absorption is included. This agrees with the conclusion of Jiang et al. [12]. The observed behaviour at high heat fluxes cannot be explained by the reaction scheme, the ignition criterion, the temperature dependency of the material properties, the surface heat losses or the radiation attenuation by pyrolyzate.

Using the model, it is concluded that the traditional coating of black carbon added on the sample does not cancel in-depth radiation absorption but its effect is to absorb at the surface around 35 % ± 5% of the incoming radiation. The

study uses the only two available sets of experimental data at high heat fluxes for both coated and uncoated black PMMA samples to reach this conclusion. This is the first time that the effect of black-carbon coating is quantified and captured in an ignition model.

The model also shows that the inclusion of the temperature dependency of the material properties does not improve the results significantly. Investigation of the surface temperature at ignition shows that it grows with the heat fluxes and thus is not a simple material property. However, it varies only slightly with imposed heat flux and thus is approximately invariant.

This chapter cannot categorically conclude on the effect of the phenomena not included in the model. These phenomena are considered much less important during the ignition of black PMMA but should be further studied to improve the understanding of solid ignition in general. These include the wavelength dependency of the attenuation coefficient, in-depth re-radiation, formation and transport of bubbles and surface oxidation reactions. Also the fundamental underlying assumption that transport and combustion times in the gas phase are negligible compared to those in the solid phase needs to be further investigated at high heat flux levels. The exact roles of these mechanisms remain a challenge to fire research and should be solved during the coming decades.

References

[1] A. Ito and T. Kashiwagi, Characterization of flame spread over PMMA using holographic interferometry sample orientation effects, Combustion and flame 71 (1988) 189-204, http://dx.doi.org/10.1016/0010-2180(88)90007-7.

[2] B.Y. Lattimer, Heat fluxes from fires to surfaces, in: The SFPE Handbook of Fire Protection Engineering, 4th edition, P.J. DiNenno et al. (Eds.), National Fire Protection Association, 2008, chapter 2.142, pp. 2.303-2.336, ISBN-10:0877658218.

[3] G. Rein, J.L. Torero, W. Jahn, J. Stern-Gottfried, N.L. Ryder, S. Desanghere, M.Lázaro, F. Mowrer, A. Coles, D. Joyeux, D. Alvear, J.A. Capote, A. Jowsey, C. Abecassis-Empis and P. Reszka, Round-robin study of a priori modelling predictions of the Dalmarnock Fire Test One, Fire safety journal 44 (2009) 590-602, http://dx.doi.org/10.1016/j.firesaf.2008.12.008.

[4] X. Silvani and F. Morandini, Fire spread experiments in the field: Temperature and heat fluxes measurements Fire safety journal 44 (2009) 279-285, http://dx.doi.org/10.1016/j.firesaf.2008.06.004.

[5] A. Lonnermark and H. Ingason, Gas temperatures in heavy goods vehicle fires in tunnels, Fire safety journal 40 (2005) 506-527, http://dx.doi.org/10.1016/j.firesaf.2005.05.003.

[6] J. Casal, Fire accidents, in: Evaluation of the Effects and Consequences of Major Accidents in Industrial Plants, Industrial Safety Series, vol. 8, Elsevier, 2008, ISBN: 2008 978-0-444-53081-3.

[7] M. Gómez-Mares, M. Muñoz and J. Casal, Radiant heat from propane jet fires, Experimental thermal and fluid science 34 (2010) 323-329, http://dx.doi.org/10.1016/j.expthermflusci.2009.10.024.

[8] Underwriters Laboratories Inc., Rapid Rise Fire Tests of Protection Materials for Structural Steel, Underwriters Laboratories Certification 1709, 2005, ISBN: 0-7629-1074-7.

[9] J.L. Torero, Flaming ignition of solid fuels, in: The SFPE handbook of fire protection engineering 4th edition, P.J. DiNenno et al. (Eds.), National Fire Protection Association, 2008, chapter 2.11, pp. 2.260-2.278, ISBN-10: 0877658218.

[10] P.A. Beaulieu and N.A. Dembsey, Flammability characteristics at applied heat flux levels up to 200 kW/m^2, Fire and materials, 32 (2007) 61-86, http://dx.doi.org/10.1002/fam.948.

[11] P.A. Beaulieu, Flammability Characteristics at Heat Flux Levels up to 200 kW/m^2 and the Effect of Oxygen on Flame Heat Flux, PhD Dissertation, Worcester Polytechnic Institute, 2005, <http://www.wpi.edu/Pubs/ETD/Available/etd-121905-082146/unrestricted/beaulieu.pdf>.

[12] F. Jiang, J.L. De Ris and M.M. Khan, Absorption of thermal energy in PMMA by in-depth radiation, Fire safety journal 44 (2009) 106-112, http://dx.doi.org/10.1016/j.firesaf.2008.04.004.

[13] E. Mikkola, I.S. Wichman, On the thermal ignition of combustible materials, Fire and materials 14 (1989) 87-96, http://dx.doi.org/10.1002/fam.810140303.

[14] J.R. Hallman, Ignition characteristics of plastics and rubber, PhD Dissertation, The University of Oklahoma, 1971.

[15] A. Tewarson and S.D. Ogden, Fire behaviour of polymethylmethacrylate, Combustion and flame 89 (1992) 237-259, http://dx.doi.org/10.1016/0010-2180(92)90013-F.

[16] D. Hopkins Jr. and J.G. Quiniere, Material fire properties and predictions for thermoplastics, Fire safety journal 26 (1996) 241-268, http://dx.doi.org/10.1016/S0379-7112(96)00033-1.

[17] B.T. Rhodes, Burning rate and flame heat flux for PMMA in the Cone Calorimeter, Master dissertation, The University of Maryland, 1994.

[18] S.M. Dakka, G.S. Jackson and J.L. Torero, Mechanisms controlling the degradation of poly(methyl methacrylate) prior to piloted ignition, Proceedings of the Combustion Institute 29 (2002) 281–287, http://dx.doi.org/10.1016/S1540-7489(02)80038-4.

[19] S.M. Olenick, Validation of the Forced Flow Ignition and Flame Spread Test (FIST), A Reduced Scale Test Apparatus, to Assess Material Flammability for Micro-Gravity Environments, Master dissertation, The University of Maryland, 1999.

[20] R.T. Long Jr., J.L. Torero, J.G. Quintiere and C. Fernandez-Pello, Scale and transport considerations on piloted ignition of PMMA, Fire safety science 6 (2000) 567-578, http://dx.doi.org/10.3801/IAFSS.FSS.6-567.

[21] J.L. Cordova, D.C. Walther, J.L. Torero and C. Fernandez-Pello, Oxidizer flow effects on the flammability of solid combustibles, Combustion science and technology 164 (2001) 253-278, http://dx.doi.org/10.1080/00102200108952172.

[22] T.H. Tsai, M-J. Li, I-Y. Shih, R. Jih and S-C. Wong, Experimental and numerical study of autoignition and pilot ignition of PMMA plates in a cone calorimeter, Combustion and flame 124 (2001) 466-480, http://dx.doi.org/10.1016/S0010-2180(00)00219-4.

[23] M.A. Delichatsios, K. Saito, Upward fire spread: key flammability properties, Similarity solution and flammability indices, FM Global Research, Internal Report, 1991.

[24] K. Saito, M.A. Delichatsios, S. Venkatesh and R.L. Alpert, Measurement and evaluation of parameters affecting the pre-heating and pyrolysis of noncharring materials, Paper Prepared for Presentation at the Fall Technical Meeting, Eastern Section, The Combustion Institute, 1988.

[25] D. Drysdale, Ignition: the initiation of flaming combustion, in: An Introduction to Fire Dynamics, second ed., John Wiley and Sons, 1999, chapter 6 pp. 193-232, ISBN-10:0471972916.

[26] C. Fernandez-Pello, The solid phase, in: Combustion Fundamentals of Fire, G. Cox (Ed.), Academic Press Ltd., 1994, chapter 2, pp. 31-100, ISBN-10:0121942309.

[27] C. Lautenberger and C. Fernandez-Pello, Approximate analytical solutions for the transient mass loss rate and piloted ignition time of a radiatively heated solid in the high heat flux limit, Fire safety science 8 (2005) 445-456, http://dx.doi.org/10.3801/IAFSS.FSS.8-445.

[28] G. Rein, From pyrolysis kinetics to models of condense-phase burning Proceedings of recent advances in flame retardancy of polymeric material 19 (2008), BCC Research, http://www.era.lib.ed.ac.uk/handle/1842/2290.

[29] H.E. Thomson and D.D. Drysdale, Flammability of plastics I: Ignition temperatures, Fire and materials 11 (1987) 163-172, http://dx.doi.org/10.1002/fam.810110402.

[30] H.R. Wesson, J.R. Welker and C.M. Sliepcevich, The piloted ignition of wood by thermal radiation, Combustion and flame 16 (1971) 303-310, http://dx.doi.org/10.1016/S0010-2180(71)80101-3.

[31] D.D. Drysdale and H.E. Thomson, Flammability of plastics II: Critical mass flux at the firepoint, Fire safety journal 14 (1989) 179–188, http://dx.doi.org/10.1016/0379-7112(89)90071-4.

[32] D. Rich, C. Lautenberger, J.L. Torero, J.G. Quintiere and C. Fernandez-Pello, Mass flux of combustible solids at piloted ignition, Proceedings of the Combustion Institute 31 (2007) 2653-2660, http://dx.doi.org/10.1016/j.proci.2006.08.055.

[33] J. Panagiotou and J.G. Quintiere, Generalizing flammability of material, Proceedings of the 10th international Interflam conference (2004) 895-905, The University of Edinburgh, UK.

[34] D.J. Rasbash, D.D. Drysdale and D. Deepak, Critical heat and mass transfer at pilot ignition and extinction of a material, Fire safety journal 10 (1986) 1-10, http://dx.doi.org/10.1016/0379-7112(86)90026-3.

[35] R.E. Lyon and J.G. Quintiere, Criteria for piloted ignition of combustible solids, Combustion and flame 151 (2007) 551-559, http://dx.doi.org/10.1016/j.combustflame.2007.07.020.

[36] R.S. Magee, R.D. Reitz, Extinguishment of radiation augmented plastic fires by water sprays, Factory Mutual Research Technical Report No. 22357-1 (1974).

[37] J.E.J. Stagg, The heat of gasification of polymers, Fire safety journal 39 (2004) 771-820, http://dx.doi.org/10.1016/j.firesaf.2004.07.001.

[38] T. Steinhaus, Evaluation of the Thermophysical Properties of Poly(Methyl Methacrylate): A Reference Material for the Development of a Flammability Test for Micro-Gravity Environments, Master dissertation, The University of Maryland, 1999. <http://www.era.lib.ed.ac.uk/handle/1842/2831>.

[39] C. Lautenberger and C. Fernandez-Pello, Generalized pyrolysis model for combustible solids, Fire safety journal 44 (2009) 819-839, http://dx.doi.org/10.1016/j.firesaf.2009.03.011.

[40] M.A. Delichatsios, Th. Panagiotou, and F. Kiley, The use of time to ignition data for characterizing the thermal inertia and the minimum (critical) heat flux for ignition or pyrolysis, Combustion and flame 84 (1991) 323-332, http://dx.doi.org/10.1016/0010-2180(91)90009-Z.

[41] R.E. Lyon, N. Safranova, S.I. Stoliarov and R.N. Walters, The role of thermal decomposition kinetics in polymer flammability, Proceedings of recent advances in flame retardancy of polymeric material 20 (2009), BCC Research.

[42] S.M. Dakka, Kinetic pyrolysis of poly(methyl methacrylate) and its effects on the ignition delay time, PhD Dissertation, The University of Maryland, 2002.

[43] C. Di Blasi, S. Crescitelli, G. Russo and G. Cinque, Numerical model of ignition processes of polymeric materials including gas-phase absorption of radiation, Combustion and flame 83 (1991) 333-344, http://dx.doi.org/10.1016/0010-2180(91)90080-U.

[44] C. Lautenberger, A Generalized Pyrolysis Model for Combustible Solids, PhD dissertation, The University of California, Berkeley, 2007, <http://escholarship.org/uc/item/7wz5m7dg>.

[45] J.E.J. Staggs, Modelling thermal degradation of polymers using single-step first-order kinetics, Fire safety journal 32 (1999) 17-34, http://dx.doi.org/10.1016/S0379-7112(98)00026-5.

[46] J. Zhang and M.A. Delichatsios, Determination of the convective heat transfer coefficient in three dimensional inverse heat conduction problems, Fire safety journal 44 (2009) 681-690, http://dx.doi.org/10.1016/j.firesaf.2009.01.004.

[47] M. Janssens, C. Gomez, Convective heat transfer in the cone calorimeter revisited, Proceedings of the 12th international Interflam conference (2010) 281-290, The University of Nottingham, UK.

[48] Y. Zhou, L. Yang, J. Dai, Y. Wang and Z. Deng, Radiation attenuation characteristics of pyrolysis volatiles of solid fuels and their effect for radiant ignition model, Combustion and flame 157 (2010) 167-175, http://dx.doi.org/10.1016/j.combustflame.2009.06.020.

[49] T.J. Ohlemiller and M. Summerfield, Radiative ignition of polymeric materials in oxygen/nitrogen mixtures, Proceedings of the symposium (international) on combustion 13 (1971) 1087-1094, http://dx.doi.org/10.1016/S0082-0784(71)80106-6.

[50] ASTM E2058-03: Standard test method for measurement of synthetic polymer material flammability using a Fire Propagation Apparatus, ASTM International, West Conshohocken PA, 2003, http://dx.doi.org/10.1520/E2058-03.

Chapter 2

Pyrolysis modelling up to ignition – Part I: Literature review on sources of uncertainty and experimental variability

Summary

Solid ignition is a key phenomenon in fire safety engineering due to its influence on the fire growth. Its prediction requires the full resolution of the mechanisms occurring in the condensed and the gas phases but the phenomenon complexity cannot be solved for most of the engineering applications and simplifications are unavoidable. Moreover, the mathematical formulation of some mechanisms is still ill-defined implying also some simplifications of the physics. The mechanisms not explicitly considered affect implicitly the value attributed to the model input parameters. Moreover, the methodology used to extract the parameters adds uncertainty to the parameter values. As a consequence of these experimental and methodological uncertainties, the value associated with the parameter is not error free and while often ignored, a range of variability exists

for each input parameter of a model. The quantification of this uncertainty has been performed in this chapter for the most common input parameters of models predicting the delay time to ignition of PolyMethylMethAcrylate (PMMA) samples. The literature review reveals some scatter in the available studies for parameters such as the solid kinetics.

Collaboration

This chapter results from a joint work performed with Dr Guillermo Rein and Prof José L. Torero from the University of Edinburgh (UK).

Nomenclature

A	Pre-exponential factor [s^{-1}]
c	Specific heat [J/(kg.K)]
E_a	Activation energy [kJ/mol]
h	Convective heat transfer coef. [$W/(m^2.K)$]
ΔH	Heat of pyrolysis [kJ/kg]
k	Thermal conductivity [W/(m.K)]
L	Sample thickness [m]
$\dot{m}''$	Mass loss rate [$g/(m^2.s)$]
n	Order of reaction [-]
$\dot{q}''$	Heat flux level [kW/m^2]
r	Surface reflectivity [-]
R	Ideal gas constant [J/(K.mol)]
t	Time [s]
T	Temperature [K]
U	Flow velocity [m/s]
V	Front velocity [m/s]
w	Mass fraction [-]
y	Depth [m]

Subscripts

∞	Ambient conditions
Ch	Char
Conv	Convective
Back	At the back
e	External
F	Flammable gases
ign	At ignition
λ	Wavelength
o	Oxygen
p	At the peak
Rad	Radiative
ref	Reference
s	At the surface
T	Thermal

Greek symbols

α	Absorbance [-]
δ	Pilot distance [m]
ε	Depth [m]
κ	Effective attenuation coef. [m^{-1}]
ρ	Density [kg/m^3]
σ	Stefan-Boltzmann coef. [$W/(m^2.K^4)$]
φ	Material properties
χ	Permeability coefficient [-]
ω	Constant kinetic rate [s^{-1}]

1. Introduction

Solid ignition is a key phenomenon in fire safety engineering due to its influence on the fire growth (e.g. initiation, secondary ignition and flame spread).

In the past, this phenomenon was considered only by ranking the materials according to their ease of ignition (i.e. qualitative analysis). By reproducing the same experimental procedure between tests (i.e. standardization of the tests), it was possible to consider that the differences between the materials at ignition were not related to the set up but only to the differences in the solid phase temperature evolution and chemical degradation (i.e. condensed phase response) [1].

However, nowadays, fire safety strategy is more and more based on the material performance and a quantitative analysis of the phenomenon of solid ignition is therefore required. An issue in the prediction of solid ignition is the characterization of the intrinsic material properties. They are mostly extracted from experiments where a high number of external variables, such as the flow field, the atmospheric composition or the thermal exposure, are controlled and the mathematical models used for the extraction are often based on strong assumptions (e.g. material properties invariant with temperature). The values attributed to the material properties can change from one study to another due to experimental and methodological variations. Generally, this uncertainty in the extracted properties is often ignored for model calibration whereas it can have a major influence on the predictions. The characterization of these uncertainties is essential.

Babrauskas [2] gathered information on most of the individual studies exploring the influence of procedural conditions but the resulting variability in the extracted parameters is not assessed.

The objective in this chapter is to analyse the origin of these experimental and methodological uncertainties in order to assess, afterwards, the parameter uncertainty in the context of solid ignition. The study is focused on PolyMethylMethAcrylate (PMMA) due to the large number of investigations available on this material.

2. Piloted solid ignition

The concept of solid ignition is covered briefly to apprehend its complexity and to understand afterwards the simplifications required to model it. Excellent theoretical reviews are available elsewhere [1,2-7]

2.1. Phenomenon complexity

When a solid sample, initially at ambient temperature T_∞, is exposed to an external heat flux $\dot{q}''_e$ (i.e. fire), its temperature starts to increases and its molecules are stimulated. Their bonds finally break-up, producing flammable gases. These pyrolysis gases leave the top surface and mix with the surrounding air to form a flammable mixture which moves upwards and ignite as soon as it reaches the pilot location.

This simple view of the solid ignition hides a large number of complex phenomena both in the condensed and gas phases (see schematic on Fig. 2.1).

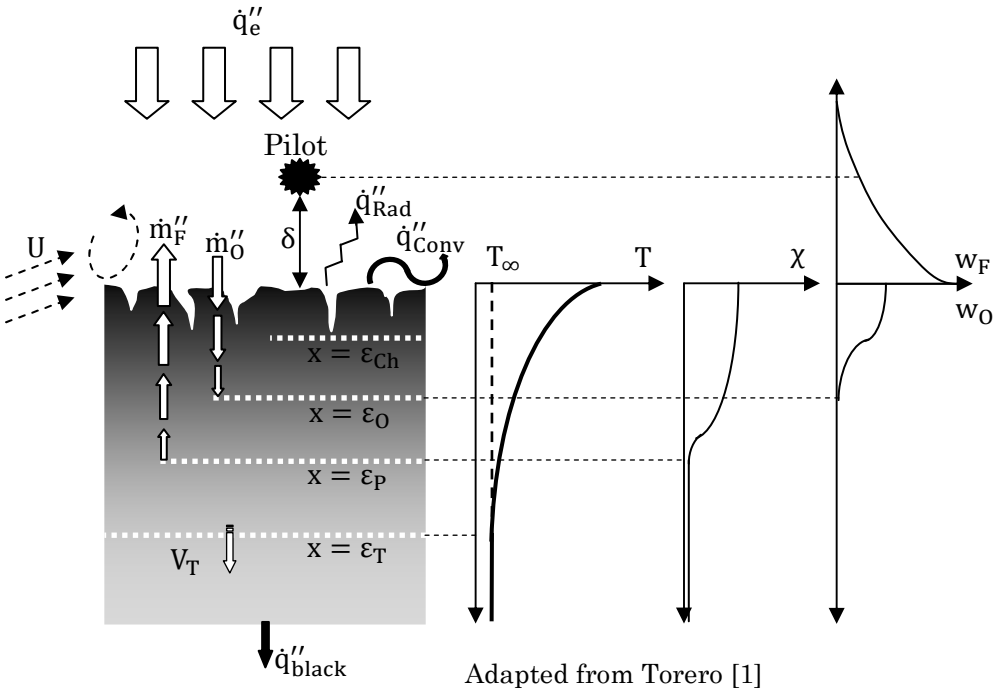

Figure 2.1: Schematic of the complexity encompassed in the pyrolysis process.

The heat flux $\dot{q}''_e$ is absorbed in-depth according to the material radiative properties and generates a thermal wave which propagates with a velocity V_T (function of the temperature) and affects a depth ε_T of the solid. The absorbed energy is balanced by the heat losses at the surface (re-radiation $\dot{q}''_{Rad}$ and convection $\dot{q}''_{Conv}$) and at the back $\dot{q}''_{back}$ (function of the boundary conditions - hypothesis of one-dimensional problem).

When local temperature increases, the solid can undergo a phase change (e.g. melting) affecting the viscosity and creating potential internal convective flow such as in a liquid phase. Any water contained inside the solid evaporates prior to the beginning of the chemical degradation process which follows a complex reaction scheme highly influenced by the atmospheric composition and the heating rate [1]. This process, globally endothermic, represents a heat sink in the heat balance.

The pyrolysis gases $\dot{m}''_F$ produced in depth by the degradation reactions and the vaporized water try to escape through the less resistant path. This mass transfer is mainly controlled by the viscosity and the permeability χ of the solid which evolves in time with the presence of bubbles along the depth ε_P where pyrolysis occurs. The oxygen present in the surrounding atmosphere, with a mass fraction w_O, diffuses in a counter flow ($\dot{m}''_O$) and penetrates inside the solid matrix up to a depth ε_O affecting the pyrolysis reaction scheme and oxidizing the pyrolysis gases released.

In the case of charring material, a carbonaceous layer ε_{Ch} is formed above the virgin material. This layer can undergo a second degradation process to form ashes.

Moreover, above the exposed surface, the fuel mass fraction w_F of the mixture is a function of the pyrolysis gases $\dot{m}''_F$ and the flow velocity U (on the three dimensions). Once the mixture reaches its lean flammability limit at the pilot location δ, the energy provided by this latter enables the combustion reaction to occur. The nascent flame propagates to the rest of the mixture and becomes sustainable if the heat produced by the combustion reaction and

provided back to the solid fuel is enough to overcome the heat loses [7]. The mass flux of pyrolysis gases $\dot{m}''_F$ leaving the sample determines the flame temperature and thus its stability. If only a flash appears, a higher $\dot{m}''_F$ is required.

The prediction of the delay time to ignition requires therefore the full description of the chemical and physical phenomena occurring in the gas phase and the condensed phase (e.g. thermal and oxidative pyrolyses, combustion reaction, heat and mass transport). The interactions between these two phases through the thermal and flow boundary conditions need also to be considered.

2.2. Modelling of the condensed phase

The complex phenomena mentioned above, while well understood, are generally poorly formulated. Large approximations are required. A simple mathematical expression for the heat balance of the solid phase (one-dimensional) is presented in Eq. 2.1 in the case where the solid is exposed to a uniform and constant heat flux at the front (Eq. 2.2 – heat losses by convection with a constant heat transfer coefficient h and by re-radiation) and is insulated at the back (Eq. 2.3 – semi-infinite solid). The influence of the gas phase is neglected [4] and the incident heat flux is assumed to be partially absorbed (absorptivity α) at the surface. The production rate of the pyrolysis gas is modelled in Eq. 2.4 with a simplified Arrhenius law (1-step reaction controlled by the pre-exponential factor A and the energy activation E_a). The power laws used in Eq. 2.4 for the mass fraction of flammable fuel and oxygen are generally unknown and taken respectively as unity and null. The endothermicity (ΔH_p) of the pyrolysis reaction appears as a heat sink in Eq. 2.1. The simplified heat balance presented in Eq. 2.1 neglects any internal mass transfer and change of conductive heat transfer due to bubble formation.

$$\rho c \frac{\partial T(y,t)}{\partial t} = k \frac{\partial^2 T(y,t)}{\partial y^2} - \Delta H_p \, \dot{m}''' \tag{2.1}$$

$$\forall t;\ -k \left.\frac{\partial T}{\partial y}\right|_{y=0} = \alpha \dot{q}''_e - h(T_s - T_0) - \sigma\alpha(T_s^4 - T_0^4) \tag{2.2}$$

$$\forall t;\ \left.\frac{\partial T}{\partial y}\right|_{y=L} = 0 \tag{2.3}$$

$$\dot{m}''' = \rho A \exp\left(\frac{-E_a}{R\,T(y,t)}\right) w_F^a\, w_O^b \tag{2.4}$$

These equations are applicable for non-charring polymer such as PMMA. While a more complete set of equations can be found elsewhere [1,8,9], Eqs. 2.1 to 2.4 correspond to the skeleton of most pyrolysis models.

Through a series of assumptions, Torero [1] and Atreya [4] arrive to two different models which respectively reflect the main concepts used nowadays for the prediction of solid ignition based on condensed phase criteria. These models have not been developed by these two authors but their respective review provides a deep understanding of them.

In the model reviewed by Torero [1], it is assumed that given the typical large activation energy E_a associated with pyrolysis reactions, the exponential characteristic of the Arrhenius law can be viewed as a step function (kinetics infinitely fast). The pyrolysis reaction rate jumps as soon as a characteristic temperature, called pyrolysis temperature, is reached. Since surface absorption is considered, the peak temperature is located at the surface and the solid is assumed inert until the pyrolysis temperature is reached at the surface. The heating process of the solid is the predominant mechanism and a surface temperature $T_{s\,ign}$ is used as ignition criterion.

For Atreya [4], the kinetics of the pyrolysis reactions have a finite-rate (use of an equation similar to Eq. 2.4). The solid ignition is reached when a critical mass flux of pyrolyzates $\dot{m}''_{F\,ign}$ is released by the sample. This concept of critical mass loss rate is related to the lean flammability limit that the mixture should reach at the pilot location. Lyon and Quintiere [10] related this critical mass flux to a critical heat release rate required to exceed the heat losses and guarantee a sustained ignition.

Long et al. [11] have added the gas phase response to the concept reviewed by Torero [1]. Flaming ignition is defining when a specific ratio fuel/air is reached at the pilot location. This sophisticated concept requires the knowledge of the flow field which is generally unknown or not well characterized. As a

consequence, a condensed phases criterion ($T_{s\,ign}$ and $\dot{m}''_{F\,ign}$) is generally considered by default, assuming that the atmospheric conditions (i.e. temperature, flow, oxygen concentration) are approximately constant and therefore that the critical values for the condensed phase criteria are only function of the material.

With the increasing understanding of the condensed phase behaviour, a large number of physical and chemical processes were introduced in pyrolysis models, increasing their global complexity. Two groups of models have emerged depending on the assumption concerning the predominant mechanism: heating process or chemical degradation. These models are however still uncoupled to the gas phase and ignition is therefore related to a condensed phase criterion. The codes developed by Rhodes and Quintiere [12] and by Wasan et al. [13] consider that the heating process controls the evolution of the solid phase (kinetics infinitely fast). On the other side, codes such as Gpyro [14], ThermaKin [15], FireFoam [16] and FDS [17] consider that the chemical degradation is fundamental (finite-rate kinetics). Different levels of complexity are possible in these models and it is therefore the responsibility of the user to choose the appropriate level of complexity. This level will control the number of parameters requiring a calibration. Even with the implementation of these mechanisms, a large number of physical and chemical phenomena presented in section 2.1 are neglected.

2.3. Experimental state-of-the-art

The phenomenon of solid ignition has mainly been studied in the past with bench-scale experiments to control the boundary conditions and the quantity observed to analyse this phenomenon has often been the delay time to reach a sustainable flame.

2.3.1 Time to ignition t_{ign}

The delay time to ignition for more than 250 black PMMA samples has been gathered in a previous chapter [18 (chap 1)] in order to assess the experimental uncertainty of piloted ignition and its apparatus dependency. Figure 2.2 represents a part of these data sets ($\dot{q}''_e$ < 100 kW/m²). The cloud of data points is the result of differences in the experimental conditions (external parameters) and in the material intrinsic properties (internal parameters).

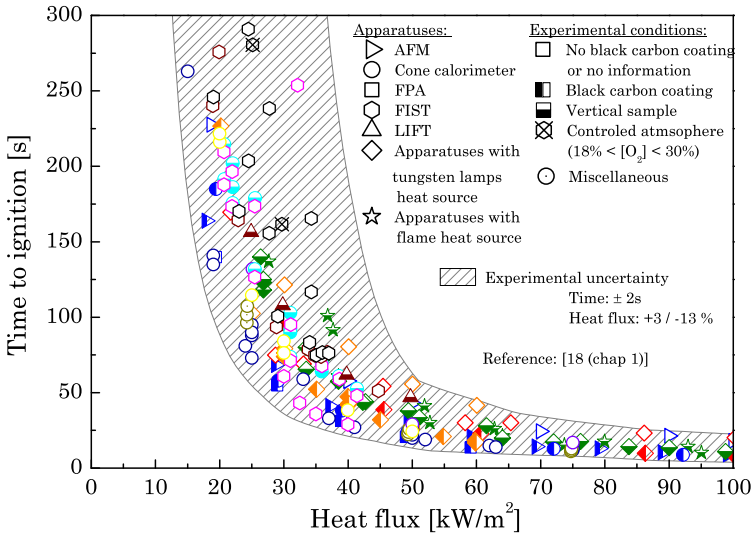

Figure 2.2: Times to piloted ignition of black PMMA samples for a wide range of experimental conditions (data extracted from the literature).

A large number of experiments have been performed to estimate the influence of the external and internal parameters on the delay time to ignition t_{ign}. As an example, Fig. 2.3 illustrates experimental sensitivity analyses performed by Cordova et al. [19] on t_{ign} varying the flow velocity and the oxygen concentration in the Forced-flow Ignition and Flame-spread Test (FIST). t_{ign} is delayed by an increase of the flow velocity and a decrease of the oxygen concentration but these effects are reduced when $\dot{q}''_e$ increases. Table 2.1 gathers the results of the main experimental sensitivity studies performed on t_{ign} with PMMA samples (non-exhaustive list).

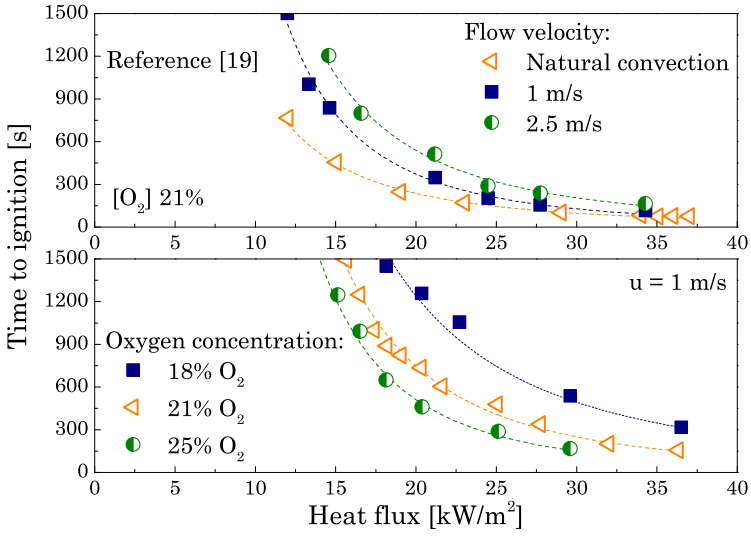

Figure 2.3: Variations of the measured delay time to ignition for different flow conditions and atmospheric compositions (black PMMA samples).

Table 2.1: Sensitivity of t_{ign} to experimental conditions for PMMA samples.

Parameters	Sensitivity results	References
Pilot distance δ	$\delta_1 < \delta_2 \Rightarrow t_{ign\ \delta_1} < t_{ign\ \delta_2}$	[11]
Thickness L	$L_1 < L_2 \Rightarrow t_{ign\ L_1} \approx t_{ign\ L_2}$ (both thermally thick) $L_1 < L_2 \Rightarrow t_{ign\ L_1} < t_{ign\ L_2}$ (low heat flux)	[20,21] [22]
Molecular weight MW	$MW_1 < MW_2 \Rightarrow t_{ign\ MW_1} > t_{ign\ MW_2}$ (thermally thin)	[23]
Flow velocity U	$U_1 < U_2 \Rightarrow t_{ign\ U_1} < t_{ign\ U_2}$ (FIST apparatus) $U_1 < U_2 \Rightarrow t_{ign\ U_1} \approx t_{ign\ U_2}$ (FPA) $t_{ign\ U_{Natural\ convection}} < t_{ign\ U_{forced\ convection}}$	[19] [21,24] [19]
Oxygen concentration $[O_2]$	$[O_2]_1 < [O_2]_2 \Rightarrow t_{ign\ [O_2]_1} > t_{ign\ [O_2]_2}$	[19]
Orientation	$t_{ign\ horizontal} < t_{ign\ vertical}$ (min for 30° from horizontal)	[20,25]
Black coating	$t_{ign\ coated} < t_{ign\ uncoated}$	[21,24]
Heater type	$t_{ign\ tungsten\ lamp} \approx t_{ign\ benzene\ flame}$ (Black PMMA) $t_{ign\ tungsten\ lamp} > t_{ign\ benzene\ flame}$ (Clear PMMA) $t_{ign\ tungsten\ lamp} > t_{ign\ conical\ heater}$ (Black PMMA)	[22] [22] [21]
Ambient pressure P	$P_1 < P_2 \Rightarrow t_{ign\ P_1} < t_{ign\ P_2}$ (existence of a minimum)	[26]
Heat flux $\dot{q}''_e$	$\dot{q}''_{e\ 1} < \dot{q}''_{e\ 2} \Rightarrow t_{ign\ \dot{q}''_{e\ 1}} > t_{ign\ \dot{q}''_{e\ 2}}$	[19,22,25]

Following the results in Table 2.1, ignition is enhanced when the sample is thin with a high molecular weight and the external variables promoting ignition are a pilot close to the surface, a stagnant flow, a large mass fraction of oxygen and a large applied heat flux level. However, these results are specific to the tested experimental conditions and the conclusion can change if these latter vary. This is the case for example with the thickness: t_{ign} is dependent only until a certain threshold corresponding to the thickness where the solid ignites before the thermal wave is able to reach the back of the sample.

Among the experimental conditions explored in Table 2.1, some reflect the influence of the gas phase (e.g. flow field or the oxygen concentration). The differences in the measured delay times to ignition resulting from gas phase mechanisms cannot be explicitly considered with models that ignored this phase. However, they will be implicitly considered within the variation of the ignition criterion. This variation is not only related to the ignorance of gas phase mechanisms but it is a consequence of the whole simplifications implemented in the models.

2.3.2 Variation of the condensed phase ignition criteria

As it has been mentioned previously, most of the models predict the occurrence of ignition based on a condensed phase criterion. The actual computational resources and the knowledge on the solid decomposition do not enable the use of a critical equivalence ratio (i.e. constant fuel/air ratio at the pilot location [11]) for realistic conditions where the external variables (e.g. flow field) are not controlled [27].

Thomson and Drysdale [28,29] measured the variability of $\dot{m}''_{F\,ign}$ (mass flux) and $T_{s\,ign}$ (surface temperature) for different plastics. They found for clear PMMA samples that $T_{s\,ign}$ was varying only slightly with the applied heat flux (from 301 to 317 °C between 17 and 38 kW/m²) except close to its critical value ($T_{s\,ign}$ = 238 °C at 13 kW/m²). Their results for $\dot{m}''_{F\,ign}$ show a narrower range (from 1.90 to 2.15 g/(m².s) between 13 and 33 kW/m²). However, they obtained these results when only the heat flux level was varied. Looking at other experimental conditions, they have demonstrated that some external

parameters could have an impact on these criteria. This has been confirmed for the flow velocity by Cordova and his co-authors. In their studies, $T_{s\,ign}$ was found to vary between 283 and 360 °C [19] and $\dot{m}''_{F\,ign}$ between 1.3 and 3.9 g/(m².s) [30]. Figures 2.4 gathers values of $T_{s\ ign}$ (Fig. 2.4a) and $\dot{m}''_{F\,ign}$ (Fig. 2.4b) reported in the literature [10,11,19,23-26,28-37] for clear and black PMMA. Each bar represents the range reported in a study while one parameter (external or internal) was varied: ambient conditions (pressure and oxygen concentration) [26,32,35], flow velocity [19,24,30,35], sample orientation [25,31], applied heat flux (magnitude and spectral characteristics) [10,11,28,29,33,34,36,37] and formulation (i.e. thermal stability) [23,38]. The results for each criterion do not present distinct trends according the visual aspect (clear or black) of the PMMA samples. As shown on Fig. 2.4, the condensed phase criteria are not invariant. Reasonable ranges for $T_{s\ ign}$ and $\dot{m}''_{F\,ign}$, extracted from bench-scale measurements, are respectively [523 ; 673 K] and [1 ; 5.6 g/(m².s)]. These ranges exclude outliers which can be explained by the experimental procedure. As an example, Rasbash et al. [35] found for $\dot{m}''_{F\,ign}$ a value higher than 10 g/(m².s) for a low oxygen concentration (18 %) and a drop below 5 g/(m².s) when the oxygen concentration is increased of 1 %. While similar quantitative measurement of $\dot{m}''_{F\,ign}$ have not been reported in literature, Rich et al. [36] observed also a sharp increase of $\dot{m}''_{F\,ign}$ when the oxygen concentration is reduced. The high value of $\dot{m}''_{F\,ign}$ recorded by Rasbash et al. [35] is probably the consequence of the increased impact of the gas phase as observed by Cordova et al. [19]. The decrease of oxygen implies an increase of the chemical time (time required for the reaction to occur when the mixture is between its flammability limits) which cannot be neglected anymore despite the presence of the pilot. The mass flux measured when flaming ignition occurs cannot be considered as a critical mass flux. This result illustrates the limitations to uncouple and neglect the gas phase response for the prediction of solid ignition.

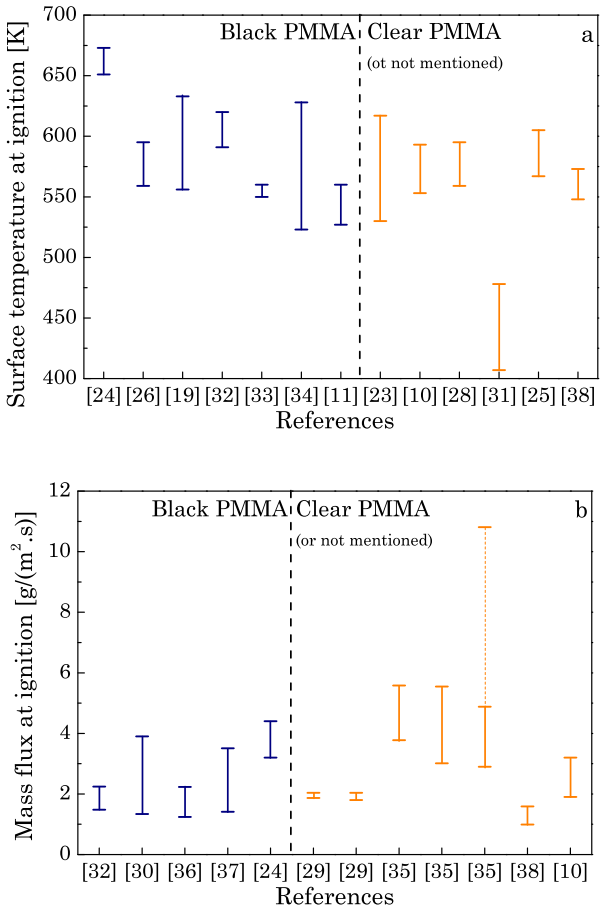

Figure 2.4: (a) Surface temperature and (b) mass flux measured at ignition with different experimental conditions for black and clear PMMA samples.

This specific phenomenon occurred only close to the critical oxygen concentration required for ignition. It is therefore reasonable to not consider this value in the range associated with $\dot{m}''_{F\,ign}$ but to constrain the use of a condensed phase criterion to atmosphere where the oxygen concentration is a few percent higher than the critical concentration. The threshold is suspected to vary with the flow velocity due to the importance of the ratio between the chemical time and the local residence time (time the reactants remain together at a specific location). This ratio is called the Damkholer number [1,6]. Moreover, Fereres et al. [32] and McAllister et al. [26] have demonstrated that the chemical time is also increased when the pressure is reduced, implying a similar issue concerning the prediction of the delay time to ignition.

Torero [1] and Fernandez-Pello [6] have concluded that in ignitibility tests, the condensed phase response is predominant only in the presence of a strong pilot, at atmospheric pressure, with a stagnant flow and in a sufficiently oxygenated atmosphere.

Figure 2.5 represents typical measurements of the surface temperature and the mass loss rate for PMMA samples exposed to a uniform external heat flux. The surface temperatures (left Y-axis) increased sharply at the beginning but reached a plateau after a certain time whereas the measured mass loss rates (right Y-axis) stay negligible for a long time (i.e. pyrolysis time) and increases exponentially once initiated. Due to the plateau reached by the surface temperature, a small variation in the value used for $T_{s\ ign}$ will have a large impact on the predicted t_{ign}. This is not the case for $\dot{m}''_{F\ ign}$ due to the exponential character of the mass loss rate measurements. However, as Kashiwagi et al. [38] have shown in their study, different polymer samples sold under the same trade name PMMA could present different mass loss rate histories resulting from different thermal stabilities while the surface temperature evolutions are similar between samples (Fig. 2.5).

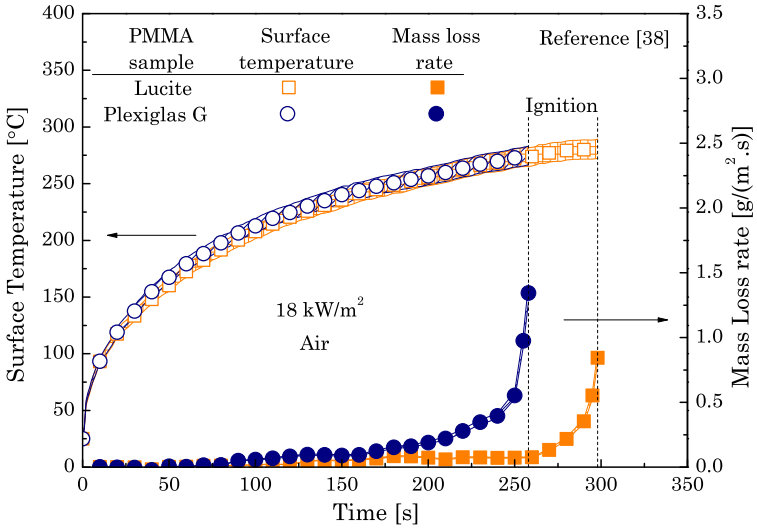

Figure 2.5: Surface temperature and mass loss rate for two samples sold under the trade name PMMA (18 kW/m² - air).

To summarize, this section illustrates issues concerning the capability to predict the onset of flaming ignition which are the consequence of the phenomenon complexity and the engineering solutions applied to overcome these difficulties. The simplifications lead to the use of a condensed phase ignition criterion and induce variations of the values for this criterion.

3. Extraction of the input parameters

Whatever is the reason why solid ignition is predicted (e.g. research, design or forensic analysis); the model used needs to be calibrated. The parameters can be extracted from different sources: independent measurements, inverse modelling, expert judgement or literature. This section explores the different sources of uncertainty associated with these methods.

3.1. Independent measurements

The use of independent experiments, as it has been performed by Stoliarov et al. [15] for most of the parameters in their study on non-charring polymers degradation, represents the best solution. However, this technique can be challenged by the capability to reproduce the experimental conditions (e.g. atmospheric composition [39,40]), by the availability of the material (e.g. thermal stability from different production batches [38,41] – Fig. 2.5) and by the methodology used (e.g. apparatus and analysis). The last point, while often not mentioned, could be an important source of uncertainty, especially when several mechanisms are coupled. Hirata et al. [42] found discrepancies in the kinetics parameters (Eq. 2.4) using two different thermal exposures (ramped or isothermal heating). Lyon et al. [43] have also recently noticed differences in the kinetics parameters according to the theoretical model used in the analyses. The issue is not only related to the chemistry decomposition. As an example, Linteris et al. [44] have demonstrated that a small change in the range of wavelengths used to study in-depth radiation absorption (Beer-Lambert's law) might have a large influence on the predicted location (in-depth) and magnitude of energy absorbed. Finally, the number of tests required by this methodology could represent a prohibitive cost.

3.2. Inverse modelling

The extraction of the input variables by inverse modelling [14,16] requires less experimental resources. The entire set of parameters is calibrated simultaneously by optimising the match between the numerical predictions and experimental measurements of a quantity of interest such as surface temperature.

The advantage with this technique is that the assumptions performed to extract the parameters are these of the model used afterwards for the prediction. However, the system studied is open [45] (i.e. more unknown than experiments to identify a unique solution for each variable [46,47]) and the mathematical technique considered for the optimisation can have a significant effect as shown recently by Lautenberger and Fernandez-Pello [46] using four different algorithms.

3.3. Expert judgment

This technique, while corresponding to the easiest, is also the most uncertain because its effect is rarely quantifiable. The parameter is estimated by a simple engineering judgment, based generally on the analogy to another study. An example of common engineering judgment calibration is the values attributed to the radiative properties of the condensed phase (i.e. absorbance, reflectance and transmittance).

3.4. Literature

The last possibility is to use the large database available in the literature. This is often the case for design and forensic analysis. The applicability of the results is questionable mainly due to the extrapolation of the results out the experimental conditions and the difference in the material used (i.e. influence of the thermal stability). However, the main advantage of a large database, as it is for PMMA, is that a large number of experimental configurations and material polymerisations have been investigated. The extracted ranges can therefore be

considered as representative of the experimental and methodological uncertainties.

Whatever methodology is used to extract the values for the input parameters, there are several sources of uncertainty (experimental and/or methodological).

4. Literature review of main input parameters

This section is dedicated to the quantification of the uncertainty associated with the most common parameters used in pyrolysis models when only the database from the literature is exploited. Some of them correspond to external variables but the majority are internal material properties. The literature review, focused on PMMA, do not pretend to be exhaustive.

The pyrolysis model have generally 12 parameters in common: the applied heat flux level $\dot{q}''_e$ [kW/m^2], the thermal conductivity k [W/(m.K)], the specific heat c [J/(kg.K)], the density ρ [kg/m^3], the in-depth radiation absorption coefficient κ [m^{-1}], called also attenuation coefficient, the ignition criterion (mainly $T_{s\,ign}$ [K] or $\dot{m}''_{F\,ign}$ [g/(m^2.s)]), the convective heat transfer coefficient h [W/(m^2.K)], the reflectivity r [-], the heat of pyrolysis ΔH_p [kJ/g] and the kinetics triplet composed of the pre-exponential factor A [s^{-1}], the activation energy E_a [kJ/mol] and the order of the reaction n [-].

4.1. Thermophysical properties

The thermal conductivity k, the density ρ and the specific heat c are the main material properties controlling the temperature evolution inside a solid sample (Eq. 2.1) and they are known to be temperature dependent. There are several techniques to estimate these properties (e.g. Differential Scanning Calorimetry - DSC - or guarded hot plate [48]). Values extracted from the literature (non exhaustive search) for k, c and ρ are plotted in Figs. 2.6 to 2.8. Excluding outliers, the observable ranges for these parameters are:

[0.13 ; 0.27] W/(m.K) for k, [1000 ; 1220] kg/m³ for ρ and [1200 ; 3050] J/(kg.K) for c.

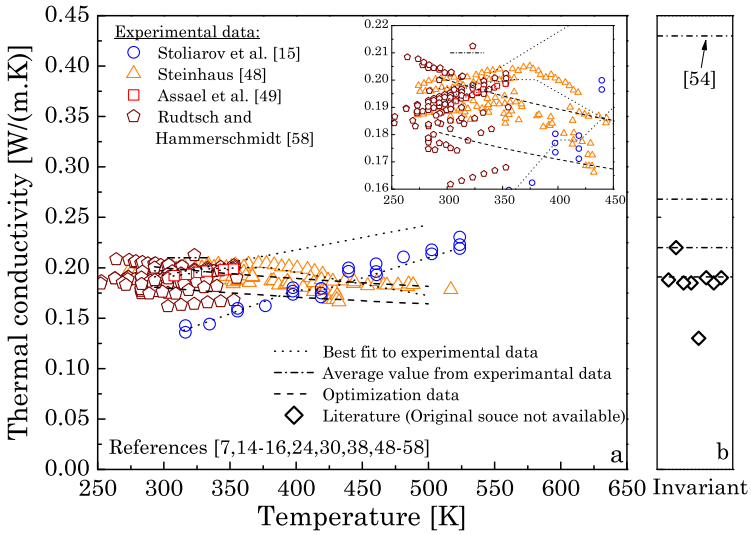

Figure 2.6: Thermal conductivity extracted from the literature for PMMA samples: (a) property function of temperature and (b) property considered as invariant.

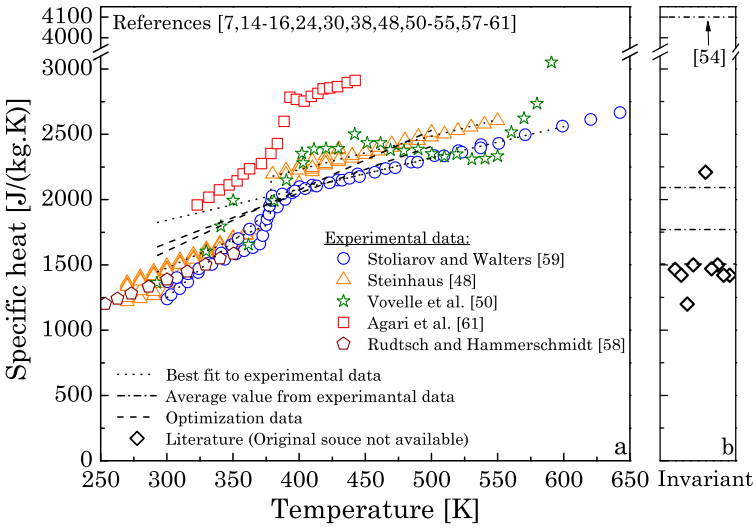

Figure 2.7: Specific heat extracted from the literature for PMMA samples: (a) property function of temperature and (b) property considered as invariant.

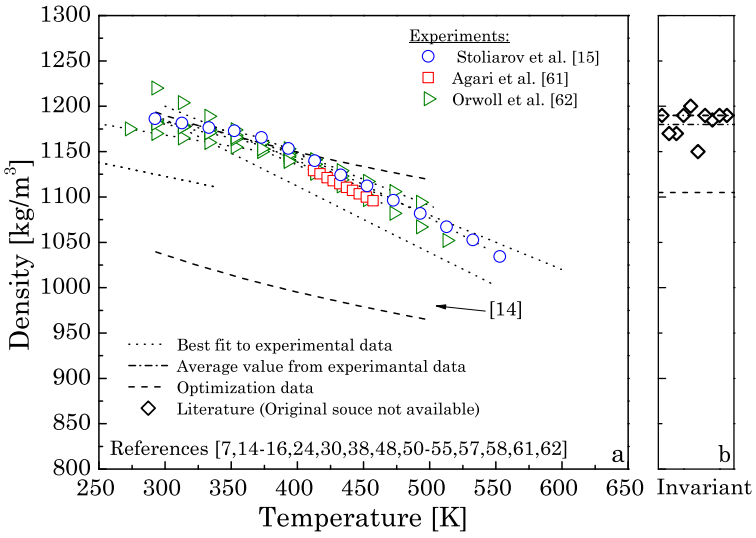

Figure 2.8: Density extracted from the literature for PMMA samples: (a) property function of temperature and (b) property considered as invariant.

The whole sets of data agree on the general trend for c and ρ: they respectively increase and decrease when the local temperature increases. The evolution of k is less unanimous. While most of the sets provide a global decrease of k as the temperature increases, some sets [15,49] show an opposite behaviour. Nevertheless, the ranges of variation in all sets are similar.

In models taking into account the temperature dependency of these parameters, the evolution is mainly assumed to be linear (Eq. 2.5 - as ThermaKin [15]) or to follow a power law (Eq. 2.6 - as Gpyro [14]). Table 2.2 gathers the best fits of Eqs. 2.5 and 2.6 to the data presented in Figs. 2.6 to 2.8. Moreover, in order to illustrate the variability of the different coefficients, the best fits to specific sets of data are also reported in Table 2.2. PMMA undergoes a glass transition around 378 K, therefore the coefficients from the best fits in Table 2.2 are associated with a temperature range located prior to or post to the glass transition.

$$\varphi = \varphi_0 + \varphi_1 T \tag{2.5}$$

$$\varphi = \varphi_0 \left(\frac{T}{T_{ref}}\right)^{\varphi_1} \tag{2.6}$$

where $\varphi \in \{k; \rho; c\}$, φ_0 and φ_1 are constant coefficients and T_{ref} is a reference temperature.

Table 2.2: Equation coefficients for PMMA thermophysical properties.

Temperature [K]	Thermal dependency models				References
	φ_0 Eq. 2.5	φ_1 Eq. 2.5	φ_0 Eq. 2.6	φ_1 Eq. 2.6[a]	
			Thermal conductivity		
[273 ; 378]	0.170	$0.90 \cdot 10^{-4}$	0.192	0.12	Best fit[b]
[378 ; 517]	0.258	$-1.67 \cdot 10^{-4}$	0.148	-0.39	Best fit[b]
[316 ; 403]	-0.008	$4.64 \cdot 10^{-4}$	0.131	1.05	[15]
[403 ; 524]	-0.001	$4.33 \cdot 10^{-4}$	0.128	1.02	[15]
[276 ; 378]	0.183	$0.598 \cdot 10^{-4}$	0.201	0.09	[48]
[378 ; 420]	0.283	$-2.08 \cdot 10^{-4}$	0.225	-0.42	[48]
			Specific heat		
[234 ; 378]	21.8	4.63	1411	0.97	Best fit[b]
[378 ; 642]	1375.7	2.04	1932	0.42	Best fit[b]
[300 ; 403]	1323	8.54	1250	1.82	[59]
[403 ; 642]	1125	2.40	1784	0.52	[59]
[300 ; 370]	146.4	4.08	1369	0.90	[59]
[379 ; 551]	1107	2.41	1793	0.50	[59]
[290 ; 360]	-515.5	6.25	1359	1.34	[48]
[390 ; 500]	1045	2.94	1892	0.55	[48]
			Density		
[273 ; 378]	1243	-0.215	1178	-0.059	Best fit[b]
[378 ; 553]	1408	-0.665	1238	-0.276	Best fit[b]
[313 ; 378]	1261	-0.255	1185	-0.074	[62]
[378 ; 533]	1438	-0.723	1255	-0.301	[62]

[a] $T_{ref} = 300$ K

[b] based on the whole data sets in Figs. 2.6 to 2.8

When the different sets of data are considered one-by-one, the coefficients resulting from the best fits of Eqs. 2.5 and 2.6 present linear correlations ($\varphi_1 = \alpha + \varphi_0\beta$ – not represented). This mathematical aspect suggests the presence of a compensation effect between these coefficients.

4.2. Pyrolysis kinetics

The main product released by the pyrolysis reaction of PMMA is its monomer MMA (Methyl MethAcrylate). However, the number of steps and the onset temperature of decomposition (i.e. thermal stability) diverge between the different small-scale studies [23,38,39,42,43,63-65]. These steps, consisting of the polymer unzipping process, result mainly from random scission and chain-end initiation. The difference in thermal stability between samples is due to the presence of abnormal structures which results from particular conditions of polymerisation and presence of additives [5]. An example of the observable variability between thermogravimetric analyses (TGA) is shown in Fig. 2.9 for experiments in inert atmosphere (nitrogen or argon) and air with a heating rate of 5 K/min. For inert atmosphere, except for one measurement, all the TGA present a main peak between 350 and 370 °C. However, prior to this main peak, the steps are totally disparate implying a difference in the onset temperature of decomposition (between 130 and 260 °C). The presence of oxygen in the atmosphere has a double effect: on the one hand, it increases the onset temperature of decomposition, but on the other hand, it enhances the random scission process shifting the main peak to lower temperature [42]. The large discrepancies observable between the TGA in air (Fig. 2.9a) cannot be neglected given the influence of the atmospheric composition on the mass loss rate. Indeed, Kashiwagi and Ohlemiller [40] first and then Vovelle et al. [66] have demonstrated by performing bench-scale experiments in different oxygen concentration that the mass flux released by the sample is influenced by the presence of oxygen. However, this sensitivity is evolving with the applied heat flux. Since $\dot{m}''_F$ acts as a counter flow (Fig. 2.1), an increasing $\dot{m}''_F$, induced by a higher heat flux level, will decrease the diffusion of oxygen and therefore avoid in-depth oxidative reactions. Nevertheless, the critical value of $\dot{m}''_F$ where oxygen has reduced effect on the decomposition corresponds to the upper range of mass

flux reported at ignition in Fig. 2.4b [40,66], thus oxidative reactions should be considered in pyrolysis models.

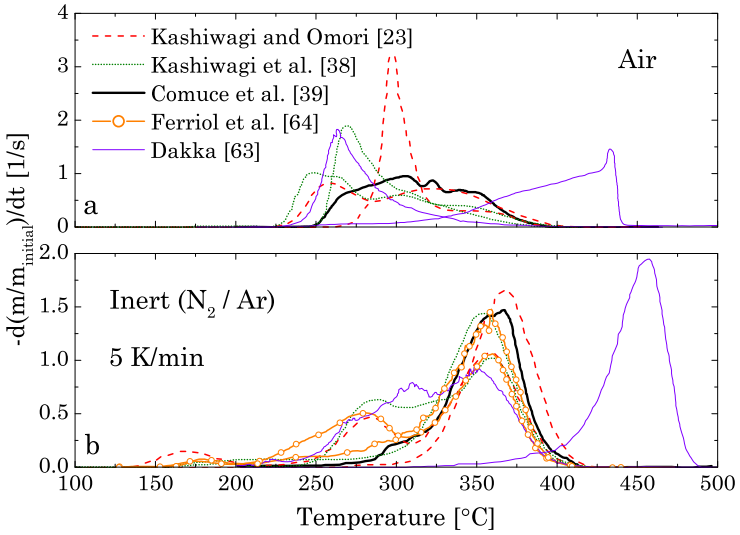

Figure 2.9: Thermogravimetric analyses extracted from the literature for PMMA at 5 K/min: (a) in air and (b) in inert gas.

Hirata et al. [42] performed two unusual but interesting sets of experiments. In the first one, they carried out a purification (i.e. chemical process) of the PMMA sample beforehand. They found that while the degradation of the sample is almost unchanged for inert atmosphere in comparison to the original sample, the reaction occurring in oxygenated atmosphere is significantly affected. The reaction scheme evolves from four stages for non purified PMMA to only one stage in air. In the second set of experiments, Hirata et al. [42] pre-heated a sample in air up to a temperature slightly lower than the onset of decomposition and finished the test under nitrogen. Once again, they found differences in the thermal stability of the pre-heated sample in comparison to the original one. This second set tends to replicate the experimental conditions where the quantity of pyrolysis gases increases and reaches a level preventing the diffusion of oxygen in the surface sample.

Dakka et al. [65] and more recently Comuce et al. [39] have coupled their thermogravimetric experiments to a gas phase analysis. Their respective

measurements show different gas product compositions. A deeper investigation is required to assess if this difference is due to the analysis or if the experimental procedures are responsible for these differences. In the latter case, the mixture flammability and therefore the ignition delay time could be affected. Rich et al. [36], performing an analysis on the dependency of $\dot{m}''_{F\,ign}$ to experimental conditions, emitted the hypothesis that at higher heat flux levels, the gases released by the sample might contained an increasing concentration level of CO, CO_2 and H_20, due to a higher level of oxidation.

Some issues are encountered in the thermogravimetric experiments concerning the heat and mass transport. The heating rates applied are generally slow (from 1 to 10 K/min) to avoid a temperature gradient and mass transport limitation. However, this heating rate is one order of magnitude lower than the heating rate applied in bench-scale ignition tests (from 0.8 to 5.8 K/s for heat fluxes between 50 and 100 kW/m^2 [43]) and in flame spread tests (from 5 to 10 K/s [5]). Moreover, when the heating rate is increased in TGA, the peak of mass loss rate shifts towards higher temperature [39,42,43,64,65]. Gao et al. [67] and Holland and Hay [68] have estimated the activation energy from TGA that they carried out at different heating rates. They found a variation between 160.6 and 260 kJ/mol for heating rates varying between 1 and 20 K/min.

Several experimentalist teams [63,42] found a heating rate threshold around 2-3 K/min above which mass transport affects the mass loss evolution. Kashiwagi and Omori [23] have shown that samples with a lower viscosity, enhancing therefore the mass transport, ignite at longer delay time. They concluded from their experiments that while the mass transport might have an impact, the thermal stability of a sample, effecting the pyrolysis reaction, has a higher effect on the ignition process.

To sum up, the chemical decomposition of PMMA presents large discrepancies from one sample to another and between different experimental conditions. The applicability of the results to larger scales remains therefore a research area.

The evolution of the mass for a solid subjected to chemical degradation is predicted by the combination of two models: the first one capturing the dependence of the reaction rate to the available mass of fuel and the second its dependence to the local temperature. Arrhenius law is generally used to express the temperature dependency (Eq. 2.4). The impact of the mass of fuel is, most of the time, an unknown function and it is therefore assumed. The submodel included in Eq. 2.4 corresponds to a $(a+b)^{th}$ order reaction model. The order of the reaction, often taken arbitrary equals to unity, was found to vary in the literature between 0.5 and 2.2 [63,64,67,68]. Once the model is assumed, a fit is performed to obtain the kinetics parameters. The most famous technique is the Kissinger's method [42,43,63] but other methodologies can be used [43].

Vyazovkin and Wight [69] in a large review of the kinetics in solids claim that the activation energy is expected to vary with the extent of the reaction and the type of reaction occurring. The usual techniques averaging this evolution of the activation energy, like the Kissinger's method, will result in the failure to predict the mass loss evolution. In a few studies [64,67], a methodology called isoconversional [69], where the activation energy is evolving with the extent of reaction, was used to investigate PMMA degradation. The activation energy was found to vary between 100 and 230 kJ/mol (maximal range).

As shown in Eq. 2.4, the two main parameters in an Arrhenius law are the activation energy E_a and the pre-exponential factor A. Around sixty couples of these parameters (constant values) extracted from the literature for PMMA decomposition are plotted in Fig. 2.10. They have been obtained for different reaction schemes consideration (1-setp in open symbols and multi-steps in solid symbols), in different atmospheres (triangles for inert conditions and circles for oxygenated atmosphere) and with different experimental methodologies (such as constant heating ramp TGA [15,23,38,42,53,63-68,70], iso-thermal heating TGA [42,67], Microscale Combustion Calorimeter (MCC) [70] or inverse modelling coupled with bench-scale experiments [14,16,18 (chap 1),30]). It is worth noticing that the couples obtained by inverse modelling are encompassed within the data obtained from small-scale experiments (Fig. 2.10).

Except for a few points (all coming from the experiments - including overlapping peaks [64]), the parameters E_a and $ln(A)$ present a linear correlation ($R^2 > 0.95$) demonstrating the presence of a compensation effect. The spread of the data is framed by the dashed lines. The range of variation for these parameters is relatively wide: [31 ; 290] kJ/mol for E_a and [1.1 ; $4.5 \cdot 10^{23}$] s^{-1} for A.

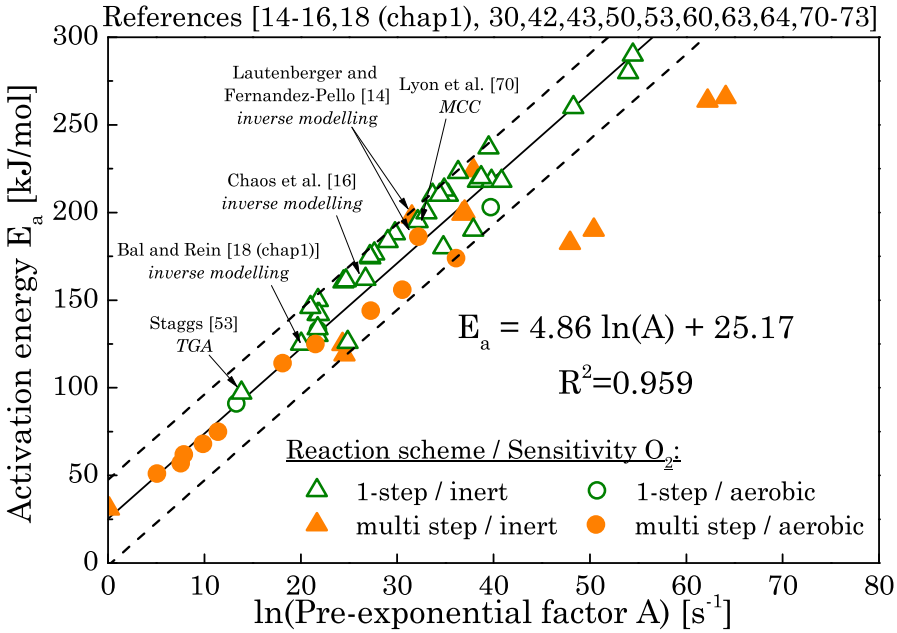

Figure 2.10: Correlation between the Arrhenius kinetics parameters (activation energy and pre-exponential factor) for the chemical decomposition of PMMA (data extracted from the literature).

Lyon et al. [70] suggested recently that the important parameter to extract from small-scale tests such as TGA is the temperature where the peak of mass loss rate occurs: T_p. Based on the definition of the Arrhenius law, they express the activation energy as a function of T_p, A and ω (the kinetics constant rate at T_p).

$$E_a = T_p \, R \, ln(A) - T_p \, R \, ln(\omega) \qquad (2.7)$$

Using the best fit between $ln(A)$ and E_a presented in Fig. 2.10 with Eq. 2.7, T_p and ω are estimated to 583 K and $5 \cdot 10^{-3}$ s^{-1}. The kinetics constant rate ω is one order of magnitude lower than the prediction by Lyon et al. [70] at 1 K/s ($\omega \approx 0.05$ s^{-1}). T_p is under estimated of about 40 to 60 K when compared to the temperature of the peaks plotted in Fig. 2.9. This can be probably attributed to the fact that the correlation between $ln(A)$ and E_a is an average over different experimental conditions (e.g. heating rate, atmospheric composition, initial mass).

In another study but following the same principle, Lyon et al. [43] provide a methodology to assess the ignition temperature $T_{s\,ign}$. Based on the data in Fig. 2.10 (583 K), $T_{s\,ign}$ is estimated to be between 499 and 556 K (for $91<E_a<290$ kJ/mol - kinetics couples with only 1-step reaction scheme. This corresponds to a lower range of the value found in Fig. 2.4a.

The variability in the chemical decomposition of PMMA samples presented in this section clearly shows that unless the thermal stability of a specimen is investigated, the uncertainty associated with the prediction of its pyrolysis decomposition is expected to be significant.

4.3. Radiative properties

The radiative properties of PMMA samples will interact with the energy absorption (location and order of magnitude). The incident energy received at the surface sample is divided in three parts: reflected, absorbed and transmitted. Absorptivity is not a surface property since in reality radiations are absorbed in-depth. This mechanism is often neglected due to the small thickness of the layer (just below the surface) where the energy is absorbed. Kashiwagi [57] claims that this approximation is valid if $\sqrt{(k/\rho c)t} \gg 1/\bar{\kappa}$, with $\bar{\kappa}$ corresponding to an effective attenuation coefficient (broadband average of the attenuation coefficient κ - dependent of the heat source and the material). Tewarson and Ogden [24] with black PMMA samples and more recently Girods

et al. [74 (chap 6)] with clear PMMA samples have shown that in-depth radiation can have a significant impact on the pyrolysis behaviour in some experimental conditions.

The reflectivity r has been often taken in the past as the complement of the absorptivity (assuming the solid as opaque) or simply neglected [54]. This parameter can be measured thanks to integrating spheres [44,75] or estimated from the refractive index [76]. Linteris et al. [44] have compared both techniques and found less than 6 % of difference for r averaged over the entire spectrum. Figure 2.11 presents the range of values found in the literature for r. The resulting range of possible values is [0 ; 0.15]. The measurements from Manohar et al. [77] are not considered in this range since the presence of noise provokes large scatters in comparison to others measurements [75,44].

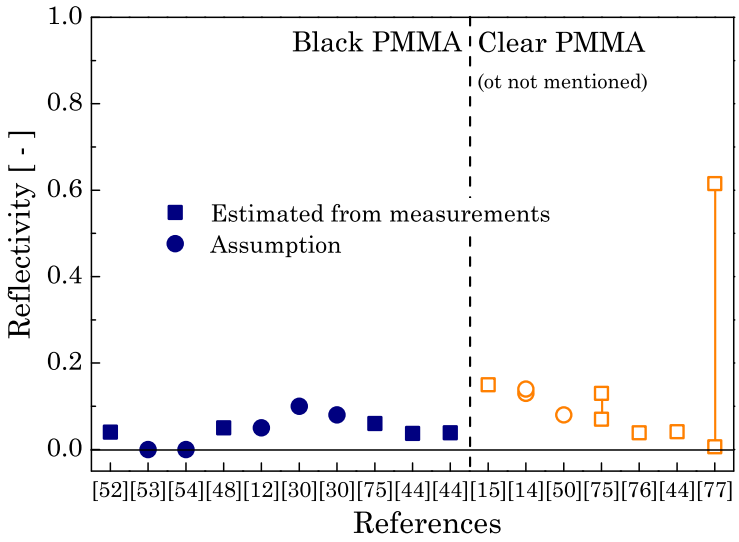

Figure 2.11: Reflectivity coefficients extracted from the literature for black PMMA.

The reflectivity is found slightly higher for clear PMMA than for black PMMA. In fact, as it is explained by Tsilingiris [76], the fraction of radiation non-reflected at the surface travels inside the medium and a part is reflected by the back surface (internal reflection), crossing again the sample to exit the front surface. This process of internal reflexion is function of the absorbance of the sample. The measurements performed with an integrating sphere correspond to

the summation of the different radiations reflected by the front or back surfaces. A higher value of the reflectivity of clear PMMA samples provides a hint on its lower absorbance.

A fundamental study [78 (chap 7)] on the radiative properties of clear PMMA shows that knowledge of the spectral distribution of the attenuation coefficient κ_λ (inverse of the mean distance before absorption or scattering) enables the characterization of the absorbance as function of the sample thickness L (Eq. 2.8).

$$\alpha_\lambda = 1 - (1 - r)^2 \exp(-\kappa_\lambda L) - r \qquad (2.8)$$

κ_λ is an intensive parameter but its effective value $\bar{\kappa}$ (broadband average) appears to be extensive as presented by Linteris et al. [44]. The current pyrolysis models, except in a few studies [27,79], allow only the use of a scalar value of the attenuation coefficient. As a consequence, the dependence of $\bar{\kappa}$ to L has to be neglected and this parameter is used often as a potentiometer [18 (chap 1),30]. Figure 2.12 gathers the different values of $\bar{\kappa}$ found in the literature for black PMMA. They range between 333 and 5340 m^{-1}. A similar graph can be obtained for clear PMMA except that lower values would be found (e.g. 10 m^{-1} [74 (chap 6)]).

The symbols in Fig. 2.12 represent measurements of $\bar{\kappa}$ carried out for specific thicknesses whereas lines are the results of estimations or optimisations. Their respective length corresponds to the thickness of the sample on which the optimisation has been performed. The optimised values agree with the global trend obtained with measurements. The high values of $\bar{\kappa}$ reported for small thicknesses demonstrate that a large part of the energy is absorbed close to the surface. By using a small value for thick sample, as suggested by Fig. 2.12, the energy absorption cannot be correctly modelled (i.e. localisation). The methodological uncertainty imposed by the broadband average of the

attenuation coefficient influences therefore the temperature evolution inside the sample.

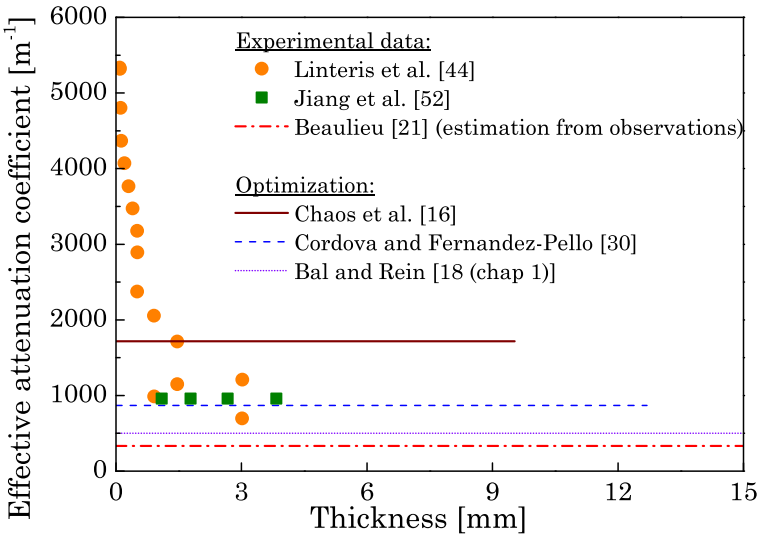

Figure 2.12: Effective attenuation coefficients extracted from the literature for black PMMA.

Moreover, although the impact of the radiative properties is well understood at ambient conditions, there is a significant absence of studies on the temperature dependency of these properties and also on the effect of the bubbles produced by the degradation process. Försth and Roos [75] are the first presenting an analysis on the bubbles impact by measuring the absorbance of PMMA samples after different exposition duration to a constant heat flux level. From their experiments using a cone calorimeter, it seems that for clear and black PMMA, the influence of bubbles is negligible.

4.4. Convective heat transfer coefficient

Newton's law is used to assess the convective heat losses (Eq. 2.2). The convective heat transfer coefficient h is a function of the gas velocity, the solid geometry and the temperature of both phases. Some standard experimental procedures imposed forced flow like ASTM E2058 [80] (used with the Fire Propagation Apparatus) whereas others like ASTM E1354 [81] (use with the

Cone Calorimeter) use only natural flow. From the fire literature, it appears that h is either estimated through theoretical correlations [54] or estimated by the inverse resolution of an energy balance on a piece of metal exposed to a constant external heat flux level [82-85]. The values found for h in the literature are reported on Fig. 2.13 with a few sets of available correlations between h and T_S. h varies between 3.5 and 34 W/(m².K) in the studies considered in Fig. 2.13.

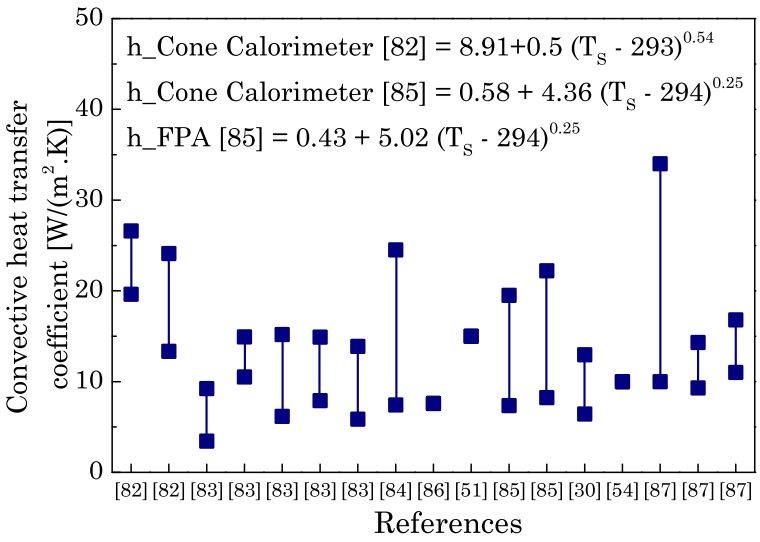

Figure 2.13: Convective heat transfer coefficients extracted from the literature for bench-scale tests.

While h is generally taken as constant in pyrolysis models, it changes according to the experimental conditions (e.g. flow velocity or heat flux level). The difference of the convective loses between vertical and horizontal sample configurations is often ignored whereas it can explain, at least, part of the differences in surface temperature [25].

4.5. Heat of pyrolysis

The heat of pyrolysis corresponds to the amount of energy required to convert a unit of solid mass to pyrolysis gas when this one is already at its pyrolysis temperature. This is different from the heat of gasification which includes also the energy required to heat the solid sample from ambient

temperature to its pyrolysis temperature. Staggs [53] and Stoliarov and Walters [59] provide excellent reviews on the heat of gasification with the methodology to extract it. In his review, Staggs [53] is looking at the methodological uncertainty associated with the definition and extraction of the heat of gasification.

Both heat of pyrolysis and heat of gasification are mainly obtained from DSC (Differential Scanning Calorimetry) analyses. The different values reported in the literature are gathers in Fig. 2.14. The ranges for the heat of pyrolysis and heat of gasification are respectively [0.42 ; 1.007] kJ/g and [1.42 ; 2.77] kJ/g.

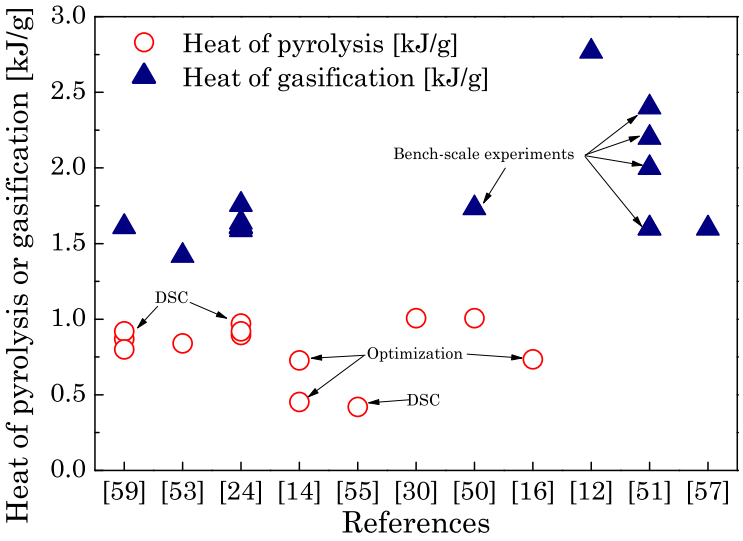

Figure 2.14: Heat of pyrolysis and gasification extracted from the literature for PMMA.

4.6. Incident heat flux level

The applied heat flux level is usually calibrated using a heat flux gauge [80,81] with an uncertainty of ± 3 %. However, the variability of the actual heat flux received by the sample (in comparison to applied heat flux) is much higher due to gas phase absorption. Kashiwagi [88] observed using an electrical conical heater at 40 kW/m² (coils at 700 °C) a reduction of 35 % of the incident heat flux (horizontal configuration for the sample) prior to auto-ignition but almost no absorption was measured for two-thirds of the exposure duration. More recently, Zhou et al. [89] have measured a reduction only up to 10 % of the incident

radiative heat flux before auto-ignition of horizontal PMMA slabs using also an electrical resistance operating between 600 and 1000 °C (26 to 57 kW/m²). Vovelle et al. [50], for vertical orientation and similar range of heat flux levels (30 kW/m² with a heater temperature estimated at 635 °C) did not observe such reduction. Due to the large number of measurements performed by Zhou et al. [89], the range of reduction is estimated to be of the order of 10 %.

The prediction of the actual heat flux received with time required the resolution of the gas phase and the consideration of the complex spectral distribution of MMA radiative properties [90]

Kashiwagi studied [57] the influence of the sample orientation on this phenomenon and found that a horizontal sample was more affected. This is related to the length of the pyrolysis gases plume crossed by the radiation which is lower for vertical sample.

Finally, a change in the spectral emission of the heat source can affect the energy absorption through the process of in-depth radiation (location and magnitude). This change of temperature evolution was demonstrated to influence the sample pyrolysis behaviour [74 (chap 6)].

4.7. Range of variability

Based on the different sections presented above, variability ranges are estimated in Table 2.3 for each of the common input parameters. In the ranges proposed, outliers have been removed. Except Steinhaus [48] who performed a similar analysis for the thermophysical properties of PMMA, the identification of the parameter variability is often ignored.

This variability is not only the result of differences in the sample properties. The change in the experimental conditions (e.g. heating rate or atmospheric composition in TGA) and the required simplifications in the extraction models provoke experimental and methodological uncertainties. The spread of possible values for one parameter reflects these uncertainties.

Table 2.3: Ranges of variability extracted from the literature for the main input parameters of pyrolysis models applied to PMMA samples.

Parameter			Range
Thermal conductivity	k	[W/(m.K)]	[0.13 ; 0.27]
Specific heat	c	[J/(kg.K)]	[1200 ; 3050]
Density	ρ	[kg/m^3]	[1000 ; 1220]
Effective attenuation coefficient (black PMMA)	$\bar{\kappa}$	[m^{-1}]	[333 ; 5340]
Surface temperature at ignition	$T_{s\,ign}$	[K]	[523 ; 673]
Mass flux at ignition	$\dot{m}''_{F\,ign}$	[g/(m^2.s)]	[1.00 ; 5.6]
Heat transfer coefficient	H	[W/(m^2.K)]	[3.5 ; 34]
Activation energy	E_a	[kJ/mol]	[31 ; 290]
Pre-exponential factor	A	[s^{-1}]	[$1.1 \cdot 10^0$; $4.50 \cdot 10^{23}$]
Order of reaction	n	[-]	[0.5 ; 2.2]
Reflectivity coefficient	r	[-]	[0 ; 0.15]
Heat flux	$\dot{q}''_e$	[kW/m^2]	[-13 % ; +3 %]
Heat of pyrolysis	ΔH_p	[kJ/g]	[0.42 ; 1.007]

The problem arises when the parameter uncertainty accumulates in a model output. As model complexity growths, the number of parameters is increased as well and the parameter uncertainty can balance the improvement obtained by a better mathematical formulation of the phenomenon (i.e. more mechanisms implemented).

While the use of the simplest models, already developed decades ago, can include error in the prediction due to the simplicity of it mechanisms, direct use of the most complex models ("brute force") has the potential of leading to spurious results due to the parameter uncertainty. This emphasizes that the appropriate level of complexity results from a balance between mechanisms simplicity and parameter uncertainty. It is therefore essential to assess the prediction uncertainty and the parameters which are responsible for this uncertainty. These investigations require performing sensitivity and uncertainty analyses which are the scope of the following chapter [91 (chap 3)].

5. Conclusion

The prediction of solid ignition is complex since it requires the full characterization of the condensed phase and the gas phase. While the phenomena occurring in both phases are generally understood philosophically, the mathematical formulation of some mechanisms is still ill-defined (e.g. bubbles formation). Moreover, the fine resolution that is required to predict accurately the occurrence of a sustainable flame above the solid is not possible for most of the engineering applications due to the resources needed. Simplifications in the models are therefore unavoidable. The effects of the mechanisms which are not explicitly embedded in pyrolysis models are implicitly considered in the values attributed to the input parameters. These assumptions generate therefore uncertainties in the parameter. As an example, the ignorance of the gas phase implies that the onset of ignition is defined by a condensed phase criterion which is shown to vary when external parameters are changed.

The parameter uncertainty is also a function of the means used to extract their values. While the use of independent experiments is expected to be the best solution for calibration, this methodology is not error free and the significant amount of resources that it requires encourage modellers to use others techniques such as inverse modelling, expert judgment or simply to pick up the parameter values from the database available in the literature. It was demonstrated that every methodology owns some drawbacks and induces methodological and experimental uncertainties which also results in parameter uncertainties

The parameter uncertainty propagates through the model. In order to assess the prediction uncertainty associated with a model, the ranges of variability of its input parameters need to be established. This has been carried out in this chapter for the most common input parameters of models predicting the ignition of PMMA samples.

Based on the parameter uncertainty reported in this chapter, a detailed investigation of the prediction uncertainty associated with the simple pyrolysis model used by Bal and Rein [18 (chap 1)] is performed in the following chapter [91 (chap 3)].

Finally, the present literature review emphasizes some issues such as the variability of the chemical degradation scheme, the gas phase absorption and the influence of bubbles and temperature gradient on the radiative properties. These mechanisms need particular attention in the future.

References

[1] J.L. Torero, Flaming ignition of solid fuels, in: The SFPE handbook of fire protection engineering 4th edition, P.J. DiNenno et al. (Eds.), National Fire Protection Association, 2008, chapter 2.11, pp. 2.260-2.278, ISBN-10: 0877658218.

[2] V. Babrauskas, Ignition of common solids, in: Ignition handbook: Principles and Applications to Fire Safety Engineering, Fire Investigation, Risk Management and Forensic Science, Fire science publishers, 2003, chapter 7, pp. 234-351, ISBN-10:0972811133.

[3] J.G. Quintiere, Ignition of solids, in: Fundamentals of fire phenomena, John Wiley and sons Ltd, 2006, chapter 7, pp. 159-190, ISBN-10 0-470-09113-4.

[4] A. Atreya, Ignition of fires, Philosophical transactions: Mathematical, physical and engineering sciences 356 (1998) 2787-2813, http://www.jstor.org/stable/55049.

[5] T. Kashiwagi, Polymer combustion and flammability – Role of the condensed phase, Proceedings of the symposium (international) on combustion 25 (1994) 1423-1437, http://dx.doi.org/10.1016/S0082-0784(06)80786-1.

[6] A.C. Fernandez-Pello, On fire ignition, Fire safety science 10 (2011) 25-42, http://dx.doi.org/10.3801/IAFSS.FSS.10-25.

[7] D. Drysdale, An introduction to fire dynamics, 3rd edition. Wiley, 2011, ISBN-10:0470319038.

[8] E. Kim, N. Dembsey and M. Janssens, SFPE Engineering guide for estimating material pyrolysis properties for fire modelling, Draft version 10012011, 2011.

[9] C. Lautenberger, A generalized pyrolysis model for combustible solids, PhD Dissertation, The University of California, 2007 <http://escholarship.org/uc/item/7wz5m7dg>.

[10] R.E. Lyon and J.G. Quintiere, Criteria for piloted ignition of combustible solids, Combustion and flame 151 (2007) 551-559, http://dx.doi.org/10.1016/j.combustflame.2007.07.020.

[11] R.T. Long, An evaluation of the lateral ignition and flame spread test for material flammability assessment for mico-gravity environments, Master dissertation, the University of Maryland, 1998.

[12] B.T. Rhodes and J.G. Quintiere, Burning rate and flame heat flux for PMMA in a cone calorimeter, Fire safety journal 26 (1996) 221-240, http://dx.doi.org/10.1016/S0379-7112(96)00025-2.

[13] S.R. Wasan, P. Rauwoens, J. Vierendeels and B. Merci, An enthalpy-based pyrolysis model for charring and non-charring materials in case of fire, Combustion and flame 157 (2010) 715-734, http://dx.doi.org/10.1016/j.combustflame.2009.12.007.

[14] C. Lautenberger and C. Fernandez-Pello, Generalized pyrolysis model for combustible solids, Fire safety journal 44 (2009) 819-839, http://dx.doi.org/10.1016/j.firesaf.2009.03.011.

[15] S.I. Stoliarov, S. Crowley, R.E. Lyon and G.T. Linteris, Prediction of the burning rates of non-charring polymers, Combustion and flame 156 (2009) 1068-1083, http://dx.doi.org/10.1016/j.combustflame.2008.11.010.

[16] M. Chaos, M.M. Khan, N. Krishnamoorthy, J.L. De Ris and S.B. Dorofeev, Evaluation of optimization schemes and determination of solid fuel properties for CFD fire models using bench-scale pyrolysis tests, Proceedings of the Combustion Institute 33 (2011) 2599-2606, http://dx.doi.org/10.1016/j.proci.2010.07.018.

[17] K. McGrattan, S. Hostikka, J. Floyd, H. Baum, R. Rehm, W. Mell and R. McDermott, Fire dynamics simulator (version 5) technical reference guide volume 1: Mathematical model, NIST internal publication 1018-5, 2010.

[18] N. Bal and G. Rein, Numerical investigation of the ignition delay time of a translucent solid at high radiant heat fluxes, Combustion and flame 158 (2011) 1109-1116, http://dx.doi.org/10.1016/j.combustflame.2010.10.014.

[19] J.L. Cordova, D.C. Walther, J.L. Torero and A.C. Fernandez-Pello, Oxidizer flow effects on the flammability of solid combustibles, Combustion science and technology 164 (2001) 253-278, http://dx.doi.org/10.1080/00102200108952172.

[20] V. Babrauskas and W. J. Parker, ignitability measurements with the Cone Calorimeter, Fire and materials 11(1987) 31-43, http://dx.doi.org/10.1002/fam.810110103.

[21] P.A. Beaulieu, Flammability Characteristics at Heat Flux Levels up to 200 kW/m^2 and the Effect of Oxygen on Flame Heat Flux, PhD Dissertation, Worcester Polytechnic Institute, 2005, <http://www.wpi.edu/Pubs/ETD/Available/etd-121905-082146/unrestricted/beaulieu.pdf>.

[22] J.R. Hallman, Ignition characteristics of plastics and rubber, PhD Dissertation, The University of Oklahoma, 1971.

[23] T. Kashiwagi and A. Omori, Effects of thermal stability and melt viscosity of thermoplastics on piloted ignition, Proceedings of the symposium (international) on combustion 22 (1988) 1329-1338, http://dx.doi.org/10.1016/S0082-0784(89)80144-4.

[24] A. Tewarson and S.D. Ogden, Fire behaviour of polymethylmethacrylate, Combustion and flame 89 (1992) 237-259, http://dx.doi.org/10.1016/0010-2180(92)90013-F.

[25] H.E. Thomson and D.D. Drysdale, Effect of sample orientation on the piloted ignition of PMMA, Proceedings of the 5th international Interflam conference (1990) 35-42, The University of Edinburgh, UK.

[26] S. McAllister, C. Fernandez-Pello, D. Urban and G. Ruff, The combined effect of pressure and oxygen concentration on piloted ignition of a solid combustible, Combustion and flame 157 (2010) 1753-1759, http://dx.doi.org/10.1016/j.combustflame.2010.02.022.

[27] Y.Y. Zhou, D.C. Walther and A.C. Fernandez-Pello, Numerical analysis of piloted ignition of polymeric materials, Combustion and flame 131 (2002) 147-158, http://dx.doi.org/10.1016/S0010-2180(02)00396-6.

[28] H.E. Thomson and D.D. Drysdale, Flammability of plastics I: Ignition temperatures, Fire and materials 11 (1987) 163-172, http://dx.doi.org/10.1002/fam.810110402.

[29] D.D. Drysdale and H.E. Thomson, Flammability of plastics II: Critical mass flux at the firepoint, Fire safety journal 14 (1989) 179–188, http://dx.doi.org/10.1016/0379-7112(89)90071-4.

[30] J.L. Cordova and C. Fernandez-Pello, Convection effects on the endothermic gasification and piloted ignition of a radiatively heated combustible solid, Combustion science and technology 156 (2000) 271-289, http://dx.doi.org/10.1080/00102200008947306.

[31] K-C Tsai, Orientation effect on cone calorimeter test results to assess fire hazard of materials, Journal of hazardous materials 172 (2009) 763-772, http://dx.doi.org/10.1016/j.jhazmat.2009.07.061.

[32] S. Fereres, C. Lautenberger, C. Fernandez-Pello, D. Urban and G. Ruff, Mass flux at ignition in reduced pressure environments, Combustion and flame 158 (2011) 1301-1306, http://dx.doi.org/10.1016/j.combustflame.2010.11.013.

[33] T-H. Tsai, M-J. Li, I-Y Shih, R. Jih and S-C. Wong, Experimental and numerical study of autoignition and pilot ignition of PMMA plates in a cone calorimeter, Combustion and flame 124 (2001) 466-480, http://dx.doi.org/10.1016/S0010-2180(00)00219-4.

[34] B.T. Rhodes, Burning rate and flame heat flux for PMMA in the Cone Calorimeter, Master dissertation, The University of Maryland, 1994.

[35] D.J. Rasbash, D.D. Drysdale and D. Deepak, Critical heat and mass transfer at pilot ignition and extinction of a material, Fire safety journal 10 (1986) 1-10, http://dx.doi.org/10.1016/0379-7112(86)90026-3.

[36] D. Rich, C. Lautenberger, J.L. Torero, J.G. Quintiere and C. Fernandez-Pello, Mass flux of combustible solids at piloted ignition, Proceedings of the Combustion Institute 31 (2007) 2653-2660, http://dx.doi.org/10.1016/j.proci.2006.08.055.

[37] J. Panagiotou and J.G. Quintiere, Generalizing flammability of material, Proceedings of the 10th international Interflam conference (2004) 895-905, The University of Edinburgh, UK.

[38] T. Kashiwagi, A. Inaba and J.E. Brown, Differences in PMMA degradation characteristics and their effects on its fire properties, Fire safety science 1 (1986) 483-493, http://dx.doi.org/10.3801/IAFSS.FSS.1-483.

[39] M. Comuce, T. Rogaume, F. Richard, T. Fateh, J. Luche and P. Rousseaux, Kinetics and mechanisms of the thermal degradation of Polymethyl Methacrylate by TGA/FTIR analysis, Proceedings of the sixth international seminar on Fire and Explosion Hazards (2011) 560-570, The University of Leeds, UK.

[40] T. Kashiwagi and T.J. Ohlemiller, A study of oxygen effects on nonflaming transient gasification of PMMA and PE during thermal irradiation, Proceedings of the symposium (international) on combustion 19 (1982) 815-823, http://dx.doi.org/10.1016/S0082-0784(82)80257-9.

[41] T. Kashiwagi, A. Omori and H. Nanbu, Effects of melt viscosity and thermal stability on polymer gasification, Combustion and flame 81 (1990) 188-201, http://dx.doi.org/10.1016/0010-2180(90)90063-W.

[42] T. Hirata, T. Kashiwagi and J.E. Brown, Thermal and oxidative degradation of Poly(methyl methacrylate): Weight loss, Macromolecules 18 (1985) 1410-1418, http://dx.doi.org/10.1021/ma00149a010.

[43] R.E. Lyon, N. Safronava and E. Oztekin, A simple method for determining kinetic parameters for materials in fire models, Fire safety science 10 (2011) 765-777, http://dx.doi.org/10.3801/IAFSS.FSS.10-765.

[44] G. Linteris, M. Zammarano, B. Wilthan and L. Hanssen, Absorption and reflection of infrared radiation by polymers in fire-like environments, Fire and materials 36 (2012) 537-553, http://dx.doi.org/10.1002/fam.1113.

[45] N. Oreskes, K. Shrader-Frechette and K. Belitz, Verification, Validation, and Confirmation of Numerical Models in the Earth, Science, New Series 263 (1994) 641-646, http://dx.doi.org/10.2307/2883078

[46] C. Lautenberger and C. Fernandez-Pello, Optimization algorithms for material pyrolysis property estimation, Fire safety science 10 (2011) 751-764, http://dx.doi.org/10.3801/IAFSS.FSS.10-751.

[47] G. Rein, C. Lautenberger, A.C. Fernandez-Pello, J.L. Torero and D.L. Urban, Application of genetic algorithms and thermogravimetry to determine the kinetics of polyurethane foam in smoldering combustion, Combustion and flame 146 (2006) 95-108, http://dx.doi.org/10.1016/j.combustflame.2006.04.013.

[48] T. Steinhaus, Evaluation of the Thermophysical Properties of Poly(Methyl Methacrylate): A Reference Material for the Development of a Flammability Test for Micro-Gravity Environments, Master dissertation, The University of Maryland, 1999. <http://www.era.lib.ed.ac.uk/handle/1842/2831>.

[49] M.J. Assael, S. Botsios, K. Gialou and I.N. Metaxa, Thermal conductivity of polymethyl methacrylate (PMMA) and Borosilicate crown glass BK7, International journal of thermoplastics 26 (2005) 1595-1605, http://dx.doi.org/10.1007/s10765-005-8106-5.

[50] C. Vovelle, J-L Delfau, M. Reuillon, J. Bransier and N. Laraqui, Experimental and numerical study of the thermal degradation of PMMA, Combustion science and technology 53 (1987) 187-201, http://dx.doi.org/10.1080/00102208708947026.

[51] P.A. Beaulieu and N.A. Dembsey, Flammability characteristics at applied heat flux levels up to 200 kW/m^2, Fire and materials 32 (2008) 61-86, http://dx.doi.org/10.1002/fam.948.

[52] F. Jiang, J.L. De Ris and M.M. Khan, Absorption of thermal energy in PMMA by in-depth radiation, Fire safety journal 44 (2009) 106-112, http://dx.doi.org/10.1016/j.firesaf.2008.04.004.

[53] J.E.J Staggs, The heat of gasification of polymers, Fire safety journal 39 (2004) 711-720, http://dx.doi.org/10.1016/j.firesaf.2004.07.001.

[54] D. Hopkins and J.G. Quintiere, Material fire properties and predictions for thermoplastics, Fire safety journal 26 (1996) 241-268, http://dx.doi.org/10.1016/S0379-7112(96)00033-1.

[55] K.D. Steckler, T. Kashiwagi, H.R. Baum and K. Kanemaru, Analytical model for transient gasification of noncharring thermoplastic materials, Fire safety science 3 (1991) 895-904, http://dx.doi.org/10.3801/IAFSS.FSS.3-895.

[56] M. Hu, D. Yu and J. Wei, Thermal conductivity determination of small polymer samples by differential scanning calorimetry, Polymer testing 26 (2007) 333-337, http://dx.doi.org/10.1016/j.polymertesting.2006.11.003.

[57] T. Kashiwagi, Effects of sample orientation on radiative ignition, Combustion and flame 44 (1982) 223-245, http://dx.doi.org/10.1016/0010-2180(82)90075-X.

[58] S. Rudtsch and U. Hammerschmidt, Intercomparison of measurements of the thermophysical properties of polymethyl methacrylate, International journal of thermophysics 25 (2004) 1475-1482, http://dx.doi.org/10.1007/s10765-004-5752-y.

[59] S.I. Stoliarov and R.N. Walters, Determination of the heats of gasification of polymers using differential scanning calorimetry, Federal Aviation Administration internal report DOT/FAA/AR-TN07/62, 2007.

[60] S.I. Stoliarov, N. Safronava and R.E. Lyon, The effect of variation in polymer properties on the rate of burning, Fire and materials 33 (2009) 257-271, http://dx.doi.org/10.1002/fam.1003.

[61] Y. Agari, A. Ueda, Y. Omura and S. Nagai, Thermal diffusivity and conductivity of PMMA/PC blends, Polymer 38 (1997) 801-807, http://dx.doi.org/10.1016/S0032-3861(96)00577-0.

[62] R. Orwoll, Densities, coefficients of thermal expansion, and compressibilities of amorphous polymers, in: J.E. Mark (Ed.), Physical properties of polymer handbook 2nd edition, Springer, 2007, pp. 93-101, http://dx.doi.org/10.1007/978-0-387-69002-5_7.

[63] S.M. Dakka, Kinetic pyrolysis of poly(methyl methacrylate) and its effects on the ignition delay time, PhD Dissertation, The University of Maryland, 2002.

[64] M. Ferriol, A. Gentilhomme, M. Cochez, N. Oget and J.L. Mielosszynski, Thermal degradation of poly(methyl methacrylate) (PMMA): modelling of DTG and TG curves, Polymer degradation and stability 79 (2003) 271-281, http://dx.doi.org/10.1016/S0141-3910(02)00291-4.

[65] S.M. Dakka, G.S. Jackson and J.L. Torero, Mechanisms controlling the degradation of poly(methyl methacrylate) prior to piloted ignition, Proceedings of the Combustion Institute 29 (2002) 281–287, http://dx.doi.org/10.1016/S1540-7489(02)80038-4.

[67] Z. Gao, T. Kaneko, D. Hou and M. Nakada, Kinetics of thermal degradation of poly(methyl methacrylate) studied with the assistance of the fractional conversion at the maximum reaction rate, Polymer degradation and stability 84 (2004) 399-403, http://dx.doi.org/10.1016/j.polymdegradstab.2003.11.015.

[68] B.J Holland and J.N Hay, The value and limitations of non-isothermal kinetics in the study of polymer degradation, Thermochimica acta 388 (2002) 253-273, http://dx.doi.org/10.1016/S0040-6031(02)00034-5.

[69] S. Vyazovkin and C.A. Wight, Kinetics in solids, Annual reviews of physical chemistry 48 (1997) 125-149, http://dx.doi.org/10.1146/annurev.physchem.48.1.125.

[70] R.E. Lyon, N. Safronava and S.I. Stoliarov, The role of thermal decomposition kinetics in the burning of polymers, Proceedings of the 12th international Interflam conference (2010) 463-474, The University of Nottingham, UK.

[71] A. Kashani and J.A. Esfahani, Interactive effect of oxygen diffusion and volatiles advection on transient thermal degradation of poly methyl methacrylate (PMMA), Heat and mass transfer 44 (2008) 641-650, http://dx.doi.org/10.1007/s00231-007-0293-0.

[72] C.P. Brescianini, G.H. Yeoh, V. Chandrasekarani and R. Yuen, A numerical model for pilot ignition of PMMA in a Cone Calorimeter, Combustion science and technology 129 (1997) 312-345, http://dx.doi.org/10.1080/00102209708935731.

[73] C. Di Blasi, S. Crescitelli, G. Russo and G. Clinque, Numerical model of ignition processes of polymeric materials including gas-phase absorption of radiation, Combustion and flame 83 (1991) 333-344, http://dx.doi.org/10.1016/0010-2180(91)90080-U.

[74] P. Girods, N. Bal, H. Biteau, G. Rein and J.L. Torero, Comparison of pyrolysis behaviour results between the Cone Calorimeter and the Fire Propagation Apparatus heat sources, Fire safety science 10 (2011) 889-901, http://dx.doi.org/10.3801/IAFSS.FSS.10-889.

[75] M. Försth and A. Roos, Absorptivity and its dependence on heat source temperature and degree of thermal breakdown, Fire and materials 35 (2011) 285-301, http://dx.doi.org/10.1002/fam.1053.

[76] P.T. Tsilingiris, Comparative evaluation of the infrared transmission of polymer films, Energy conversion and management 44 (2003) 2839-2856 http://dx.doi.org/10.1016/S0196-8904(03)00066-9.

[77] S.S. Manohar, A.K. Kulkarni and S.T. Thynell, In-depth absorption of externally incident radiation in nongray media, Journal of heat transfer 117 (1995), 146-152, http://dx.doi.org/10.1115/1.2822295.

[78] N. Bal, Experimental study of radiative heat transfer in a translucent fuel sample exposed to different spectral sources (chapter 7), Uncertainty and complexity in pyrolysis modelling, The University of Edinburgh, 2012.

[79] Y. Sohn, S.W. Baek and T. Kashiwagi, Transient modelling of thermal degradation in non-charring solids, Combustion science and technology 145 (1999) 83-108, http://dx.doi.org/10.1080/00102209908924204.

[80] ASTM E2058-03: Standard test method for measurement of synthetic polymer material flammability using a Fire Propagation Apparatus, ASTM International, West Conshohocken PA, 2003, http://dx.doi.org/10.1520/E2058-03.

[81] ASTM E1354-10a: Standard test method for heat and visible smoke release rates for materials and products using an oxygen consumption calorimeter", ASTM International, West Conshohocken PA, 2010, http://dx.doi.org/10.1520/E1354-10A.

[82] J.E.J. Staggs, Convection heat transfer in the cone calorimeter, Fire safety journal 44 (2009) 469-474, http://dx.doi.org/10.1016/j.firesaf.2008.10.002.

[83] J. Zhang and M.A. Delichatsios, Determination of the convective heat transfer coefficient in three-dimensional inverse heat conduction problems, Fire safety journal 44 (2009) 681-690, http://dx.doi.org/10.1016/j.firesaf.2009.01.004.

[84] J.E.J. Staggs, A reappraisal of convection heat transfer in the cone calorimeter, Fire safety journal 46 (2011) 125-131, http://dx.doi.org/10.1016/j.firesaf.2010.12.002.

[85] T. Steinhaus, Determination of intrinsic material flammability properties from material tests assisted by numerical modelling, PhD dissertation, The University of Edinburgh, 2009.

[86] J.L. De Ris and M.M. Khan, A sample holder for determining material properties, Fire and materials 24 (2000) 219-226, http://dx.doi.org/10.1002/1099-1018(200009/10)24:5<219::AID-FAM741>3.0.CO;2-7.

[87] M. Janssens, C. Gomez, Convective heat transfer in the cone calorimeter revisited, Proceedings of the 12th international Interflam conference (2010) 281-290, The University of Nottingham, UK.

[88] T. Kashiwagi, Experimental observation of radiative ignition mechanisms, Combustion and flame 34 (1979) 231-244, http://dx.doi.org/10.1016/0010-2180(79)90098-1.

[89] Y. Zhou, L. Yang, J. Dai Y. Wang and Z. Deng, Radiation attenuation characteristics of pyrolysis volatiles of solid fuels and their effect for radiant ignition model, Combustion and flame 157 (2010) 167-175, http://dx.doi.org/10.1016/j.combustflame.2009.06.020.

[90] S.H. Park, A.J. Stretion and C.L. Tien, Infrared Radiation Properties of Methyl Methacrylate Vapor, Combustion science and technology 62 (1988) 257-271, http://dx.doi.org/10.1080/00102208808924012.

[91] N. Bal, Pyrolysis modelling up to ignition - Part II: Parametric sensitivity and uncertainty analyses (chapter 3), Uncertainty and complexity in pyrolysis modelling, The University of Edinburgh, 2012.

Chapter 3

Pyrolysis modelling up to ignition – Part II: Parametric sensitivity and uncertainty analyses

Summary

The level of confidence associated with the prediction from a pyrolysis model is a function of the model accuracy but also of the spread of the predictions resulting from the parameter uncertainty. The assessment of this level of confidence requires the quantification of the governing parameters and of the effect of the parameter variability. In this chapter, several parametric sensitivity and uncertainty analyses are performed on a pyrolysis model predicting the delay time to ignition at high heat flux levels for PolyMethylMethAcrylate samples. The results between the different techniques used are complementary and consistent. They show that while the specific heat, the attenuation coefficient, the kinetics, the applied heat flux level and the density have a large influence on the predictions, the uncertainty found in the

literature for the three first parameters is responsible for most of the prediction spread. The influence of the uncertainty associated with the attenuation coefficient is increasing when the applied heat flux increases, whereas an opposite behaviour is observed for the kinetics. The influence of the specific heat stays stable over the range of heat flux studied. When a large set of simulations is performed (random sampling of the input parameters), the interval defined by one standard deviation on either side of the average prediction capture the experimental uncertainties. However, the global dispersion of the predictions is found to be significantly higher than this interval. The investigation reveals therefore that one of the main issues in the prediction of solid ignition based on literature calibration is the uncertainty of the governing parameters.

Collaboration

This chapter results from a joint work performed with Dr Guillermo Rein from the University of Edinburgh (UK).

Nomenclature

A	Pre-exponential factor [s^{-1}]	u	Uncertainty coefficient
c	Specific heat [J/(kg.K)]	w	Mass fraction [-]
E_a	Activation energy [kJ/mol]	X	Input quantity of interest
f	Model	y	Depth [m]
h	Convective heat transfer coef. [W/(m^2.K)]	Y	Output quantity of interest
k	Thermal conductivity [W/(m.K)]	Subscripts	
L	Sample thickness [m]	∞	Ambient conditions
$\dot{m}''$	Mass loss rate [g/(m^2.s)]	i	Parameter
n	Power law [-]	ign	At ignition
$\dot{q}_e''$	Heat flux [kW/m^2]	s	At the surface
r	Surface reflectivity [-]		
R	Ideal gas constant [J/(K.mol)]	Greek symbols	
s	Sensitivity coefficient	κ	Attenuation coefficient [m^{-1}]
t	Time [s]	ρ	Density [kg/m^3]
T	Temperature [K]	σ	Stefan-Boltzmann coef. [W/(m^2.K^4)]

1. Introduction

A model is a simplified representation of a phenomenon. The capability of predicting this phenomenon prior its actual realization is of great importance in design and especially in safety fields. However, the predictions extracted from a model are irrelevant if the level of confidence associated is low. This is related to the difference between the concepts of trueness and uncertainty. The first one corresponds to the agreement between the predictions and the experimental results while the second corresponds to the dispersion of the predictions due to the uncertainty associated with the parameters [1]. The last concept should be also included in the validation process of a model.

The parameter uncertainty is function of the technique used to calibrate them. While the determination from direct measurements represents the ideal solution, the values are often difficult to extract due to limitations in the experimental and methodological states-of-the-art (e.g. coupling between different mechanisms, required resources, scale effect or model hypotheses) [2 (chap 2)]. Modellers are therefore obliged to use other methodologies and sources such as inverse modelling, expert judgement and the literature [2 (chap 2)]. The required accuracy for a parameter is a function of its influence (i.e. sensitivity analysis) on the predicted quantity. A parameter having a negligible effect will not provoke a large dispersion of the predictions whatever is its uncertainty and it does not need a particular attention during the calibration process. The relative influence of the input parameters is therefore required to prioritize their determination and optimise the resources available for the model calibration.

In the context of fire safety, the prediction of piloted solid ignition is a challenge due to its importance on fire growth (e.g. initiation, flame spread and secondary ignition). This phenomenon has been subject to intense research for several decades. A theory (called classical ignition theory) expresses the delay time to ignition t_{ign} of thermally thick samples as a function of the applied heat flux $\dot{q}''_e$ (Eq. 3.1). A full description of this theory with a review of the assumptions made can be found elsewhere [3].

$$t_{ign} = k\rho c \frac{\pi}{4} \frac{\left(T_{s\,ign} - T_\infty\right)^2}{\dot{q}_e''^2} \quad (3.1)$$

In this theory, the occurrence of flaming ignition is specified by a surface temperature criterion $T_{s\,ign}$ which is assumed invariant. However, due to the simplifications required to reach the simple analytical solution presented in Eq. 3.1, changes in the ignitability tests (e.g. flow conditions, sample orientation or heater used) provoke some variations of its value [2 (Chap 2)].

While the simple approach of the classical ignition theory provides correct orders of magnitude for most materials and for most parts of the heat flux range encountered in fire safety, it fails to capture the experimental ignition behaviour of translucent polymers at large heat flux levels [4,5]. Jiang et al. [6] have shown that the mechanism of in-depth radiation absorption could explain these experimental observations. This statement has been confirmed and completed by Bal and Rein [7 (chap 1)] who have investigated a large number of condensed phase mechanisms and have found that the only one which was able to explain the discrepancy between the experimental results and the classical ignition theory was in-depth absorption.

Bal and Rein [7 (chap 1)] have confronted the predictions (dashed line in Fig. 3.1) of their simple pyrolysis model including in-depth absorption to more than 250 bench-scale measurements of delay time to ignition for black PolyMethylMethAcrylate (PMMA) samples.

While the model predictions are enclosed inside the experimental uncertainty, traducing the concept of trueness, it is essential to identify the controlling parameters and to assess the influence of the variability (i.e. uncertainty). These investigations represent the scope of this chapter.

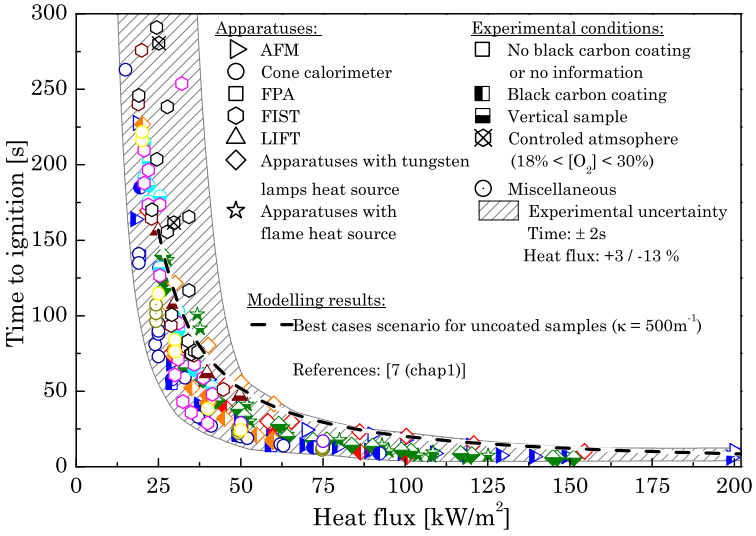

Figure 3.1: Delay times to piloted ignition of black PMMA samples for a wide range of experimental conditions (data from literature).

Linteris [8] conducted a sensitivity analysis on the pyrolysis model Thermakin [9] for the predictions of the delay time to ignition t_{ign} of a non-charring material with nominal properties close to PMMA. Based on variability ranges for the input parameters which have been fixed arbitrary, Linteris [8] has estimated the sensitivity graphically (i.e. qualitative analysis) using a methodology called scatter plot (SP) where only one parameter is varied over its range at the time (more details provided in section 3.1.1). For few input parameters, Linteris [8] has fitted with a power law the evolution of the predicted t_{ign} when the input parameter studied is varied (i.e. quantitative analysis) and compared this power with the theoretical dependency of t_{ign} according to Eq. 3.1. He concluded that the specific heat c has the largest influence on the prediction of t_{ign} and that the uncertainty for the predictions of t_{ign} evolves proportionally to the variation applied to c. By looking the sensitivity of t_{ign} at different heat flux level $\dot{q}''_e$, Linteris [8] observed that the effect of some parameters evolves with the applied heat flux level. This is the case for the thermal conductivity k which presents a decreasing effect when $\dot{q}''_e$ increases.

While the sensitivity analysis performed by Linteris [8] provides good insight on the governing mechanisms, its remains mainly qualitative and the effect of

the different parameters are not linked to the parameter uncertainty to estimate the level of confidence associated with the prediction of the delay time to ignition. Stoliarov et al. [10] have included in their study (using also Thermakin [9]) such approach by looking the difference in the predicted t_{ign} when the parameters are at their nominal value or at the bounds of their respective variability ranges. However, they looked at only one parameter at a time, keeping the other at their nominal values (more details provided in section 3.2.1). Stoliarov et al. [10] used variability ranges for the input parameters which correspond to the values found in the literature for a large variety of polymers, so their results cannot provide information on the uncertainty associated with the predictions of the delay time for one particular material.

In both studies, solid ignition is specified by a critical value of $\dot{m}''_{F\,ign}$. This quantity is predicted in Thermakin [9] by an Arrhenius law. Both modelling teams assumed a correlation, called compensation effect, between the pyrolysis kinetics of the Arrhenius law: the pre-exponential factor A and the activation energy E_a. Linteris [8] used a fixed correlation whereas Stoliarov et al. [10] have considered variations in the correlation. In the present chapter both techniques will be investigated to provide a full characterization of the sensitivity and uncertainty on the prediction of t_{ign}.

A different pyrolysis model is used in this chapter, allowing an inter-model comparison with the studies from Linteris [8] and Stoliarov et al. [10]. Moreover, in this chapter, the predictions of the delay time to ignition are confronted to experimental results at the opposite of both studies previously mentioned. Due to the diversity in the experimental procedures and formulations of black PMMA used in Fig. 3.1, the experimental uncertainty is considered representative of the current experimental state-of-the-art for this material. The level of confidence associated with the pyrolysis model and the uncertainty of its input parameters can therefore be assessed.

2. Piloted ignition model

The one-dimensional model used in this chapter is described in detail elsewhere [7 (chap 1)], however, the equations are presented briefly here for completeness.

A semi-infinite and translucent slab of PMMA, initially at ambient temperature T_∞, is subjected to external radiation $\dot{q}''_e$ on its free surface (y = 0). While a fraction r of the radiation intensity is reflected away at the surface, the remaining part is crossing the solid interface and undergoes an exponential attenuation quantified by the attenuation coefficient κ also called in-depth radiation absorption coefficient (Beer-Lambert's law). The slab loses heat at its free surface due to convection (controlled by a constant heat transfer coefficient h) and re-radiation with an emissivity equivalent to the fraction of radiation not reflected (1 − r) (Kirchhoff's law for opaque material).

The temperature evolution is governed by an energy balance (Eq. 3.2) with its boundary conditions (Eqs. 3.3 and 3.4)

$$\rho c \frac{\partial T(y,t)}{\partial t} = k \frac{\partial^2 T(y,t)}{\partial y^2} + (1-r)\dot{q}''_e \, \kappa \, e^{(-\kappa y)} \tag{3.2}$$

$$\forall t;\ -k\frac{\partial T}{\partial y}\Big|_{y=0} = -h(T_S - T_\infty) - \sigma(1-r)\left(T_S^4 - T_\infty^4\right) \tag{3.3}$$

$$\forall t;\ \frac{\partial T}{\partial y}\Big|_{y=L} = 0 \tag{3.4}$$

The solid decomposition is assumed to follow a 1-step reaction scheme modelled by a first order Arrhenius law (Eq. 3.5).

$$\dot{m}'' = \rho \int_{y=0}^{y=L} A \exp\left(\frac{-E_a}{R\,T(y,t)}\right) w \, dz \tag{3.5}$$

When the pyrolysis gases leave the free surface, they mix with the surrounding air and ignite once a flammable mixture is reached at the pilot

location. A full resolution of the flow, species and temperature fields through momentum, mass transport and gas-phase chemistry equations are required to predict accurately the delay time to ignition [3]. Due to the presence of a pilot and the short distance separating it to the solid free surface (similar in most of the bench-scale apparatuses), the prediction of flaming ignition can be simplified by considering a condensed phase ignition criterion [3]. In this chapter, a critical mass flux of pyrolysis released by the sample $\dot{m}''_{F\,ign}$ is used to define the occurrence of ignition.

The particularity of this model is that mass conservation is neglected (e.g. no surface regression) and the energy sink by endothermicity of the pyrolysis reaction is neglected in the energy balance (Eq. 3.2). Both of these simplifications are justified by the range of applied heat fluxes considered: $\dot{q}''_e \geq 40$ kW/m². At these heat flux levels, the delay time to ignition is short and the surface regression is therefore negligible. The heat losses by the reaction represent less than 10 % of the energy received above 40 kW/m² [7 (chap 1)]. These simplifications able to uncouple the energy balance from the pyrolysis decomposition process.

The model has been calibrated by Bal and Rein [7 (chap 1)] based on the sets of data from Fig. 3.1 corresponding to uncoated samples (opened symbols).

3. Sensitivity and uncertainty analyses: concepts and methodologies

3.1. Sensitivity analyses

A parametric sensitivity study consists of assessing the impact on the output Y of a model f when a small variation is applied to a input parameter X_i. This effect, corresponding to the derivative $\partial f / \partial X_i$, is called sensitivity coefficient s_i [11]. The complexity of some models does not allow the expression of an analytical solution for s_i and needs to be estimated numerically.

Moreover, for non-linear model f, s_i is local and can evolve according to the position of the other parameters in the hyperspace.

Morris [12] identified four different classes for s_i: (#1) negligible suggesting that Y is non-sensitive to X_i, (#2) constant ($\neq 0$) indicating that the effect of X_i is linear and additive, (#3) non-constant function of X_i traducing a non-linear effect and (#4) non-constant function of one or more $X_{j\neq i}$ showing an interaction between the input parameters.

In this study, an increasing complexity of the techniques to assess s_i is explored. However, only a few sets of techniques is investigated. A review of a large number of sensitivity techniques is available elsewhere [13].

3.1.1 Scatter-plot (SP)

This technique consists of representing graphically the evolution of Y while varying only one X_i over its range of potential values and keeping the others constant.

These plots provide double information. First, the sensitivity of the different parameters can be assessed qualitatively. Then, using curve fitting, s_i can be assessed quantitatively by performing the derivative of the obtained best fit function. In this study, only linear and power laws are explored.

3.1.2 One-At-a-Time (OAT)

With this technique, the derivative $\partial f/\partial X_i$ is assessed numerically by estimating Y at the nominal value $X_{i,0}$ and at $(X_{i,0} + \Delta X_i)$. ΔX_i should represent a small variation.

The input parameters X_i do not have the same units and the comparison of their sensitivity is possible only by evaluating a nondimensionalized s_i called effective sensitivity coefficient $\bar{s}_i$ (Eq. 3.6). This is achieved by multiplying s_i by the ratio $X_{i,0}/Y(X_{i,0})$.

$$\bar{s}_i = \frac{Y(X_{i,0}+\Delta X_i)-Y(X_{i,0})}{\Delta X_i}\frac{X_{i,0}}{Y(X_{i,0})} = \frac{f(X_1\ ;\ldots;X_{i,0}+\Delta X_i\ ;X_k)-f(X_1\ ;\ldots;X_{i,0}\ ;X_k)}{\Delta X_i}\frac{X_{i,0}}{Y(X_{i,0})} \quad (3.6)$$

This methodology enables only the quantification of the first order derivatives of a Taylor series expansion of f around the nominal value $X_{i,0}$.

One issue related to this methodology is the determination of ΔX_i. In Eq. 3.6, f is implicitly assumed linear over ΔX_i, which can be reasonably considered for small ΔX_i. However, when $\Delta X_i \to 0$, numerical instabilities appear. As a consequence, $\bar{s}_i$ should be assessed for different ΔX_i to estimate its appropriate value. ΔX_i is taken, in this chapter, as a percentage of $X_{i,0}$.

3.1.3 Design of Experiments (DoE)

With this technique, the understanding is pushed one step further by including the mixed partial derivative of the Taylor series expansion of f. This permits therefore to distinguish the Morris's class #4 (only locally due to the small variations imposed). The concept of DOE is explained in detail somewhere else [14].

3.2. Uncertainty analyses

A parameter is never known with a perfect accuracy. The uncertainty $u(X_i)$ corresponds to the lack of knowledge of the parameter X_i. It represents the dispersion around the quantity (i.e. range of possible value) that results from its calibration. There are two ways to evaluate this uncertainty [11]: the first one is based on repeated observations (i.e. statistics) whereas the second is based on scientific judgement.

The uncertainty on the different parameters $u(X_i)$ induces an uncertainty on the predictions (i.e. spread of the predictions) $u(Y)$. In this chapter, only two techniques are explored to assess the uncertainty on the prediction of t_{ign} but others can be found elsewhere [15].

3.2.1 Prediction intervals

This simple technique consists of assessing the spread of the predictions resulting only from the uncertainty of one parameter $u(X_i)$ while the others parameters are kept constant. The spread represents the largest interval existing between two predictions when only one parameter is varied.

This technique is simple to apply but it does not consider the interactions existing between the different parameters and more important, it neglects the uncertainty associated with the others parameters.

3.2.2 Monte Carlo analysis

Monte Carlo is a more sophisticated methodology for the propagation of uncertainty [16]. In this technique, the value of each parameter is attributed randomly among their respective range of variation. The uncertainty associated with the predicted quantity of interest $u(Y)$ is assessed by performing a large number simulation [16], varying at each simulation the parameter values. The non-linearity of the model f and the interactions between the parameters are therefore considered with the parameter uncertainty. A major drawback of this technique is its computational cost.

4. Input parameters

The model from Bal and Rein [7 (chap 1)] requires 10 parameters: the applied heat flux level $\dot{q}''_e$ [kW/m^2], the thermal conductivity k [W/(m.K)], the specific heat c [J/(kg.K)], the density ρ [kg/m^3], the attenuation coefficient κ [m^{-1}], the critical mass flux at ignition $\dot{m}''_{ign}$ [g/(m^2.s)], the convective heat transfer coefficient h [W/(m^2.K)], the reflectivity coefficient r [-], the pre-exponential factor A [s^{-1}] and the activation energy E_a [kJ/mol].

A detailed literature review of the parameter values has been performed for black PMMA in a previous chapter [2 (chap 2)]. The variability range for each of the parameters is reported in Table 3.1 with their nominal value used to predict

the delay time to ignition (dashed line in Fig. 3.1) of uncoated black PMMA samples (open symbols in Fig. 3.1).

Table 3.1: Input parameters and uncertainty ranges extracted from literature for PMMA samples.

Parameter			Range	Nominal value
Thermal conductivity	k	[W/(m.K)]	[0.13 ; 0.27]	0.21
Specific heat	c	[J/(kg.K)]	[1200 ; 3050]	1664.66
Density	ρ	[kg/m^3]	[1000 ; 1220]	1187.80
Attenuation coefficient	κ	[m^{-1}]	[333 ; 5340]	500
Mass flux at ignition	$\dot{m}''_{ign}$	[g/(m^2.s)]	[1.00 ; 5.6]	2.42
Convective heat transfer coefficient	h	[W/(m^2.K)]	[3.5 ; 34]	10
Activation energy	E_a	[kJ/mol]	[91 ; 290]	125
Pre-exponential factor	A	[s^{-1}]	[$7.6 \cdot 10^5$; $4.6 \cdot 10^{23}$]	$5 \cdot 10^8$
Reflectivity	r	[-]	[0 ; 0.1]	0.055
Heat flux	$\dot{q}''_e$	[kW/m^2]	[-13 % ; +3 %]	[50 - 200]

Reference [2 (Chap 2)]

As demonstrated in the previous chapter [2 (chap 2)], $ln(A)$ and E_a present a strong correlation called compensation effect [10]. This is illustrated in Fig. 3.2 with the data sets of $\{E_a; ln(A)\}$ extracted from the literature for 1-step pyrolysis reaction (PMMA $\rightarrow$ GAS) [2 (chap 2)].

Bal and Rein [7 (chap1)] have calibrated their kinetics couple $\{A; E_a\}$ by fitting their predictions of t_{ign} to the bench-scale measurements from Fig. 3.1 at heat flux levels lower than 70 kW/m^2. It is worth noticing that the values found for $ln(A)$ and E_a match perfectly with the best fit correlation expressed on Fig. 3.2.

For the rest of this chapter, only one parameter is considered for $\{A; E_a\}$. The second is deduced from the best fit correlation suggested in Fig. 3.2 by the continuous line. However, other linear relationships can be fitted between the two dashed lines representing the boundaries of the spread extracted in the

literature for {A; E_a}. The dash-dotted lines in Fig. 3.2 correspond to the extreme correlations. The consequences of the uncertainty on the correlation will be investigated as part of the sensitivity and uncertainty analyses.

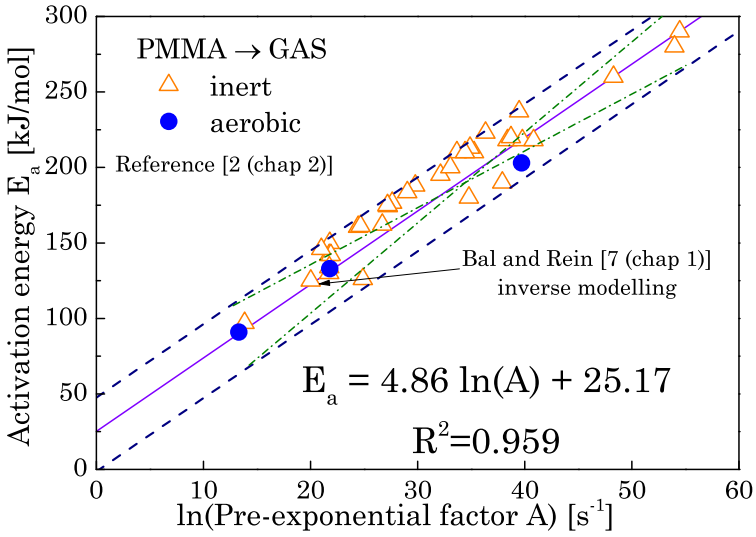

Figure 3.2: Correlation between the Arrhenius kinetics parameters for the chemical decomposition of PMMA samples simulated with 1-step reaction scheme (data extracted from the literature).

5. Results of parametric sensitivity analyses

The three sensitivity techniques presented in section 3.1 are used to assess the governing parameters among the nine required by the model to predict t_{ign} (A and E_a being assumed as one). The study is performed at four different heat flux levels (50, 100, 150 and 200 kW/m²) to assess potential evolution of the sensitivity.

5.1. Scatter plot (SP)

The evolution of the predicted t_{ign} when only one parameter is varying along its variability range (Table 3.1) is assessed for each parameter. An example is plotted in Fig. 3.3 for κ. The dash-dotted lines frame the range of variability of the parameter. In this particular case, the predictions of t_{ign} do not evolve linearly, so $\bar{s}_\kappa$ is not constant and κ belongs to Morris's class #3. The same

non-linear behaviour occurs for $\dot{m}''_{ign}$, the couple $\{A; E_a\}$ and $\dot{q}''_e$. The other parameters have a constant $\bar{s}_i$ and are therefore from Morris's classes #1 or #2. However, this technique cannot state on the parameter belongings to Morris's class #4.

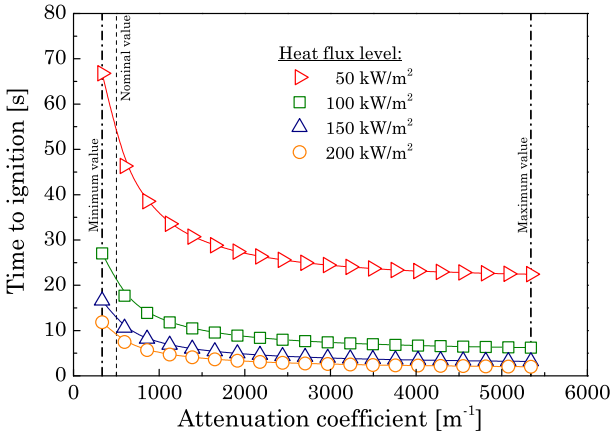

Figure 3.3: Evolution of the predicted delay time to ignition at four heat flux levels over the range of variation of the attenuation coefficient (SP technique).

By fitting the evolution of the predicted t_{ign} to simple relationships such as linear ($g = aX_i + b$) or power ($g = m\,X_i^n$) laws, $\bar{s}_i$ can be expressed quantitatively by multiplying the analytic expression of $\partial g/\partial X_i$ by the ratio $X_{i,0}/Y(X_{i,0})$. For the particular case of the power law, $\bar{s}_i$ is equivalent to the power n.

The results are reported on Table 3.2. For low coefficient of determination R^2 obtained with the best fit, the law was not considered as applicable to the data and "N.A." is reported in Table 3.2.

The laws complement each other since they do not necessarily fit the predictions of the same parameters. In the cases of k, ρ and c, both laws fit and the results present a very good agreement (difference between $\bar{s}_i \leq 10^{-2}$). When none of the laws suits, a more sophisticated sensitivity technique is required to assess $\bar{s}_i$.

Table 3.2: Effective sensitivity coefficient $\bar{s}_i$ from SP and OAT techniques.

		Applied heat flux [kW/m²]	k [W/(m.K)]	c[J/(kg.K)]	ρ [kg/m³]	κ [1/m]	r [-]	$\dot{m}''_{ign}$ [g/(m².s)]	h [W/(m².K)]	{A ; E} [1/s;kJ/mol]	$\dot{q}''_e$ [kW/m²]
SP	Power law	50	0.26	1	0.88	N.A.	N.A.	0.12	N.A.	N.A.	-1.47
		100	0.17	1	0.90	N.A.	N.A.	0.10	N.A.	N.A.	-1.29
		150	0.14	1	0.90	N.A.	N.A.	0.10	N.A.	N.A.	-1.22
		200	0.11	1	0.90	N.A.	N.A.	0.09	N.A.	N.A.	-1.19
	Linear law	50	0.27	1.00	0.89	N.A.	$7.9 \cdot 10^{-2}$	N.A.	$7.9 \cdot 10^{-2}$	N.A.	N.A.
		100	0.18	1.00	0.90	N.A.	$7.2 \cdot 10^{-2}$	N.A.	$4.1 \cdot 10^{-2}$	N.A.	N.A.
		150	0.15	1.01	0.90	N.A.	$6.9 \cdot 10^{-2}$	N.A.	$2.9 \cdot 10^{-2}$	N.A.	N.A.
		200	0.12	0.99	0.91	N.A.	$6.7 \cdot 10^{-2}$	N.A.	$2.3 \cdot 10^{-2}$	N.A.	N.A.
OAT		50	0.27	1.01	0.87	-0.60	$7.8 \cdot 10^{-2}$	0.12	$7.8 \cdot 10^{-2}$	0.20[a] (-1.03 ; 1.33)[b]	-1.41
		100	0.18	1	0.9	-0.70	$7.4 \cdot 10^{-2}$	0.10	$4.0 \cdot 10^{-2}$	0.14 [a] (-0.88 ; 1.16) [b]	-1.26
		150	0.14	0.99	0.89	-0.74	$6.6 \cdot 10^{-2}$	$8.9 \cdot 10^{-2}$	$2.5 \cdot 10^{-2}$	0.13 [a] (-0.79 ; 1.11) [b]	-1.18
		200	0.12	0.99	0.89	-0.77	$7.0 \cdot 10^{-2}$	$9.3 \cdot 10^{-2}$	$2.3 \cdot 10^{-2}$	0.093[a] (-0.79 ; 1.06) [b]	-1.14

[a] $\bar{s}_i$ obtained from best fit linear correlation in Fig. 3.2.
[b] Range of variation of $\bar{s}_i$ due to possible linear correlations between $ln(A)$ and E_a.

5.2. One-At-a-Time (OAT)

This methodology enables, whatever is the law of evolution of t_{ign}, the assessment of $\bar{s}_i$ using Eq. 3.6. The main issue of this technique is the definition of ΔX_i. In case of a non-linear law, $\bar{s}_i$ evolves until it reaches a stable value for small ΔX_i corresponding to the actual tangent to the curve t_{ign} versus X_i at $X_{i,0}$. An example of this behaviour is plotted Fig. 3.4 for κ. The results for $\bar{s}_i$ are reported in Table 3.2. Figure 3.4 demonstrates that using a high ΔX_i for κ results in an overestimation of $\bar{s}_\kappa$.

The different possibilities of the linear correlation between $ln(A)$ and E_a (consequence of the data spread around the best fit correlation - Fig. 3.2), is considered by assessing $\bar{s}_{\{A;E_a\}}$ for extreme correlations (dash-dot lines in

Fig. 3.2). The results, for the extreme correlations, are reported between brackets in Table 3.2.

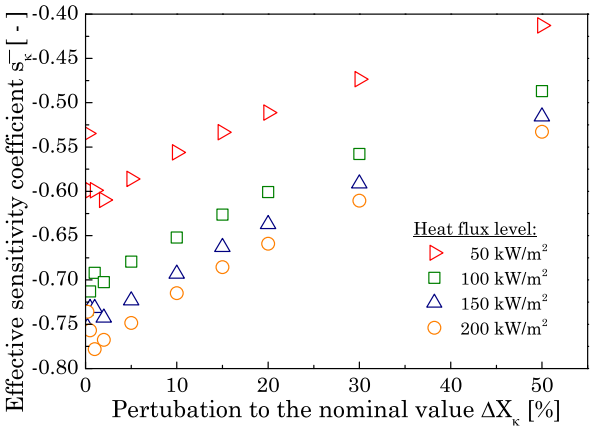

Figure 3.4: Change in the effective sensitivity coefficient $\bar{s}_\kappa$ at four heat flux levels as a function of the variation ΔX_i.

5.3. Design of Experiments (DoE)

The assessment of the local interactions (Morris's class #4) using DoE demonstrated that they are negligible. A high confidence is associated with these results because the technique enables also the estimation of the first order derivatives and it provides similar results as SP and OAT for the different parameters.

5.4. Analysis and discussion

Table 3.2 gathers the numerical values of $\bar{s}_i$ obtained from the SP and OAT techniques. For the parameters presenting a linear or power correlation with t_{ign}, an excellent agreement is observed between OAT and SP techniques, even if $\bar{s}_i$ evolves with $\dot{q}''_e$, as is the case for k ($\bar{s}_k$ changes from 0.26 to 0.12 when $\dot{q}''_e$ increases from 50 to 200 kW/m²). This agreement obtained between both techniques strengthens the results.

The negative values for $\bar{s}_{\dot{q}''_e}$ and $\bar{s}_\kappa$ indicate that the predictions of t_{ign} decrease when $\dot{q}''_e$ and κ increases. The kinetics parameters $\{A; E_a\}$ are particular

due to the possible linear correlations between $ln(A)$ and E_a that result from the spread of data plotted in Fig. 3.2. While the predictions of t_{ign} increase with E_a when the best fit linear correlation is applied, there are some correlations where the opposite occurs ($\bar{s}_{\{A;E_a\}} < 0$).

Figure 3.5 represents, for each parameter, the absolute value of its relative sensitivity $\bar{s}_i/\bar{s}_{i\,max}$ where $\bar{s}_{i\,max}$ is the highest effective sensitivity coefficient ($\bar{s}_{\dot{q}''_e}$ according to Table 3.2).

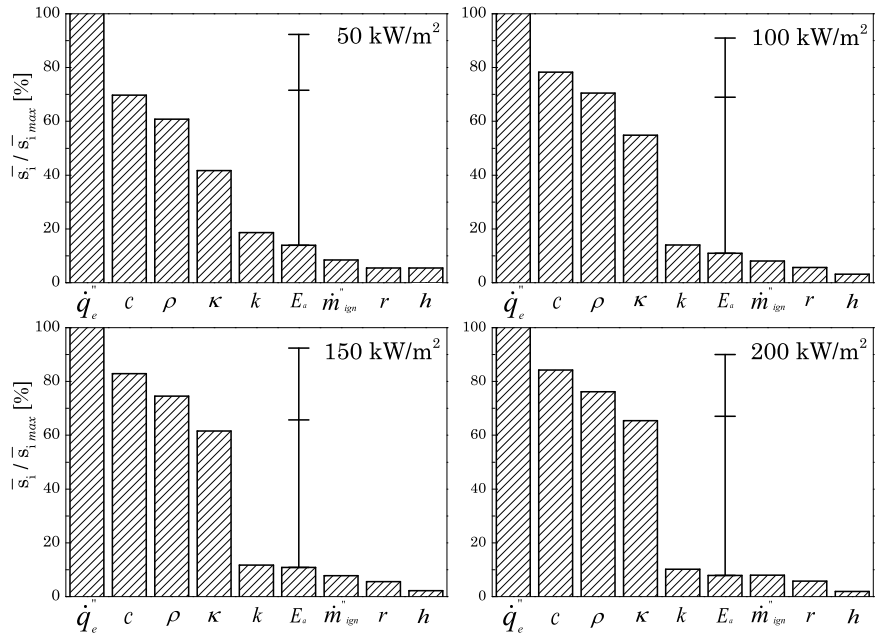

Figure 3.5: Relative sensitivity $\bar{s}_i/\bar{s}_{i\,max}$ of the different parameters (assessed from SP and OAT techniques) at four heat flux level.

From Fig. 3.5 and Table 3.2, two distinct groups of parameters appear: one composed of $\dot{q}''_e$, c, κ, and ρ, corresponding to the influential parameters (i.e. t_{ign} is sensitive to these parameters) while the other, with $\dot{m}''_{ign}$, h, k and r, includes parameters considered of secondary importance.

The relative sensitivity of the kinetic $\{A; E_a\}$ represented on Fig. 3.5 is obtained from the best fit linear correlation given on Fig. 3.2. According to the figure, its effect can be considered as secondary ($\bar{s}_{\{A;E_a\}} < 15$ % of $\bar{s}_{\dot{q}''_e}$) but the

relative sensitivity of $\{A; E_a\}$ becomes significant (second in the rank) if the uncertainty associated with the correlation used is considered (error bars in Fig. 3.5). $\{A; E_a\}$ should therefore be included in the group of parameters that need to be considered for calibration (i.e. influential group).

The uncertainty associated with the prediction of t_{ign} is therefore expected to be low if the parameters from the influential group are characterised with a high level of accuracy. These results suggest that an experimentalist willing to extract the parameters from independent experiments to calibrate the model would need to focus in priority on $\dot{q}''_e$, $\{A; E_a\}$, c, κ, and ρ (decreasing order) to be cost effective.

The rank of the parameters does not evolve over the range of heat flux levels studied. However, as $\dot{q}''_e$ increases, the relative sensitivities of c , ρ and κ increase. For c and ρ, this increase is only due to the reduction of $\bar{s}_{\dot{q}''_e}$ ($\bar{s}_c$ and $\bar{s}_\rho$ are constant in Table 3.2) whereas in the case of κ, it is also due to the raise of its effect $\bar{s}_\kappa$.

The effective sensitivity coefficients $\bar{s}_i$ can be compared to the power of evolution of the different parameters present in Eq. 3.1. In this latter, the power of k, ρ and c is 1 and does not evolve with the applied heat level. This is in close agreement with the results in Table 3.2 for ρ and c, but the sensitivity of t_{ign} to k is found lower in the present study and it decreases when the applied heat flux increases (from 0.27 at 50 kW/m² to 0.12 at 200 kW/m²). The effect of $\dot{q}''_e$ presents also discrepancies. In Eq. 3.1, the power of $\dot{q}''_e$ is -2 and is invariant whereas it is estimated to vary between -1.41 and -1.14 respectively at 50 and 200 kW/m². The other parameters do not appear in Eq. 3.1. These disagreements can be directly related to the different assumptions included in the models. This can be demonstrated by performing identical analysis with another analytical solution for the prediction of t_{ign} (Eq. 3.7) which is based on a finite reaction rate and critical mass flux ignition criterion [17].

$$t_{ign} = \frac{\pi}{4} k\rho c \left(\frac{T_\infty}{\dot{q}''_e}\right)^2 \left(\left(\frac{\dot{q}''_e \, \dot{m}''_{ign}}{D \, \rho \exp(-E_a/(RT_1)) \, k \, A \, T_\infty} \right)^{(R\,T_2)/E_a} - 1 \right)^2 \quad (3.7)$$

where T_1, T_2 and D represent constant parameters.

Except for c, the values of $\bar{s}_i$ in Eq. 3.7 are different from Eq. 3.1 since k, ρ and $\dot{q}''_e$ are present in the bracket at the most right. Using either the nominal values suggested by Lautenberger and Fernandez-Pello [17] or by Table 3.1, the ratio $(RT_2)/E_a$ is estimated to be of the order of $5 \cdot 10^{-2}$. Multiplying this coefficient by 2 due to the squared character of the equation, ρ is found to evolve theoretically with a power of 0.9 as predicted by the present sensitivity analysis (Table 3.2). The agreement is also very good for $\dot{m}''_{ign}$ which evolves with a power of 0.1 in Eq. 3.7.

The estimations of $\bar{s}_k$ and $\bar{s}_{\dot{q}''_e}$ present again discrepancies with the theoretical powers from Eq. 3.7, respectively of 0.9 and -1.9. This can be explained by the presence of the in-depth absorption mechanism in the pyrolysis model used in this study (Eq. 3.2). While analytical solutions have been developed for models including in-depth radiation absorption [6,18], their formulations does not allow a direct comparison with a power law. With both analytical formulations, κ increases the delay time to ignition when its value decreases, implying a negative value for $\bar{s}_\kappa$ as predicted in Table 3.2.

The pyrolysis model used by Linteris [8] is closer to the model studied in this chapter considering the assumptions performed. In his study, Linteris [8] has quantified only $\bar{s}_i$ for k, κ and c. The values for κ and c are similar to the values presented in Table 3.2, even when the heat flux level is changed (i.e. the trend is respected). However, $\bar{s}_k$ is in agreement only qualitatively and discrepancies exits quantitatively. This is probably due to the nominal values used by Linteris [8] which are different for some parameters.

The changes in the parameter evolution powers between the different models show the impact that the assumptions (i.e. equations of a model) can have on the results. This demonstrates that a sensitivity analysis is not only local on the hyperspace (i.e. function of the nominal values of the parameters) but can change between models, even if they predict the same quantity of interest.

It is worth noticing that while local interactions between the parameters are not significant according the DoE techniques (i.e. mixed partial derivatives negligible); there are global interactions between parameters since $\bar{s}_i$ changes for some parameters when the applied heat flux is increased.

6. Uncertainty analyses

In this section, the objectives are to assess the uncertainty associated with the prediction of t_{ign} and also to determine which parameters are responsible for the dispersion of the predictions.

6.1. Prediction intervals

Within this section, the spread of the predictions for t_{ign} (i.e. maximum prediction interval) induces by the parameter uncertainty is assessed varying only one parameter at the time. The prediction interval is then divided by the nominal prediction of t_{ign} (i.e. prediction with the nominal values of the parameters - Table 3.1) in order to assess the relative importance of the prediction uncertainty (Table 3.3).

Table 3.3: Ratios between the prediction interval and the nominal prediction of t_{ign}.

	Applied heat flux [kW/m²]	k [W/(m.K)]	c [J/(kg.K)]	ρ [kg/m³]	κ [1/m]	r [-]	$\dot{m}''_{ign}$ [g/(m².s)]	h [W/(m².K)]	{A ; E} [1/s;kJ/mol]	$\dot{q}''_e$ [kW/m²]
Prediction intervals	50	18%	111%	16%	86%	14%	21%	24%	19%	27%
	100	12%	111%	17%	104%	13%	18%	12%	13%	23%
	150	10%	111%	17%	111%	12%	17%	9%	11%	22%
	200	8%	111%	17%	115%	12%	16%	7%	9%	21%

The uncertainty on c and κ produce the biggest effects with a spread larger than the nominal prediction (ratio > 100 %). For the other parameters, the spread of the predictions represent less than 30 % of the nominal prediction.

While the effect of the uncertainty associated with c and ρ are stable when $\dot{q}''_e$ increases; the uncertainty in κ has a growing importance. The opposite behaviour occurs for k, $\dot{q}''_e$, h and $\{A; E_a\}$.

In fact, the influence of $\{A; E_a\}$ in Table 3.3 is only estimated considering the best fit correlation from Fig. 3.2. If the uncertainty in the correlation is taken into account, the effect resulting from the uncertainty on $\{A; E_a\}$ is still found to decrease when $\dot{q}''_e$ increases, but the ratio between the prediction interval and the nominal prediction of t_{ign} takes the first position in the rank of importance: from 177 % at 50 kW/m² to 128 % at 200 kW/m².

6.2. Monte Carlo

The uncertainty associated with the prediction of t_{ign} is investigated applying a Monte Carlo methodology with 10 000 simulations by heat flux level studied. The variability range of each parameter (Table 3.1) is sampled randomly following an uniform distribution, as recommended by the Joint Committee for Guides in metrology [11]. For each heat flux level studied, the probability density function (*pdf*) obtained from the predictions of t_{ign} is plotted in Fig. 3.6 with the average and standard deviation (estimated following Ref. [16]). The best fit for the *pdf*, obtained with a Generalized Extreme Value distribution, is also represented in Fig. 3.6 for completeness.

While the standard deviation of the predictions is getting narrower with increasing heat flux level, the spreads of the predictions (called $u(t_{ign})$ in Fig. 3.6) are significant, especially at 50 kW/m² (≈ 320 s).

The measured delay times to ignition from Fig. 3.1 are plotted bellow each *pdf* in order to compare the spread of the predictions with the experimental uncertainty.

A drawback of Monte Carlo technique is its incapacity to assess the respective contributions of the different parameters to the spread of the predictions.

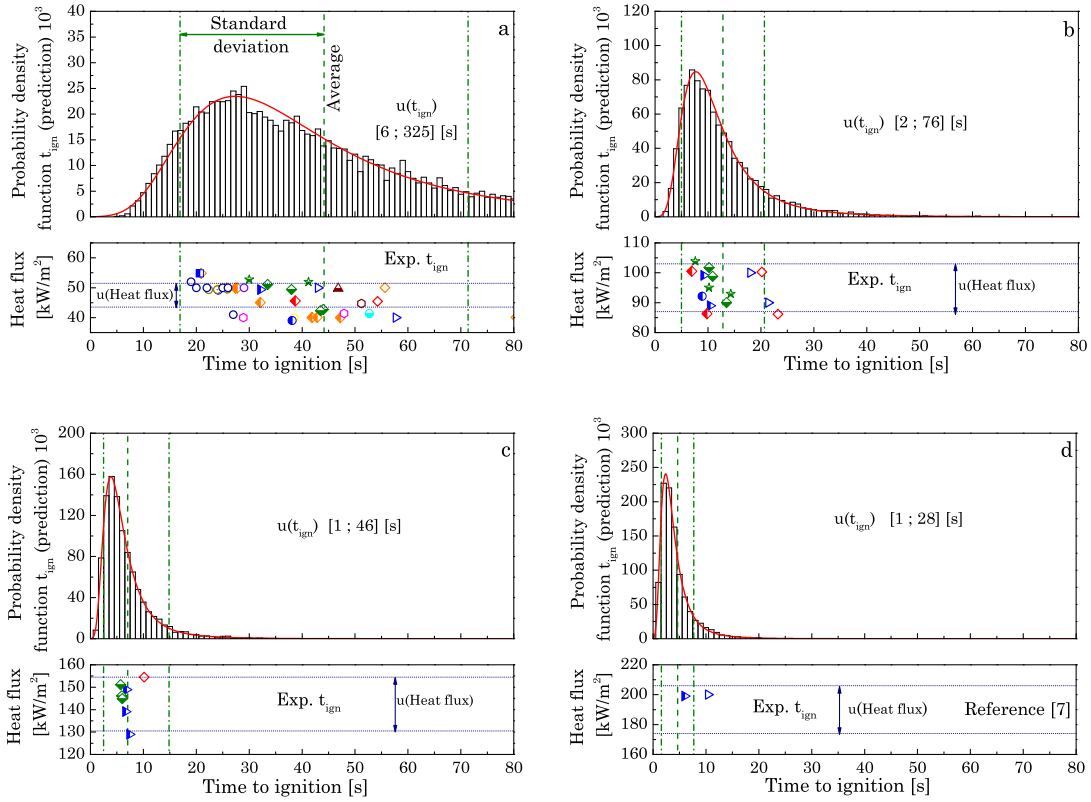

Figure 3.6: Probability density functions of the predicted delay time to ignition resulting from the parameter uncertainty: (a) 50 kW/m², (b) 100 kW/m², (c) 150 kW/m² and (d) 200 kW/m².

For the parameters revealed by the sensitivity analysis as being influential ($\dot{q}''_e$, c, ρ, κ and {A; E_a}), a second set of Monte Carlo simulations has been performed (2 500 simulations each) where one parameter is kept fixed at its nominal value while the others are sampled randomly over their ranges. The objective is to assess the evolution of the spread if one parameter is assumed to be known without uncertainty.

Figure 3.7 shows the influence on the *pdf* at 100 kW/m² when κ and {A; E_a} are fixed. For κ, the distribution is significantly different. The average and standard deviation of the predictions are respectively increased by 117 and

33 %. On the contrary, the *pdf* for the set of simulations with $\{A; E_a\}$ fixed presents almost no changes. The variation in the average prediction is lower than 1 % and the standard deviation is only reduced by 15 %.

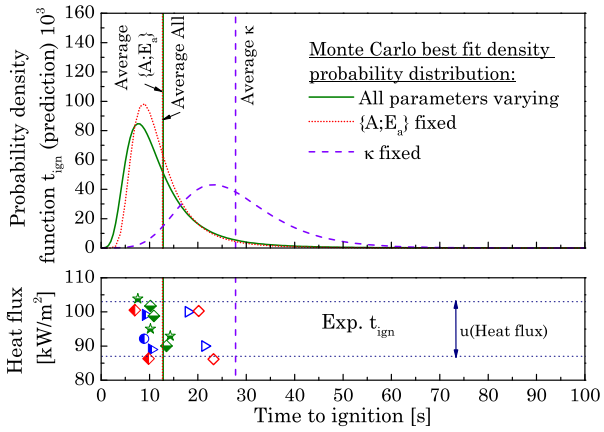

Figure 3.7: Impact on the probability density function best fit at 100 kW/m² when a parameter is kept constant.

Figure 3.8 reports the relative difference in the average and standard deviation of the predictions between the simulations where all the parameters vary simultaneously and the simulations where only one parameter is fixed at its nominal value.

The effect of kinetics parameters has been studied from different angles: first both parameters have been fixed (columns with the nomenclature $\{A; E_a\}$ in Fig. 3.8) and then only the correlation between the parameters was fixed (correlation suggested in Fig. 3.2 - columns with the nomenclature $E_a = f(A)$ in Fig. 3.8). Figure 3.8 shows that fixing κ has the biggest influence on the average of the predictions. This influence is increasing with $\dot{q}''_e$.

By fixing the value of c, κ or $\{A; E_a\}$ (parameters or correlation), the standard deviation of the predictions is significantly changed. They have therefore a high effect on the uncertainty of t_{ign}. While the perfect knowledge (i.e. no uncertainty) of c has a relative constant impact over the heat flux range studied, the

knowledge of κ and $\{A; E_a\}$ has respectively an increasing and decreasing impact as $\dot{q}''_e$ increases. The uncertainty of $\dot{q}''_e$ and ρ do not influence significantly the spread of the predictions, confirming the results from the prediction interval methodology.

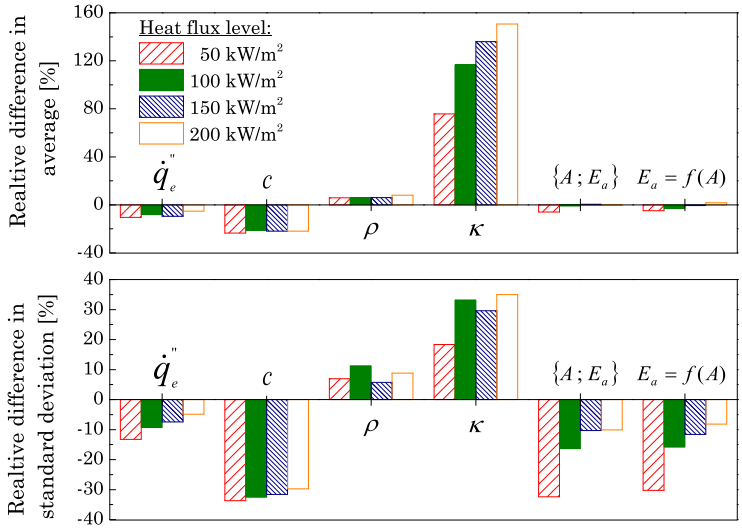

Figure 3.8: Relative differences in the average and standard deviation between the simulations where all parameters vary simultaneously and the simulations where one parameter is fixed: applied heat flux $\dot{q}''_e$; specific heat c; density ρ; attenuation coefficient κ; kinetics parameters $\{A; E_a\}$ or kinetics correlation $E_a = f(A)$.

6.3. Analysis and discussion

From these uncertainty studies, a clear and uniform message is obtained: the uncertainty on c, κ or $\{A; E_a\}$ when extracted from the literature is responsible for a large part of the spread in the prediction of t_{ign}. In the mean time, the relatively low uncertainties in the values attributed to $\dot{q}''_e$ and ρ imply that these two parameters explain only a small part of the dispersion of the prediction around the nominal prediction.

With both methodologies it is found the effect of u(κ) increases in importance when $\dot{q}''_e$ increases whereas the opposite behaviour occurs for $u(\{A; E_a\})$. However, the methodologies diverge on the rank of importance between u(κ) and

$u(\{A; E_a\})$. With the prediction intervals, $u(\{A; E_a\})$ is found to have the biggest influence whereas the opposite is reached with Monte Carlo.

This change in the rank demonstrates that $u(t_{ign})$ is not only the summation of the effects resulting from the uncertainty of the different parameters when studied independently. The interactions between the different mechanisms, considered with Monte Carlo methodology, are responsible for this change.

Using a methodology equivalent to the prediction intervals, Stoliarov et al. [10] found also that the uncertainty on $\{A; E_a\}$ (with the correlation uncertainty) has the highest effect on the predictions of t_{ign}. However, their results diverge from Table 3.3 for the other parameters. This can be justified by the differences in the range applied for each parameter and c and κ in particular. Moreover, Stoliarov et al. [10] performed their analyses at lower heat flux levels: $\dot{q}''_e \leq 75$ kW/m².

The experimental delay times to ignition shown in Fig. 3.1 are reported in Fig. 3.6 to compare the experimental and predictions uncertainties. When the parameter variability from the literature is considered, the spread of the predictions is significantly higher than the experimental uncertainty. However, the experimental uncertainty falls within a range defined by one standard deviation on either side of the average prediction.

When $\dot{q}''_e$ increases, two distinct groups of experimental results are observed. The reason for this difference is mostly the application of black-carbon coating on the exposed surface for some sets of data (semi-opened symbols in Figs. 3.1 and 3.6). This experimental artefact, applied to improve the radiation absorption, is influencing the experimental uncertainty at high heat flux level. The effect of black-carbon coating on the radiation absorption can be captured by increasing the effective value of κ [7 (chap 1)]. By fixing κ to its nominal value (Table 3.1), the predictions get closer to the experimental delay time to ignition for uncoated samples (Fig. 3.7). The uncertainty on κ is therefore not just related to the material but also to the experimental set up.

7. Conclusion

The sensitivity and uncertainty analyses of a pyrolysis model predicting the delay time to ignition have been performed using several methods. The sensitivity studies provide the governing parameters to predict ignition whereas the uncertainty analysis characterizes the prediction uncertainty. In order to make these uncertainty analyses realistic, they have been based on the parameter variability found in the literature for black PMMA [2 (chap 2)]. Moreover, both sensitivity and uncertainty analyses have been studied at four heat flux levels (from 50 to 200 kW/m^2) in order to capture the potential evolution of the parameter sensitivity and of the prediction uncertainty.

The sensitivity analysis shows that the predictions of the delay time to ignition for heat flux levels higher than 50 kW/m^2 are sensitive to the applied heat flux, the specific heat, the density and the attenuation coefficient (decreasing order of important). The kinetics parameters are particular since their sensitivity is a function of the correlation used between the activation energy and the pre-exponential factor. The best fit correlation over the kinetics found in the literature provide a sensitivity which is relatively low, whereas the possible correlation uncertainty implied by the data spread around this best fit can position the kinetics couple as the second most influential parameter. The relative sensitivity of these influential parameters in comparison to the group of parameters considered as secondary increases with heat flux level. The research and the calibration efforts should be focused on the group of parameters considered as influential.

The uncertainty analyses demonstrate that the uncertainty on the attenuation coefficient, the specific heat and the kinetics parameters is responsible for most of the spread in the predictions. The influence of the uncertainty associated with the attenuation coefficient is shown to increase with the heat flux level, whereas an opposite behaviour is observed for the kinetic parameters.

Neglecting the interactions between the different input parameters over their respective range of variability, as it is with the prediction interval methodology, is shown to change the rank of importance attributed to the parameter uncertainty. The uncertainty on the attenuation coefficient has more influence on the prediction spread if the variability of the other parameters is considered. Nevertheless, both uncertainty analyses emphasize the same parameters.

Moreover, the applied heat flux level and the density which are two influential parameters (sensitivity analyses) produce only a low effect on the spread due to their low uncertainty.

The combination of both analyses is important. The sensitivity enabled the identification of five influential parameters reducing the research domain of the uncertainty analysis.

For the first time, the spread of model predictions is compared to actual experimental data. These measurements of the delay time to ignition of black PMMA samples gathered in a previous chapter [7 (chap 1)] represent the experimental state-of-the-art of piloted ignition for this material: large sets of protocol and formulations of black PMMA.

When a high number of simulations is performed varying the value of the input parameters at each run, the interval defined by one standard deviation on either side of the average prediction captures the experimental uncertainty. However, the global spread of the predictions is significantly higher than this interval. The level of confidence that can be attributed to one specific prediction, when the model is calibrated thanks to the literature database, is therefore relatively low. Modellers are required to define the probable range of evolution for each of the parameters to obtain statistically a higher level of confidence in their predictions.

The spreads observed in this study tend to show that one of the main issues in solid ignition prediction is the variability of the parameters if they are extracted from the literature.

Finally, it is worth noticing that in the case of real fire the heat flux received is not constant and well controlled as in a bench-scale experiment. The sensitivity of the delay time to ignition to this parameter suggests that an accurate determination of its evolution is essential for the prediction capability of a model.

References

[1] Joint Committee for Guides in Metrology, International vocabulary of metrology – Basic and general concepts and associated terms (VIM), JCGM 200:2008 (2008).

[2] N. Bal, Pyrolysis modelling up to ignition - Part I: Literature review on sources of uncertainty and experimental variability (chapter 2), Uncertainty and complexity in pyrolysis modelling, The University of Edinburgh, 2012.

[3] J.L. Torero, Flaming ignition of solid fuels, in: The SFPE handbook of fire protection engineering 4th edition, P.J. DiNenno et al. (Eds.), National Fire Protection Association, 2008, chapter 2.11, pp. 2.260-2.278, ISBN-10: 0877658218.

[4] P.A. Beaulieu and N.A. Dembsey, Flammability characteristics at applied heat flux levels up to 200 kW/m2, Fire and materials 32 (2008) 61-86, http://dx.doi.org/10.1002/fam.948.

[5] M.A. Delichatsios, K. Saito, Upward fire spread: key flammability properties, Similarity solution and flammability indices, FM Global Research, Internal Report, 1991.

[6] F. Jiang, J.L. De Ris and M.M. Khan, Absorption of thermal energy in PMMA by in-depth radiation, Fire safety journal 44 (2009) 106-112, http://dx.doi.org/10.1016/j.firesaf.2008.04.004.

[7] N. Bal and G. Rein, Numerical investigation of the ignition delay time of a translucent solid at high radiant heat fluxes, Combustion and flame 158 (2011) 1109-1116, http://dx.doi.org/10.1016/j.combustflame.2010.10.014.

[8] G.T. Linteris, Numerical simulation of polymer pyrolysis rate: Effect of property variations, Fire and materials 35 (2011) 463-480, http://dx.doi.org/10.1002/fam.1066.

[9] S.I. Stoliarov and R.E. Lyon, Thermo-Kinetic model of burning, Federal Aviation Administration internal report DOT/FAA/AR-TN08/17, 2008.

[10] S.I. Stoliarov, N. Safronava and R.E. Lyon, The effect of variation in polymer properties on the rate of burning, Fire and materials 33 (2009) 257-271, http://dx.doi.org/10.1002/fam.1003.

[11] Joint Committee for Guides in Metrology, Evaluation of measurement data – Guide to the expression of uncertainty in measurement, JCGM 100:2008 (2008).

[12] M.D. Morris, Factorial sampling plans for preliminary computational experiments, Technometrics 33 (1991) 161-174, http://dx.doi.org/10.2307/1269043.

[13] D.M. Hamby, A review of techniques for parameter sensitivity analysis of environmental models, Environmental monitoring and assessment 32 (1994) 135-154, http://dx.doi.org/10.1007/BF00547132.

[14] NIST/SEMATECH e-Handbook of Statistical Methods, 2010, <http://www.itl.nist.gov/div898/handbook/>.

[15] A.M. Hasofer, Modern sensitivity of the CESARE-Risk computer fire model, Fire safety journal 44 (2009) 330-338 http://dx.doi.org/10.1016/j.firesaf.2008.07.007.

[16] Joint Committee for Guides in Metrology, Evaluation of measurement data – Supplement 1 to the "Guide to the expression of uncertainty in measurement" – Propagation distributions using Monte-Carlo method, JCGM101:2008 (2008).

[17] C. Lautenberger and A.C. Fernandez-Pello, Approximate analytical solutions for the transient mass loss rate and piloted ignition time of a radiatively heated solid in the high heat flux limit. Fire safety science 8 (2005) 445-456 http://dx.doi.org/10.3801/IAFSS.FSS.8-445.

[18] T.J. Ohlemiller and M. Summerfield, Radiative ignition of polymeric materials in oxygen/nitrogen mixtures, Proceedings of the symposium (international) on combustion 13 (1971) 1087-1094, http://dx.doi.org/10.1016/S0082-0784(71)80106-6.

Chapter 4

Relevant model complexity for non-charring polymer pyrolysis

Summary

The choice of the heat, mass and chemical mechanisms included in a pyrolysis model is often subjective, and detailed justifications of the inclusion or exclusion of the different mechanisms are infrequent. The implicit assumption that models with a higher number of mechanisms reproduce more accurately the reality has led to the recent growth of complexity in pyrolysis modelling seen in the literature. However, the comparison of several models predicting the same experimental results does not support this assumption, but reveals the presence of unnecessary complexity. Using a novel approach corresponding to a mechanism sensitivity, the influence of the heat, mass and chemical mechanisms on the transient predictions of surface temperature and mass loss rate (non flaming conditions) for PolyMethylMethAcrylate samples is

investigated. While a small change in the chemical degradation mechanism has a large effect on the predictions of the mass loss rate in oxygen atmospheres, the surface temperature is not affected. The heat transfer mechanisms appear to have however a significant effect on both quantities of interest. This study tends to demonstrate that the use of complex chemical mechanisms (e.g. multi-step reaction scheme or oxidative reaction) is not justified if the mechanisms of the heat transfer are kept simple. The calibration of the energy distribution and the heat losses should be considered as a priority.

Collaboration

This chapter results from a joint work performed with Dr Guillermo Rein from the University of Edinburgh (UK).

Nomenclature

A	Pre-exponential factor [s^{-1}]
c	Specific heat [J/(kg.K)]
E_a	Activation energy [kJ/mol]
k	Thermal conductivity [W/(m.K)]
$\dot{m}''$	Mass loss rate [g/(s.m^2)]
M	Model
n	Order of reaction [-]
N	Number of experimental points
T	Temperature [K]

Subscripts

∞	Ambient conditions
exp	Experiment
i	Model number
m	Mass loss rate
ref	Reference T_{ref} = 300 K
s	At the surface
sim	Simulation
T_s	Surface temperature

Greek symbols

γ	Power properties evolution [-]
Δ	Prediction error
ε	Absorptivity / emissivity [-]
κ	Attenuation coefficient [m^{-1}]
υ	Yield of reaction [-]
ρ	Density [kg/m^3]
φ	Material properties
ϕ	Measurements

1. Introduction

While the choice of a model is a major step in the prediction of a phenomenon, its justification is often subjective, and detailed justifications of inclusion or exclusion of the different mechanisms are infrequent. Assumptions and simplifications decrease the complexity of a model and define somehow its limitations. The implicit hypothesis that models with a higher number of

mechanisms reproduce more accurately the reality has led modelling in general and fire modelling in particular to undergo recently a large growth in complexity [1-3].

Chwif et al. [4] have listed some of the reasons for this growth in complexity. Among the non-technical, they highlight the "include all" syndrome and the "possibility" factor. The first one is the consequence of the inexperience of the modellers who might feel insecure and include the maximum number of mechanisms just in case. The second one is due to the increasing computational power available which makes possible to include a significantly higher number of mechanisms without increasing the running time. One example of the technical reasons listed is the willingness of gathering the needs of several users, thus increasing the scope of the model and the number of mechanisms.

However, as the global level of complexity increases in models, the number of input parameters required increases as well. These parameters could be, for example, physical properties (or effective properties), mathematical constants, experimental constants or calibration factors, and all carry some degree of uncertainty. Their respective uncertainty accumulates in the model and contributes to the global uncertainty associated with the numerical predictions. The discrepancy between the experiments and the predictions is a combination of errors due to the lack of important mechanisms (continuous line in Fig. 4.1) and the parameter uncertainty (dashed line in Fig. 4.1) [5,6].

An equilibrium is therefore required between the error related to the simplicity of the model equations and the prediction uncertainty in order to find an appropriate level of model complexity as shown in Fig. 4.1. The parameter uncertainty can be reduced by a calibration process, decreasing the resulting prediction uncertainty. The appropriate level of complexity is therefore moving in the direction of growing complexity.

As the number of available mechanisms (i.e. complexity) grows rapidly, the issue of how determining the most beneficial level of model complexity to predict a phenomenon is becoming a major concern, not only in fire science [6].

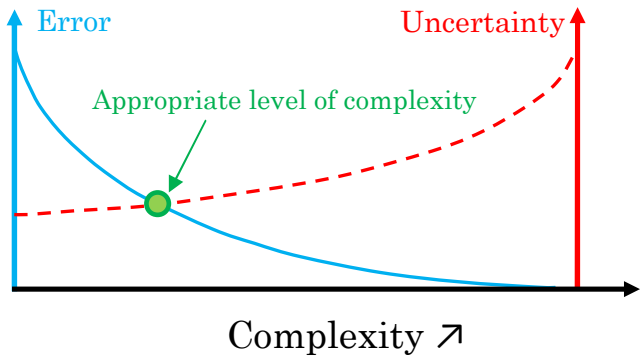

Figure 4.1: Schematic of the relationship between prediction error, prediction uncertainty and model complexity.

This paper explores the relationship between complexity and prediction error in the pyrolysis modelling of a non-charring material. This is one of the most important and best known problems in fire science. Moreover, this phenomenon is fundamental in the context of solid ignition and fire growth.

The predictions from a range of pyrolysis models are compared in order to investigate their sensitivity to the heat, mass and chemical mechanisms. This approach diverges from previous sensitivity analyses found in the literature which focused on the parameter sensitivity [7-9]. Instead, this methodology studies the evolution of the predictions by adding one-by-one assumptions to a base model corresponding to the highest complexity (i.e. most complete set of pyrolysis mechanisms available in the literature), until a relatively simple model is reached.

2. Several model complexities for one set of experiments

2.1. Comparison to experiments

The prediction capability of a pyrolysis model is usually inferred from comparisons against transient measurements of mass loss rate $\dot{m}''$ and surface temperature T_S. One of the most complete sets of pyrolysis measurements in the

literature is that by Kashiwagi and Ohlemiller [10]. They exposed vertical samples of PolyMethylMethAcrylate (PMMA), 15 mm thick, to two different radiative heat flux levels (17 and 40 kW/m²) in several atmospheric compositions (from 0 to 40 % in oxygen concentration) and provided measurements of $\dot{m}''$ and T_S. They have estimated their measurement uncertainty to be of 5 % for $\dot{m}''$ and 3 % for T_S.

These high quality experiments have been used for comparison to model predictions by Lautenberger and Fernandez-Pello [1], Kashani and Esfahani [11] and Staggs [12]. Part of the comparisons between these predictions and the measurements is shown in Fig. 4.2. Note that among the experiments considered, Staggs [12] predict only one set of conditions (40 kW/m² and inert atmosphere) whereas Lautenberger and Fernandez-Pello [1] and Kashani and Esfahani [11] compared to all four sets.

The predictions of T_S from the three models are in good agreement with the experimental results for all conditions. While the predictions from Lautenberger and Fernandez-Pello [1] are almost always within the experimental uncertainty at 40 kW/m² for both atmospheric compositions, they slightly overestimate T_S at 17 kW/m². Their predictions are overall the best, but Kashani and Esfahani [11] predict slightly better the results at 17 kW/m² in 20 % of oxygen.

From a general point of view, the predictions of $\dot{m}''$ by the three modelling teams in Fig. 4.2 present more discrepancies and do not stay within the experimental uncertainty. Similarly to the prediction of T_S, the predictions of Lautenberger and Fernandez-Pello [1] are the most accurate at 40 kW/m², even if the model does not capture correctly the early stages (< 3 g/(m².s)) in the presence of oxygen (maximum error ≈ 1 g/(m².s) at 60 s). At 17 kW/m² in the presence of oxygen, it is again the predictions from Kashani and Esfahani [11] which predict best the transient $\dot{m}''$. Overall, all three models capture approximately the shape of $\dot{m}''$ but fails to predict the onset of pyrolysis.

Due to the relative similarity in their predictions, it is interesting to compare the mechanisms included in the models.

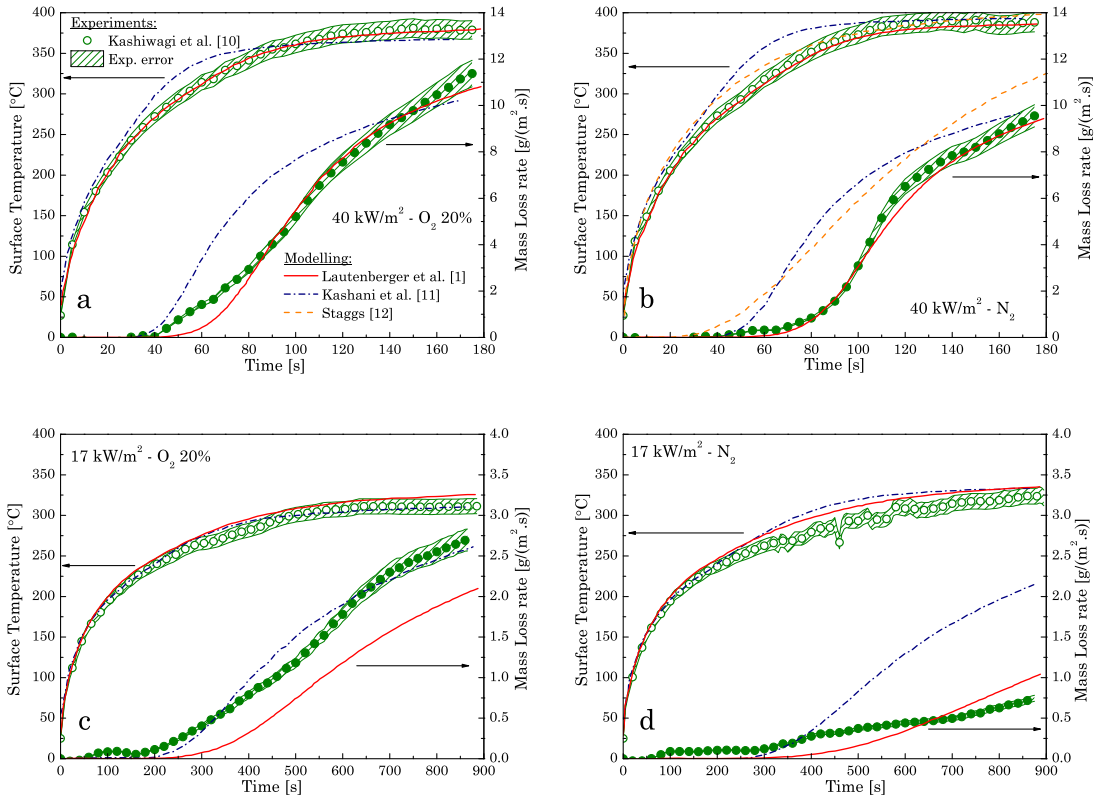

Figure 4.2: Numerical predictions of surface temperature and mass loss rate from literature against experimental measurements for clear PMMA: (a-b) at 40 kW/m²; (c-d) at 17 kW/m²; (a-c) in 20 % of oxygen concentration and (b-d) in nitrogen atmosphere.

2.2. Differences in the model equations

The three models solve the energy conservation equation in the solid, but the mass of the condensed phase is not always conserved (regression assumed negligible by Kashani and Esfahani [11]).

The gas phase treatment differs between the three models. Stagg [12] does not consider any. Lautenberger and Fernandez-Pello [1] solve the momentum equation for the gases moving across the solid matrix and assume thermal equilibrium between the condensed and gas phases. Finally, Kashani and Esfahani [11] solve the energy and species conservation equations only for the gas above the front surface.

Although the three models have based the quantification of $\dot{m}''$ on an Arrhenius kinetics model, the reaction schemes differ. Lautenberger and

Fernandez-Pello [1] used a 3-steps reaction scheme whereas Kashani and Esfahani [11] and Stagg [12] considered only 1-step. Stagg [12] is the only one that does not include oxidative reaction. For Lautenberger and Fernandez-Pello [1] (only one step sensitive to oxygen) and Kashani and Esfahani [11], the Arrhenius term of the oxidative reaction includes a factor varying with the oxygen concentration.

The mechanism of energy absorption of the incident radiative heat flux is also different. Staggs [12] assumes that the radiation is absorbed at the surface (boundary condition), whereas the two other models consider in-depth radiation absorption (Beer-Lambert's law). While Lautenberger and Fernandez-Pello [1] keep the attenuation coefficient constant and uniform, Kashani and Esfahani [11] use a transient attenuation coefficient to account for bubble formation during in-depth degradation. Lautenberger and Fernandez-Pello [1] model the bubbles impact by introducing an intermediate solid species with different material properties than the virgin PMMA (PMMA → β PMMA - where β PMMA stands for bubbled PMMA).

Only Lautenberger and Fernandez-Pello [1] uses thermal properties varying with temperature whereas the others assume constant and uniform properties.

Finally, the treatment of the convective heat losses varies also between the models. Lautenberger and Fernandez-Pello [1] considered the convective heat transfer coefficient as constant at both boundaries whereas Kashani and Esfahani [11] take it as function of T_S. Staggs [12] assumed a constant convective heat transfer coefficient at the front surface but the back boundary was insulated (heat losses negligible).

2.3. Parameter values

The three models have been calibrated differently. Staggs [12] used data extracted from the literature except for the determination of the kinetics couples (independent study). Kashani and Esfahani [11] used also mainly the data from the literature but the radiative properties (attenuation coefficient and reflectivity) and the oxygen sensitivity of the pyrolysis degradation have been

optimised based on the measurements from Kashiwagi and Ohlemiller [10]. Lautenberger and Fernandez-Pello [1] optimised most of their parameters by inverse modelling with the full set of measurements from Kashiwagi and Ohlemiller [10].

The material properties used by the modelling teams have different values but they all fit inside the ranges of variability for PMMA observed from the literature [13 (chap 2)]. In particular, the kinetics couple (pre-exponential factor A and activation energy E_a) used falls inside the range of variability shown in Fig. 4.3 (60 kinetics couples). The techniques employed to extract theses couples are emphasized in Fig. 4.3.

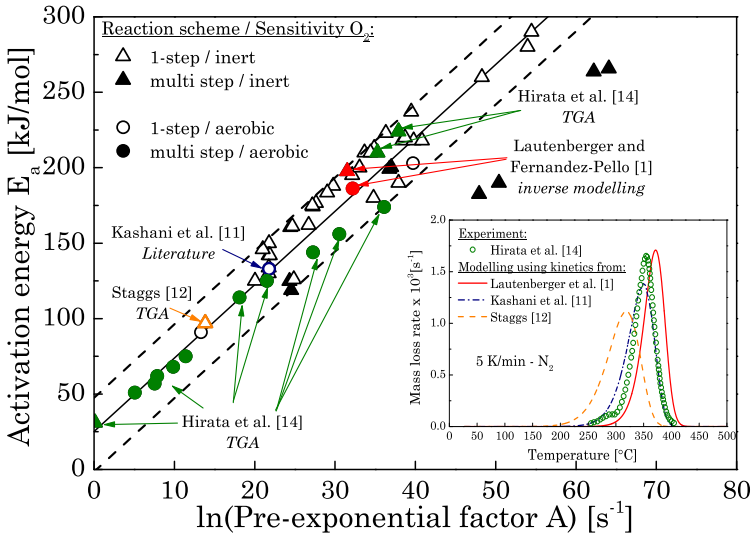

Figure 4.3: Kinetics parameters collected from the literature for PMMA decomposition. Inset: Comparison between experimental and numerical results of TGA at 5 K/min in inert atmosphere.

Hirata et al. [14], performed thermogravimetric analyses (TGA) on PMMA samples from the same supplier as in Kashiwagi and Ohlemiller [10]. They found that while a 1-step reaction suffices to describe the chemical degradation in nitrogen atmosphere, three steps were required in air.

Using a 1-step Arrhenius model (PMMA → GAS) with the kinetics couples applied in the three models [1,11,12], the thermogravimetry is predicted in nitrogen at 5 K/min and compared in the inset of Fig. 4.3 to the experimental

results reported by Hirata et al. [14]. Kashani and Esfahani [11] have introduced a calibration factor in the Arrhenius law to calibrate the oxygen sensitivity. This factor has been considered for the calculation. Staggs' kinetics [12], obtained from independent TGA performed at 10 K/min, predicts the temperature for the peak mass loss within 10 % of error. However, the magnitude of the peak mass loss is predicted within 32 % of error. Lautenberger and Fernandez-Pello [1] who performed an inverse modelling using the experimental data from Kashiwagi and Ohlemiller [10] (estimated heating rate < 1K/s [15]) predict the temperature and the magnitude of the peak with less than 5 % of error. The predictions using the kinetics from Kashani and Esfahani [11] (found in the literature) fall between the two previous.

The discrepancy between the thermogravimetry simulations and the experimental results in air is significantly higher (number of peaks and location).

Even if agreement is not consistent, the different models present similarities in the results whereas the mechanisms included in the models and the values of the input parameters present large differences. This demonstrates that there is some degree of unnecessary complexity in the models and some non-relevant parameters that nonetheless add modelling uncertainty. It is therefore important to identify the mechanisms that control the modelling accuracy.

3. Mechanism sensitivity

3.1. Taxonomy of model complexity

In this section, the predictions of different models are compared to the experimental results from Kashiwagi and Ohlemiller [10] at 40 kW/m^2 (Fig. 4.2). The taxonomy of the models is obtained by adding, one-by-one, assumptions to the model used by Lautenberger and Fernandez-Pello [1] and called M_1 hereafter. It represents the highest level of complexity (i.e. most complete set of mechanisms). At each assumption or approximation, a new model M_{i+1} is obtained and used to predict surface temperature and mass loss rate with the

same values for the input parameters as for M_1. In this novel approach based on a mechanism sensitivity, the values of the input parameters are kept unchanged in order to reveal the influence of the simplifications.

M_1 is based on mass, species and energy balances for the condensed phase. The source terms included in the energy conservation encompass the energy consumed by the chemical reactions and the in-depth radiation absorption. On top of that, the mass, species and momentum conservation equations are solved for the pyrolysis gases inside the solid matrix. The momentum equation enables the consideration of the gas pressure evolution and the description of the mass flux of gases released at the front surface instead of assuming an instantaneous release of the pyrolysis gases produced in depth. The pyrolysis degradation is composed of 3 steps (Eqs. 4.1 to 4.3).

$$\mathrm{PMMA} \rightarrow \beta\ \mathrm{PMMA} \tag{4.1}$$

$$\beta\ \mathrm{PMMA} \rightarrow \mathrm{GAS} \tag{4.2}$$

$$\beta\ \mathrm{PMMA} + \upsilon_{O_2} O_2 \rightarrow \upsilon_{GAS}\mathrm{GAS} \tag{4.3}$$

In the first reaction (Eq. 4.1), the solid species PMMA produces another solid species called β PMMA. This reaction allows variations of the material properties to account for the formation of bubbles. This reaction does not absorb energy (i.e. heat of pyrolysis $\Delta H = 0$ kJ/kg). The two other reactions produce pyrolysis gases: one by thermal degradation (Eq. 4.2) whereas the other by oxidation (Eq. 4.3). They are both assumed endothermic. These reactions are modelled by Arrhenius laws with the kinetics triplet: pre-exponential factor A, activation energy E_a and order of reaction n. The material properties (thermal conductivity k, specific heat c and density ρ), expressed generically by φ, are allowed to vary with temperature in Eq. 4.4 following a power law controlled by γ_φ. This temperature dependency implies a potential swelling or shrinking only due to thermal impact.

$$\varphi = \varphi_\infty \left(\frac{T}{T_{ref}}\right)^{\gamma_\varphi} \qquad \varphi \in \{k\,;\ \rho\,;\ c\} \tag{4.4}$$

The radiation absorption (non-reflected fraction of the incident radiation based on the absorptivity/emissivity ε) is assumed to occur in-depth using Beer-Lambert's law with a finite attenuation coefficient κ. The full set of equations is available elsewhere [1].

From this model, a set of assumptions is added to decrease the model complexity. Table 4.1 gathers the different assumptions referenced by letters from A to I. These ones can be classified in 3 groups: (1) mass transfer {A}, (2) chemical degradation {B ; C ; E ; G} and (3) heat transfer {D ; F ; H ; I}.

Table 4.1: Assumptions and simplifications added to model M_1.

Letter	Assumption	Groups	Definition and implementation
A	Gases released instantaneously	(1)	The gases produced are released without resistance (low viscosity). Gas phase momentum equation is not solved
B	Oxidation negligible	(2)	The solid decomposition is anaerobic. The reaction in Eq. 4.3 is removed
C	1-step chemical reaction	(2)	The chemical degradation is described with only one reaction. Eqs. 4.1 and 4.2 are replaced by PMMA → GAS
D	Heat of pyrolysis negligible	(3)	The energy consumed (or produced) by a chemical reaction is negligible. Heat of pyrolysis sets to 0 kJ/kg.
E	Solid phase consumption negligible	(2)	The mass lost by the solid is negligible. The 1-step reaction is replaced by PMMA → PMMA
F	Thermo-physical parameters invariant	(3)	The material properties are considered independent of temperature. γ_φ from Eq. 4.4 sets to 0
G	Inert solid	(2)	The chemistry degradation process is negligible. The chemical reaction is removed.
H	In-depth absorption negligible	(3)	The incident radiative heat flux is absorbed at the surface. Attenuation coefficient sets to infinity.
I	Reflectivity negligible	(3)	All the incident heat flux is absorbed by sample. Absorptivity/Emissivity equal to unity.

The order in which each assumption is invoked is not unique. The impact of this order could be important and so it is also investigated in this study. A total of 17 models have been created. An *a priori* order, illustrated in Fig. 4.4, has

been investigated first. It specifies the taxonomy α which reflects the general ranking of complexity found in the literature. Some examples follow. Stoliarov et al. [7] used a model similar to M_4. The difference resides in the mathematical formulation of some mechanisms such as for in-depth absorption. Bal and Rein [16 (chap 1)] predicted the delay time to ignition at high heat fluxes with a model equivalent to M_6. Cordova and Fernandez-Pello [17] used a model equivalent to M_7 for the same purpose. Their model differs slightly from M_7 since it considers the endothermicity of the pyrolysis reaction (assumption D not invoked). Jiang et al. [18] developed an analytical solution of a model similar to M_8. The difference being that they assumed linear heat losses at the front surface (combination of convective and radiative heat losses). Finally, the classical ignition theory [19] corresponds to M_{10} but without the heat losses at the boundary.

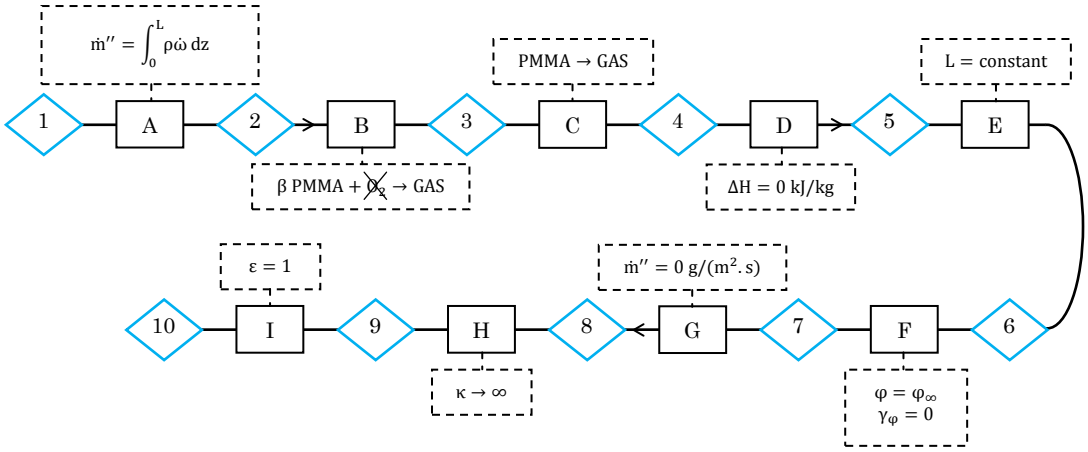

Figure 4.4: Model taxonomy α (diamond: models - square: assumptions).

3.2. Results and discussion

The error, called Δ, between the experimental and numerical results is defined in Eq. 4.5. The experimental data set used is from Kashiwagi and Ohlemiller [10] at 40 kW/m² (see Figs. 4.2a and 4.2b).

$$\Delta = 1 - \left(\left(\frac{1}{N} \sum \left(\frac{\phi_{exp}}{diff(\phi_{exp} - \phi_{sim}) + 0.05\ \phi_{exp}} \right)^2 \right) \Big/ \left(\frac{1}{0.05} \right)^2 \right) [\%] \qquad (4.5)$$

$$diff(\phi_{exp} - \phi_{sim}) = \begin{cases} |\phi_{exp} - \phi_{sim}| & \text{if } \phi_{sim} \text{ not} \in \text{ in experimental error} \\ 0 & \text{if } \phi_{sim} \in \text{ in experimental error} \end{cases}$$

where ϕ is the quantity of interest and N is the number of data points considered.

There are two errors considered: Δ_m associated with $\dot{m}''$ and Δ_{T_S} associated with T_S.

3.2.1 Taxonomy α

The models from the taxonomy α are used to simulate $\dot{m}''$ and T_S at 40 kW/m² in 20 % of O_2, keeping the values of the input parameters suggested by Lautenberger and Fernandez-Pello [1]. The simulations of the different models are plotted in Fig. 4.5.

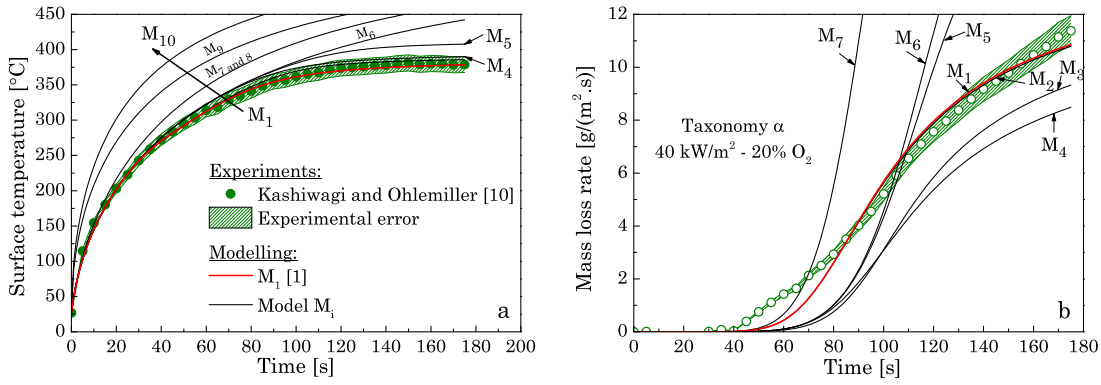

Figure 4.5: Predictions against experimental measurements at 40 kW/m² in 20 % of O_2 for models in taxonomy α: (a) surface temperature and (b) mass loss rate.

The predictions of T_S with the models M_1 to M_4 show a good agreement with the experimental results since they are in the experimental uncertainty (not entirely for M_4). For M_5 and simpler models ($M_{i>5}$), T_S is over estimated. Cordova et al. [20] reported similar behaviour using a model close to M_{10}. They claimed that this overestimation was due to the assumption of negligible endothermic

pyrolysis reaction (assumption D, M_4 to M_5). However, assumption D implies overestimations only after a certain threshold (≈ 325 °C).

The assumptions related to the heat transfer, F (thermo-physical parameters invariant, M_6 to M_7) and H (in-depth absorption negligible, M_8 to M_9) are also very influent (Fig. 4.5a) since they increases significantly the overestimation.

Concerning the predictions of $\dot{m}''$, the assumption of instantaneous release of the pyrolysis gases produced (assumption A, M_1 to M_2) seems to not influence the prediction.

Assumption of negligible oxidation reaction (assumption B, M_2 to M_3 - Eq. 4.3) affects significantly the magnitude of $\dot{m}''$ but not its shape. Simplifying the reaction scheme to only one reaction, where PMMA produces directly gases (assumption C, M_3 to M_4), provokes change in $\dot{m}''$ only after 4 g/(s.m^2) whereas neglecting the endothermicity (assumption D, M_4 to M_5) influences considerably its shape. This assumption affects directly the energy balance. Note that for the prediction of ignition using a critical mass flux, the results show that the endothermicity has a negligible effect since the ignition threshold is generally considered ≤ 3 g/(m^2.s) and predictions from M_4 and M_5 are close up to this threshold (Fig. 4.5b). $\dot{m}''$ is not calculated for model $M_{i>7}$ since assumption G considers the solid as inert.

The error Δ has been assessed following Eq. 4.5 in order to quantify the evolution of the predictions as a function of the model complexity (Fig. 4.6).

The relationship between model complexity and error Δ is monotonic but varies according to the quantity of interest studied: $\dot{m}''$ or T_S. The error Δ_{T_S} ranges from 7 % to 98 % between M_1 and M_{10} whereas the error Δ_m spreads between 45 % and 85 % for $\dot{m}''$ between M_1 and M_7.

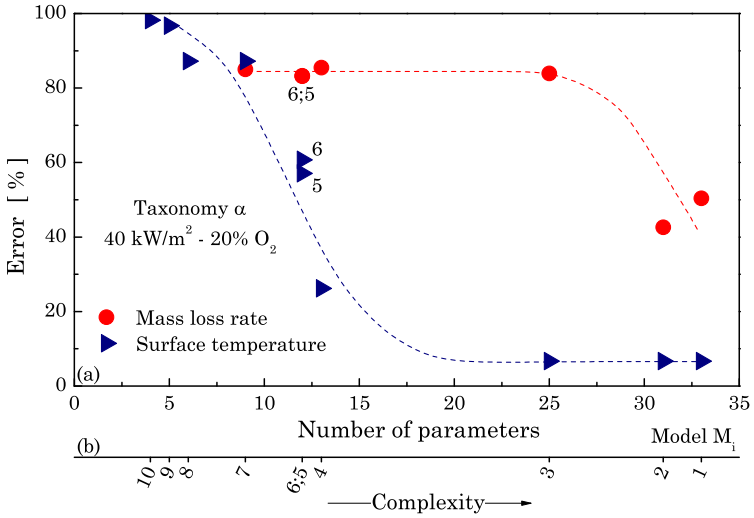

Figure 4.6: Relationship between model complexity (taxonomy α) and prediction error for surface temperature and mass loss rate at 40 kW/m² in 20 % of oxygen. The x-axes represent (a) the number of parameters in the models and (b) the reference number of the models.

The complexity-error relationship for T_S presents a plateau at around 7 % for high complexity (beginning of the taxonomy - high number of parameters) and suddenly increases below 25 parameters. The assumption C (1-step chemical reaction, M_3 to M_4) increases the error of 20 %. This significant increase, not visible on Fig. 4.5a, comes from the closeness between the numerical predictions and the experimental uncertainty. The predictions fall outside the experimental uncertainty at some time intervals which results in an increase of the numerical value for Δ_{T_S}. A large impact on the complexity-error relationship for T_S is caused by assumption D (heat of pyrolysis negligible, M_4 to M_5). The assumption of negligible regression (assumption E, M_5 to M_6) does not affect the numerical quantification of the error Δ_{T_S} whereas in Fig. 4.5a, its effect on the prediction shape is important: T_S present smoother curvature after 375 °C when the surface regression is considered.

While assumption F (thermo-physical parameters invariant, M_6 to M_7) and assumption H (in-depth absorption negligible, M_8 to M_9) provoke similar influence in Fig. 4.5a, only assumption F induces a significant jump in the error Δ_{T_S}. Assumption H does not seem to have an impact because the error with M_8 is already poor.

T_S is therefore predicted in reasonable accuracy (26 % error) with only 1-step reaction including losses by endothermicity, thermal dependency of the material properties and in-depth radiation absorption. Following this taxonomy, simpler models would result in an error at least of 57 %. M_4 required only 13 parameters instead of the 33 of M_1, reducing therefore the required effort for calibration.

The shape of the relationship between the error Δ_m and model complexity presents an opposite trend. The predictions of $\dot{m}''$ diverge drastically from the experimental measurements as soon as a single simplification is performed on the chemical degradation complexity. The error Δ_m goes from 43 % to 84 % when the oxygen sensitivity is neglected (assumption B, M_2 to M_3).

After only a few assumptions, Δ_m reaches a plateau at around 84 %. At the opposite of the plateau observed for the error Δ_{T_S} which is the consequence of no improvement when the complexity is increased, in the case of Δ_m, the plateau results from a large disagreement with the measurement. Even if assumptions C to F (added between M_3 and M_7) provokes changes in the predictions of $\dot{m}''$, the fit between the prediction of M_3 and the measurement is already poor (Fig. 4.5b) and the simplifications do not influence Δ_m. The error does not increase above 84 % because in the early stages (< 40 s), the experimental and predicted $\dot{m}''$ are both null. The 16 % of agreement correspond therefore to the prediction of the pyrolysis time.

It is worth mentioning that assumption A (gases released instantaneously, M_1 to M_2) improves the predictions (43 % error with M_2 instead of 50 % with M_1). While the physical phenomenon of mass transfer inside the solid matrix is observed experimentally, its mathematical formulation or its calibration, in M_1, is not satisfactory.

The thermogravimetric analysis (TGA) performed by Hirata et al. [14] reveals a large complexity of the reaction scheme in oxygenated atmosphere (three steps) whereas it seems to be composed only of one reaction in nitrogen.

By performing an equivalent analysis in nitrogen with the models from the taxonomy α, the sensitivity of $\dot{m}''$ to the oxidation reaction is avoided and it is possible to assess the impact of the following assumptions. The models predictions for inert atmosphere are plotted in Fig. 4.7.

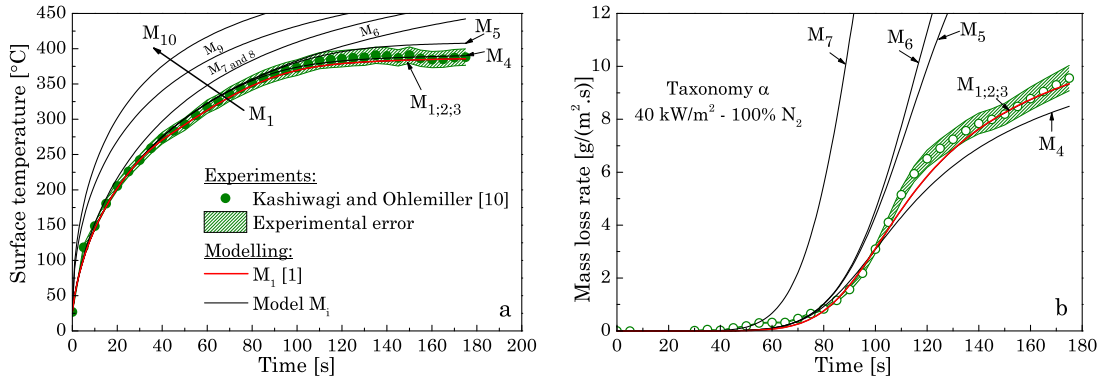

Figure 4.7: Predictions against experimental measurements at 40 kW/m² in nitrogen for models in taxonomy α: (a) surface temperature and (b) mass loss rate.

For T_S, the evolution of the predictions with model complexity provides similar results as in 20 % of O_2. Only models simpler than M_4 (i.e. $M_{i>4}$) predict T_S outside of the experimental uncertainty. Whatever chemical reaction is occurring, the predictions of the surface temperature have a similar level of accuracy.

As expected, $\dot{m}''$ is not influenced by assumption B (oxidation negligible, M_2 to M_3) due to the inert atmosphere surrounding the sample. The simplification of the reaction scheme with the assumption C (1-step chemical reaction, M_3 to M_4), which removes the intermediate species β PMMA, affects the prediction of $\dot{m}''$ after 4 g/(m².s). However, the predictions of $\dot{m}''$ evolves with time in a similar manner than the experimental measurement. However, when the endothermicity of the reaction is neglected (assumption D, M_4 to M_5), the shape of the predicted $\dot{m}''$ is drastically changed.

The quantification of the complexity-error relationship for the taxonomy α in inert atmosphere is plotted in Fig. 4.8. As it was observed in Fig. 4.7a, T_S is relatively well accurate up to M_4. The overestimation using M_5 appears only above 400 °C, which corresponds to a higher threshold than in oxygenated atmosphere. As a consequence, Δ_{T_S} is only at 25 % of error with M_5, which is equivalent to the level of error reached with M_4 in oxygenated atmosphere. This decrease in required complexity (only 12 parameters with M_5) shows that the experimental conditions affect the mechanisms sensitivity. Indeed, the reduction of $\dot{m}''$, caused by the absence of oxidative reaction (Eq. 4.3), provokes a lower level of heat losses by endothermicity and therefore a lower influence of the assumption D (heat of pyrolysis negligible, M_4 to M_5).

Assumption F (thermo-physical parameters invariant, M_6 to M_7) induces an increase of the error Δ_{T_S} which reaches a similar level (≈ 87 %) that in oxygenated atmosphere for the same number of parameters.

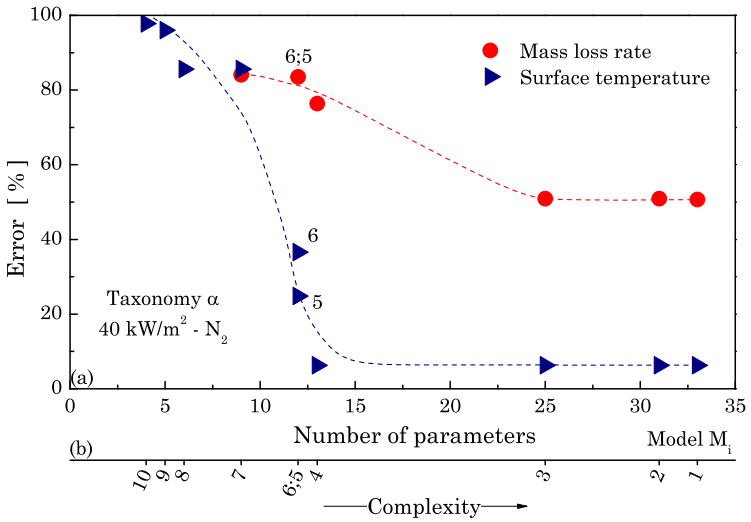

Figure 4.8: Relationship between model complexity (taxonomy α) and prediction error for surface temperature and mass loss rate at 40 kW/m² in nitrogen. The x-axes represent (a) the number of parameters in the models and (b) the reference number of the models.

The prediction of $\dot{m}''$ appears again sensitive to a change of the reaction scheme. The error Δ_m increases from 51 % to 84 % with the simplification of the

reaction scheme to only 1-step (assumption C, M_3 to M_4). Eq. 4.1 is not a limiting reaction in models $M_{i<4}$, meaning that the pyrolysis reaction producing the gas (Eq. 4.2) is not regulate by the production of solid species β_{PMMA}. The suppression of this species by assumption C induces changes only on the material properties. The production rate of gases is affected by the change of density and local temperature.

While the shape of $\dot{m}''$ with M_4 appears close to the experimental measurements in Fig. 4.7b, the quantification of the error Δ_m indicates that the predictions are only slightly better than the predictions using M_5.

As a conclusion of the investigations performed on taxonomy α, the mechanisms controlling the prediction of $\dot{m}''$ and T_S tend to be different. In the case of $\dot{m}''$, the prediction accuracy is affected as soon as an assumption is performed on the chemical mechanisms. While in air the experimental results show that the chemical decomposition is relatively complex, in nitrogen, the degradation is well described with only 1step. A detailed analysis of the predictions in inert atmosphere shows that $\dot{m}''$ is affected also by the evolution of the temperature (mechanisms of heat transfer).

In the case of T_S, accurate predictions can be achieved with a relatively low complexity: only 12 or 13 parameters (depending of the atmosphere) instead of 33 with M_1. The mechanisms impacting significantly the results are from the group of the heat transfer mechanisms (i.e. group (1) from Table 4.1: heat of pyrolysis negligible -assumption D-, thermo-physical parameters invariant -assumption F- and in-depth absorption negligible -assumption H).

The taxonomy α reveals that $\dot{m}''$ requires a high level of complexity concerning the chemical mechanisms, whereas T_S does not. Some results indicate that heat transfer can also affects $\dot{m}''$. The implementation of the assumptions following the taxonomy α does not allow the investigation of the sensitivity of $\dot{m}''$ to the heat transfer mechanisms. For this reason, a second taxonomy, called β and presented Fig. 4.9, is investigated.

3.2.2 Taxonomy β

Taxonomy β is such that the assumptions related to the heat transfer are added before reducing the chemical degradation complexity. This taxonomy is applied at 40 kW/m² in 20 % of O_2 and the predictions for T_S and $\dot{m}''$ are shown in Fig. 4.10.

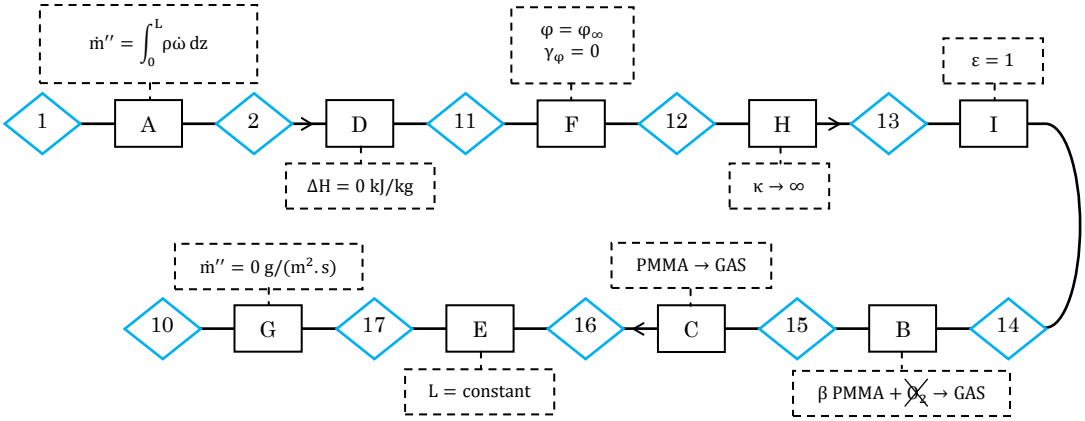

Figure 4.9: Model taxonomy β (diamond: models - square: assumptions).

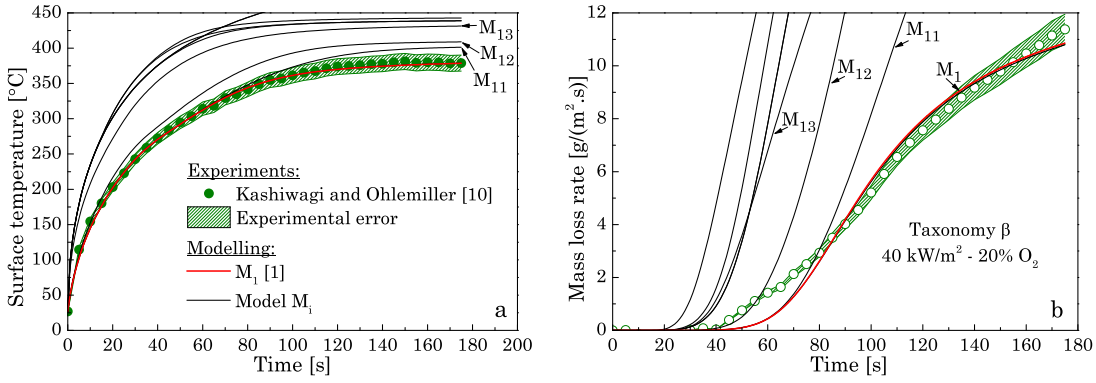

Figure 4.10: Predictions against experimental measurements at 40 kW/m² in 20 % of O_2 for models in taxonomy β: (a) surface temperature and (b) mass loss rate.

As in taxonomy α, neglecting the endothermic heat losses (assumption D, M_2 to M_{11}) provokes the prediction of T_S to fall outside the experimental uncertainty

after a certain temperature threshold (around 375 °C for taxonomy β). However, at the opposite of taxonomy α, the complete reaction scheme (Eqs. 4.1 to 4.3) is still considered when assumption D is performed. This result confirms that the increase of error in the prediction of T_S is not coupled to the assumption performed on the chemical mechanisms. This is of great importance since it makes possible to calibrate the heat losses by endothermicity without predicting the exact reaction scheme but by using the measured mass loss rate.

The prediction of T_S falls mainly out of the experimental uncertainty once the material thermal dependency is neglected (assumption F, M_{11} to M_{12}). However, the predictions using M_{12} stays close to the experimental range and the largest effect on the transient evolution of T_S is obtained by the simplification of the radiation absorption mechanism (assumption H, M_{12} to M_{13}).

The predictions of $\dot{m}''$ (Fig. 4.10b) are also significantly influenced by the simplifications of the heat transfer mechanisms: endothermic heat losses negligible (assumption D, M_2 to M_{11}), invariant material properties (assumption F, M_{11} to M_{12}) and radiation absorption as the surface (assumption H, M_{12} to M_{13}).

The complexity-error relationship Δ resulting from the taxonomy β is plotted in Fig. 4.11. The two curves representing the relationship between model complexity and the predictions error have a similar shape in this taxonomy for both quantities T_S and $\dot{m}''$. This demonstrates that the accuracy of the predictions is affected by the same simplifications.

As it is observed in Fig. 4.11, with only three assumptions (endothermic heat losses negligible, invariant material properties and absorption of the external radiation at the surface, respectively D, F and H, M_2 to M_{13}), the error Δ_{T_S} increases from 7 to 95 %. This influence of the heat transfer mechanisms on Δ_{T_S} is in agreement with the result from taxonomy α. However, the quantification of the error Δ_{T_S} gives more influence to assumption F (thermo-physical parameters invariant, M_{11} to M_{12}) than assumption H (in-depth absorption negligible, M_{12} to M_{13}) whereas the transient prediction shows the opposite in Fig. 4.10a.

The quantification of the error Δ_m confirms that the heat transfer mechanisms have also a large influence on $\dot{m}''$, since Δ_m increases when a simplification from this group is performed. The plateau reached by Δ_m in this taxonomy is higher (95 %) than in taxonomy α (84 %) because the models predict a shorter pyrolysis time (onset of decomposition) in this taxonomy (Fig. 4.10b).

The prediction capability of a pyrolysis model is therefore intimately linked to the accuracy of the energy distribution inside the solid sample and the heat losses. Considering the importance of these aspects, in-depth temperature measurements are required to validate the correct implementation of these mechanisms. Unfortunately, measurements of this quantity are rare in the literature.

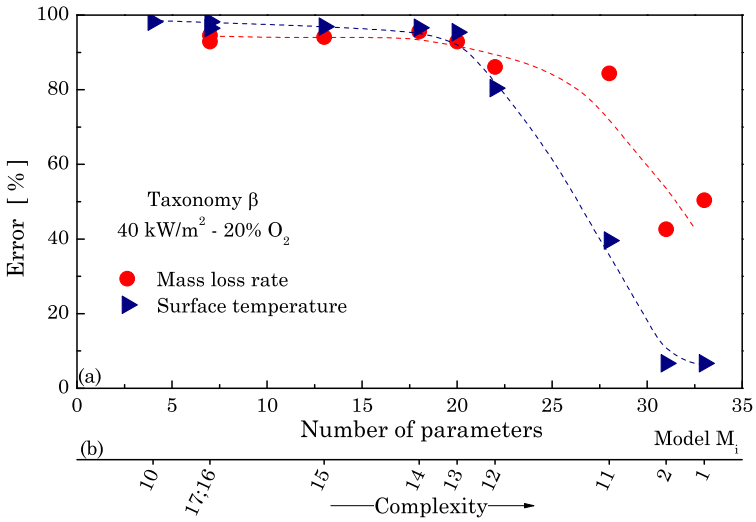

Figure 4.11: Relationship between model complexity (taxonomy β) and prediction error for surface temperature and mass loss rate at 40 kW/m² in 20 % of oxygen. The x-axes represent (a) the number of parameters in the models and (b) the reference number of the models.

4. Conclusion

While one of the first modelling tasks is to select the appropriate model to simulate a physical phenomenon, detailed justifications of the inclusion or exclusion of the different mechanisms are infrequent and the model complexity

is often subjective. A brief comparison of three models used for predicting the same experimental results reveals that some degree of complexity in their mechanisms is unnecessary. Moreover, the complexity of two of the models required the use of inverse modelling for the parameter calibration.

Considering that each parameter owns some uncertainty, the multiplication of the number of mechanisms can only increase the prediction uncertainty. It is therefore important to identify the governing mechanisms.

A novel approach corresponding to a mechanism sensitivity (parameters kept constant) is used to identify the predominant mechanisms for transient pyrolysis. From one of the most complex pyrolysis models for non-charring polymer available in the literature, a series of assumptions and simplifications have been performed; reducing step-by-step its complexity. The specific order of these assumptions defined a taxonomy of model complexity and the influence of this order is investigated via two taxonomies (17 different models in total).

The capability of these models to predict the pyrolysis behaviour of clear PMMA has been observed from the transient evolution of the mass loss rate and the surface temperature at 40 kW/m^2 in two different atmospheric compositions. The qualitative and quantitative evaluations of the disagreement between experimental and numerical results show an increase of the prediction error when model complexity is decreased. While this increase is expected, the shape of the complexity-error relationship is unknown a priori and the study shows that this one is dependent of the observed quantity of interested.

The mechanisms of heat transfer appear to be the most important since their simplifications provokes a large increase of the prediction error for the surface temperature whatever complexity is considered for the chemical mechanisms. In the case of simple chemical complexity (1-step reaction), neglecting the endothermic heat losses, the thermal dependency of the material properties and the mechanism of in-depth absorption implied in this study an increase from 25 to 96 % for the error on the surface temperature predictions (taxonomy α). If the

full reaction scheme is considered (3-steps reaction), the same simplifications implied an increase from 7 to 96 % for the surface temperature (taxonomy β). Moreover, in the latter case, the mass loss rate is also significantly impacted by these simplifications (error from 43 to 83 %).

The complexity associated with mass transfer (i.e. gas pressure evolution) appears negligible in this study.

The transient predictions of $\dot{m}''$ is significantly affected by the level complexity of the chemical mechanisms. However, according to this study, without a good prediction of the energy distribution and the heat losses, the prediction of $\dot{m}''$ could not be accurate neither. It is therefore recommended to not include a large complexity to simulate the chemical degradation if the heat transfer mechanisms included in the model are kept simple.

The knowledge of the predominant mechanisms enables the reorientation of the research concerning their formulations and their ranking for calibration purposes. Fundamental studies are required to improve the submodels linked to heat transfer and more generally energy distribution. An accurate implementation of these mechanisms can be achieved by selecting appropriate quantities of interest (e.g. temperature profile) and experimental conditions where the mechanisms are influent.

Like a parametric sensitivity study, the results are specific to the cases studied (i.e. experimental conditions). Similar investigations are required varying experimental conditions and taxonomies. A global optimisation of the required mechanisms might be assessed using sophisticated techniques such as genetic algorithms applied on the selection of the mechanisms.

References

[1] C. Lautenberger and C. Fernandez-Pello, Generalized pyrolysis model for combustible solids, Fire safety journal 44 (2009) 819-839, http://dx.doi.org/10.1016/j.firesaf.2009.03.011.

[2] S.I. Stoliarov, S. Crowley, R.E. Lyon and G.T. Linteris, Prediction of the burning rates of non-charring polymers, Combustion and flame 156 (2009) 1068-1083, http://dx.doi.org/10.1016/j.combustflame.2008.11.010.

[3] M. Chaos, M.M. Khan, N. Krishnamoorthy, J.L. De Ris and S.B. Dorofeev, Evaluation of optimization schemes and determination of solid fuel properties for CFD fire models using bench-scale pyrolysis tests, Proceedings of the Combustion Institute 33 (2011) 2599-2606, http://dx.doi.org/10.1016/j.proci.2010.07.018.

[4] L. Chwif M.R.P. Barretto and R.J. Paul, On simulation model complexity, Proceedings of the 2000 Winter simulation conference vol.1 (2000) 449-455, http://doi.ieeecomputersociety.org/10.1109/WSC.2000.899751

[5] S.D. Snowling and J.R. Kramer, Evaluation modelling uncertainty for model selection, Ecological modelling 138 (2001) 17-30, http://dx.doi.org/10.1016/S0304-3800(00)00390-2

[6] R. Astrup, K.D. Coates and E. Hall, Finding the appropriate level of complexity for simulation model: an example with forest growth model, Forest ecology and management 256 (2008) 1659-1665, http://dx.doi.org/10.1016/j.foreco.2008.07.016

[7] S.I. Stoliarov, N. Safronava and R.E. Lyon, The effect of variation in polymer properties on the rate of burning, Fire and materials 33 (2009) 257-271, http://dx.doi.org/10.1002/fam.1003.

[8] G.T. Linteris, Numerical simulation of polymer pyrolysis rate: Effect of property variations, Fire and materials 35 (2011) 463-480, http://dx.doi.org/10.1002/fam.1066.

[9] N. Bal, Pyrolysis modelling up to ignition - Part II: Parametric sensitivity and uncertainty analyses (chapter 3), Uncertainty and complexity in pyrolysis modelling, The University of Edinburgh, 2012.

[10] T. Kashiwagi and T.J. Ohlemiller, A study of oxygen effects on nonflaming transient gasification of PMMA and PE during thermal irradiation, Proceedings of the symposium (international) on combustion 19 (1982) 815-823, http://dx.doi.org/10.1016/S0082-0784(82)80257-9.

[11] A. Kashani and J.A. Esfahani, Interactive effect of oxygen diffusion and volatiles advection on transient thermal degradation of poly methyl methacrylate (PMMA), Heat and mass transfer 44 (2008) 641-650, http://dx.doi.org/10.1007/s00231-007-0293-0.

[12] J.E.J Staggs, A theory for quasi-steady single step thermal degradation of polymers, Fire and materials 22 (1998) 109-118, http://dx.doi.org/10.1002/(SICI)1099-1018(1998050)22:3<109::AID-FAM643>3.0.CO;2-C

[13] N. Bal, Pyrolysis modelling up to ignition - Part I: Literature review on sources of uncertainty and experimental variability (chapter 2), Uncertainty and complexity in pyrolysis modelling, The University of Edinburgh, 2012.

[14] T. Hirata, T. Kashiwagi and J.E. Brown, Thermal and oxidative degradation of Poly(methyl methacrylate): Weight loss, Macromolecules 18 (1985) 1410-1418, http://dx.doi.org/10.1021/ma00149a010

[15] R.E. Lyon, N. Safronava and E. Oztekin, A simple method for determining kinetic parameters for materials in fire models, Fire safety science 10 (2011) 765-777, http://dx.doi.org/10.3801/IAFSS.FSS.10-765.

[16] N. Bal and G. Rein, Numerical investigation of the ignition delay time of a translucent solid at high radiant heat fluxes, Combustion and Flame 158 (2011) 1109-1116, http://dx.doi.org/10.1016/j.combustflame.2010.10.014

[17] J.L. Cordova and C. Fernandez-Pello, Convection effects on the endothermic gasification and piloted ignition of a radiatively heated combustible solid, Combustion science and technology 156 (2000) 271-289, http://dx.doi.org/10.1080/00102200008947306.

[18] F. Jiang, J.L. De Ris and M.M. Khan, Absorption of thermal energy in PMMA by in-depth radiation, Fire safety journal 44 (2009) 106-112, http://dx.doi.org/10.1016/j.firesaf.2008.04.004.

[19] J.L. Torero, Flaming ignition of solid fuels, in: The SFPE handbook of fire protection engineering 4th edition, P.J. DiNenno et al. (Eds.), National Fire Protection Association, 2008, chapter 2.11, pp. 2.260-2.278, ISBN-10: 0877658218.

[20] J.L. Cordova, D.C. Walther, J.L. Torero and A.C. Fernandez-Pello, Oxidizer flow effects on the flammability of solid combustibles, Combustion science and technology 164 (2001) 253-278, http://dx.doi.org/10.1080/00102200108952172

Chapter 5

Uncertainty in the calibration process by inverse modelling for polymer pyrolysis

Summary

Polymer pyrolysis is a key phenomenon in solid ignition, flame spread and fire growth. It is therefore an essential part in the understanding of fire behaviour. Advances in pyrolysis modelling during the last decade have mainly resulted in an increase of the number of physical and chemical mechanisms implemented in the models. This stems from the implicit assumption that models with a higher level of complexity should be more accurate. However, a direct consequence of this growth in complexity is the addition of new parameters and the accumulation of modelling uncertainty by the lack of knowledge of their values. Their large number and the difficulty to quantify their values from direct measurements often oblige modellers to solve an inverse

problem to perform the calibration of their models. With this technique, the model equations and the experimental data are consequently coupled to the parameter values. This phenomenon, which is most often ignored, is investigated in this study using different levels of model complexity for the simulation of transient pyrolysis of PolyMethylMethAcrylate in non-flaming conditions. Among the wide range of possible model complexities, five models with a number of parameters going from 30 to 3 are considered. Models with different number of mechanisms achieve a similar level of accuracy by virtue of using different parameter values. The results show the strong presence of multiple compensation effects between different mechanisms, and that an increase of model complexity induces accumulation of uncertainty in the parameter values. It is expected that the use of more and specific data can help to break down the compensation effects. It is therefore desirable that an appropriate equilibrium between model complexity and data quality is drawn in the future.

Collaboration

This chapter results from a joint work performed with Dr Guillermo Rein from the University of Edinburgh (UK).

Nomenclature

A	Pre-exponential factor [s^{-1}]
c	Specific heat [J/(kg.K)]
E_a	Activation energy [kJ/mol]
k	Thermal conductivity [W/(m.K)]
n	Order of reaction [-]
N	Number of experimental points
T	Temperature [K]

Subscripts

∞	Ambient conditions
exp	Experiment
ref	Reference T_{ref} = 300K
sim	Simulation

Greek symbols

γ	Power properties evolution
ε	Absorptivity coefficient [-]
κ	Attenuation coefficient [m^{-1}]
ρ	Density [kg/m^3]
υ	Yield of reaction
φ	Material properties
ϕ	Measurements

1. Introduction

Despite the extensive use and constant development of fire modelling tools, the current state of the art is still not capable of predicting fire growth rate from first principles. The pyrolysis process of the condensed phase represents one of the main challenges related to this problem. It is a key phenomenon in solid ignition, flame spread and therefore in the global understanding of fire behaviour. Advances in pyrolysis modelling during the last decade have mainly resulted in an increase of the number of physical and chemical mechanisms implemented in the models. This stems from the implicit assumption that models with a higher level of complexity should be more accurate. However, a direct consequence of this growth in complexity is the addition of new parameters and the accumulation of modelling uncertainty by the lack of knowledge of their values.

A computational model is based on three main components: the equations of the model, the input parameters, and the experimental data used to validate the model. The equations, direct function of the assumptions performed, describe mathematically the physical and chemical mechanisms which are then solved in time based on the assumed boundary conditions. The input parameters are a set of values required to perform a simulation. This set is composed of material properties (e.g. kinetic triplet, attenuation coefficient), initial and boundary conditions (e.g. incident heat flux, sample thickness, convective cooling) and numerical aspects (e.g. grid size and time steps). The experimental data is made of the measurements to which the model predictions are to be compared (e.g. mass loss rate, surface temperature and in-depth temperature profile).

The goal of a model is to be able to predict the evolution of the pyrolysis behaviour. In practice, the change of experimental conditions can influence the controlling mechanisms [1 (chap 6),2], implying the necessity of adding more mechanisms (simple models are often valid only for specific experimental conditions) or to compensate the simplified mechanisms by considering effective properties which become dependent on the experimental procedure [3,4

(chap 2)]. The first models for the prediction of ignition were simple analytical expressions based on heat conduction. The most recent ones are numerical and multi-physics models of the heat and kinetic transient response of the polymer. Issues grow rapidly with the number of possible mechanisms that can be added.

Once the model equations are chosen, the input parameters are then quantified through a process called calibration. Recently, Stoliarov et al. [5] showed that is possible to quantify many of the material properties from multiple independent experiments. However, for some materials (especially charring materials), challenging experimental difficulties arise and some key input parameters cannot be measured independently [3,6]. Moreover, the scarce availability of experimental data in fire science (especially for new materials) and the large number of parameters required (including new more specific ones) imply that model calibration using independent experiments quickly becomes a prohibitive economic and time cost. The applicability of this methodology is therefore limited.

The number of experiments can be reduced by exploiting the data base available in the literature. However, the variability of the results can be significant [4 (chap 2)]. As an example, Kashiwagi et al. [7] have demonstrated that two materials supplied by different manufacturers, but sold under the same trade name, can present large differences in their pyrolysis behaviour. This material variability cannot be ignored and it is expected to increase with the use of new technologies such as fire retardant and nanocomposites.

The mentioned difficulties associated with the calibration process inspired the concept of inverse modelling. In this case, the experimental data become entirely integrated in the calibration process and an optimisation routine is used to quantify the best set of parameters which explain the observed pyrolysis behaviour. The most used experimental data for model calibration have been the mass loss rate and the surface temperature [8-10]. The optimisation technique used is a function of the number of variables and their interactions. In the past, only the few most uncertain parameters (i.e. the kinetics parameters) were

generally used as potentiometers [11]. However, sophisticated mathematical procedures have been developed to increase the number of parameters optimised simultaneously (e.g. Genetic Algorithm GA [8,12] or Shuffled Complex Evolution SCE [9]). Lautenberger and Fernandez-Pello [10] have shown recently the influence that the choice of algorithm can have on the optimised parameters.

With this calibration technique, the optimised parameters become coupled to the set of equations included in the model and to the experimental data. The objective of this study is to assess the influence of the model complexity (i.e. mechanisms), most often ignored, on the calibration process using inverse modelling. The investigation is performed for the most understood non-charring polymer, PolyMethylMethAcrylate (PMMA), in non-flaming conditions.

This modern topic of model complexity goes beyond polymer pyrolysis but applies to modelling of physical process in general [13,14]. The question of how to determine the most beneficial level of model complexity escapes simplistic approaches. This study is an approach to assess the prediction uncertainty caused by the selection of the model complexity.

2. Experimental data

The results from Kashiwagi and Ohlemiller [15] are used in this study as experimental data. They exposed 15 mm thick PMMA samples, vertically oriented, to a constant level of heat flux using a graphite plate heated at 1260 °C. While they performed tests in different atmospheric compositions and at different heat flux levels, only the results obtained in [O_2] 20% / [N_2] 80% at 40 kW/m^2 are used. The influence of the experimental data on the calibration process by inverse modelling is out of the scope of this work.

The mass loss rate and surface temperature measurements are plotted in Fig. 5.1. The experimental error has been estimated at 3 and 5 % respectively for the surface temperature and the mass loss rate according to the information given in Ref. [15].

3. Model equations

3.1. Reference model

Lautenberger and Fernandez-Pello [8], using their pyrolysis model called GPYRO, have performed an inverse modelling analysis with the full set of experimental data provided by Kashiwagi and Ohlemiller [15]. Their best predictions for the experiments studied in this work are also shown in Fig. 5.1.

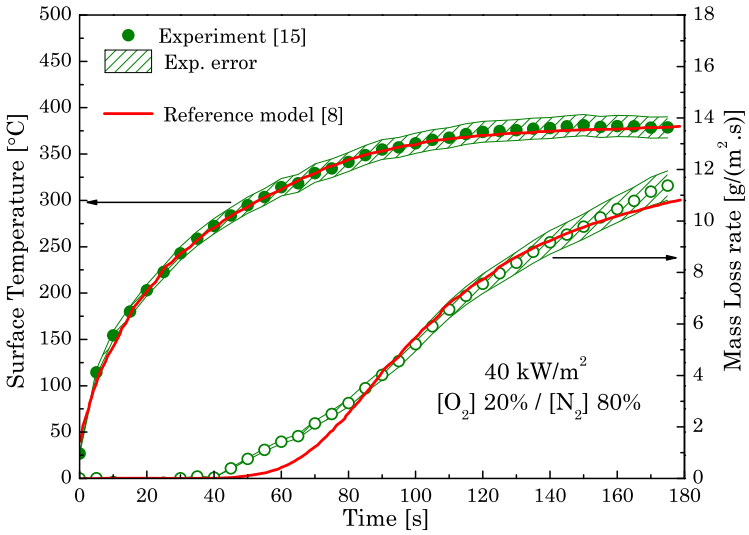

Figure 5.1: Mass loss rate and surface temperature of clear PMMA at 40 kW/m² in 20 % oxygen (non flaming conditions): measurements and predictions.

The simulated mass loss rate follows closely the experimental measurements (within experimental errors). However, in the early (< 80 s) and final (> 160 s) stages, the mass loss rate is under-predicted. In the case of the surface temperature, the predictions capture the experimental behaviour even better.

The model used by Lautenberger and Fernandez-Pello [8], called the "reference model" in the rest of this study, is based on mass, species and energy balances for the condensed phase. The source terms include in the energy conservation encompass the energy consumed by the chemical reactions and the

in-depth radiation absorption. On top of that, the mass, species and momentum conservation equations are solved for the pyrolysis gases inside the solid matrix. The momentum equation enables the consideration of the gas pressure evolution and a description of the mass flux of gases released at the front surface instead of assuming an instantaneous release of the pyrolysis gases produced in depth.

The pyrolysis chemical degradation used by Lautenberger and Fernandez-Pello [8] is composed of three steps (Eqs. 1 to 3).

$$\mathrm{PMMA} \rightarrow \beta\ \mathrm{PMMA} \tag{5.1}$$

$$\beta\ \mathrm{PMMA} \rightarrow \mathrm{GAS} \tag{5.2}$$

$$\beta\ \mathrm{PMMA} + \upsilon_{O_2} O_2 \rightarrow \upsilon_{GAS}\mathrm{GAS} \tag{5.3}$$

In the first reaction (Eq. 5.1) the solid species PMMA produces another solid species called β PMMA. This reaction allows variations of the material properties to account for the formation of bubbles. This reaction does not absorb energy (i.e. heat of pyrolysis $\Delta H = 0$ kJ/kg). The other two reactions produce pyrolysis gases: one by thermal degradation (Eq. 5.2) whereas the other by oxidation (Eq. 5.3). They are both assumed endothermic. These reactions are modelled by Arrhenius's laws with the kinetics triplet: pre-exponential factor A, activation energy E_a and order of reaction n. The material properties (thermal conductivity k, specific heat c and density ρ), expressed generically by φ, are allowed to vary with temperature in Eq. 5.4, following a power law controlled by γ_φ. This temperature dependency implies a potential swelling or shrinking only due to thermal impact.

$$\varphi = \varphi_\infty \left(\frac{T}{T_{ref}}\right)^{\gamma_\varphi} \qquad \varphi \in \{k\,;\ \rho\,;\ c\} \tag{5.4}$$

The radiation absorption (non-reflected fraction of the incident radiation - based on the absorptivity/emissivity ε) is assumed to occur in-depth using Beer-Lambert's law with a finite attenuation coefficient κ. The full set of equations is available elsewhere [16].

3.2. Model taxonomy

In this study, the model GPYRO is used with different levels of complexity. The most complex model, called M_1, is identical to the reference model with the exception that the pressure evolution inside the condensed phase is considered negligible (i.e. gas phase momentum equation not solved). Lautenberger et al. [17] used a similar level of complexity for the pyrolysis behaviour of fibre reinforced polymer. The other models, ranked from M_2 to M_5 (decreasing level of complexity), correspond to simplifications of M_1. The total number of parameters evolves from 30 to 3 between M_1 and M_5.

M_2 assumes that among the mechanisms included in M1, the predominant ones are related to the chemical decomposition of the solid sample. The evolution of the material properties with temperature is therefore considered negligible ($\gamma_\varphi = 0$) and the energy is integrally ($\varepsilon = 1$) absorbed at the surface ($\kappa \to \infty$). On top of that, the heat sinks due to the endothermicity of the reactions are assumed not to be significant ($\Delta H = 0$ kJ/kg).

M_3 considers only 1 step reaction ($\mathrm{PMMA} \to \mathrm{GAS}$) but the heat transfer mechanisms from M_1 are all considered. Cordova and Fernandez-Pello [11] estimated with a similar model the time to reach critical mass flux (ignition criterion) for black PMMA subjected to a constant heat flux level.

M_4 suggests that the chemical degradation is secondary (opposite assumption as M_2) and more importance is put to the heat transfer mechanisms. The solid is therefore assumed inert (i.e. no reaction) but the in-depth radiation absorption and the temperature dependency of the material properties are modelled. Jiang et al. [18] provided an analytical solution for a model close to M_4 but without the temperature dependency mechanism.

Finally, the simplest model M_5, is equivalent to M_4, except that the solid is assumed to absorb at the surface ($\varepsilon = 1$ and $\kappa \to \infty$) and the material properties are constant ($\gamma_\varphi = 0$). Rhodes and Quintiere [19] used a similar approach to estimate the ignition time of non-charring polymers.

Table 5.1 summarizes the assumptions of the different models studied in this paper and the number of parameters to optimise. There are many possible model taxonomies but the selected one serves to illustrate the global levels of complexity that can be found in the literature for finite-rate chemistry pyrolysis models.

Table 5.1: Taxonomy of models complexity.

Assumption invoked	Models				
	M_1	M_2	M_3	M_4	M_5
Heat of pyrolysis negligible: $\Delta H = 0$ kJ/kg		✓		✓	✓
1-step chemical degradation: PMMA → GAS			✓	✓	
Inert solid: no kinetics, no mass loss				✓	✓
Constant thermo-physical parameters: $\gamma_\varphi = 0$		✓			✓
Radiation absorption at the surface: $\varepsilon = 1$, $\kappa \to \infty$		✓			✓
Number of input parameters	30	18	12	8	3
Reference similar models	[17]	-	[11]	[18]	[19]

4. Optimisation process

The process of inverse modelling has been performed in this study with a genetic algorithm (GA) implemented in GPYRO. This technique, based on Darwinian evolution, enables the optimisation of several parameters for non-linear models. Details on the principle and its implementation in GPYRO are available in the user and technical reference guides of the software [16].

For each model, a GA with a population of 250 individuals has been run, in order to obtain the best set of parameters which predicts the measured mass loss rate and the surface temperature evolution presented on Fig. 5.1. The process of optimisation has been performed over 500 generations, except for M_1 which was judged more ambitious and for which the process was performed over 1000 simulations.

The fitness, $f_{sim \to exp}$, between experiments and simulations is estimated thanks to Eq. 5.5.

$$f_{sim \to exp} = \frac{1}{N} \sum \left(\frac{\phi_{exp}}{|\phi_{exp} - \phi_{sim}| + 0.05\phi_{exp}} \right)^2 \quad (5.5)$$

where ϕ is the quantity of interest (either surface temperature or mass loss rate) and N is the number of times experimental data and predictions are compared.

There are two possible $f_{sim \to exp}$, one for the mass loss and one for the surface temperature. For the calibration of M_1, M_2 and M_3, the fitness used is the sum of both, whereas for M_4 and M_5, only the surface temperature fitness is used since the inert solid assumption leads to no mass loss predictions.

The research domain is based on a literature review of the parameter variability for PMMA [4 (chap 2)]. These ranges have been taken wider on purpose to avoid any possible restriction derived from limitation of the current literature.

5. Results and discussion

The set of the 10 best simulations obtained with GA for each model is plotted on Figs. 5.2 to 5.5. The results obtained with the reference model are also represented for comparison. The calculated fitness spreads between 372 and 383 for M_1, 358 and 387 for M_2 and between 382 and 403 for M_3. A better fitness is therefore obtained for a model which does not have the highest level of complexity.

By claiming different values for the input parameters, all models are capable of following the measurements with some degree of scatter. This scatter is more pronounced for the mass loss rate than for the surface temperature and it is found more significant with M_2 (Fig. 5.3). Note that the simulations obtained with M_2 which over predict or under-predict significantly the surface

temperature (Fig. 5.3b), are not the same simulations failing to simulate the mass loss rate (Fig. 5.3a).

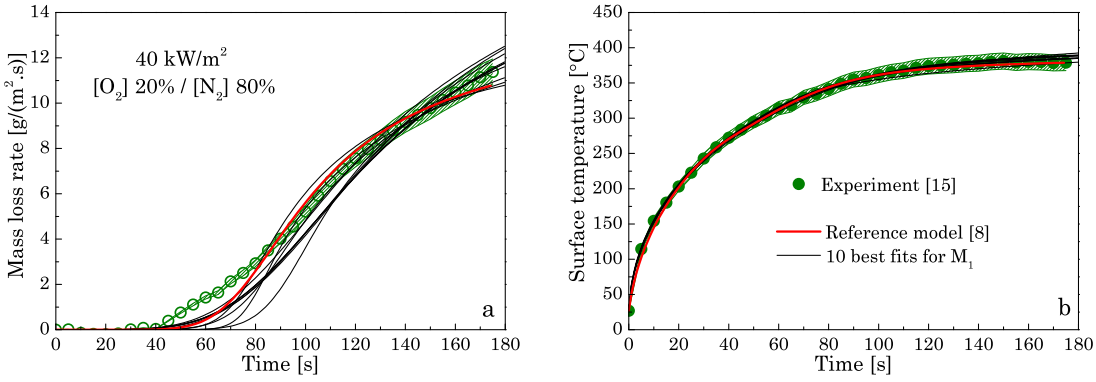

Figure 5.2: Comparison of the 10 best simulations obtained with model M_1 against the experimental results: (a) mass loss rate and (b) surface temperature.

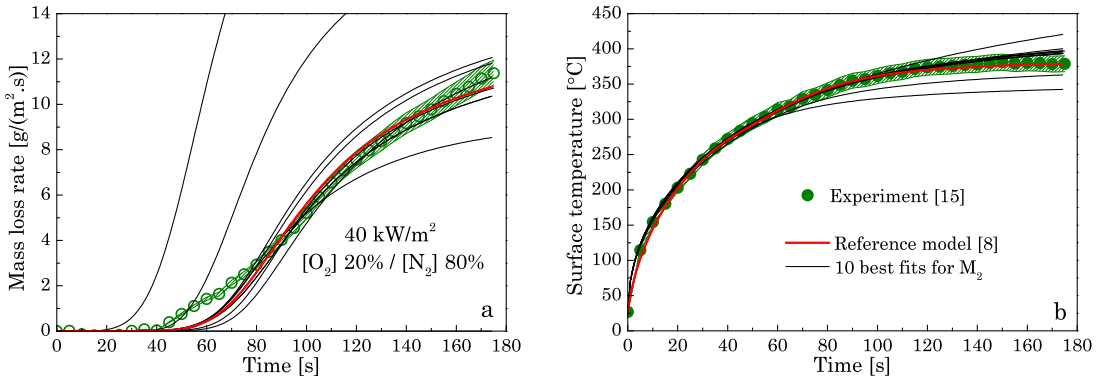

Figure 5.3: Comparison of the 10 best simulations obtained with model M_2 against the experimental results: (a) mass loss rate and (b) surface temperature.

The predictions from M_4 and M_5 are shown in Fig. 5.5. These models assume that the solid is inert, and therefore only the surface temperature can be compared. In both cases, the 10 best fit simulations predict accurately the surface temperature with negligible scatter up to a threshold temperature around 370 °C (Fig. 5.5). The inclusion of in-depth absorption (M_4) leads to a slight improvement of 10 °C but the over prediction above 380 °C remains. The failure of inert assumption models to predict the surface temperature above this

threshold has been observed also by Cordova et al. [20] (using an approximate analytical solution of M_5). They claimed that the failure is related to the absence of heat losses by endothermicity of the pyrolysis reaction. The effect of endothermic pyrolysis can be further explored by looking at the improved surface temperature predictions of M_1 and M_3 (Figs. 5.2b and 5.4b). With both models, the surface temperature predictions are inside the experimental error. There are two mains differences between the model couples {M_1 ; M_3} and {M_4 ; M_5}: the chemical reaction scheme and the heat losses by endothermicity. The model M_2, which includes a reaction scheme but does not consider endothermic pyrolysis, fails to predict correctly the surface temperature above 375 °C. This result confirms the findings by Cordova et al. [20]: the accurate prediction of the surface temperature above 375 °C requires inclusion of endothermic pyrolysis. The failure of the inert assumption models is not linked to the change of solid species, induced by the reaction scheme and which can influence the heat transfer by conduction. However, the heat loss mechanism can be compensated in the prediction of the mass loss rate since M_2 can provide predictions as good as those of the reference model (Fig. 5.6).

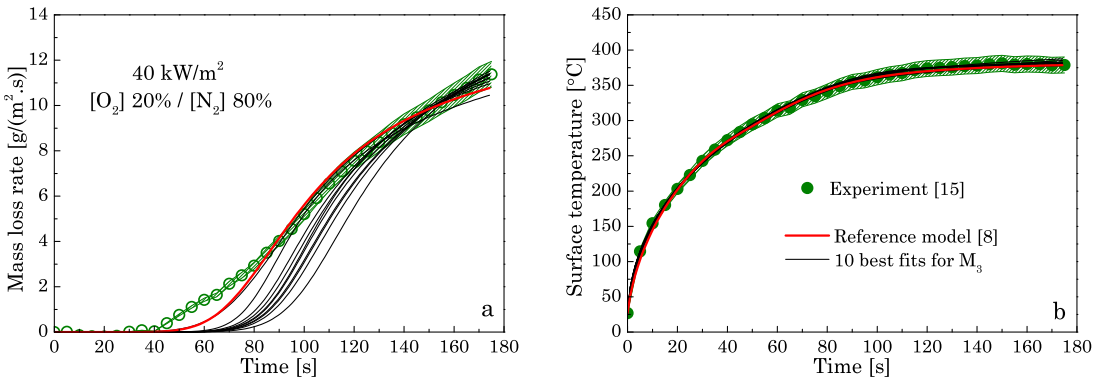

Figure 5.4: Comparison of the 10 best simulations obtained with model M_3 against the experimental results: (a) mass loss rate and (b) surface temperature.

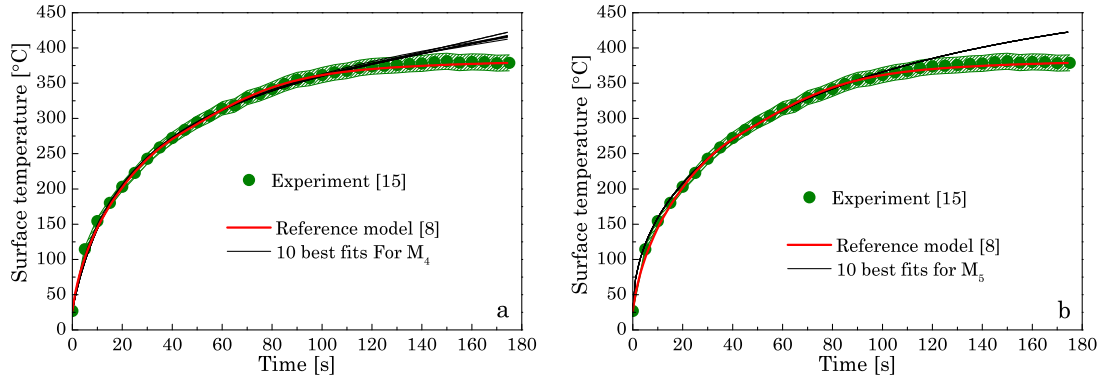

Figure 5.5: Comparison of the 10 best simulations obtained with model (a) M_4 and (b) M_5 against the experimental results for the surface temperature.

Figure 5.6 shows, for each model M_1, M_2 and M_3, the best single match to the mass loss rate prediction from the reference model. There is at least, for each model, one simulation presenting a similar level of accuracy to the reference model. The agreement between different models using different parameter values illustrates the process of compensation effect. This artefact, which is commonly recognised in chemical kinetics [21], is shown in this study to apply also for heat transfer.

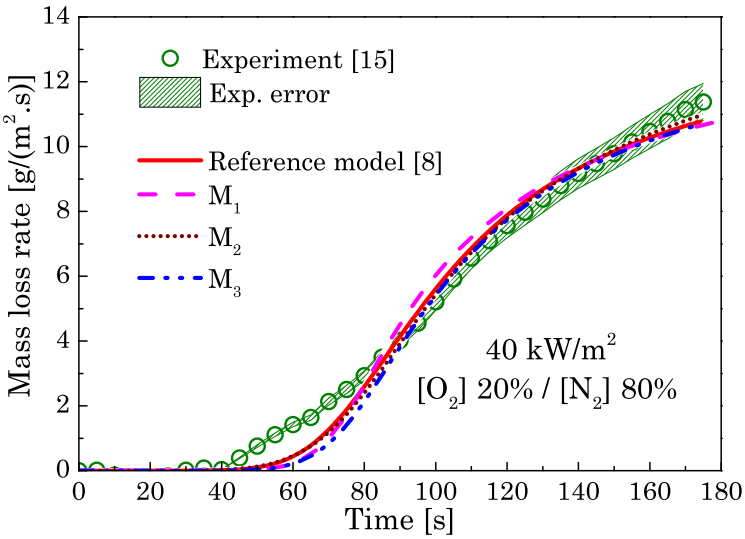

Figure 5.6: Mass loss rate evolution of the single best match from M_1, M_2 and M_3 to reference model prediction.

Figure 5.7 shows the different values of the input parameters for the 10 best fits of each model. The spread of values is wider for the models with higher complexity (i.e. widest spread is for M_1 and M_2). This is an indication that the number of compensation effects increases significantly with the number of parameters. Many of the optimised values go significantly over the range found in the literature, indicating that unphysical values are found during the optimisation.

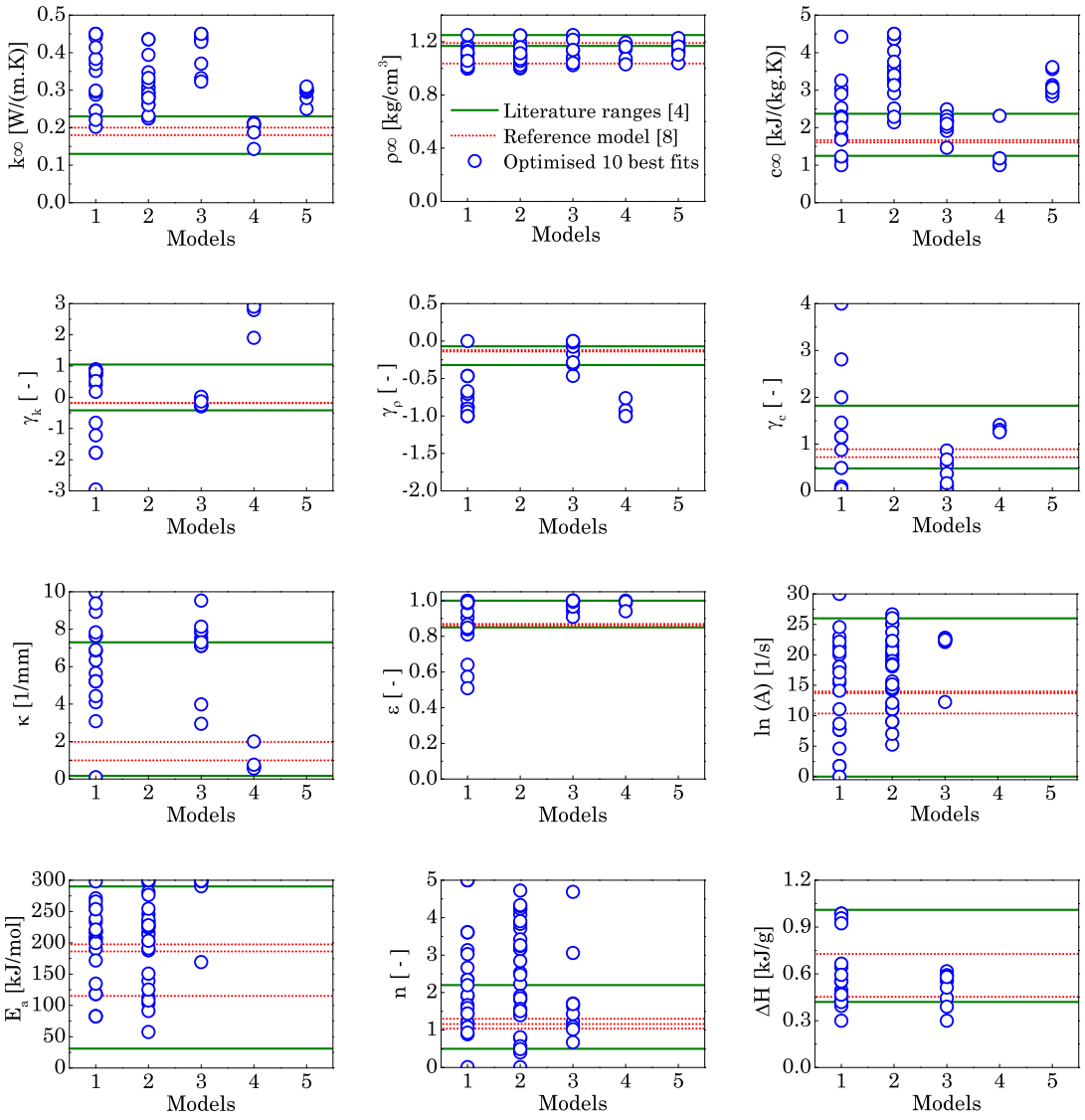

Figure 5.7: Comparison of the optimised parameters from the 10 best fits for each model M_1 to M_5 with ranges found in the literature (solid lines) and values obtained with the reference model (dotted lines).

One issue related to inverse modelling is that it is difficult to take into consideration known correlations existing between parameters. As an example, for the thermo-physical properties described by Eq. 5.4, the coefficient γ_φ and the value at ambient temperature φ_∞ are linked to each other [4 (chap 2)]. As a consequence, even if the values for φ_∞ and γ_φ can both be found separately to be inside the literature ranges after optimisation, their combination could be unrealistic. This issue is observed more strongly in model M_1. As an example, for one of the best fits obtained with M_1, the parameters γ_φ and φ_∞ for the specific heat are found to be equal respectively to 0.88 and 2900 J/(kg.K). Both of these values are included in the literature ranges but their combination provides unrealistic values for temperature higher than 100 °C.

As has been mentioned, models M_1 to M_3 can reproduce almost identically the prediction of the mass loss rate (Fig. 5.6) and of the surface temperature obtained by the reference model [8]. These do not represent necessarily the best predictions obtained with the models but their comparison is interesting due to the observable compensation effect. Table 5.2 compares the parameters of these simulations. While most of the values obtained with M_2 and M_3 agree approximately with the order of magnitude of those found by Lautenberger and Fernandez-Pello [8], the ones obtained with M_1 are not in agreement and seem unrealistic.

Note that the mass loss rate simulations (M_1 to M_3 and reference model) fail to capture the early stage (Figs. 5.2a to 5.4a) of the pyrolysis behaviour. This failure cannot be explained with the results presented here. It is probably the consequence of the change of the oxidative pyrolysis effect when the mass flux released at the free surface grows and displaces ambient oxygen as claimed by Kashiwagi and Ohlemiller [15] and Vovelle et al. [22]. This failure is a hint that another mechanism (probably in the gas phase) is required to capture the full mass loss evolution. However, more numerical and experimental evidence combined with fundamental studies are needed to confirm this theory before

oxygen displacement can be readily added to a pyrolysis model without accumulating uncertainty with new unknown parameters. The level of complexity associated with a model should be increased only when investigations show that the failure of the predictions to capture the experimental behaviour is related to its high degree of simplifications and that it is possible to quantify the new parameters added with the extra mechanisms.

Table 5.2: Ranges of optimised values for best matched predictions of the mass loss rate between the reference model and M_1 to M_3.

Variables	Reference model [8]	M_1	M_2	M_3
k [W/(m.K)]	[0.16 ; 0.20]	[0.29 ; 0.82]	[0.28 ; 0.32]	[0.26 ; 0.32]
c [J/(kg.K)]	[1572 ; 3327]	[1122 ; 32565]	[3402 ; 3614]	[2109 ; 3704]
ρ [kg/m^3]	[923 ; 1193]	[470 ; 1250]	[1007 ; 1158]	[885 ; 1146]
κ [1/m]	[1000 ; 1980]	[4430 ; 6870]	N.A.	7106
ε [-]	[0.86 ; 0.87]	[0.51 ; 0.99]	N.A.	0.91
log(A) [1/s]	[10^{10} ; 10^{16}]	[10^{17} ; 10^{25}]	[10^{12} ; 10^{19}]	$10^{12.3}$
E_a [kJ/mol]	[115 ; 198]	[218 ; 259]	[125 ; 246]	169
n [-]	[1.04 ; 1.31]	[0.8 ; 5]	[1.51 ; 4.72]	1.71
ΔH [kJ/g]	[0.45 ; 0.73]	[0.3 ; 0.96]	N.A.	0.39

M_1, M_2 and M_3 can predict similar mass loss evolution to the reference model (Fig. 5.6) but this is achieved by using different parameter values. These differences have a significant influence on the in-depth temperature profile as shown in Fig. 5.8. Temperature differences up to 50 °C are observed between the simulations.

The accuracy of thermocouples positioned close to the surface is low due to the presence of bubbles and melted polymer. However, the temperature evolution in-depth and away from the free surface, where the bubbles are not present, can be measured with an accuracy much lower than 50 °C and used as experimental data in order to reduce the uncertainty on the parameter during

the calibration process. The level of complexity of a model should be related to the resources available to calibrate it.

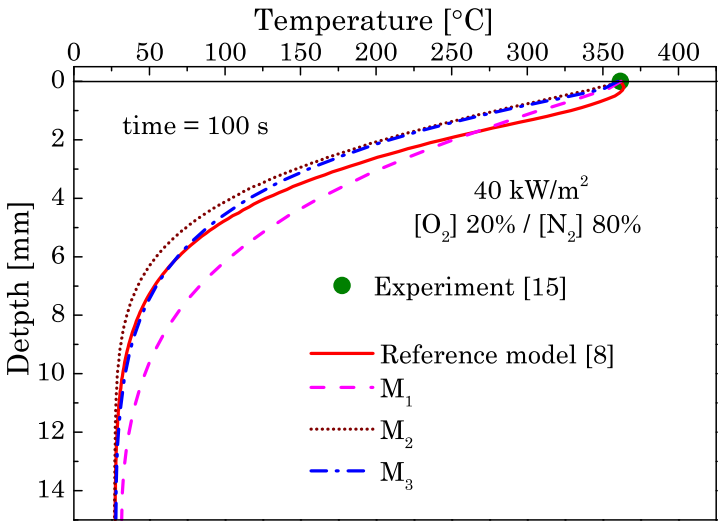

Figure 5.8: Comparison of the in-depth temperature prediction for the simulations presenting equivalent predictions of the mass loss rate.

6. Conclusion

The influence of the model complexity on the calibration process by inverse modelling has been investigated in this study using genetic algorithms. It is shown that the same experimental data can be accurately predicted with different levels of complexity by using different parameter sets (number and values). This reveals the presence of multiple compensation effects between the mechanisms. They are shown to increase with model complexity and can lead to unphysical values for the optimised input parameters. These compensation effects in excessively complex models can prevent the understanding of the essential mechanisms.

While inverse modelling is a powerful tool, the current state-of-the-art is such that uncertainty is created by the possible compensation effect when the level of complexity is increased arbitrarily. A model should be kept as simple as possible unless investigations enable the identification of the reason of failure of

its predictions. The comparison of the predictions from the different model equations suggests that a certain level of complexity is required to capture the experimental pyrolysis behaviour.

The calibration conducted in this study considers surface temperature and mass loss rate. The process of calibration can be improved by using data obtained from different experimental conditions (e.g. different heat fluxes, ambient gas concentrations) where the importance of the parameters (i.e. sensitivity) is changed but it can be also improved by varying the type of measurements (e.g. in-depth temperature profile). It is expected that the use of more and better quality data can help to break down the compensation effects. In the future, it is therefore desirable that a more appropriate level of complexity is reached by considering the quality of the available data.

References

[1] P. Girods, N. Bal, H. Biteau, G. Rein and J.L. Torero, Comparison of pyrolysis behaviour results between the Cone Calorimeter and the Fire Propagation Apparatus heat sources, Fire safety science 10 (2011) 889-901, http://dx.doi.org/10.3801/IAFSS.FSS.10-889.

[2] T.J. Ohlemiller and M. Summerfield, Radiative ignition of polymeric materials in oxygen/nitrogen mixtures, Proceedings of the symposium (international) on combustion 13 (1971) 1087-1094, http://dx.doi.org/10.1016/S0082-0784(71)80106-6.

[3] E.S. Oztekin, S.B. Crowley, R.E. Lyon, S.I. Stoliarov, P. Patel and T.R. Hull, Sources of variability in fire test data: a case study on poly(aryl ether ether ketone) (PEEK), Combustion and flame 159 (2012) 1720-1731, http://dx.doi.org/10.1016/j.combustflame.2011.11.009

[4] N. Bal, Pyrolysis modelling up to ignition - Part I: Literature review on sources of uncertainty and experimental variability (chapter 2), Uncertainty and complexity in pyrolysis modelling, The University of Edinburgh, 2012.

[5] S.I. Stoliarov, S. Crowley, R.E. Lyon and G.T. Linteris, Prediction of the burning rates of non-charring polymers, Combustion and flame 156 (2009) 1068-1083, http://dx.doi.org/10.1016/j.combustflame.2008.11.010.

[6] S.I. Stoliarov, S. Crowley, R.N. Walters and R.E. Lyon, Prediction of the burning rates of charring polymers, Combustion and flame 157 (2010) 2024-2034, http://dx.doi.org/10.1016/j.combustflame.2010.03.011

[7] T. Kashiwagi, A. Inaba and J.E. Brown, Differences in PMMA degradation characteristics and their effects on its fire properties, Fire safety science 1 (1986) 483-493, http://dx.doi.org/10.3801/IAFSS.FSS.1-483.

[8] C. Lautenberger and C. Fernandez-Pello, Generalized pyrolysis model for combustible solids, Fire safety journal 44 (2009) 819-839, http://dx.doi.org/10.1016/j.firesaf.2009.03.011.

[9] M. Chaos, M.M. Khan, N. Krishnamoorthy, J.L. De Ris and S.B. Dorofeev, Evaluation of optimization schemes and determination of solid fuel properties for CFD fire models using bench-scale pyrolysis tests, Proceedings of the Combustion Institute 33 (2011) 2599-2606, http://dx.doi.org/10.1016/j.proci.2010.07.018.

[10] C. Lautenberger and C. Fernandez-Pello, Optimization algorithms for material pyrolysis property estimation, Fire safety science 10 (2011) 751-764, http://dx.doi.org/10.3801/IAFSS.FSS.10-751.

[11] J.L. Cordova and C. Fernandez-Pello, Convection effects on the endothermic gasification and piloted ignition of a radiatively heated combustible solid, Combustion science and technology 156 (2000) 271-289, http://dx.doi.org/10.1080/00102200008947306.

[12] G. Rein, C. Lautenberger, A.C. Fernandez-Pello, J.L. Torero and D.L. Urban, Application of genetic algorithms and thermogravimetry to determine the kinetics of polyurethane foam in smoldering combustion, Combustion and flame 146 (2006) 95-108, http://dx.doi.org/10.1016/j.combustflame.2006.04.013

[13] N. Oreskes, K. Shrader-Frechette and K. Belitz, Verification, Validation, and Confirmation of Numerical Models in the Earth, Science, New Series 263 (1994) 641-646, http://dx.doi.org/10.2307/2883078

[14] R. Astrup, K.D. Coates and E. Hall, Finding the appropriate level of complexity for simulation model: an example with forest growth model, Forest ecology and management 256 (2008) 1659-1665, http://dx.doi.org/10.1016/j.foreco.2008.07.016

[15] T. Kashiwagi and T.J. Ohlemiller, A study of oxygen effects on nonflaming transient gasification of PMMA and PE during thermal irradiation, Proceedings of the symposium (international) on combustion 19 (1982) 815-823, http://dx.doi.org/10.1016/S0082-0784(82)80257-9.

[16] C. Lautenberger, A Generalized Pyrolysis Model for Combustible Solids, PhD dissertation, The University of California, Berkeley, 2007, <http://escholarship.org/uc/item/7wz5m7dg>.

[17] C. Lautenberger, E. Kim, N. Dembsey and C. Fernandez-Pello, The role of decomposition kinetics in pyrolysis modelling - Application to a fire retardant polyester composite, Fire safety science 9 (2009) 1201-1212 http://dx.doi.org/10.3801/IAFSS.FSS.9-1201

[18] F. Jiang, J.L. De Ris and M.M. Khan, Absorption of thermal energy in PMMA by in-depth radiation, Fire safety journal 44 (2009) 106-112, http://dx.doi.org/10.1016/j.firesaf.2008.04.004.

[19] B.T. Rhodes and J.G. Quintiere, Burning rate and flame heat flux for PMMA in a cone calorimeter, Fire safety journal 26 (1996) 221-240, http://dx.doi.org/10.1016/S0379-7112(96)00025-2

[20] J.L. Cordova, D.C. Walther, J.L. Torero and A.C. Fernandez-Pello, Oxidizer flow effects on the flammability of solid combustibles, Combustion science and technology 164 (2001) 253-278, http://dx.doi.org/10.1080/00102200108952172

[21] M.C. Bruns, J.H. Koo and O.A. Ezekoye, Population-based models of thermoplastic degradation: Using optimization to determine model parameters, Polymer degradation and stability, 94 (2009) 1013-1022, http://dx.doi.org/10.1016/j.polymdegradstab.2009.02.007.

[22] C. Vovelle, R. Akrich and J-L. Delfau, Mass loss rate measurements on solid materials under radiative heating, Combustion science and technology 36 (1984) 1-18, http://dx.doi.org/10.1080/00102208408923722

Chapter 6

Comparison of pyrolysis behaviour results between the Cone Calorimeter and the Fire Propagation Apparatus heat sources

Summary

The Cone Calorimeter and the Fire Propagation Apparatus (FPA) are often used to carry out flammability studies of materials. There are various differences in the set up of these two devices that could lead to different fire behaviour for the same material. Among these, the impact of the different heat sources used is studied here. The Cone Calorimeter employs electric coils and the FPA uses tungsten lamps to radiate a given heat flux level to the sample. Experiments are conducted in the FPA set up using a conical resistance or tungsten lamps as the heat source with clear PMMA and wood samples. Mass loss and temperature measurements are taken during the tests, and the bubble

layer depth is measured after the tests. Significant differences in the pyrolysis behaviour of both samples between the Cone Calorimeter and the FPA are consistently observed at the same heat flux level. The theory of radiative heat transfer and qualitative modelling show that the wavelength dependency of the radiation, reflectance and in-depth radiation absorption are the main reasons explaining the different pyrolysis behaviours. The conclusion reached experimentally in this chapter confirmed the theoretical findings from previous studies.

Collaboration

This chapter results from a joint work performed with Dr Pierre Girods from ENSTIB, the University of Nancy (France), Dr Hubert Biteau, Dr Guillermo Rein and Prof José L. Torero from the University of Edinburgh (UK).

Nomenclature

L	Optical path [m]
r	Reflectivity [-]
t	Time [s]
T	Temperature [K]
Subscripts	
alu	In aluminium block
ign	At ignition
ini	Initial condition
λ	Wavelength dependent
Greek symbols	
α	Absorbance [-]
γ	Dimensionless mass loss [-]
κ	Attenuation coefficient [m^{-1}]

1. Introduction

Research in fire safety related to material characterization typically involves the use of bench-scale apparatus such as the Cone Calorimeter [1] or the FM Global Fire Propagation Apparatus (FPA) [2]. Both apparatuses aim to provide similar information on the behaviour of materials exposed to an external heat flux [3,4]: ignitability (time to ignition, critical heat flux), heat release rate, combustion gases, mass loss and others. Accurate measurements of these variables are essential to understand the response of materials to fire and to obtain relevant flammability properties. Knowledge of the latter allows an

advanced description of the chemical and physical mechanisms taking place during burning, i.e. modelling.

The designs of the Cone Calorimeter [3] and the FPA [4] were defined more than 30 years ago. While the exhaust and gas collection systems are relatively similar, the heating system and the geometry of the combustion chamber contain significant differences. Under similar experimental conditions, there is an expectation that similar results will be obtained since both apparatuses were designed to be able to extract material properties. However, experimental measurements have shown otherwise (Fig. 6.1).

The time to ignition measurements carried out with the Cone Calorimeter and the FPA (or slight variants of this apparatus) for black PolyMethylMethAcrylate (PMMA) samples (Fig. 6.1) show two distinct groups of data. The samples of black PMMA ignite faster with the Cone Calorimeter than with the FPA.

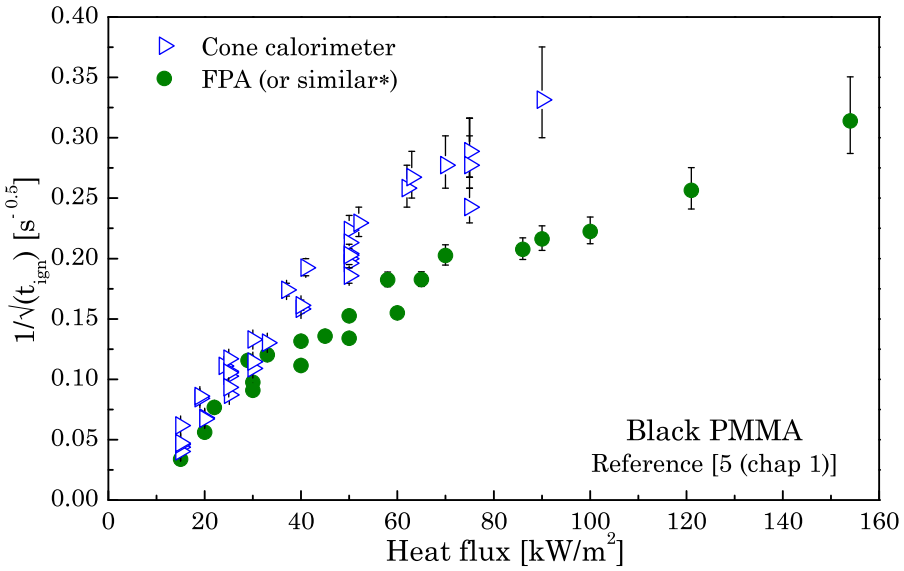

*Factory Mutual Research Corporation's Flammability apparatus and Advanced Flammability Measurements apparatus

Figure 6.1: Inverse square root of the time to ignition for black PMMA samples extracted from the literature. The uncertainty is estimated at ± 2 s.

Given the importance of the flammability properties when defining standard material classification or when using fire models, the origins of these differences

need to be fully understood. The magnitude and consistency of the differences between the two test methods makes it unlikely that it stems only from errors inherent to heterogeneities of the tested materials or from errors associated with the measurements. Consequently, potential biases relative to the methodology need to be investigated.

To be relevant, the argument has to emphasize the main differences between both apparatuses:

- The sample holder: it is square (stainless steel) for the Cone Calorimeter and square or circular (aluminium) for the FPA. Dimensions are nevertheless consistent.
- The design of the combustion chamber: different geometry.
- The pilot used for ignition: spark for the Cone Calorimeter and air/ethylene flame for the FPA.
- The heating source type: truncated cone made of electrical coils for the Cone Calorimeter and 6 tubular quartz-filled with halogen gas placed in a rectangular-shaped enclosure (4 lamps) for the FPA.
- The heating source position: directly above the sample for the Cone Calorimeter and on the side for the FPA.
- The experimental protocols: the main difference is linked to the presence of air supply (200 l/min recommended) blowing under the sample in the case of the FPA.

The equipment design and the experimental protocols of both apparatuses are explicitly mentioned in the corresponding standards: ASTM 1354-10a (Cone Calorimeter) [1] and ASTM E2058-03 (FPA) [2].

The degree of influence of these differences on the experimental results is best assessed on a one-to-one basis (uncoupled manner).

A non-exhaustive literature review [6–11] shows that the influence of the radiative characteristics of the heater source on the results is an area of concern.

Thomson and Drysdale [6] studied the impact of the spectral distribution on the time to ignition for PMMA using a conical heater. In order to assess the impact, they used the same heater but with two different experimental protocols. First, they varied the heat flux by increasing and decreasing the

temperature of the heater element while they kept the distance to the sample constant. Then, they carried out a new series of tests changing the heat flux level by varying the vertical elevation of the heater above the sample but with a constant heater temperature. According to Wien's law, variations in the emitter temperature have a direct influence on the spectral distribution and the position on the peak of emission. Thomson and Drysdale [6] concluded that ignition time measurements depend on the spectral distribution of the radiant heater. Finally, they compare their previous time to ignition to tests carried out with a CO_2 laser beam providing a heat flux of 34 kW/m^2. The time measured with the laser was up to 6 times larger. In this work Thomson and Drysdale [6] focussed on the surface temperature at ignition and they found that for PMMA, the surface temperature tends to be independent of the emission wavelengths. They confirmed this with their laser tests. They compared their results with Kashiwagi [7] who also used a CO_2 laser beam as the heater source. The time to ignition could not be compared since he performed his experiments at heat flux levels higher than 70 kW/m^2. However, their surface temperature measurements can be compared. Kashiwagi's measurements [7] were found to be relatively high. They claimed that this discrepancy in the surface temperature measurements came from the pilot used and the fact that the part of radiation absorbed by the gas phase was significantly higher in the range of heat flux levels used by Kashiwagi [7].

Hallman [8] compared the ignition delay time for black, clear and white PMMA with two different heaters: a tungsten lamp and a benzene flame (see Fig. 6.2). The experiments were carried out with the sample mounted in the vertical position to reduce the dependence on the flow conditions. Hallman's [8] results show that the impact of the heater does not appear with all the types of PMMA. Ignition of black PMMA is independent of the heater used. However, the ignition of clear and white PMMA samples is a function of the heater source used and the difference in the delay time to ignition between both heaters increases with the flux level.

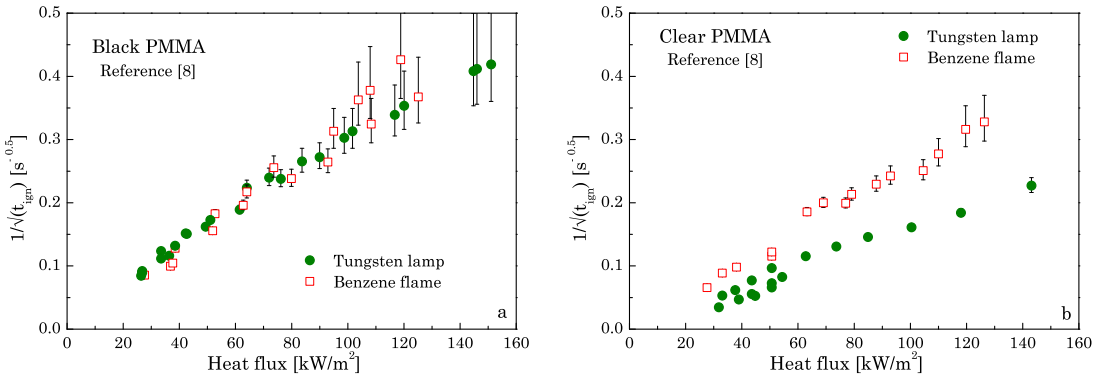

Figure 6.2: Ignition test measurements for (a) black PMMA and (b) clear PMMA with two heater sources: tungsten lamp and benzene flame. The uncertainty is estimated at ± 2s.

Wesson et al. [9] carried out similar experiments to Hallman [8] (same apparatus, vertical orientation and same heaters) with the difference that they used wood samples (6 different types of wood for ignition tests). By taking into account the relative absorbance of their samples under a benzene flame and tungsten lamps, and the effect of the density and the thickness of the different types of wood, they were able to explain the discrepancy between the ignition delay times measured with both heater sources for all wood types. They concluded that the time to ignition is strongly dependent on the spectral distribution of the incident radiation since the absorbance of wood is low (with a minimum of 0.16) between 0.6 µm and 2 µm and becomes higher (with a maximum of 0.95) at longer wavelengths. They presented absorbance measurements as a function of the wavelength for only two kinds of wood but they claimed that the results for the 14 types of wood tested are similar. They provided the effective absorptivity (across a range of wavelengths included between 0.3 µm and 5.45 µm) for the 14 types of wood: the data spreads over a narrow range with an average value of 0.76 ± 0.01 for benzene flame radiation and 0.48 ± 0.08 for tungsten lamps.

Recently, Försth and Roos [10] have carried out a large experimental study on absorptivity measurements for different material types. They assessed theoretically the impact of the heater temperature by calculating the effective

absorptivity of their sample as a function of the emissive power of the radiative source. They also provide some interesting results on the evolution of the absorptivity of the sample after being exposed to an external heat flux for different times.

Linteris et al. [11] have studied the concept of the absorbance in detail and provide experimental results where they clearly show a dependency on thickness. On top of that, they show that according to the range of wavelengths analysed, the measurements of absorbance can give results differing by an order of magnitude. Their results emphasize the relative caution that experimentalist and modelling teams need when they deal with in-depth radiation absorption.

As a consequence of these studies, experimental teams [12-14] have resorted to using a black coating on all tested samples to try to guarantee that the heat flux measured by a gauge is the same as that absorbed by the material surface, independently of the radiative properties of the material. While this guarantees consistency between tests, it changes the impact of the effective radiative properties of the material and also results in non-quantified degradation issues of the coating. A recent study [5 (chap 1)] tends to prove that a black coating on the exposed surface does not guarantee a total surface absorption.

The present work focuses on how the heating systems of the Cone Calorimeter and the FPA affect the pyrolysis behaviour of flammable materials. Experiments have been conducted using clear PMMA and wood (Spruce) samples. Comparisons of visual observations and mass loss and temperature measurements are performed. These complement previous experimental findings concerning the impact of the radiative source on the ignition delay times and confirm theoretical ones. Indeed, a deeper analysis of the pyrolysis behaviour (not only on delay time to ignition) enables an emphasis of the agreement with theoretical findings on the impact of the heater source type.

2. Experimental section

2.1. Sample preparation

The present study incorporates several modifications to the standard sample holders to minimize the effect of these on the results. The main differences between the sample holders are associated with the insulation of the sample and the way the sample edges are treated. Therefore, for the present study, the sizes of the samples were reduced to 65 × 65 × 65 mm for the wood and 75 × 75 × 25 mm for the clear PMMA. The sample edges were treated in an identical manner. The lateral sides of the samples were insulated with ceramic fibre (10 mm width) coated with aluminium foil that also covered the edges of the sample. Heat transfer through the back of the sample was standardized by introducing an insulated aluminium block [15]. The back surface of the sample was thus in contact with an aluminium block that was insulated on the sides and back (see Fig. 6.3). High thermal conductivity glue (Dow Corning 340) was added between the back surface of the sample and the aluminium block to ensure good contact. In the case of wood, the samples are placed such that the wood fibres are perpendicular to the vertical axis. More detailed justifications for the sample holder arrangement can be found in Carvel et al. [15].

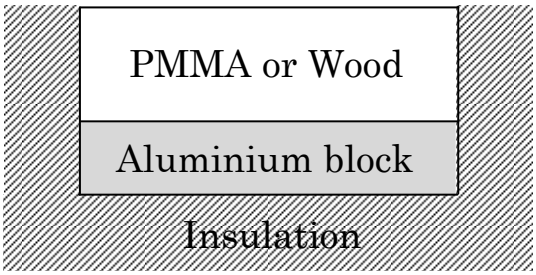

Figure 6.3: Schematic of the sample holder.

2.2. Experimental procedure

Experiments have been performed with the two types of heaters (conical resistance and tungsten lamps) at 20 kW/m^2. To make the tests comparable, they have both been carried out within the chamber of the FPA apparatus. In

the case of the test with the conical resistance, the FPA has been modified (see Fig. 6.4) by placing the electrical cone heater above the sample as it is in the Cone Calorimeter.

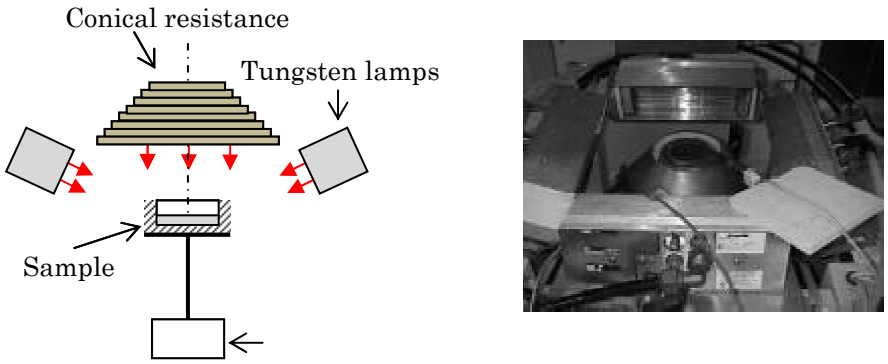

Figure 6.4: Schematic and picture of the experimental apparatus with both heaters: tungsten lamps and conical resistance.

In the FPA configuration, four heaters composed of six tungsten tubular quartz lamps filled with halogen (Research Inc. model 5208) have been used. The conical resistance is made of inconel and its temperature is regulated by a PID (Proportional Integral and Derivative) temperature controller. Both heater types has been calibrated using a heat flux meter to ensure that the radiant heat on the top surface of the sample is kept within ± 10 % in time and space during the course of the experiment.

Natural convection conditions are chosen in order to reduce the perturbation of the flow caused by the presence of the conical resistance just above the sample. To increase the time before ignition, the tests have been performed without pilot.

The mass loss of the sample has been measured for both materials studied. The temperature profile has been recorded in-depth only for the wood samples. The measurements have been carried out with three Type-K thermocouples (1 mm of diameter) inserted parallel to the exposed surface at 5, 15 and 25 mm depths. For the PMMA samples, only the temperature of the aluminium block has been measured. In-depth temperature measurements with clear PMMA

were avoided because this material has a high transmittance and the measured temperature would correspond to a complex mixture of the absorption of the radiation by the thermocouple and conduction from the material, thus introducing further sources of uncertainty.

Temperature and mass loss were not taken simultaneously due to the large perturbation on the mass loss reading caused by the vibrations of the thermocouples wires. Basic visual observations were noted on the sample shape after the experiments and of the thickness of the bubble layer appearing due to in-depth thermal degradation.

2.3. Experimental results

For both heaters set up at 20 kW/m^2, auto-ignition was not observed for both types of materials (wood and clear PMMA), thus the discussion concerns only the interaction between the heaters and the samples.

2.3.1 Clear PMMA samples

The temperature increase of the aluminium block located at the back is shown in Fig. 6.5 for only 500 s over the more than 2000 s the tests lasted. The repeatability of the results for both heater types is excellent (± 2 °C over 35 min). It appears that the aluminium block located under the sample exposed to the tungsten lamps is heated as soon as the exposure starts. Its temperature is increased of 10 % in less than 100 s whereas it takes around 350 s for the same increase when the sample is exposed to the electrical conical resistance

Mass loss measurements are shown in Fig. 6.6 based on the dimensionless mass loss parameter γ which is defined as the mass lost since the beginning of the test divided by the initial mass (percentage). The samples exposed to the lamps heaters do not pyrolyse as fast as the ones exposed to the conical resistance.

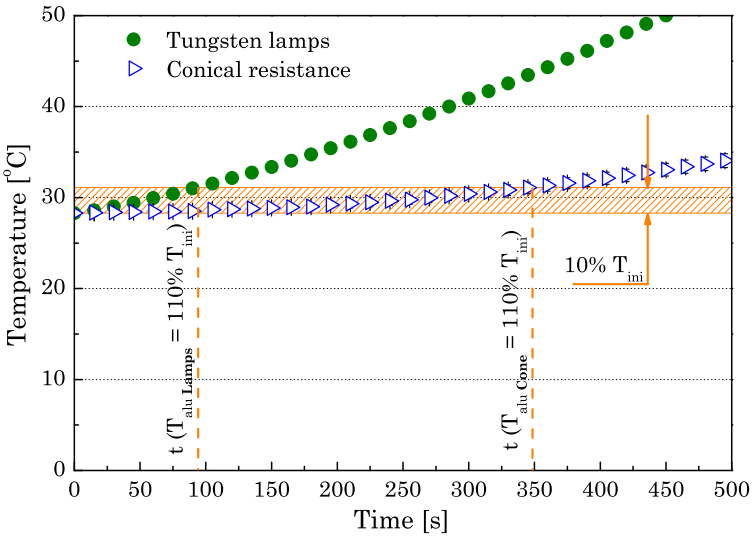

Figure 6.5: Temperature increase of the aluminium block located at the back of the clear PMMA samples for experiments with tungsten lamps and conical resistance.

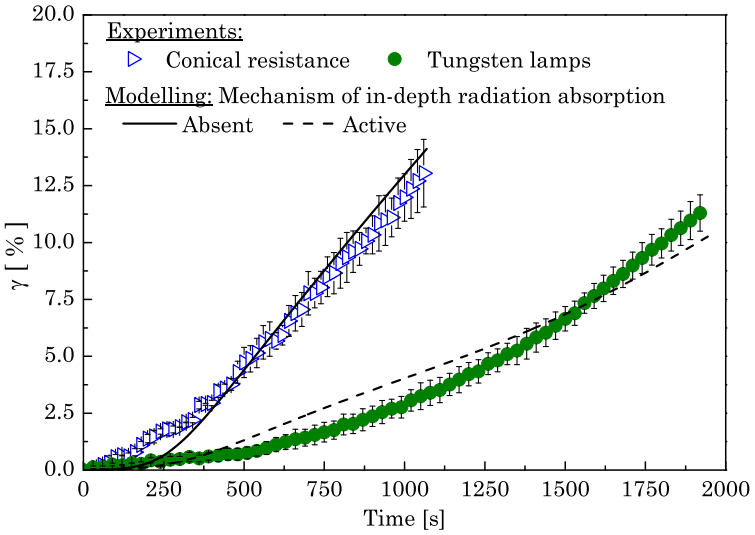

Figure 6.6: Dimensionless mass loss coefficient γ versus time for tungsten lamps and conical resistance experiments with clear PMMA samples.

During the experiments, bubbles appeared on the exposed side of the samples. After the tests, the samples were cut (Fig. 6.7) in order to observe the thickness of the bubble layer on the cross section. It is observed that the bubble layer is thicker when the sample is exposed to the lamps. This indicates that the in-depth temperature profile depends on the heater type. In the case of the

conical resistance, heating takes place on a thin layer close to the top surface. In contrast, clear PMMA seems to absorb energy at a greater thickness when it is exposed to the tungsten lamps.

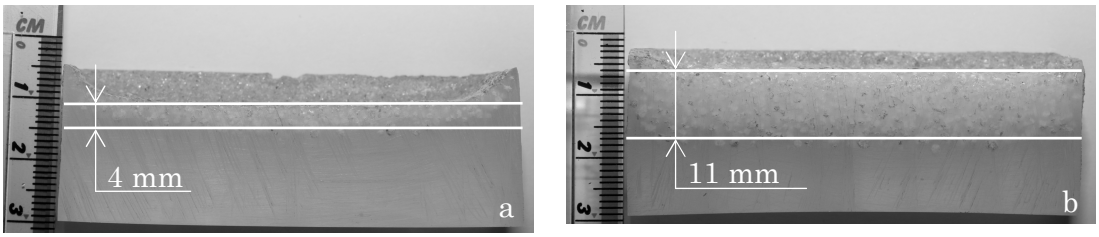

Figure 6.7: Vertical sections of clear PMMA samples showing the bubble layer depth. Samples were exposed to a heat flux level of 20 kW/m^2 for 35 min with: (a) conical resistance and (b) tungsten lamps.

The differences in sample observations, mass loss measurements and aluminium block heating are the result of different radiation attenuations according to the heater used. The non-reflected radiation in the clear PMMA surface is passing through the sample and it is subjected to in-depth attenuation as it is presented in Eq. 6.1. The energy is not absorbed at the surface but in-depth (Beer Lambert's law) and the value of the attenuation coefficient κ controlling this absorption is not the same for both heaters.

$$\alpha_\lambda = 1 - (1 - r)^2 e^{(-\kappa_\lambda L)} - r \qquad (6.1)$$

A consequence of the in-depth radiation absorption is the presence of a peak of temperature inside the solid and not at the surface. This characteristic is more apparent as the heat flux level increases [5 (chap 1)]. The peak location is related to the depth penetration by radiation which is proportional to the inverse of the attenuation coefficient. The radiative penetration depth is independent of the heat flux level and is established instantaneously, whereas the thermal depth penetration by conduction grows at a rate decreasing with time.

In order to estimate the value of the attenuation coefficient κ, measurements of the transmittance of the clear PMMA (by means of a heat flux gauge) for two different sample thicknesses (5 and 25 mm) have been carried out with the tungsten lamps. This experimental protocol corresponds to the one operated by Jiang et al. [16] for a range of wavelengths estimated between 0.46 µm and 2.08 µm (60 % of the energy irradiated). The slope obtained by plotting the logarithm of the transmittance measured against the sample thickness gives an approximate value of the order of 10 m^{-1} for κ.

In order to support the statement about the heater dependence of the attenuation coefficient, a qualitative analysis was performed with a pyrolysis model. This model, presented by Chaos et al. [17], solves kinetics, energy and mass conservation with the inclusion of the in-depth radiation absorption. The model is similar of the model GPYRO which is explained in detail elsewhere [18,19]. For the qualitative analysis, a single step reaction following a first order Arrhenius law with only two species (PMMA → GAS) is considered.

Considering that the bubble layer thickness for the clear PMMA exposed to the conical resistance indicates a high attenuation coefficient ($\kappa \to \infty$), it is first assumed that the material does not absorb in-depth but at the surface. Then, the most uncertain parameter values (kinetics parameters) have been modified in order to obtain numerically the same mass loss measured experimentally (see Fig. 6.6). The rest of the parameters are taken from those measured by Steinhaus [20]. In-depth radiation absorption is then included but no other parameter values changed. The measured value for the attenuation coefficient with the lamps of 10 m^{-1} was used. By only adding in-depth radiation absorption, the mass loss measurements for samples exposed to the tungsten lamps is captured (see Fig. 6.6). While these modelling results are only approximate and that the results should not be taken as quantitative, this simple analysis enables a confirmation that the in-depth radiation absorption mechanism is important and depends on the nature of the emission from the heaters.

2.3.2 Wood specimens

During the tests with wood specimens, thermocouples were used to measure the temperature profile of the samples (see Fig. 6.8). The repeatability of the tests is worse than for the aluminium block measurements but this was predictable considering the non-homogeneity of the material properties (e.g. thermal conductivity) of the wood samples.

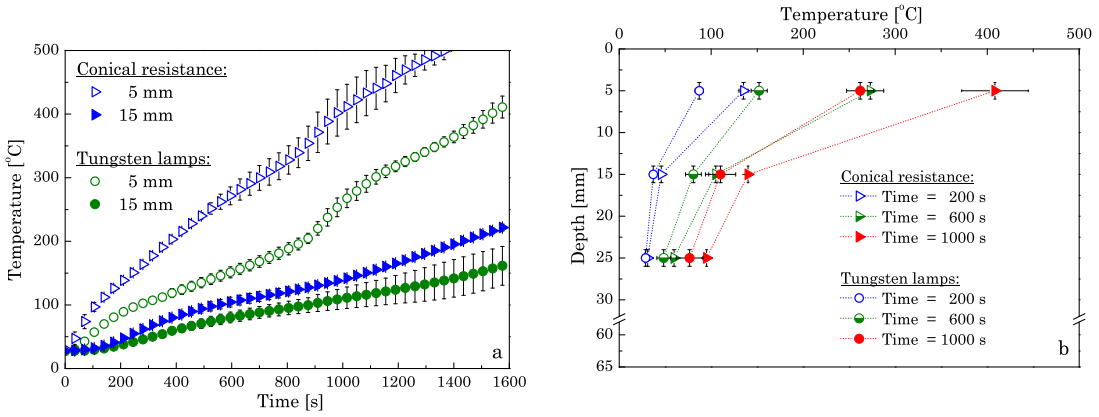

Figure 6.8: Temperature measurement in-depth (below the exposed surface) for wood sample exposed to tungsten lamps and conical resistance: (a) temperature vs. time and (b) depth vs. temperature.

Among the temperature measurements plotted in Fig. 6.8, the temperatures 5 mm below the surface of the samples present the higher difference between each type of heaters. The samples exposed by the conical resistance have the highest temperature at 5 mm under the surface.

The mass loss measurements for the wood samples (Fig. 6.9) present the same behaviour as the ones presented in Fig. 6.6 for clear PMMA. Once again, the samples exposed to the conical resistance have a mass loss at similar time which is more significant than the ones exposed to the lamps. From Figs. 6.6 and 6.9, it can be seen that the uncertainty on the measurements performed with the conical resistance are higher. This seems to be due to the rate of the mass loss which is more important for the samples exposed to the conical resistance.

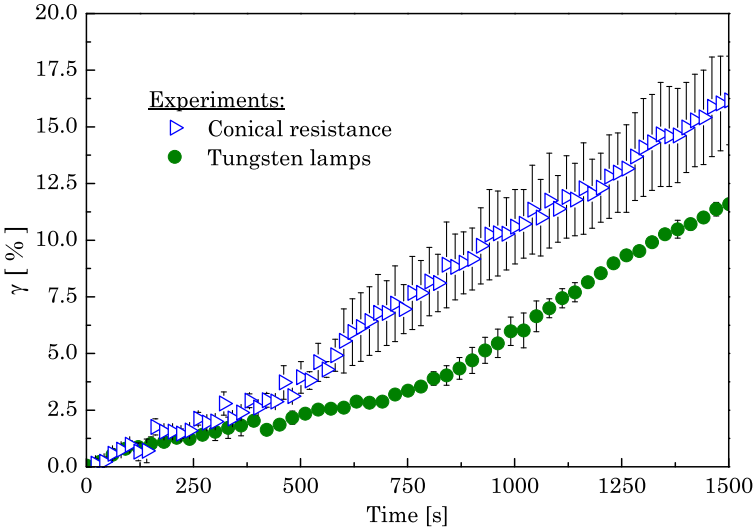

Figure 6.9: Dimensionless mass loss coefficient γ versus time for tungsten lamps and conical resistance experiments with wood samples.

3. Discussion

In order to assess the possible causes of the discrepancy in the observed pyrolysis behaviour of the same material exposed by two different heat sources, the differences in the experimental set up have to be investigated more in depth.

The first one is link to the position of the source. In the case of the Cone Calorimeter the heater is located just above the sample (at 2.5 cm [1] – see Fig. 6.4). This could have an impact for two reasons: the presence of an obstacle perturbs the flow and the high temperature of the conical heater elements (see Table 6.1) creates buoyancy. In the case where tungsten lamps are used, there is no obstacle directly above the sample. In order to reduce the impact that the flow could have on the results, it has been decided, given the protocol presented in Refs. [1,2], to perform the test in a horizontal position but without any injected air (natural convection). The ideal solution to avoid this perturbation would be to use a vertical orientation [8,9].

The second difference which is significant is the temperature range of the radiative source. Indeed, the conical resistance temperature is lower than 1000 K for heat flux levels under 40 kW/m², whereas the tungsten lamps (four in the FPA) are working in a temperature range greater than 2000 K for heat flux levels above 10 kW/m² (see Table 6.1).

As a first approximation, it is assumed that these heat sources radiate as black bodies. Planck's distribution of blackbody emissive power [21] gives the temperature and wavelength dependency of the emissive power. From this, it is shown that the difference in the operating temperature ranges of the heaters change significantly the wavelengths at which the emissive power is distributed (Fig. 6.10).

Table 6.1: Operating temperatures for heat sources for Cone Calorimeter and FPA.

Heat flux [kW/m^2]	Conical resistance	Tungsten lamps
	Operating temperature [K]	
10	725	1970
20	855	2280
40	1013	2625

Hallman [8] and Wesson et al. [9] measured respectively the absorbance of PMMA and wood. Figure 6.10 compares the spectral distribution of the absorbance for clear PMMA (a-b) and wood (c-d) with the emissive power distribution as a function of the wavelength for the conical heater (a-c) and the tungsten lamps (b-d). For both materials, the absorbance is relatively high in the operating wavelengths range of the conical heater and relatively low for the range of the infrared heater lamps. In general, clear PMMA and wood absorbs energy mostly for wavelengths higher than 2 µm. Below this threshold, the tungsten lamps emit around 60 % of their energy (see shaded are in Figs 6.10b and 6.10d). The same level of energy is emitted by the conical heater for wavelengths higher than 5 µm.

Försth and Roos [10], in their recent study, confirmed this global trend for wood and plastic samples (sometimes with a decrease between 4 µm and 6 µm). Their numerical results of the effective absorptivity over the emitting ranges of different heater temperatures corroborate the global observation explained

above concerning the difference of absorption between radiation emitted at wavelengths below and above 2 µm.

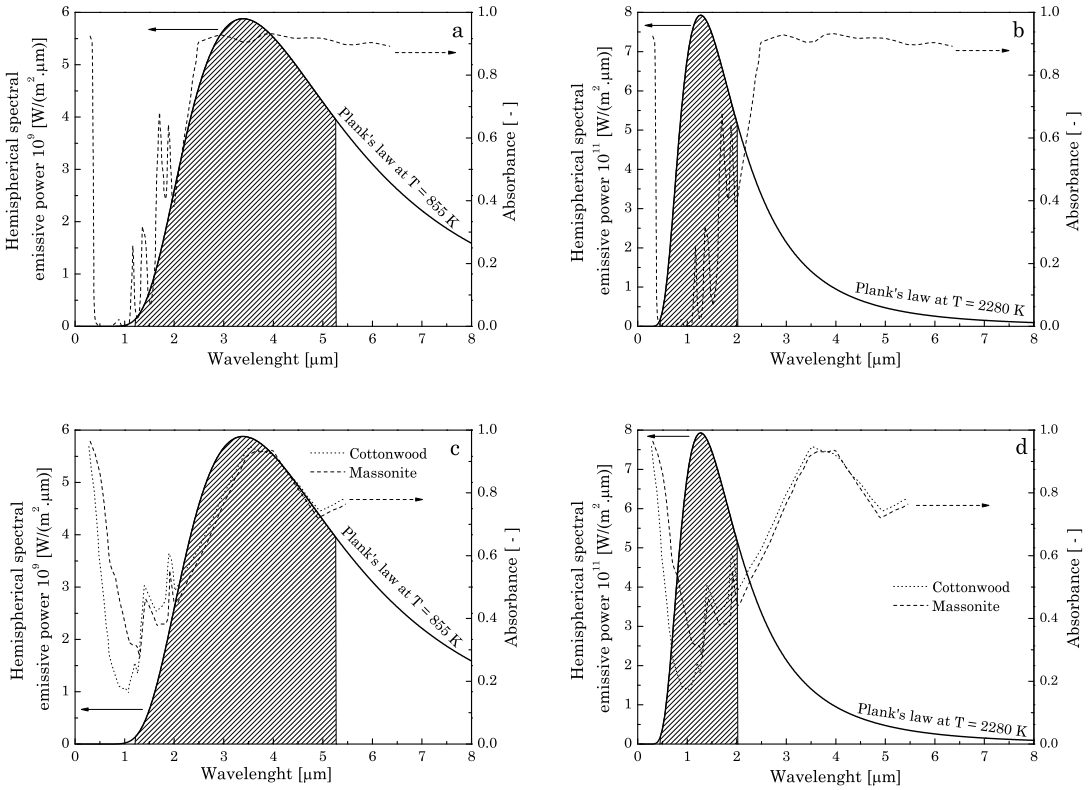

Figure 6.10: Spectral distribution of the absorbance against the emissive power of a blackbody at the corresponding heater temperature providing a heat flux of 20 kW/m². (a) conical resistance, clear PMMA; (b) tungsten lamps, clear PMMA; (c) electrical cone resistance, wood; (d) tungsten lamps, wood. Shaded area is 60 % of the total intensity and centred on the peak emissive power value.

In Ref. [8], Hallman indicates that he measured a non-negligible transmittance at low wavelengths for his clear PMMA samples (Fig. 6.11).

From Figs. 6.10 and 6.11, it is seen that for clear PMMA not all the incident radiation is absorbed by the sample and the transmitted part is high for wavelengths lower than 2 µm. For wood, the transmittance is very low (for the whole spectrum) and can be assumed equal to 0. As a consequence, the low absorbance at wavelengths below 2 µm means that a large fraction of the

incident radiation is reflected [9]. These two different radiation behaviours explain well the measurements presented here.

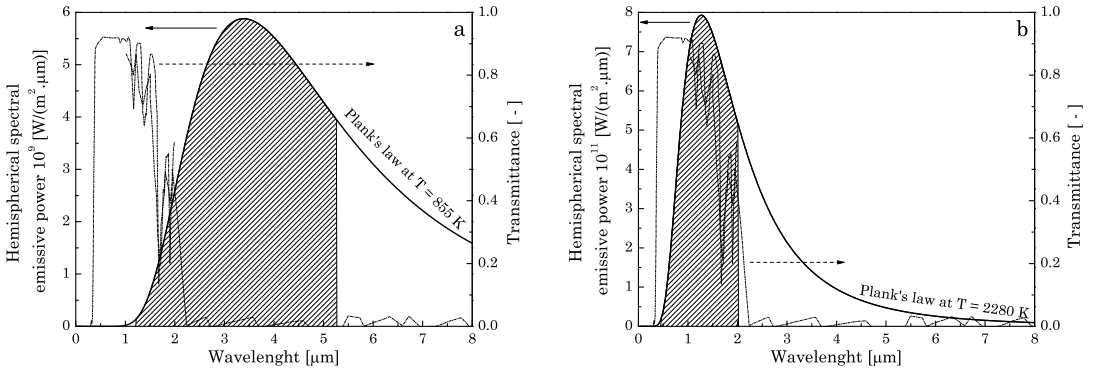

Figure 6.11: Spectral distribution of the transmittance of clear PMMA against the emissive power of a blackbody at the corresponding heater temperature providing a heat flux of 20 kW/m²: (a) conical resistance; (b) tungsten lamps. Shaded area is 60 % of the total intensity and centred on the peak emissive power value.

For clear PMMA, the relatively high increase in temperature of the aluminium block when the tungsten lamp is used (wavelength below 2 µm) is due to higher transmission of the incident radiation. This high ratio of transmitted radiation means that the attenuation coefficient κ is low which is confirmed by the order of magnitude found by measurement: 10 m^{-1}. In addition, a low coefficient κ leads to a larger radiation penetration depth (confirmed by the visual thickness of the bubble layer in Fig. 6.7). The presence of bubbles indicates the thermal decomposition of the solid into pyrolysis gases. However, the mass loss rate is lower for the samples exposed to tungsten lamps in Fig. 6.6. This is the consequence of a lower amount of energy absorbed but also of a wider distribution inside the sample.

The presence of the bubbles in-depth goes against the main hypothesis of most of the pyrolysis models which states that pyrolysis gases are instantaneously released out of the sample. This observation tends to show that the transport of the pyrolysates may play an important role.

For the wood, higher temperature measurements, just below the surface, are observed when the conical heater is used (wavelength above 2 µm). This is explained by the significant part of the incident radiation being reflected by the wood sample exposed to the lamps. The higher mass loss attributed to the samples exposed to the conical resistance in Fig. 6.9 is therefore only the consequence of a higher quantity of energy absorbed and not of the thickness through which the energy is distributed.

Finally, the third difference between the two heater sources studied here is linked also to the position of the heaters. Due to their respective position (Fig. 6.4) the incident radiation does not arrive with the same angle on the sample. The conical resistance provides incident radiations intercepting the sample with a large range of angles (due to its inclined shape) whereas tungsten lamp radiations arrive with an angle between 70 ° and 80 ° to the normal of the surface. Hallman [8] studied the angular variation of the absorbance for clear PMMA and showed that the variation from a normal orientation to 70 ° is included within 15 % for wavelengths lower than 2 µm. A supplementary study, with the relation given by Jiang et al. [16] to calculate the reflectivity at a particular wavelength (linked to reflective index), shows that the reflected ratio varies between 0.038 and 1 when the angle formed with the normal of the sample is between 0 and 90 ° (0.17 for an angle of 70 ° and 0.39 for an angle of 80 °).

According to the experimental results from Hallman [8] and from Försth and Roos [10], the absorbance of the black PMMA is approximately constant over the wavelength range covered by the conical resistance and the tungsten lamps. Therefore a significant difference between these heaters should not appear. Figure 6.2a is in perfect agreement with this statement whereas Fig. 6.1 is not. The difference between these two sets of data is the experimental protocols. In Fig. 6.2, the experiments were carried out with only one apparatus in a vertical orientation to avoid any flow disturbance whereas in Fig. 6.1 the measurements are obtained from Cone Calorimeter and FPA (or similar apparatuses) ignition tests.

The discrepancies between the ignition delay times in Fig. 6.1 do not seem to be linked to the wavelength dependency of the material but could come from

the flow field and the sample holder differences. In [12], Beaulieu claims, according to measurements performed with black PMMA, that the shape and the thickness of the sample do not bring significant difference on the time to ignition but the Cone Calorimeter sample holder (due to conduction through it at its edges) and the flow are responsible for some discrepancies. The pilot used (flame or spark) seems not to cause a significant difference to the piloted ignition time since these two types of pilot are used indifferently with the Cone Calorimeter and the FPA (or similar) among the data set presented in Fig. 6.1.

4. Conclusion

The impact on the results obtained with a Cone Calorimeter and a Fire Propagation Apparatus (FPA) heater source has been studied here. This chapter builds on previous work which studied the impact of the heater source on time to piloted ignition. It confirms and expands previous studies by including temperature, mass loss and pyrolysis observations for clear PMMA and spruce wood samples.

Planck's wavelength distribution shows that the conical resistance wire from the Cone Calorimeter emits most of its intensity in a range of wavelengths greater than 2 µm whereas for the tungsten lamps from the FPA, the range is mainly situated under 2 µm. Moreover, it appears from previous studies on absorbance measurement (Hallman [8], Wesson et al. [9] and Försth and Ross [10]), that most of the energy absorbed by clear PMMA and wood samples is for wavelengths above 2 µm. However, different behaviour appears for clear PMMA and wood when the wavelength is lower than 2 µm: clear PMMA transmits the energy whereas wood reflects it. Mass loss and temperature measurements confirm that this mechanism explains the significantly different pyrolysis behaviour observed in the experiments. Therefore, it appears important to pay careful attention to the radiative properties of the material under study before making conclusions from the experimental results.

It should be noted that in Ref. [2], it is recommended to use a quartz tube between the lamps and the sample. However, the tube filters the wavelengths greater than 2 µm. So with its use, the difference between the two heaters would

be increased. Moreover, for the typical uses of the Cone Calorimeter and the FPA, when the experimentalist desires to increase the heat flux imposed on the sample, the temperature of the heater is increased. This increase of temperature could therefore have an impact according to the radiative properties of the material.

Finally, it appears that although some materials like black PMMA do not have a significant wavelength dependency in their radiation material properties, some small discrepancies appear between the Cone Calorimeter and the FPA ignition tests. These differences could be caused by many other variables and need to be explored in more detail.

References

[1] ASTM E1354-10a: Standard test method for heat and visible smoke release rates for materials and products using an oxygen consumption calorimeter", ASTM International, West Conshohocken PA, 2010, http://dx.doi.org/10.1520/E1354-10A.

[2] ASTM E2058-03: Standard test method for measurement of synthetic polymer material flammability using a Fire Propagation Apparatus, ASTM International, West Conshohocken PA, 2003, http://dx.doi.org/10.1520/E2058-03.

[3] V. Babrauskas, Development of the Cone Calorimeter – A Bench-Scale Heat Release Rate Apparatus Based on Oxygen Consumption, Fire and materials 8 (1992) 81-95, http://dx.doi.org/10.1002/fam.810080206.

[4] A. Tewarson and R.F. Pion, Flammability of Plastics, I-Burning Intensity, Combustion and flame 26 (1976) 85-103, http://dx.doi.org/10.1016/0010-2180(76)90059-6.

[5] N. Bal and G. Rein, Numerical investigation of the ignition delay time of a translucent solid at high radiant heat fluxes, Combustion and flame 158 (2011) 1109-1116, http://dx.doi.org/10.1016/j.combustflame.2010.10.014

[6] H.E. Thomson and D.D. Drysdale, Flammability of plastics I: Ignition temperatures, Fire and materials 11 (1987) 163-172, http://dx.doi.org/10.1002/fam.810110402.

[7] T. Kashiwagi, Experimental observation of radiative ignition mechanisms, Combustion and flame 34 (1979) 231-244, http://dx.doi.org/10.1016/0010-2180(79)90098-1.

[8] J.R. Hallman, Ignition characteristics of plastics and rubber, PhD Dissertation, The University of Oklahoma, 1971.

[9] H.R. Wesson, J.R. Welker and C.M. Sliepcevich, The piloted ignition of wood by thermal radiation, Combustion and flame 16 (1971) 303-310, http://dx.doi.org/10.1016/S0010-2180(71)80101-3.

[10] M. Försth and A. Roos, Absorptivity and its dependence on heat temperature and degree of thermal breakdown, Fire and material 35 (2010) 285-301, http://dx.doi.org/10.1002/fam.1053.

[11] G. Linteris, M. Zammarano, B. Wilthan and L. Hanssen, Absorption and reflection of infrared radiation by polymers in fire-like environments, Fire and materials 36 (2012) 537-553, http://dx.doi.org/10.1002/fam.1113.

[12] P.A. Beaulieu, Flammability Characteristics at Heat Flux Levels up to 200 kW/m2 and the Effect of Oxygen on Flame Heat Flux, PhD Dissertation, Worcester Polytechnic Institute, 2005, <http://www.wpi.edu/Pubs/ETD/Available/etd-121905-082146/unrestricted/beaulieu.pdf>.

[13] A. Tewarson and S.D. Ogden, Fire behaviour of polymethylmethacrylate, Combustion and flame 89 (1992) 237-259, http://dx.doi.org/10.1016/0010-2180(92)90013-F.

[14] M.A. Delichatsios, T. Panagiotou and F. Kiley, The use of time to ignition data for characterizing the thermal inertia and the minimum (critical) heat flux for ignition or pyrolysis, Combustion and flame 84 (1991) 323-332, http://dx.doi.org/10.1016/0010-2180(91)90009-Z.

[15] R. Carvel, T. Steinhaus, G. Rein and J.L. Torero, Determination of the flammability properties of polymeric materials: A novel method, Polymer degradation and stability 96 (2010) 314-319, http://dx.doi.org/10.1016/j.polymdegradstab.2010.08.010.

[16] F. Jiang, J.L. De Ris and M.M. Khan, Absorption of thermal energy in PMMA by in-depth radiation, Fire safety journal 44 (2009) 106-112, http://dx.doi.org/10.1016/j.firesaf.2008.04.004.

[17] M. Chaos, M.M. Khan, N. Krishnamoorthy, J.L. De Ris and S.B. Dorofeev, Evaluation of optimization schemes and determination of solid fuel properties for CFD fire models using bench-scale pyrolysis tests, Proceedings of the Combustion Institute 33 (2011) 2599-2606, http://dx.doi.org/10.1016/j.proci.2010.07.018.

[18] C. Lautenberger, A Generalized Pyrolysis Model for Combustible Solids, PhD dissertation, The University of California, Berkeley, 2007, <http://escholarship.org/uc/item/7wz5m7dg>.

[19] C. Lautenberger and C. Fernandez-Pello, Generalized pyrolysis model for combustible solids, Fire safety journal 44 (2009) 819-839, http://dx.doi.org/10.1016/j.firesaf.2009.03.011.

[20] T. Steinhaus, Evaluation of the Thermophysical Properties of Poly(Methyl Methacrylate): A Reference Material for the Development of a Flammability Test for Micro-Gravity Environments, Master dissertation, The University of Maryland, 1999. <http://www.era.lib.ed.ac.uk/handle/1842/2831>.

[21] R. Siegel and J. Howell, Fundamental and material properties for radiative transfer in absorbing, emitting and scattering media, in: Thermal radiation heat transfer 4th edition, Taylor and Francis, 2002, chapter 11, pp 419-500, ISBN-10:1560328398.

Chapter 7

Experimental study of radiative heat transfer in a translucent fuel sample exposed to different spectral sources

Summary

Radiative heat transfer to a solid is a key mechanism in fire dynamics, and in-depth absorption is especially of importance for translucent fuels. The sample-heater interaction for radiative heat transfer is experimentally investigated in this study with two different heaters (electrical resistance and tungsten lamp) using clear PolyMethylMethAcrylate (PMMA) samples from two different formulations (*Plexiglass* and *Lucite*). First, the significant effects of the heater type and operating temperature on the radiative heat transfer are revealed with broadband measurements of transmittance on samples of different thicknesses. Then, the attenuation coefficient in Beer-Lambert's law has been calculated from detailed spectral measurements over the full wavelength range encountered in real fires. The measurements present large spectral

heterogeneity. These experimental results and calculation of in-depth absorption are used to explain the reason behind the apparent variation of the fuel absorbance with the sample thickness observed in previous studies. The measurement of the spectral intensity emitted by the heaters verifies that the common assumption of blackbody behaviour is correct for the electrical resistance, whereas the tungsten lamp does not even behave as a grey body. This investigation proves the necessity of a multi-band radiation model to calculate accurately the radiative heat transfer which affects directly the in-depth temperature profiles and hence the pyrolysis process for translucent fuel.

Collaboration

This chapter results from a joint work performed with Mr Jean Raynard from Airbus (France), Dr Michael Försth from SP (Sweden), Dr Pascal Boulet, Dr Gilles Parent, Dr Zoubir Acem from LEMTA, the University of Nancy (France), Dr Gregory Linteris from NIST (U.S.A.), Dr Guillermo Rein and Prof José L. Torero from the University of Edinburgh (UK).

Nomenclature

J	Intensity of emitted radiation [W/(m².sr.μm)]
L	Thickness [m]
$\dot{q}''$	Heat flux [kW/m²]
r	Reflectivity [-]
T	Temperature [K]

Subscripts

0	Incident flux
BACK	Flux at the back surface
FRONT	Flux at the front surface
λ	Wavelength
τ	Transmitted flux

Greek symbols

α	Absorbance [-]
κ	Attenuation coefficient [m^{-1}]
ρ	Reflectance [-]
τ	Transmittance [-]

1. Introduction

Heat absorption for solid fuels is a key mechanism in fire growth (ignition and flame spread) [1]. Bench-scale tests have been developed in order to rank different fuels according to their flammability (e.g. Cone Calorimeter [2], Fire Propagation Apparatus (FPA) [3]. In these tests, the incident radiation on the

fuel sample is generally thought to be well known by virtue of assuming that the heat flux is emitted by a black body and received at the sample's free surface with a constant absorptivity coefficient close to unity. These assumptions allow characterization of the incident heat flux simply by means of a heat flux meter.

Past studies have challenged this assumption of total absorption by varying the type of heater [2-6], the heater-sample distance [6], the sample orientation [5] or by adding carbon coating [7]. These studies have revealed that the radiative heat transfer between the heater and the sample, which is essential for the understanding of pyrolysis and fire, is dependent on the experimental set up.

Significant research is available on the experimental characterization of the material radiative properties. Hallman [4] measured the spectral absorbance α_λ for 36 polymers up to 6.5 μm under different incidence angles and for two thicknesses (3.175 and 1.27 mm). The variations in the measurements of the ignition delay time depending on the heat source (tungsten lamp or benzene flame) was explained by the spectral distribution of the absorbance.

Försth and Roos [8] measured α_λ (6 mm thick samples) for 62 materials over a wavelength range [0.3-20 μm]. Given the spectral intensity emitted by the source J_λ, they estimated the broadband effective absorbance $\bar{\alpha}$ with Eq. 7.1:

$$\bar{\alpha}(L) = \frac{\int_0^\infty \alpha_\lambda(L) J_\lambda(T) d\lambda}{\int_0^\infty J_\lambda(T) d\lambda} \quad (7.1)$$

where λ is the wavelength, T the heater temperature and L the sample thickness.

Equivalent expressions can be developed for the effective transmittance $\bar{\tau}$ and reflectance $\bar{\rho}$ respectively based on their spectral distribution τ_λ and ρ_λ.

Försth and Roos [8] specified J_λ assuming blackbody behaviour for a conical electrical resistance (operating temperature between 674 and 1300 K providing a heat flux between 10 and 100 kW/m^2). They observed a weak dependency of $\bar{\alpha}$

to the heater temperature (e.g. for clear PolyMethylMethAcrylate (PMMA) $0.87 < \bar{\alpha} < 0.93$).

Linteris et al. [9] measured α_λ over [1.5-15.1 μm] for 11 thermoplastics using samples with L lower than 3.5 mm. They estimated $\bar{\tau}$ through the sample as a function of L using an equivalent expression to Eq. 7.1. Moreover, they studied the ratio of spectral radiative fluxes $\dot{q}''_\tau/\dot{q}''_0$ (where $\dot{q}''_\tau$ is the radiative flux transmitted through the sample and $\dot{q}''_0$ the incident flux on the free surface - see set up in Fig. 7.1). This ratio $\dot{q}''_\tau/\dot{q}''_0$ is equivalent to $\bar{\tau}$ in Eq. 7.1 with the approximation that the view factor of the source to the top surface is equal to the view factor of the source to the back surface [10]. Linteris et al. [9], using a conical electrical resistant, observed discrepancies between $\bar{\tau}$ and $\dot{q}''_\tau/\dot{q}''_0$ that were assumed to be the consequence of the narrowness of the spectral range explored. They show also that most of the radiation (> 80 %) is absorbed in-depth over a thin layer (~1 mm for clear PMMA). Moreover, they also observed that $ln(\dot{q}''_\tau/\dot{q}''_0)$ varies non-linearly with L , indicating that Beer-Lambert's law [10] is not satisfied broadband.

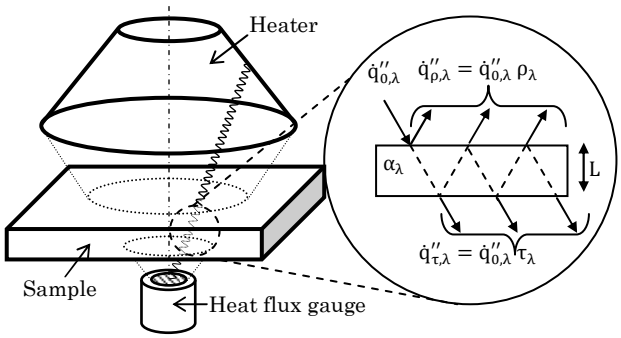

Figure 7.1: Experimental set up of the heat source, the sample and the heat flux meters. Inset: Schematic of the multiple reflection mechanism.

Most of previous investigations on radiative heat transfer to solid fuel have been performed with a conical electrical resistance as heat source, whereas other sources are used in flammability tests such a benzene flame [4] or tungsten lamps in the FPA [5,11 (chap 6)-13 (chap 1)]. Girods et al. [11 (chap 6)] conducted pyrolysis experiments on clear PMMA and wood samples using two of these sources: a tungsten lamp and an electrical resistance. They showed that

the pyrolysis behaviour is strongly dependant on the heater type and that it is essential to better understand the physical mechanism of in-depth heat absorption through fundamental measurements.

Standard ignition tests aim at eliminating the impact of the radiative material properties by adding a carbon coating on the free surface and hence facilitate the assumption of absorptivity equal to 1. Bal and Rein [13 (chap 1)] recently demonstrated that this assumption is incorrect and that around 65 % of the radiation is transmitted through the coating layer and absorbed in-depth. Linteris et al. [9] further supported this finding by showing that the transmittance of thin black PMMA (L < 0.2 mm) is around 60 %. Thus, in-depth radiative heat transfer through the material is of importance in pyrolysis for translucent fuels, even in the presence of carbon coating.

While the flammability results extracted from standard tests (e.g. time to ignition and ignition temperature) are commonly used for the calculation of fire growth, the differences in the radiative heat transfer between tests have been largely ignored in the past. This paper investigates experimentally the radiative heater-sample interaction by using the heat sources of the two most important flammability bench-scale apparatuses (tungsten lamp and electrical resistance) on two types of clear PMMA samples (*Plexiglass* and *Lucite*) over a range of sample thicknesses.

2. Broadband measurements of the sample transmittance

The ratios $\dot{q}''_\tau/\dot{q}''_0$ of transmitted to incident radiative heat fluxes were measured for clear PMMA samples of different thicknesses when exposed to a tungsten lamp and an electrical resistance. A heat flux gauge was used to measure $\dot{q}''_\tau$ and $\dot{q}''_0$ following a methodology similar to that in Linteris et al. [9] (Fig. 7.1).

The tungsten lamp heater is made of six tubular quartz bulbs filled with halogen gas placed in a rectangular-shaped enclosure with a quartz window. The resistance heater is a truncated cone made of electrical coils. Both heaters, positioned normal to the free surface, were set to provide 20 kW/m^2 at the centre of the sample's free surface. This heat flux level is achieved for the resistance when located 25 mm away from the sample and with the coil temperature sets at 858 K (controlled by a proportional integral-derivative device). The heat flux level is reached for the lamp when located 160 mm from the sample and with the filament at 2610 K (data based on the operating voltage from manufacturer for only one lamp). These heat flux levels and heater positions correspond to typical conditions used in bench scale tests.

The samples of PMMA used come from two different suppliers and are sold under the commercial names of *Plexiglass* and *Lucite*. Samples from both extruded and cast manufacturing processes are explored. In total, ten different thicknesses from 0.375 to 51 mm were tested.

The ratio $\dot{q}''_\tau/\dot{q}''_0$, measured and reported on Fig. 7.2 as a function of the sample thickness L, corresponds to averages over three consecutive tests (lasting only a few seconds each). The maximum deviation from the average was 0.045 for the electrical resistance and 0.03 for the lamp.

Given that the radiation sources are not collimated, the heat flux continuously decays with distance from the source. Therefore, the incident heat flux $\dot{q}''_0$ is neither the incident heat flux measured at the distance of the free surface $\dot{q}''_{0\,\mathrm{FRONT}}$, nor the one measured at the distance of the back surface (without sample) $\dot{q}''_{0\,\mathrm{BACK}}$, but it is in-between these two. The true ratio is therefore inside in the range $\{\dot{q}''_\tau/\dot{q}''_{0\,\mathrm{FRONT}}\,;\dot{q}''_\tau/\dot{q}''_{0\,\mathrm{BACK}}\}$, represented in Fig. 7.2 by the dashed area for 20 kW/m^2. The good repeatability of the measurements is also visible in Fig. 7.2 (e.g. *Lucite* for L equals 9 or 20 mm).

Figure 7.2 shows that $\dot{q}''_\tau/\dot{q}''_0$ decreases non-linearly with L, and that the trend is different for each heater. A 1 mm thick sample exposed to 20 kW/m^2 with the lamp transmits between 63 and 69 % of the incident heat flux, while

only 9 to 10 % is transmitted with the resistance. For a 50 mm sample (typical upper size in bench-scale testing), more than 20 % of the lamp radiation is transmitted through the sample whereas less than 1 % is transmitted with the conical resistance.

In-depth radiation heat transfer is not significantly affected by the formulation (*Plexiglass / Lucite* Fig. 7.2) or by the manufacturing process (cast/extruded; not represented in Fig. 7.2 for clarity).

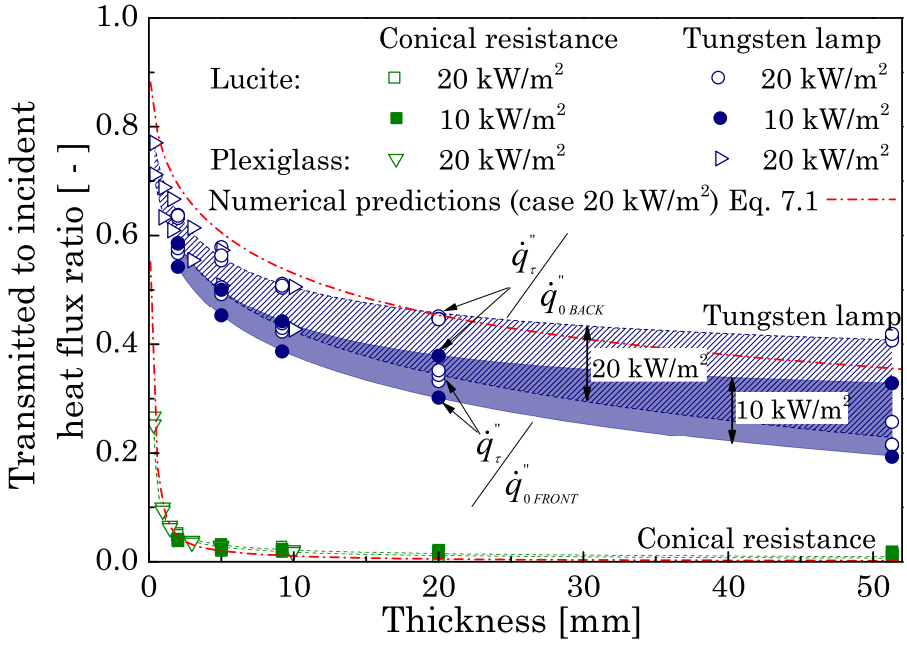

Figure 7.2: Transmitted to incident heat flux ratio for clear PMMA samples (*Plexiglass* and *Lucite*) exposed to a radiative source (conical resistance and tungsten lamp) providing 10 and 20 kW/m² for thicknesses ranging between 0.375 and 51 mm.

The influence of the distance heater-sample was investigated by keeping the same emitting temperature but moving the heaters from their initial position of distances between 20 and 50 mm. This is the same technique employed by Thomson and Drysdale [6] which leads to changes for $\dot{q}''_0$. The resulting differences in the $\dot{q}''_\tau/\dot{q}''_0$ measured are lower than 5 % (comparable to the repeatability error) and therefore the effect of distance is considered negligible.

The sensitivity to the heater operating temperature was investigated by lowering the voltage to provide 10 kW/m² (at the original distance heater-sample). This change leads to lower operating temperatures of the sources. The 10 kW/m² level is reached with operating temperatures of 723 K for the resistance and 2248 K for the lamp, representing approximately a decrease of 15 % from the operating temperatures at 20 kW/m². The resulting variation of $\dot{q}''_\tau/\dot{q}''_0$, shown in Fig. 7.2 (range represented by filled area) is significant only for the lamp, whereas it is negligible for the resistance. This confirms the relatively low dependency of $\bar{\alpha}$ to operating temperatures measured by Försth and Roos [8] for clear PMMA samples of similar thickness (6 mm) using a resistance heater. However, the effect of the operating temperature depends on L and is significant for thin samples.

In summary, measurements reported in Fig. 7.2 prove that radiative heat transfer through a sample depends strongly on thickness (or depth) and of the emitting source (type and operating temperature), but it is independent of the clear PMMA formulation and of the relative distance heater-sample. Both of these strong dependencies appear in Eq. 7.1 via α_λ which is function of the depth L, and via the spectral emitted intensity J_λ which depends on the operating temperature T and the source. These two variables are investigated in the next sections.

3. Sample in-depth absorption

When a radiative beam crosses a gas-solid interface, a fraction r is reflected. The crossing part $(1-r)$ undergoes an exponential attenuation $e^{(-\kappa_\lambda L)}$ inside the solid according Beer-Lambert's law [10] (where κ_λ is the attenuation coefficient) up to the next interface where a fraction r of the remaining beam is reflected (Fig. 7.1).

α_λ is the complement to the reflectance $\rho_\lambda(r)$ and the transmittance $\tau_\lambda(r)$ as pointed out in Eq. 7.2a. These quantities express respectively, the total reflected and transmitted components of the radiation resulting from multiple internal reflections [12].

$$\alpha_\lambda = \begin{cases} 1 - \tau_\lambda(r) - \rho_\lambda(r) & \text{(a) multiple reflections} \\ 1 - (1-r)^2\, e^{(-\kappa_\lambda L)} - r & \text{(b) simple reflection} \end{cases} \qquad (7.2)$$

The spectral distributions of α_λ were measured for eight *Plexiglass* samples of thicknesses ranging from 0.375 to 30 mm. Results are plotted in Fig. 7.3 for the thinnest and the thickest samples only. ρ_λ and τ_λ were measured using integrating spheres with a Perkin Elmer Lambda 900 double beams spectrometer in the wavelength interval [0.3-2.5 μm] and with a Bruker Tensor single beam spectrometer in the interval [2.5-20 μm]. Details of the procedure can be found elsewhere [8]. The repeatability of the measurements, based on three repeats, is good with a standard deviation lower than $3.5 \cdot 10^{-3}$ on average over the wavelength interval [0.3-20 μm] and a maximum of 0.033.

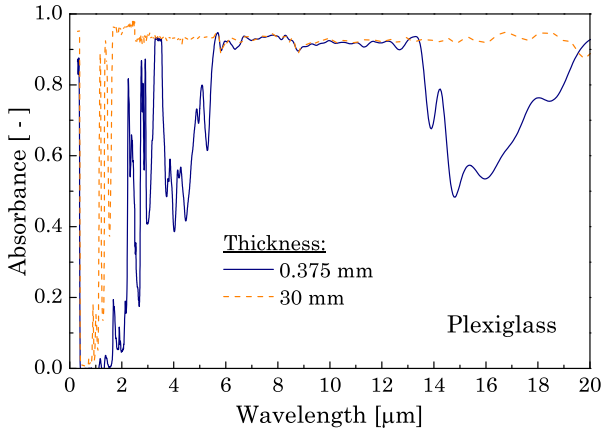

Figure 7.3: Absorbance measurements for 0.375 mm and 30 mm thick *Plexiglass* samples.

The observed independence of $\dot{q}''_\tau/\dot{q}''_0$ on the type of clear PMMA reported in Fig. 7.2, is confirmed spectrally by the near perfect agreement of α_λ (not plotted - standard deviation lower than $4.5 \cdot 10^{-3}$ in average) for *Plexiglass* and *Lucite* (cast and extruded).

The measurements of α_λ in Fig. 7.3 show large heterogeneities over their spectral dimension (non-grey property) between 0 and the maximum $(1-\rho_\lambda)$. When L increases, a larger part of the irradiation is absorbed (as predicted by Beer-Lambert's law) and the width of the bands where α_λ is not maximum (visible and near-infrared bands) is reduced.

Using these measurements of α_λ, the spectral distribution of κ_λ has been calculated numerically by solving the 3rd-order equation in $e^{(-\kappa_\lambda L)}$ resulting from multiple reflections (see [14] for details). The solution is most challenging for wavelength bands where the transmission is close to 0 or close to $(1-\rho_\lambda)$. Most of the problems of signal saturation (high transmission for visible and near-infrared bands) and of low signal-to-noise ratio (low transmission for infrared bands) were avoided by using respectively, thick samples (L = 30 mm) to reduce the bands of high transmission and thin samples (L = 0.375 mm) to reduce the bands of low transmission. For the bands where the problem was still present, κ_λ was set to 0 m^{-1} for bands of high transmission and 12000 m^{-1} for bands of low transmission (best estimation for a reasonable signal-to-noise ratio).

Figure 7.4 shows the calculated spectral distribution of κ_λ for *Plexiglass*. κ_λ is lower than 1000 m^{-1} only in the range [0.5-2.7 μm]. Given that κ_λ is the inverse of the mean penetration distance, almost the entire radiation spectrum of interest to fire science is absorbed in a thin layer within 1 mm of the top of the exposed surface. This is in agreement with the recent experimental observations of Linteris et al. [9]. The only measurements of κ_λ available in the literature are those of Manohar et al. [15] (symbols in Fig. 7.4) over the narrow band [1.59-5.56 μm]. These have been included in Fig. 7.4 to show that the agreement is good over the band although Manohar et al.'s [15] measurements carry a very large noise and only average values are presented.

Once κ_λ is known, it can be used to calculate α_λ for any sample thickness inside the studied range. When ρ_λ is not known, the multiple reflections need to be neglected and Eq. 7.2b for a simple reflection should be used as first

approximation (r is estimated from the refractive index taken as 1.49 for *Plexiglass* [14]). This calculation is used to predict in Fig. 7.5 the independent measurements of α_λ conducted by Hallman [4] and Linteris et al. [9] for L = 3.175 and 3.15 mm respectively. A good agreement is observed and it is expected that even more accurate calculations can be obtained with a good knowledge of ρ_λ.

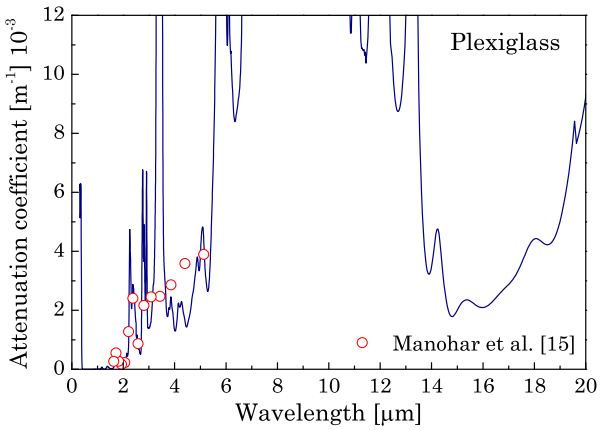

Figure 7.4: Spectral distribution of the attenuation coefficient for *Plexiglass*.

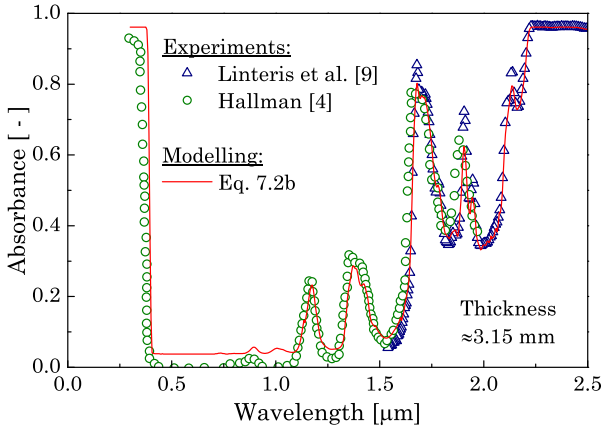

Figure 7.5: Comparison of independent measurements of the absorbance with predictions based on the measured attenuation coefficient.

Knowledge of κ_λ serves to quantify the depth of the absorption but the magnitude absorbed depends on the spectral distribution of the radiation from

the source. In the following section, the spectral intensity of the two sources is measured to complete the understanding of the sample-heater interaction.

4. Spectral emission from heaters

The two heaters used in this study (conical resistance and tungsten lamp) are different in multiple senses such as the physical principle, material, operating temperature, shape and distance to sample.

The spectral intensity J_λ of the heaters has been measured by comparing the emission received by a spectrophotometer from the heaters to that from a reference black body (Mikron M330 EU) at high temperature. The spectrometer (Vertex 80V) is used with different detectors (DTGS and Si) and beam splitters (Ge-KBr and CaF2 – function of the investigated range). The ranges of study are respectively [1.6-22 μm] for the conical resistance and [0.5-22 μm] for the lamp. Outside these ranges, the accuracy of the measurements would be low but the emission from the heaters is negligible as well. More details on the methodology can be found in [16]. The temperature of the heaters was set to 858 K and 2610 K, like for the broadband measurements reported in the second section. Each measurement has been repeated twice and the error is estimated to be lower than 5 %.

Figure 7.6 shows the measurements for the spectral distribution of J_λ. Significant differences are apparent between both heaters. The resistance emits 90 % of its intensity over the range [1.66-10.1 μm] with a peak at 3.40 μm. The lamp emits the same percentage on the narrower range, [0.5-2.8 μm], with its peak at 1.08 μm. The lamp's peak is more than 40 times higher than the resistance's peak. Also, the measurements at different operating temperatures (not represented) provide similar curves but the peak shifts to lower wavelength for higher temperature, as expected.

Fig. 7.6b shows that the calculated spectral intensity from a black body using Planck's law at 858 K matches the experimental J_λ for the electrical

resistance near perfectly. This demonstrates that the electrical coils emit as blackbodies and validates this common assumption for this heater. The lamp, which emits strongly in the visible and the near-infrared (signal weak for $\lambda > 4.3$ µm), does not present a blackbody behaviour. Fig. 7.6a also includes comparison to the intensity emitted by a grey body at 2610 K with an emissivity of 0.17 and allows the conclusion that the lamp spectral emission does not behave as a grey body either. It is believed that this non-greybody behaviour is induced by the spectral emissivity of tungsten [10], but also by the bulbs, the window and the cooling system (water and air) of the lamp.

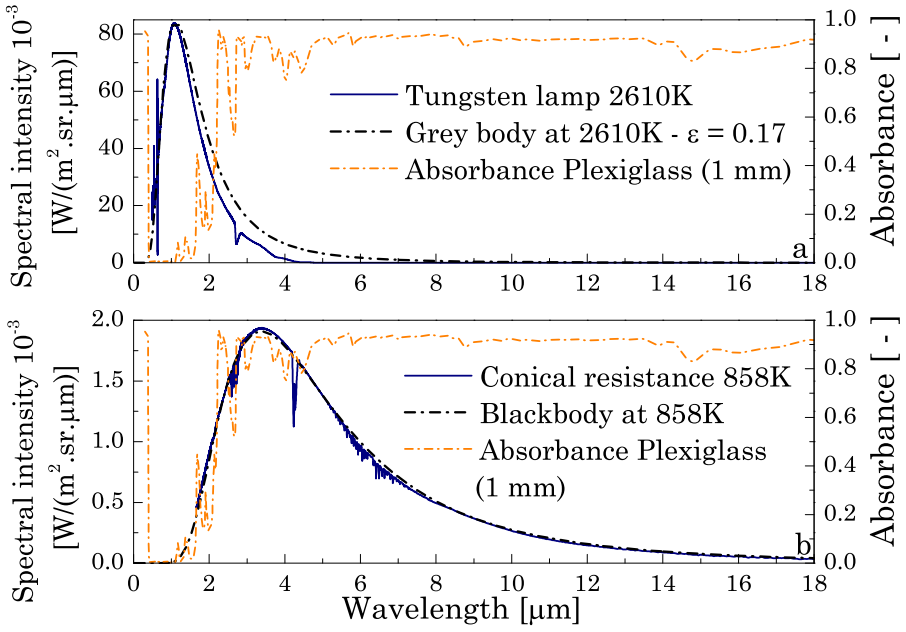

Figure 7.6: Spectral distribution of the emitted intensity (left axes) for (a) the tungsten lamp at 2610 K and (b) the conical resistance at 858 K. The absorbance for the 1 mm *Plexiglass* sample is shown on the right axes for comparison.

5. Discussion

The previous two sections provide fundamental insights which enable a better understanding of the radiative sample-heater interaction presented in Fig. 7.2.

The measurement of κ_λ, which is shown here to be strongly heterogeneous for clear PMMA with variation from 0 to 12000 m^{-1} (Fig. 7.4), allows

understanding how α_λ varies with L (Fig. 7.5). This large heterogeneity explains the reason why Linteris et al. [9] found $\bar{\kappa}$ (average of κ_λ obtained from broadband measurements) to be dependent on L instead of being an intensive property. An opaque material (no transmitted heat flux) does not necessarily absorb all the radiation close to the surface and the opacity criterion is dependent on the sample thickness. Only the spectral distribution of κ_λ or the broadband quantity $\dot{q}''_\tau/\dot{q}''_0$ for different thicknesses provide the necessary information on the absorbing depth. However, $\dot{q}''_\tau/\dot{q}''_0$ integrates the dependency associated to the heater and cannot be applied to other radiation scenarios.

Then, J_λ provides the magnitude of radiation received by the sample. In case of heaters behaving as a black body, such as the resistance, Planck's law provides the spectral variation of J_λ and the only additional required information is the heater operating temperature. If the heater can be considered as a grey body instead, the value of its emissivity is also required. In the other cases (heater neither black nor grey), like for the lamp in this study, a full characterization of J_λ is required.

The direct comparison in Fig. 7.6 of α_λ (right axes) and J_λ shows that the majority of the radiation emitted by the resistance is absorbed in the top 1 mm layer, whereas only a small fraction is absorbed in this layer for the lamp. This is confirmed in Fig. 7.2 where the resistance transmits only around 10 % of the incident heat flux for L = 1 mm while the lamp transmits between 63 % and 69 %. The numerical prediction of $\bar{\tau}$ using Eq. 7.1 with the measured values of κ_λ and J_λ is plotted in Fig. 7.2. The predictions agree well with the measurements of $\dot{q}''_\tau/\dot{q}''_0$ and capture the dependence with L and the heater type despite the assumptions made. The main assumptions are that the heater and the sample have perfectly diffusive surfaces, that the temperature distribution over the resistance coils and tungsten filaments is uniform, that radiation beams are collimated (i.e. the view factors of the source to the top surface is equal to the view factor of the source to the back surface) and that no other surface or media exchange radiation. These assumptions explain the relatively small discrepancies in Fig. 7.2 between experimental measurements and numerical predictions. While the heaters are positioned normal to the sample, all the

incident beams are not normal to the free surface. The influence of the incident angle, investigated using Fresnel's equation, has not been included in Eq. 7.1 due to the negligible improvement when it is considered. Eq. 7.1 should be taken as a qualitative tool with enough complexity to capture the main dependencies of the sample-heater interaction.

Because radiation absorption is directly dependent on the sample-heater interaction, these results prove experimentally the necessity of a multi-band radiation model to calculate accurately the heat transfer to the free surface of a translucent fuel. Manohar et al. [15] and Sohn et al. [17] have shown this numerically but only for a small spectral range [1.59-5.56 μm]. In fact, this will affect the in-depth temperature profile and hence the pyrolysis process. The number of bands required would depend on the applications (e.g. thickness and heat source). For example, to predict the penetration depth within 1 mm accuracy, only the spectral distribution of κ_λ over the range [0.5-2.7 μm] ($\kappa_\lambda < 1000$ m^{-1}) is required.

The temperature profile of a fuel sample absorbing significant radiation inside the interval [0.5-2.7 μm] will therefore be significantly different from the temperature profile of a sample absorbing outside this interval. For the same amount of energy absorbed, the first sample has a thicker thermal layer but the local temperatures are lower, significantly affecting its pyrolysis behaviour [11 (chap 6)] and the time to ignition [4].

At high heat flux levels, radiative heat transfer becomes predominant over conduction [13 (chap 1),18,19] and the spectral distribution of κ_λ needs to be considered over a wider band.

Regarding the limitations of the findings, we note that the radiative properties have been measured for a short period of exposure such that the heat absorbed by the sample is negligible and the sample temperature remains close to ambient. The in-depth temperature gradient and bubbling phenomenon (typical of PMMA pyrolysis) are expected to affect these radiative properties and the sample-heater interaction. The gas phase could also influence this

interaction by absorbing part of the incident radiation [20]. The evolution of the attenuation coefficient as a function of these phenomena should be investigated further as advanced in [8].

Due to the significant effects that J_λ can have on the pyrolysis results, the use of the electrical resistance alone will not allow the radiative heat transfer to be captured correctly since it is not a good representation of real fires (wildland [16], industrial facilities (liquid fuel) [4], common items [21]). On the other hand, the use of the lamp increases the complexity of flammability tests since experimentalist teams need to consider the difference in the heat absorbed by two fuels. The combined use of both the resistance and the lamp sources is therefore recommended. Moreover, while the tungsten lamp is a more complex spectral source, it offers other advantages over the resistance in flammability testing not related to radiation alone. For examples, the lamp prevents the pyrolysis gases from being in direct contact with a hot source possibly affecting the time to ignition and the absence of vertical obstacles just above the sample allows a better control of the flow field.

6. Conclusion

The sample-heater interaction for radiative heat transfer has been experimentally investigated for clear PMMA samples with two different heaters (electrical resistance and tungsten lamp).

Broadband measurements of transmittance through samples of different thicknesses show that radiative heat transfer is strongly dependent on the heater type and the operating temperature. For example, less than 10 % of the incident heat flux is transmitted through a 1 mm thick clear PMMA sample when exposed to the electrical resistance, whereas at 50 mm, a sample exposed to the lamp transmits more than 20 % of the incident radiation.

However, clear PMMA formulation (*Plexiglass/Lucite*), manufacturing process (extruded/cast) and the relative distance heater-sample are shown to have a negligible influence on the transmittance.

The main dependencies observed on the broadband measurements were investigated more fundamentally through the quantification of the sample spectral absorbance and the spectral intensity emitted by the heater.

The attenuation coefficient, controlling the spectral absorbance through Beer-Lambert's law, has been estimated in this study for clear PMMA. It is the first time that this is performed over the full wavelength range encountered in real fires. The sufficiency of these calculations was shown by comparing to independent measurements in the literature. The attenuation coefficient presents strong spectral heterogeneity (variation from 0 to 12000 m^{-1}). The assumption of a single effective value for this coefficient, as used nowadays in most of the pyrolysis models, cannot accurately capture in-depth absorption.

The spectral measurements of the emitted intensity by the heaters led to three main conclusions. First, both heaters emit in significantly different wavelengths ranges. Second, the conical resistance behaves almost as a black body; its spectral intensity can be described therefore by Planck's distribution and the operating temperature is the only required information. Third, the lamp does not even behave as a grey body and a full description of its spectral intensity is required. The blackbody assumption, usually accepted as first approximation is shown to not be always applicable.

Knowledge of the spectral distribution for these two fundamental variables (attenuation coefficient and emitted intensity) enables a better understanding the radiative heat transfer for a translucent fuel. This investigation proves the necessity of a multi-band radiation model to calculate accurately the heat transfer to the free surface of a translucent fuel on fire, which affects directly the in-depth temperature profile and hence the pyrolysis process. However, the required complexity of the spectral heterogeneity for the attenuation coefficient is dependent on the application and the level of accuracy expected.

References

[1] J.L. Torero, Flaming ignition of solid fuels, in: The SFPE handbook of fire protection engineering 4th edition, P.J. DiNenno et al. (Eds.), National Fire Protection Association, 2008, chapter 2.11, pp. 2.260-2.278, ISBN-10: 0877658218.

[2] ASTM E1354-10a: Standard test method for heat and visible smoke release rates for materials and products using an oxygen consumption calorimeter", ASTM International, West Conshohocken PA, 2010, http://dx.doi.org/10.1520/E1354-10A.

[3] ASTM E2058-03: Standard test method for measurement of synthetic polymer material flammability using a Fire Propagation Apparatus, ASTM International, West Conshohocken PA, 2003, http://dx.doi.org/10.1520/E2058-03.

[4] J.R. Hallman, Ignition characteristics of plastics and rubber, PhD Dissertation, The University of Oklahoma, 1971.

[5] T. Kashiwagi, Effects of sample orientation on radiative ignition, Combustion and flame 44 (1982) 223-245, http://dx.doi.org/10.1016/0010-2180(82)90075-X.

[6] H.E. Thomson and D.D. Drysdale, Flammability of plastics I: Ignition temperatures, Fire and materials 11 (1987) 163-172, http://dx.doi.org/10.1002/fam.810110402.

[7] A. Tewarson and S.D. Ogden, Fire behaviour of polymethylmethacrylate, Combustion and flame 89 (1992) 237-259, http://dx.doi.org/10.1016/0010-2180(92)90013-F.

[8] M. Forsth and A. Roos, Absorptivity and its dependence on heat source temperature and degree of thermal breakdown, Fire and materials 35 (2011) 285-301, http://dx.doi.org/10.1002/fam.1053.

[9] G. Linteris, M. Zammarano, B. Wilthan and L. Hanssen, Absorption and reflection of infrared radiation by polymers in fire-like environments, Fire and materials 36 (2012) 537-553, http://dx.doi.org/10.1002/fam.1113.

[10] T.L. Bergman, A.S. Lavine, F.P. Incropera and D.P.Dewitt, in: Fundamentals of heat and mass transfer 7th edition, Wiley, 2011, chapter 12 768-860, ISBN-10:0470501979

[11] P. Girods, N. Bal, H. Biteau, G. Rein and J.L. Torero, Comparison of pyrolysis behaviour results between the Cone Calorimeter and the Fire Propagation Apparatus heat sources, Fire safety science 10 (2011) 889-901, http://dx.doi.org/10.3801/IAFSS.FSS.10-889.

[12] M. Chaos, M.M. Khan, N. Krishnamoorthy, J.L. De Ris and S.B. Dorofeev, Evaluation of optimization schemes and determination of solid fuel properties for CFD fire models using bench-scale pyrolysis tests, Proceedings of the Combustion Institute 33 (2011) 2599-2606, http://dx.doi.org/10.1016/j.proci.2010.07.018.

[13] N. Bal and G. Rein, Numerical investigation of the ignition delay time of a translucent solid at high radiant heat fluxes, Combustion and flame 158 (2011) 1109-1116, http://dx.doi.org/10.1016/j.combustflame.2010.10.014.

[14] P.T. Tsilingiris, Comparative evaluation of the infrared transmission of polymer films, Energy conversion and management 44 (2003) 2839-2856 http://dx.doi.org/10.1016/S0196-8904(03)00066-9.

[15] S.S. Manohar, A.K. Kulkarni and S.T. Thynell, In-depth absorption of externally incident radiation in nongray media, Journal of heat transfer 117 (1995), 146-152, http://dx.doi.org/10.1115/1.2822295.

[16] P. Boulet, G. Parent, Z. Acem, A. Kaiss, Y. Billaud, B. Porterie, Y. Pizzo, C. Picard, Experimental investigation of radiation emitted by optically thin to optically thick wildland flames, Journal of combustion (2011), http://dx.doi.org/10.1155/2011/137437.

[17] Y. Sohn, S. W. Baek and T. Kashiwagi, Transient modeling of thermal degradation in non-charring solids, Combustion science and technology 145 (1999) 83-108, http://dx.doi.org/10.1080/00102209908924204.

[18] T.J. Ohlemiller and M. Summerfield, Radiative ignition of polymeric materials in oxygen/nitrogen mixtures, Proceedings of the symposium (international) on combustion 13 (1971) 1087-1094, http://dx.doi.org/10.1016/S0082-0784(71)80106-6.

[19] G. Linteris, Numerical simulations of polymer pyrolysis rate: effect of property variations, Fire and material 35 (2011) 463-480, http://dx.doi.org/10.1002/fam.1066.

[20] S.H. Park, A.J. Stretton and C.L. Tien, Infrared radiation properties of methyl methacrylate vapor, Combustion science and technology 62 (1988) 257-271, http://dx.doi.org/10.1080/00102208808924012.

[21] J.J. Comeford, The spectral distribution of radiant energy of a gas-fired radiant panel and some diffusion flames, Combustion and flame 18 (1972) 125-132, http://dx.doi.org/10.1016/S0010-2180(72)80233-5.

Achievements and prospects

1. Outcomes of the present research

The state-of-the-art in pyrolysis modelling has evolved over a few decades resulting in a large growth of model complexity by the addition of new physical and chemical mechanisms. Taken individually, these mechanisms represent realistic concepts (e.g. temperature dependency of the material properties). They are added into the models with the implicit assumption that models with a higher number of mechanisms tend to be more accurate. In the present work, this assumption has been challenged by exploring the relation between prediction uncertainty and model complexity for the pyrolysis modelling of PolyMethylMethAcrylate (PMMA) in non-flaming conditions (process prior to ignition). The present research can be divided into three parts.

The first part gathers investigations on the model equations. Two approaches were used. In the first one, the minimum level of complexity required to explain the experimental delay time to ignition of black PMMA samples is assessed by exploring the influence of the mechanisms one by one. Applying the rule that simplifications are required where the expected precision does not warrant the inclusion of higher levels of complexity, it was demonstrated that the complexity usually considered (e.g. thermal dependency of the material properties or multiple reaction scheme) cannot explain the experimental behaviour encountered when high heat flux levels are applied in bench-scale tests. The mechanism of in-depth radiation absorption is shown to be essential to predict the ignition at extreme heat fluxes.

In the second approach, a different methodology is applied. The most complex model available in the literature is employed and assumptions or simplifications are added step by step, reducing its global complexity in order to assess the importance of the mechanisms. Using different taxonomies, it was demonstrated that for the prediction of the pyrolysis process prior to ignition, the mechanisms of heat transfer, including the in-depth absorption mechanism, have a large impact on the surface temperature and mass loss rate, whereas the chemical degradation only impacts the mass loss rate. Without a good formulation and calibration of these mechanisms, an *a posteriori* optimisation of the mass loss rate is required to compensate the prediction error. More fundamental investigations are required on the heat transfer to ensure an accurate modelling of the local temperature.

The two approaches correspond in fact to sensitivity studies. However, they diverge from usual sensitivity analyses which are parametric. Moreover, these two studies operate differently. In the first one, the initial model is simple and the mechanisms are explored one by one but they are not added whereas in the second one, the model is deliberately taken to be complex and simplifications accumulate. These two methodologies can complement each other.

The second part of this work is dedicated to the assessment of the level of confidence that a modeller can have in his predictions. The global growth of complexity in pyrolysis modelling implies an increase of the number of input parameters. The problem is when the uncertainties associated with the different parameters accumulate in the model output. The global error induced by the parameter uncertainty balances the improvements obtained with the incorporation of new mechanisms, leading to the existence of an optimum of model complexity (or at least a more appropriate level of complexity decreasing the global error).

The parameter uncertainty is directly linked to the calibration process. This can be achieved mainly by three different processes: the realisation of independent studies, inverse modelling or the use of the literature database. The first one presents some problems related to the methodology (scale, experimental conditions, ...) and to the required resources (human, material and financial) but it is expected to be the best solution. This technique is generally reserved to research and high technology. The present research explores the uncertainty associated with the parameter calibration using the last two techniques which appear to be more and more employed, especially in the context of performance-based design and forensic analyses.

A large literature review of the main parameters encountered in pyrolysis modelling is performed for PMMA which the simplest and best known non-charring polymer. The large number of available studies for this material enables the characterization of the experimental uncertainty for bench-scale tests and for the model input parameters extracted from such tests. The obtained parameter variability needs to be considered when the literature database is used to calibrate a model. Using sensitivity and uncertainty analyses, the controlling parameters and the global level of confidence associated with a solid ignition model has been assessed. The results show that the variability of only a few parameters (all internal parameters) is important for the prediction of solid ignition of black PMMA. The parameters which are non-influent (low sensitivity for the predictions) or the ones presenting a small variability can be chosen directly from the literature. The prediction uncertainty has been compared to the experimental one obtained by gathering more than

250 tests results. Using a simple pyrolysis model, it was shown that the range of prediction is significantly wider than the experimental uncertainty. However, it is worth noticing that the standard deviation associated with the predictions captures the experimental uncertainty.

The influence of the model complexity on the calibration process by inverse modelling has been investigated using genetic algorithms. Identical matches to experiments were achieved for various levels of complexity, demonstrating the presence of compensation effects between the mechanisms and optimised parameters. The phenomenon grows in importance with model complexity leading to unrealistic values for the calibrated parameters. The study demonstrates also that the model complexity needs to be related to the available resources. A large model complexity implies a high number of parameters and the optimisation algorithm does not manage to reach a unique solution if a sufficient number of measurements is not performed.

The third part of the present work results from the observation performed in the two previous parts. The mechanism of in-depth radiation absorption appears to be critical in specific conditions for the prediction of the pyrolysis process up to ignition. Moreover, the variability of the parameter controlling this mechanism (i.e. the attenuation coefficient) was found to be large in the literature. Experimental investigations were therefore carried out in order to understand the variability of the attenuation coefficient (scalar). The use of different heat sources reveals its dependency to the emission wavelengths. Fundamental investigation enabled the quantification of this dependency. The impact of the heat source on the radiation absorption (depth and magnitude) is shown to be predictable thanks to the detailed measurements of the attenuation coefficient of PMMA and of the emissive power of the heat sources. Moreover, the spectral measurement of the attenuation coefficient is able to explain independent studies performed with other types of PMMA, demonstrating that the variability of this coefficient in the literature results mainly from the simplifications performed on the mathematical formulation of the mechanism (impact of the heat source neglected). These simplifications can however be justified in some experimental conditions.

To conclude, the pyrolysis models available in the literature reached a level of complexity such that parameter uncertainty can control the prediction error. The study of the process of calibration is therefore important. This process is a function of the available resources. Independent experiments are highly resource demanding. Advanced techniques such as inverse modelling present some problems due to the coupling between the model equations and the optimised parameters. The database in the literature provides ranges for the input parameters which are already too wide for simple models. The choice of model equations cannot be purely arbitrary. A combination of numerical (sensitivity and uncertainty) analyses and experimental studies is required to avoid unnecessarily increase of the level of complexity of a pyrolysis model. The two main questions that should drive the specification of a model are: what is the minimum level of complexity required to explain the experimental results and what level of complexity can be afforded due to the resources available to calibrate the model?

2. Future work

Pyrolysis modelling is unavoidable in the prediction of the fire growth. Due to its importance, fundamental studies are required in order to understand the phenomenon and improve the models' predictive capabilities. These studies need to be experimental but also numerical. Indeed, the failure of a model to predict a particular behaviour can be investigated numerically thanks to sensitivity and uncertainty analyses. Once an issue is identified, a specifically designed experiment can help to characterize a physical or chemical phenomenon, prior to adding a mechanism simulating it into the model. Pointing out failures is an essential work which is often not acknowledged as it should be.

Moreover, most of the experimental investigations on pyrolysis are performed at small and bench scales. These tests are convenient due to the possibility of fixing some external variables. However, by controlling part of the experimental conditions, the protocol steps away from the reality. It is important to identify the differences between the reality and the experimental

procedure and to assess their influences on the extracted parameters. The perfect example is the radiative heat source as it has been shown in this work. In order to go beyond the present study, since a fire is not a black body, it is important to assess the error induced by using values for parameters that have been extracted from bench-scale tests using blackbodies heat source. To the knowledge of the author, the influence of the atmosphere composition and the radiative heat transfer on the pyrolysis process are real challenges for the future.

However, as the present work has also demonstrated, the global prediction capability is not only a function of the model equations and significant improvements in pyrolysis modelling would be achieved only if the parameters calibration process is considered simultaneously with the model equations. Due to the large number of parameters present in the current models, the process of inverse modelling is more and more frequently used. In this process, the measurements used were often chosen by default. The sensitivity of the quantity predicted to the different input parameters was not investigated. The obvious coupling between the data and the model equations in the process of inverse modelling could be overcome if each of the input parameters were to be optimised over a range of experiments where the most influent external variables for each parameter are varied.

Another potential improvement resides in the implementation of sensitivity and uncertainty analyses during the process of optimisation. Sensitivity studies would help to identify, at each step, the predominant parameters in order to focus the optimisation. As an example, for techniques similar to genetic algorithms, the results from the sensitivity studies could assist in having an adaptive level of mutation to look most of the research domain for the predominant parameters. The parameter uncertainty, characterized by the width of the parameter ranges providing similar matches to the experimental results, is useful in detecting if a parameter can be calibrated accurately given the experiments performed. A high level of variability indicates that the level of complexity implemented in the model is not adapted.

On top of that, the process of inverse modelling should integrate the possibility to optimise not only the parameters but also the mechanisms as a function of the available experimental data.

In the case where the calibration using experimental data is not possible, as it is most of the time in the context of performance based design, a probabilistic approach is required in order to integrate the parameter variability. Monte Carlo is a very good technique but it is hard to implement due to its computational cost. Techniques using surrogate functions need to be developed and implemented in the pyrolysis model in order to assess the global predictions uncertainty.